STUDIES ON ANTIMICROBIAL ACTIVITY OF ARGININE-BASED SURFACTANTS AND CHEMO-ENZYMATIC SYNTHESIS OF NOVEL AMPHIPHILES BASED ON L-ARGININE AND D-FAGOMINE

José Antonio Castillo Expósito

Thesis, 2006

UNIVERSIDAD AUTÓNOMA DE BARCELONA
FACULTAD DE QUÍMICA

INSTITUTO DE INVESTIGACIONES QUÍMICAS
Y AMBIENTALES DE BARCELONA
CONSEJO SUPERIOR DE INVESTIGACIONES CIENTÍFICAS
(IIQAB-CSIC)

Studies on antimicrobial activity of arginine-based surfactants and chemo-enzymatic synthesis of novel amphiphiles based on L-arginine and D-fagomine

José Antonio Castillo Expósito
Barcelona, September 2006

Thesis submitted to Universitat Autónoma de Barcelona
in partial fulfilment of the requirements for the degree of PhD
(field of Chemistry)

Dr. Pere Clapés (director)
Dr. Àngels Manresa (director)
Dr. José Peral (tutor)

Dejar de aprender es como ir sentado en un vagón de espaldas a lo que venga,
se te va escapando el paisaje y siempre es tarde para ver lo que venía.

Antoine Martán

ACKNOWLEDGEMENTS

Firstly, I would like to acknowledge Dr. Pere Clapés and Dr. Àngels Manresa for the opportunity to perform this thesis in their research groups. During these years, they have perfectly supervised my dialy work and I have learned more than I expected. Moreover, I always could participate in the working plans and in my opinion, this is especially important for the formation of PhD students.

The present thesis has involved some collaborations with different research groups. I would like to thank all the following supervisors in chronological order for their assistance and their kind predisposition to collaborate with our group: Josep Carilla and Dr Isabel Haro from IIQAB-CSIC, Prof. Dr. Mª Asunción Alsina from Dept. Physical Chemistry, Faculty of Pharmacy, University of Barcelona, Dr. Jaume Comas from Servei cientifico-técnic, Parc Científic de Barcelona and Prof. Dr. Georg A. Sprenger from Institut of Microbiology, University of Stuttgart. I would like to acknowledge specially Dr. Jesús Joglar from IIQAB-CSIC for his helpful advises in Organic Chemistry.

Biological assays with compounds synthesised in the present thesis have been carried out by Jordi Calveras and Dr. Fina Casas from IIQAB-CSIC, Montse Mitjans and Dr. Pilar Vinardell from Dept. Physiology, Faculty of Pharmacy, University of Barcelona and Dr Jaume Carrió and Dr. Roser Fisa from Dept. Parasitology, Faculty of Pharmacy, University of Barcelona. To all of them, I want to acknowledge for their collaboration.

To work in different laboratories for some years has involved having many colleagues. I have been really lucky because in all these places I have found very nice people and pleasant environments to work. For all this reasons I would like to thank Carmen, Laia, Jordi, Xavi, Susana, Carles, Ari, Sonia, Guillem and Anna from IIQAB-CSIC, Jaume, Éscar, Mònica and Adrià from Faculty of Pharmacy, University of Barcelona and Tomoyuki from University of Stuttgart. After doing the PhD, I do not know what I will do in the future nor where, but I would like to find people like them.

Finally, I would like to thank my family and especially my mother for their support and comprehension during these years.

FOREWORD

The present thesis has been performed at the Department of Peptide and Protein Chemistry IIQAB-CSIC (Barcelona), under the supervision of Dr. Pere Clapés and at the laboratory of Microbiology, Faculty of Pharmacy, University of Barcelona, under the supervision of Dr. Àngels Manresa. Experimental parts of this thesis that have been performed in other laboratories are the following:

- Physico-chemical analyses using a Langmuir's film balance at Department of Physical Chemistry, Faculty of Pharmacy, University of Barcelona, supervised by Prof. Dr. Mª Asunción Alsina.

- Analyses by differential scanning calorimetry at laboratory of thermal analyses, IIQAB-CSIC, supervised by Josep Carilla.

- Leakage assay by fluorescent spectroscopy at Department of Peptide and Protein Chemistry, IIQAB-CSIC, supervised by Dr. Isabel Haro.

- Flow cytometry analyses at Servei cientifico-técnic, Parc Científic de Barcelona, supervised by Dr. Jaume Comas.

- Overexpression on *E. coli* and purification of fructose 6-phosphate aldolase at Institut of Microbiology, University of Stuttgart, supervised by Prof. Dr. Georg A. Sprenger:

Assays carried out in collaboration with other laboratories have been the following:

- Assays of inhibition of glycosidases by the iminocyclitols synthesised in this thesis were carried out by Jordi Calveras and supervised by Dr. Fina Casas (Research Unit on Bioactive Molecules (RUBAM), IIQAB-CSIC).

- Cytotoxic assays of the bis(PhAcArg) derivatives and of the iminocyclitols synthesised in this thesis were carried out by Dr. Montse Mitjans and supervised by Dr. Pilar Vinardell (Department of Physiology, Faculty of Pharmacy, University of Barcelona).

- Assays of the antileishmanial activity of the bis(PhAcArg) derivatives synthesised in this thesis were carried out by Dr. Jaume Carrió and supervised by Dr. Roser Fisa (Department of Parasitology, Faculty of Pharmacy, University of Barcelona)

Financial support from the Ministry of Science and Education MYCT projects PPQ2000-1687-CO2-01, PPQ2000-04625-CO2-01, PTR1995-0514-OP, CTQ-2004-771-CO2-01/PPQ, a CSIC I3P postgraduate scholarship programme and the COST D25 STSM are acknowledged.

ABBREVIATIONS

ANTS = 8-aminonaphtalene-1,3,6-trisulfonic acid
Bis-oxonol = bis-(1,3-diethylthiobarbituric acid)trimethine
Br s = broad singlet
BSA = bovine serum albumin
$C_3(CA)_2$ = bis(N^{α}-caproyl-L-arginine)-1,3-propanediamide dihydrochloride
$C_3(OA)_2$ = bis(N^{α}-octanoyl-L-arginine)-1,3-propanediamide dihydrochloride
Cbz = benzyloxycarbonyl
cfu = colony forming units
CHX = chlorhexidine dihydrochloride
de = diastereoisomeric excess
D = detection (wavelength)
DI = denaturation index
DTAB = dodecyltrimethylammonium bromide
DHA = dihydroxyacetone
DMSO = dimetilsufoxid
DPPC = 1,2-dipalmitoyl-*sn*-glycero-3-phosphocholine
DPPG = 1,2-dipalmitoyl-*sn*-glycero-3-[phospho-*rac*(1-glycerol)] sodium salt
DPX = *N,N'-p*-xylenebis(pyridinium) bromide
DTT = 1,4-dithio-D,L-threitol
Eq = equivalent
F = flow
FC = flow cytometry
FSA = fructose 6-phosphate aldolase
FU = fluorescence units
Gly-3-P = DL-glyceraldehyde-3-phosphate
Glu-6-P-DH = glucose-6-phosphate dehydrogenase
Hepes = 4-(2-hydroxyethyl)piperazine-1-ethanesulfonic acid
HLB = hydrophilic-lipophilic balance
HTAB = hexadecyltrimethylammonium bromide
HPLC = high performance liquid chromatography
HC_{50} = concentration that induces the haemolysis of 50 % of the cells
I = injection
IC_{50} = 50% inhibitory concentration
L/D = lysis/denaturation ratio
LAE = N^{α}-lauroyl-L-arginine ethyl ester hydrochloride
LAM = N^{α}-lauroyl-L-arginine methyl ester hydrochloride
LPS = lipopolysaccharides
LUV = large unilamelar vesicles
MIC = minimum inhibitory concentration
MLV = multillamelar vesicle
MRSA = methicillin-resistant *S. aureus*
Mw = molecular weight
NADP: β-nicotinamide adenine dinucleotide phosphate disodium salt
n = number of methylenes
nd = not determined
nr = no reaction

PBS = Phosphate buffered saline
P = pressure
PGI = phosphoglucose isomerase
OMPs = outer membrana proteins
PBS = phosphate buffered saline
PI = propidium iodide
RAMA = rabbit muscle aldolase
rpm = revolutions per minute
QACs = quaternary ammonium compounds
QSAR = quantitative structure-activity relationships
SEM = standard error media
SDS-Page = sodium dodecyl sulphate polyacrilamide gel electrophoresis
Spp. = specie (of micro-organism)
Suppl. Mat. = supplementary material
TEM = transmission electronic microscopy
TSA = tryptocase soy agar
TSB = tryptone soy broth
U = enzymatic unit

CONTENTS *Page*

1. INTRODUCTION

1.1. Bacteria and antibacterial agents

Bacteria constitute the major portion of biomass on Earth. These prokaryotic cells are central to the functioning of the biosphere and they establish relationships with higher organisms that can be either beneficial or harmful. Many of them carry out a range of biochemical reactions such as the synthesis of proteolytic enzymes or vitamins (*e.g.* vitamin K, niacin, thiamine and riboflavin). Moreover, the bacterial populations that are present normally in living beings (*i.e.* normal microflora) have a protective role against exogenous pathogenic organisms. Bacteria are also widely used in many industrial processes such as production of antibiotics and enzymes or fermentations in food industry. These micro-organisms also can cause many infectious diseases and therefore, the control of microbial growth is necessary in many practical situations and significant advances in agriculture, medicine and food science have been made through study of this area of microbiology.

Microbial control in living tissues requires antimicrobial agents which reduce or prevent microbial growth and cause no harm to the host cell. This goal is achieved by a variety of chemotherapeutic agents. A common target of these products is the bacterial cytoplasmic membrane. To reach this target, the molecules must cross through the cell envelopes. Therefore, the knowledge of the bacterial cell biology may help to the rational design of new antibacterial agents with improved biocidal capabilities.

1.1.1. Bacterial cell biology

Bacteria are prokaryotic cells which appear as rods (bacilli), as spherical cocci or as spiral-shaped cells. These micro-organisms show different arrangements depending of the species; single units (cocci), pairs (*Neisseria gonorrhoeae*), chains (*Streptococcus* spp.) or bunches (*Staphylococcus* spp.). In some instances, there is not a characteristic cell

shape associated with a bacterium and it may be described as pleiomorphic. Mycoplasmas are an example, they lack a rigid and shape-defining cell wall. Bacteria also vary in size, with diameters ranging from 0.1 to 50 μm, being the average diameter around 1 μm.

The natural mode of growth of bacteria is a community of cells in an ordered structure known as biofilm. These bacterial aggregates consist of adsorbed cells in a surface with the associated glycocalix (*i.e.* extracellular polymeric substances). This polymer constitutes a physical barrier which can hinder antimicrobial agents from reaching target organisms within the biofilm. Moreover, bacteria within a biofilm have both nutrient limitation and reduced growth rates which appears to influence their physiology altering their sensitivity to biocides.[1] A current strategy against biofilm infections is the impregnation of surfaces with antimicrobial agents which delay bacterial colonization.[2]

Sporulation is another example of bacterial resistance to antimicrobial agents. The bacterial spore is a complex entity which is resistant to inactivation by many chemical and physical agents.[3] Sporulation is a serious problem in food preservation and medical microbiology. A typical example is botulism, a form of food poisoning caused by the toxins of *Clostridium botulinum*. This source of infection is common in home-canned food that has not been heated sufficiently to kill the spores.

Description of the bacterial ultrastructure

Electron microscopy has provided a detailed view of the bacterial ultrastructure, revealing the absence of both a nuclear membrane enclosing the chromosomal DNA and other membrane-bound organelles.

The prokaryotic envelopes can be defined as the complex of membranes, basically the cytoplasmic membrane and the cell wall, associated with macromolecules which together form the boundary between

the inside and the outside of the cell. These envelopes play several important functions: give cell shape and rigidity, protect against osmotic lysis, act as permeability barrier-selective, involvement in cell division, etc.[4]

Bacteria are broadly divided into two major groups: Gram-positive and Gram-negative bacteria. Both types of bacteria show different permeability to the dye used in the Gram test. The different structure and composition of cell envelopes is the cause of their different permeability (see Figures 1 and 2).

Gram-positive cell wall

Peptidoglycan is the main component of the Gram-positive bacterial cell wall, being between 20 and 40 layers thick. This polymer is composed by strands which are interconnected either by direct cross-links between peptide chains or by means of a peptide interbridge. Peptidoglycan synthesis is the target for a number of commonly used antibiotics such as penicillins and cephalosporins.

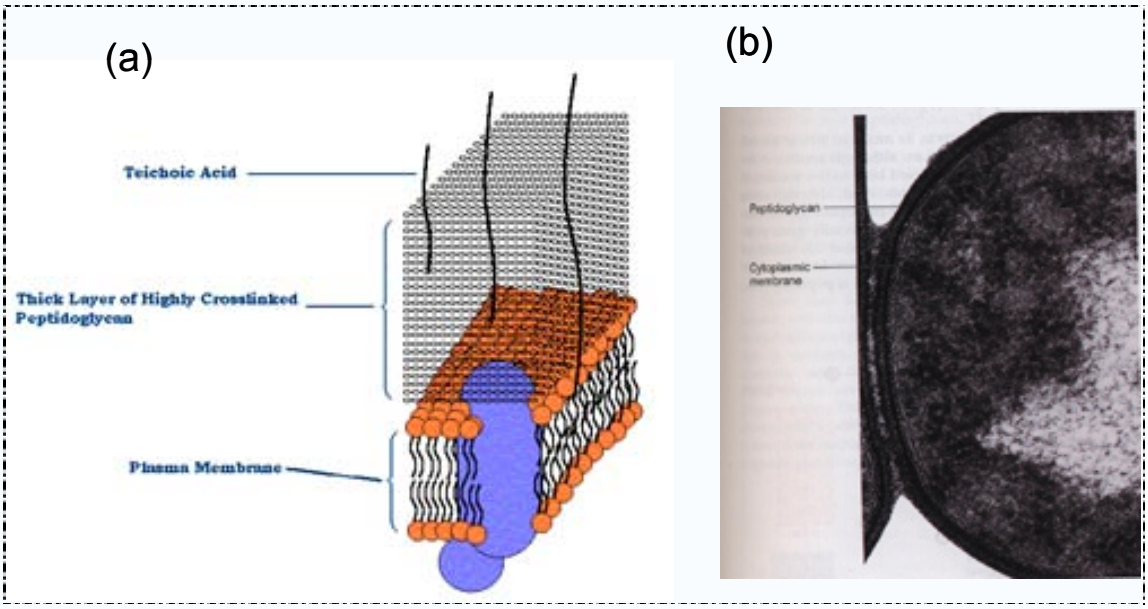

Fig. 1 (a) Scheme of the structure of cell envelopes of Gram-positive bacteria. (b) Transmission electron micrographs of *Arthobacter crystallopoites* as example of Gram-positive bacteria. Source: Brock Biology of Microorganisms.[5]

The outer major components of the cell wall are anionic polymers such as teichoic and lipoteichoic acids. These molecules may contribute to the net negative charge of Gram-positive bacteria. Their function remains unclear, although they may be involved in the adhesion process and to maintain the cell wall structure.

Gram-negative cell wall

The cell wall of Gram-negative bacteria has a more complex multilayered structure than that of Gram-positive bacteria. The peptidoglycan layer is much thinner, only one or two layers are present, and lies between the cytoplasmic membrane and a second membrane, the outer membrane. This outer membrane consists of a phospholipid bilayer connected with an external leaflet of lipopolysaccharides (LPS). LPS renders the Gram-negative bacteria highly hydrophilic with a net negative charge.

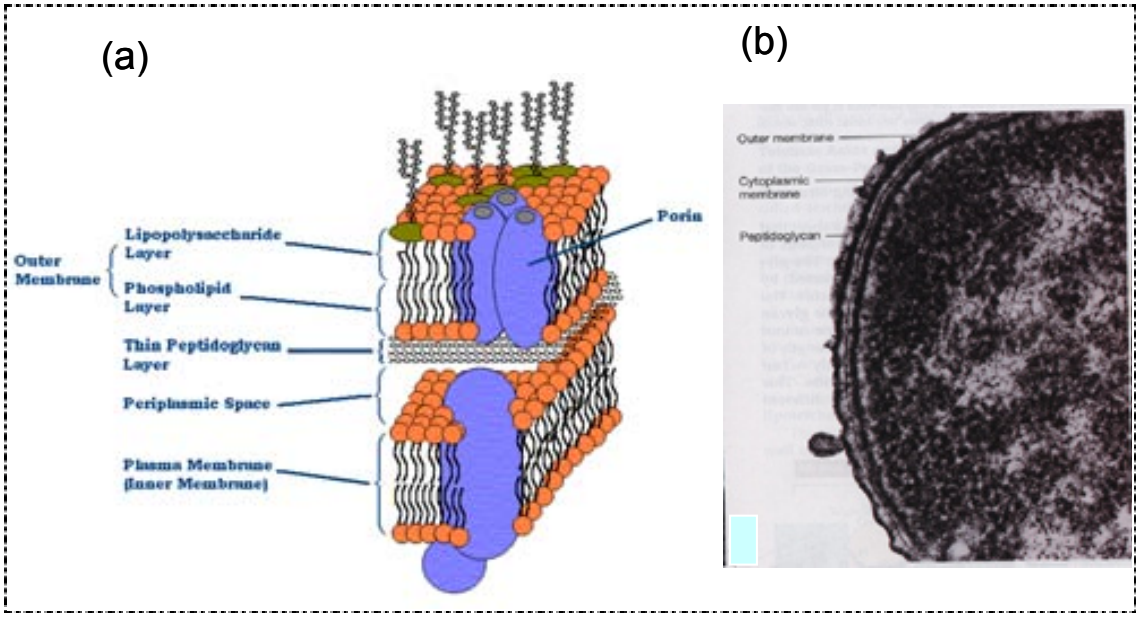

Fig. 2. (a) Scheme of the structure of cell envelopes Gram-negative bacteria. (b) Transmission electron micrograph of *Leucothrix mucor* as example of Gram-negative bacteria. Source: Brock Biology of Microorganisms.[5]

Some bacteria can rapidly change the nature of the LPS to avoid host immune defences. The outer membrane also contains a large number of proteins, namely outer membrane proteins, OMPs. These proteins include porins which create small channels of about 1 nm of diameter, allowing the transport of relative hydrophilic molecules up to around 700 Da in size.

Cytoplasmic membrane

The inner layer of cell envelope in both Gram-positive and Gram-negative bacteria is the cytoplasmic membrane. This semipermeable barrier consists of a phospholipid bilayer in which integral proteins are embedded. This bacterial membrane differs from that of eukaryotic cells in lacking cholesterol, although some bacteria may contains other compounds that probably have similar functions. The cytoplasmatic membrane holds the cell respiration and the synthesis of cell wall components. Hence, this structure is of paramount importance for the cell because of its fundamental metabolic and structural role. Therefore, the cytoplasmic membrane is the target of most biocides.[6,7]

1.1.2. Microbial growth control

In some cases, microbial growth can be eliminated using physical methods (heat, radiation or filtration). Decontamination of objects involves physical agents or specialized chemicals, namely disinfectants. These compounds are biocides that destroy micro-organisms but due to their toxicity, their application is restricted to house cleaning products. They are used against spoilage in a wide range of industrial applications (Table 1). It is also noticeable that the use of some chemicals as heavy metals and phenols produce environmentally hazardous waste products.

Table 1. Industrial uses of disinfectants (Source: Brock Biology of Microorganisms[5]).

Industry	Disinfectant	USE: Inhibition of bacterial growth
Metal	Cationic detergents	in aqueous cutting emulsions
Plastic	Cationic detergents	in aqueous dispersions of plastics
Petroleum	Cationic detergents, mercurics, phenols	during storage of petroleum products
Leather	Mercurics, phenols	in final products
Wood	Heavy metals, phenols	on wooden structures
Textile	Heavy metals, phenols	on fabrics exposed in the environmental
Paper	Heavy metals, phenols	during manufacture
Air conditioning	Chlorine, phenols	in cooling towers
Electrical power	Chlorine	in condensers and cooling towers
Nuclear	Chlorine	of radiation-resistant bacteria in nuclear reactors

Microbial control in living beings requires compounds with higher selectivity and lower toxic profile than that of disinfectants. Thus, antibiotics and antiseptics are the chemotherapeutic agents of choice. Antibiotics are used in the treatment of infections whereas antiseptics are used to wash or/and to disinfect external living tissues. Antiseptics are also extensively used in hospitals for a variety of topical and hard-surface applications.

As shown in Table 2, many antiseptics are cationic organic compounds which are present in many dermatological and pharmaceutical formulations.

Table 2. Common antiseptics and their applications (Source: Cosmetic and Drug Preservation.[8])

Antiseptics	Applications
Triclosan (2,4,4'-trichloro-2'-hydroxydiphenylether)	Use concentrations 0.1-0.3 % in deodorants, shampoos, soap, toothpaste. Also used as skin disinfectant.
Parabens (esters of *p*-hydroxy-benzoic acid)	Use concentrations 0.4 % for the single ester and 0.8 % for the mixture of esters. Also used as preservative for pharmaceuticals.
Hexetidine (5-amino-1,3-bis-(2-ethylhexyl)-5-methyl-hexahydropirimidine)	Oral disinfectant 0.1 % in mouthwashes, preservative with good fungistatic activity.
Chorhexidine (bis(*p*-chlorphenyl-diguanidino)hexane)	Use concentrations 0.1 % in toothpaste, deodorants, antiperspirants, preservative in eye drops, 0,02 % in topical and uterine antiseptic 0.1-1.0 % in powder and creams.
Polyhexamethylene biguanide hydrochloride	Use concentrations 0.1 % in cosmetic applications. Also used as disinfectant for technical products.
Alkyltrimethylammonium bromide	Additive of deodorants, also used as cationic detergent, antiseptic, disinfectant and preservative.
Benzalkonium chloride	Use concentrations 0.1 % in deodorants, 0.01-0.1 % in eyedrops, also in hair conditioner. Preoperative antiseptic for skin or for wounds.

One of the most representative antiseptic is chlorhexidine (CHX, see Figure 3). This bisbiguanide is widely used in oral products as anti-plaque agent, due to its broad spectrum efficacy against Gram-positive and Gram-negative bacteria and its low irritation.[9] Hence, CHX is present in many commercial formulations of toothpastes (~0.1 %), mouthrinse (~0.1-0.2 %), pills for low throat infections (~0.4 %) and topical disinfectant solutions (~1 %).

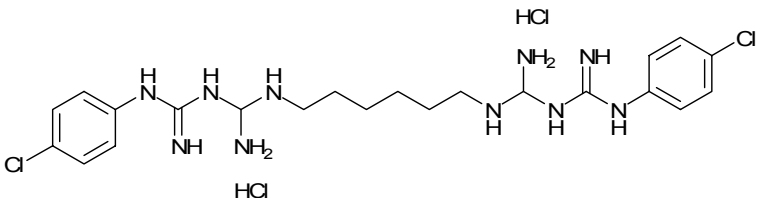

Fig. 3. Structure of chlorhexidine dihydrochloride (CHX).

A common feature of the cell envelopes of the Gram-positive and Gram-negative bacteria is the presence of large amounts of negative charged phospholipids. On the other hand, in human erythrocyte membranes the zwitterionic phospholipids occur predominantly in the membrane leaflet.[10] This appears to be one of the main reasons why cationic organic compounds show selectivity against bacteria.

Food preservatives

Biocides are also widely used for the preservation of products such as foods and beverages. These preservatives inhibit the microbial growth and they must be non-toxic by oral administration (Table 3). A small number of biocides are used as preservatives because of new food additives require lengthy and costly testing programs.

Table 3. Examples of common food preservatives. (Source: Brock biology of microorganisms[5] and www.textbookofbacteriology.net/control.html.)

Preservative	Foods
Sodium propionate (0.3 %)	Bread, cakes
Sorbic acid (0.2 %)	Citrus products, cheese, salads
Sulfur dioxide, sulfites (250 ppm)	Dried fruits and vegetables, wine
Formaldehyde	Meat, fish
Ethylene oxide	Spices, dried fruits
Sodium nitrite (200 ppm)	Cured meats, fish
Sodium chloride	Meat, fish
Sugar	Jams, syrups, jellies.
Sodium benzoate (0.1 %)	Carbonated beverages, fruit juices, margarine

Bacterial resistance to biocides

Bacterial resistance to biocides and in particular to antibiotics is hampering seriously the bacterial growth control. This resistance is

manifested by changes in the permeability of the cell envelopes, chemical modification of the antimicrobial agent, enzymatic degradation of antibiotics and the presence of membrane efflux systems which pump out the antimicrobial agents from the cytosol.[11-13] Acquired resistance to antimicrobial agents results from genetic changes in a cell and arises either by mutation or by the acquisition of genetic material (*e. g.* plasmids) from another cell.

Table 4. Possible mechanisms of plasmid-mediated biocide resistance (data from Russell[13]).

Mechanism	Example	Comment
Inactivation	Mercurials	Hydrolases and reductases
Inactivation	Chlorhexidine	Possible chromosomally-mediated mechanism
Inactivation	Formaldehyde	Formaldehyde dehydrogenase responsible
Decreased uptake	Silver nitrate	Inactivation unlikely
Decreased uptake	Chlorhexidine?	Unproven
Cell surface alterations	Formaldehyde	Outer membrane proteins appear to be involved
Efflux	Acridines	Multiresistant *S. aureus* strains
Efflux	Diamidines	
Efflux	QACs	
Efflux	Chlorhexidine	

Methicillin-resistant *S. aureus* (MRSA) strains are a problem in hospital infection because they often show multiple antibiotic resistance. Furthermore, increased resistance to some cationic agents (QACs, chlorhexidine, acridines and diamidines) is found in MRSA strains carrying genes encoding resistance to gentamicin, an aminoglycoside antibiotic.[13]

Bacterial resistance to biocides is also found in food industry, where the focus on hygiene has resulted in an increasing use of chemical disinfection. The resistant food-related staphylococci contains plasmids harbouring *qac* genes (*qacA*, *qacB*, *qacC*, *qacG* and *qacH*) which encode

membrane-embedded proteins by which staphylococci resist the bactericidal effect of QACs compounds through a drug efflux system.[14]

The problem of bacterial resistance to biocides is normally solved applying higher concentrations of the antimicrobial agent or treatment by a combination of unrelated agents. Consequently, an alternative against the bacterial resistance to biocides may be the design of novel products. The molecular diversity of biocides offers a multiplicity of potentially damaging effects on the bacterial cell. The precise knowledge and comprehension of the interactions between biocides and bacteria offers a powerful tool in the search for novel agents. Besides, the design of novel chemical structures can also tailor other important features as their toxicity and physico-chemical properties required for different formulations.

1.1.3. Mode of action of cationic biocides

In general, biocides have a broader spectrum of activity than antibiotics and, while antibiotics tend to have specific intracellular targets, biocides may have multiple targets. Table 5 shows some of the most common antiseptics and disinfectants with their targets and mechanisms of action.

General mechanism of action of cationic biocides

As mentioned previously, many antiseptics are cationic compounds such as cationic surfactants. In the following paragraphs, the general mechanism of action of this group of antimicrobial agents is described.

Initially, cationic biocides must cross the cell wall (*i.e.* external cell envelopes). Therefore, these compounds target the cytoplasmic membrane (*i.e.* inner cell envelope). The outermost surface of the cytoplasmic

membrane carries a net negative charge, often stabilized by the presence of divalent cations such as Mg^{2+} and Ca^{2+}.

Table 5. Summary of mechanisms of antibacterial action of antiseptics and disinfectants (data from McDonell *et al.*[9])

Chemical	Target	Mechanism of action
Chlorhexidine (biguanide)	Cytoplasmic membrane	Low conc.: cytoplasmic membrane damage integrity. High conc.: congealing of cytoplasm
Polymeric biguanides	Cytoplasmic membrane	Phase separation and domain formation of membrane lipids
QACs	Cytoplasmic membrane	Generalized cytoplasmic membrane damage involving phosphoplipid bilayer
Pentamidine (diamidine)	Cytoplasmic membrane	Induction of leakage of amino acids and inhibition of O_2 uptake
Phenols	Cytoplasmic membrane	Leakage of intracellular constituents
Silver compounds	Enzymes	Interaction with thiol groups of enzymes
Glutaraldehyde	Cell envelope	Cross-linking of proteins at cell envelope
Halogens	DNA Oxidizing agent	Inhibition of DNA synthesis Oxidation of thiol groups
H_2O_2	DNA Oxidizing agent	DNA strand breakage Radicals ($^{\cdot}OH$) oxidizes thiol groups of proteins

Cationic biocides display a high binding affinity for the cytoplasmic membrane. After that, the hydrophobic region of the agent penetrates into the hydrophobic core of the membrane (see Figure 4). This leads to a progressive leakage of cytoplasmatic materials to the environment, perturbing membrane-located physiologies such as respiration, solute transport and cell wall biosynthesis. These effects are sufficient to affect the cell growth (*i.e.* bacteriostatic effect) or even, to cause the cell die (*i.e.* bactericide effect). In fact, for many decades these compounds have been named "membrane-active agents".[6,9,15,16]

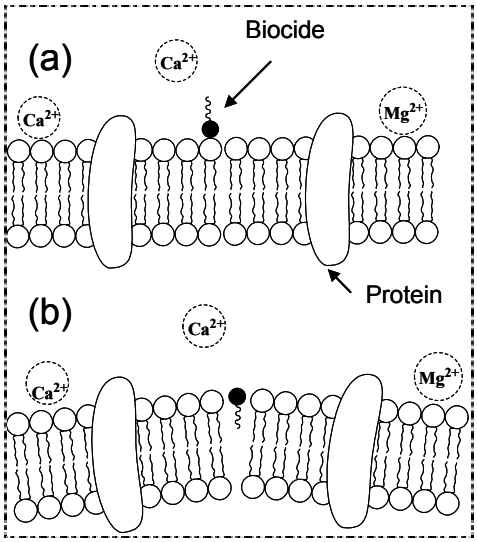

Fig. 4. Mechanism of action for cationic biocides: (a) adsorption of the head group of the biocide onto acidic phospholipids in the cytoplasmic membrane, (b) followed by insertion of the hydrophophic region of the biocide into the hydrophobic core.

Representative structures of cationic biocides are the quaternary ammonium compounds (QACs). Their antibacterial activity is approximately a parabolic function of their lipophilicity. Daoud *et al.*[17] found that alkyldimethylbenzylammonium chlorides with *n*-alkyl chain length of $n < 4$ and $n > 18$ were inactive while the optimal activity was achieved for compounds with chain lengths of n = 12-14 and n = 14-16 towards Gram-positive and Gram-negative bacteria, respectively.

Bisbiguanides antiseptics such as chlorhexidine have a very similar mechanism of action to that of QACs. However, a major difference is that the long alkyl chains of QACs become solubilised within the hydrophophic core of the cell membrane while the aromatic moieties of chlorhexidine do not.[15] Thus, the action of multi-drug efflux pumps is able to moderate the action of QACs but they only have low effect upon the action of bisbiguanides. Interestingly, the distance between phospholipid head-groups in a closely packed monolayer is roughly equivalent to the length of a hexamethylene chain, suggesting that chlorhexidine is capable of binding to two adjacent phospholipid headgroups.[15]

1.2. Amino acid-based surfactants: classification and structure

Biosurfactants are surface active molecules produced by living cells, such as micro-organisms and plants, and include glycolipids, polysaccharide lipid complexes, lipoamino acids, lipopeptides, polymeric surfactants composed of proteins, phospholipids and lipopolysaccharides. Biosurfactants have applications in medicine as antimicrobial agents and anti-adhesives and the use of liposomes made from biosurfactants constitutes an important strategy for gene transfection.[18,19]

Bio-based surfactants are synthetic amphipathic structures based on natural structures of biosurfactants. Among them, amino acid-based surfactants (or lipoamino acids) constitute an interesting class of speciality surfactants with excellent adsorption and aggregation properties, high biodegradability, low potential toxicity, low environmental impact and broad antimicrobial activity. Bio-based surfactants tend to make up a small percentage of dermatological and pharmaceutical formulations and thus, they are produced at a scale of few tonnes per annum with major applications in the areas such as health and personal care.[20]

Amino acid lipid conjugates are natural α-amino acids linked to long aliphatic chain groups through the –amino or -COOH (see Figure 5). Hence, the use of acidic, basic or neutral amino acids as starting material can furnish anionic, cationic or non-ionic surfactants, respectively.

Amino acid-based surfactants have been prepared in our group by means of chemical[21-23] and chemoenzymatic[24-26] methodologies. Long aliphatic chains and amino acids and can be combined to each other to generate four main structures (Figure 6) of amino acid-based surfactants namely single chain or linear **I**, dimeric or gemini **II**, glycerolipid-like structures **III** and bola-amphiphiles **IV**.

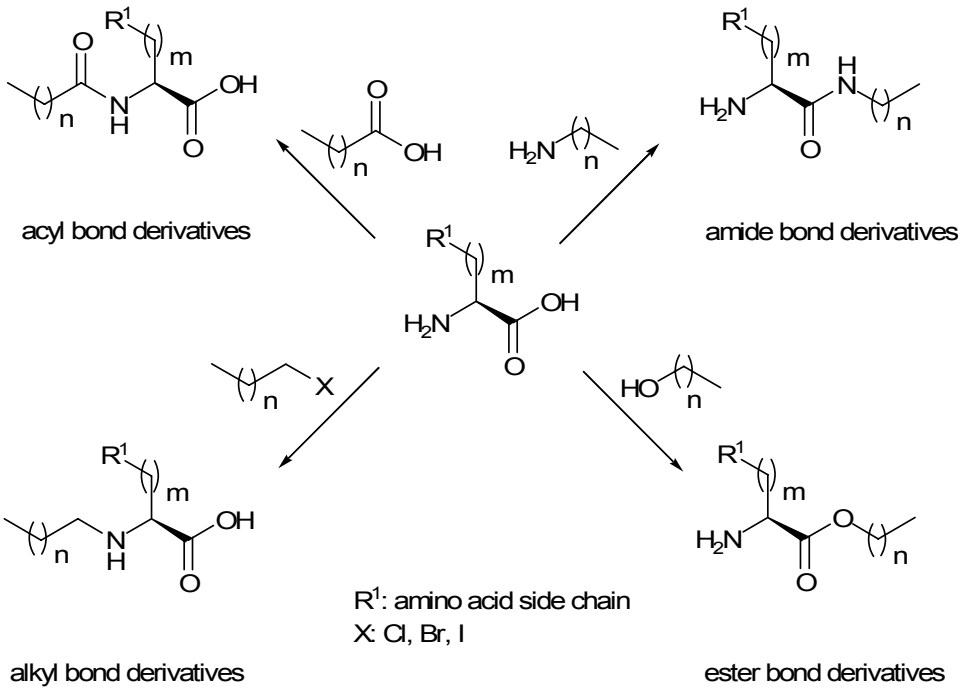

Fig. 5. Different types of linkages between an amino acid and an aliphatic chain.

Single chain structures consist of an amino acid bearing at least one hydrophobic tail. Gemini are amphipathic structures with two polar heads (*i.e.* two amino acids) and two hydrophobic tails per molecule. Glycerolipid-like structures can be considered analogues of mono-, diglycerides and phospholipids. They consist of one polar head and one or two hydrophobic moieties linked together through a glycerol skeleton. Bola-amphiphiles contain two polar heads connected at each extreme edge of an aliphatic hydrocarbon chain.

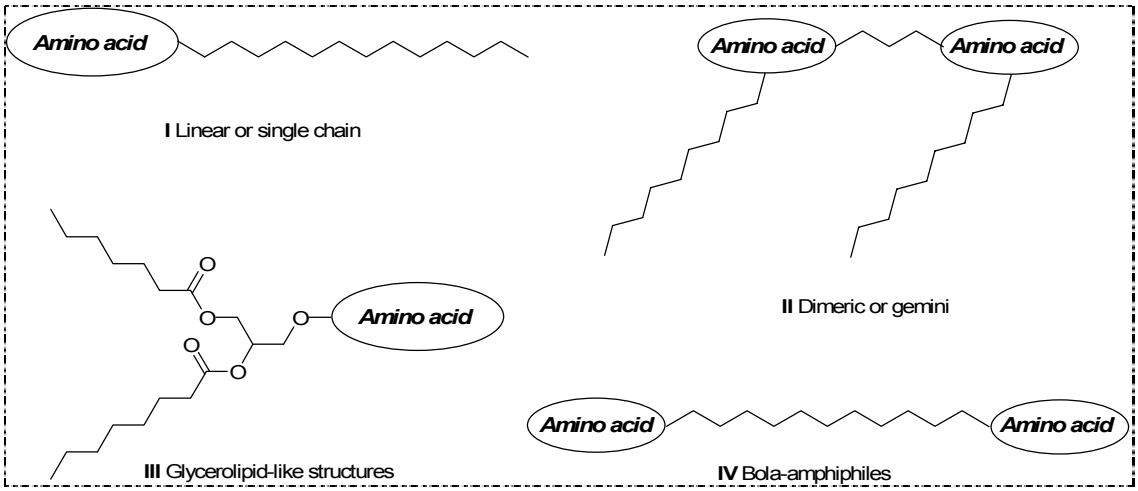

Fig. 6. Scheme of the four main structures of amino acid-based surfactants.

Among the different amino acid-based surfactants prepared in our research group, arginine-based surfactant have turned out to be an important class of cationic surface active compounds with antimicrobial activity against a broad spectrum of bacteria, biodegradability and low toxicity.[27,28] These features and the use of natural raw materials such as arginine and fatty acids for their synthesis, make them interesting candidates as preservatives and antiseptics in pharmaceutical, food and cosmetic formulations.

One example of amino acid-based surfactants as food preservative is Mirenat-N, a solution of lauric arginate. This is a novel antimicrobial compound derivative of lauric acid, L-arginine and ethanol, all naturally occurring substances. The molecule was first synthesized by the Department of Surfactant Technology, CSIC, in Barcelona in 1984, then patented and commercialized by the Vedeqsa Lamirsa Group. Its most notable features are a broad spectrum of antimicrobial efficacy; high partition coefficient (meaning the product concentrates in the water phase of products, where most bacterial action occurs); activity over a wide pH range (3 to 7); and safety. Mirenat-N is hydrolyzed in the human body and it has "generally recognized as safe" (GRAS) by the Food and Drug Administration. Thus, Mirenat-N is used as food preservative in deli meats and sausages, which are long worrisome potential sources of contamination. (Source: http://www.foodprocessing.com/articles/2005/454.html)

1.2.1. Arginine-based surfactants: preparation and properties

Synthesis of single chain arginine-based surfactants

Single chain arginine-based surfactants can be classified into three series (Figure 7): N^{α}-acyl-arginine, arginine-*N*-alkyl amide and arginine-*O*-alkyl-ester derivatives.

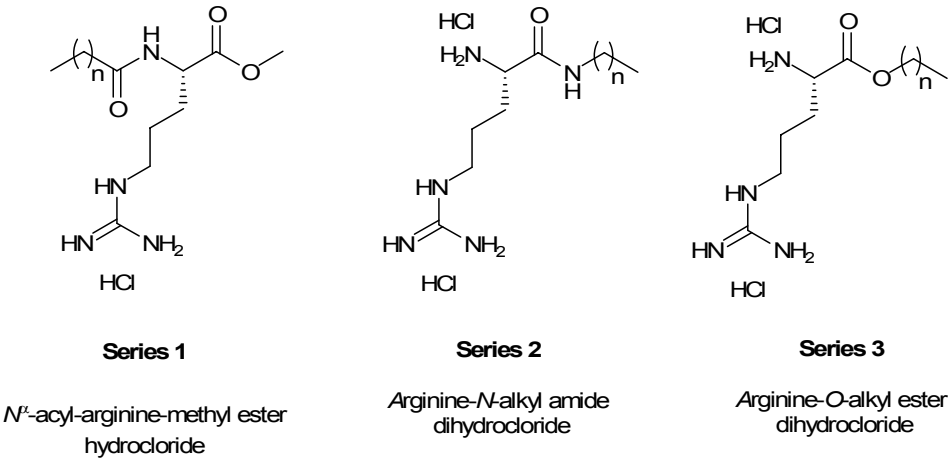

Fig. 7. Chemical structures of single chain arginine-based surfactants.

N^{α}-acyl-arginine derivatives (Figure 7, series 1) were prepared by condensation of fatty acids to arginine methyl ester using chemical methods widely used in peptide synthesis.[29] The enzymatic N^{α}-acylation of arginine has been found to be a difficult task for hydrolases and changes in the reaction medium or in the synthetic approach (*i.e.* thermodynamic or kinetic conditions) did not result in any improvement.[20]

Arginine *N*-alkyl amide derivatives (Figure 7, series 2) were firstly prepared by chemical procedures.[30] Later, papain from *Carica papaya* latex was found to be a suitable catalyst for the formation of amide bonds between *N*-Cbz-Arg-OMe and long chain alkyl amines (see Figure 8).[25]

Arginine-*O*-alkyl-ester derivatives (Figure 7, series 3) were prepared using *N*-Cbz-Arg-OMe and fatty alcohols as starting materials and papain as biocatalyst (Figure 8).[25] The transesterification reaction was carried out in solvent free systems using the same alcohol reagent[25] at elevated temperature (50°C for octanol and 65°C for dodecanol and papain from *Carica papaya* latex showed remarkable thermostability under these conditions).

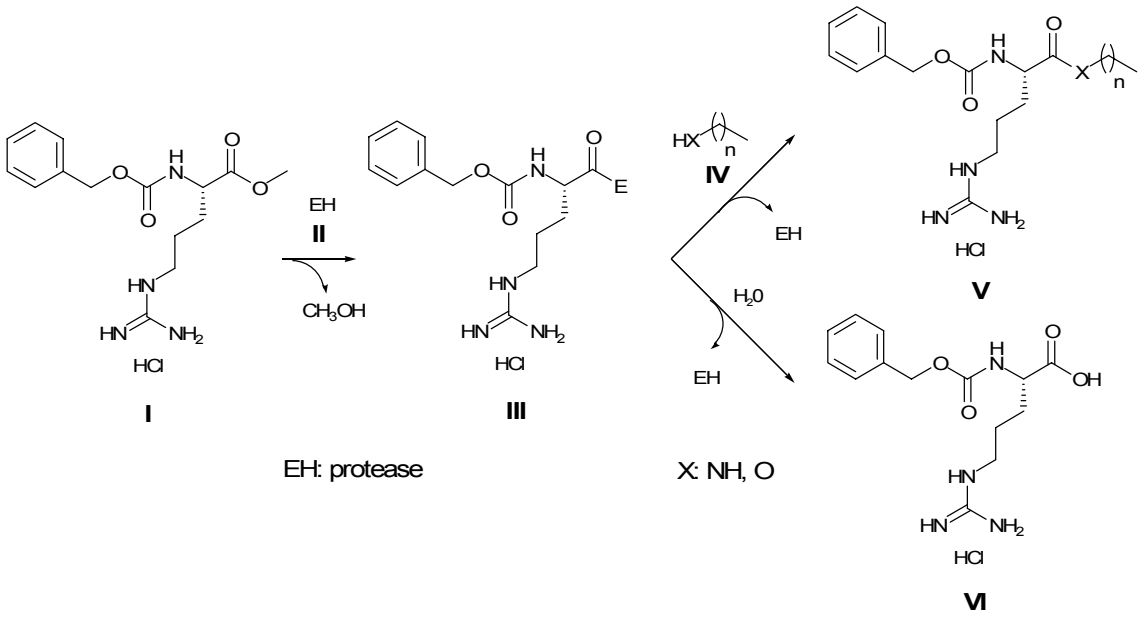

Fig. 8. Scheme of the reaction of *N*-Cbz-Arg-OMe (**I**) and fatty amine or alcohol catalyzed by papain: (**I**) acyl-donor, (**II**) protease, (**III**) acyl-enzyme, (**IV**) nucleophile, (**V**) *N*-Cbz-alkyl amide or ester and (**VI**) hydrolyzed substrate.

Synthesis of arginine-based gemini surfactants, bis(Args)

Arginine-based gemini surfactants (bis(Args)) have been prepared by both chemical[21] and chemoenzymatic methodologies. *Piera et al.*[26] have reported a chemoenzymatic synthesis of bis(Args) using the protease papain (Figure 9).

a) One-step synthesis:

Initially, the enzymatic synthesis of arginine-based gemini surfactants was planned as single pot reaction starting from 2 eq. of long chain N^{α}-acyl-arginine alkyl ester derivatives **I** and α,ω-diaminoalkane. This strategy afforded too low yields to preparative purposes.

b) Two-step synthesis:

First, the quantitative acylation of one amino group of the spacer by the carboxylic ester of the N^{α}-acyl-arginine alkyl ester **I** took place spontaneously at the melting point of the α,ω-diaminoalkane in a solvent free system. The second step was the papain-catalyzed reaction between

another N^{α}-acyl alkyl ester **I** and the free aliphatic amino group of the derivative formed in the first step (**II**). This strategy allowed the preparation of bis(Args) at gram scale.

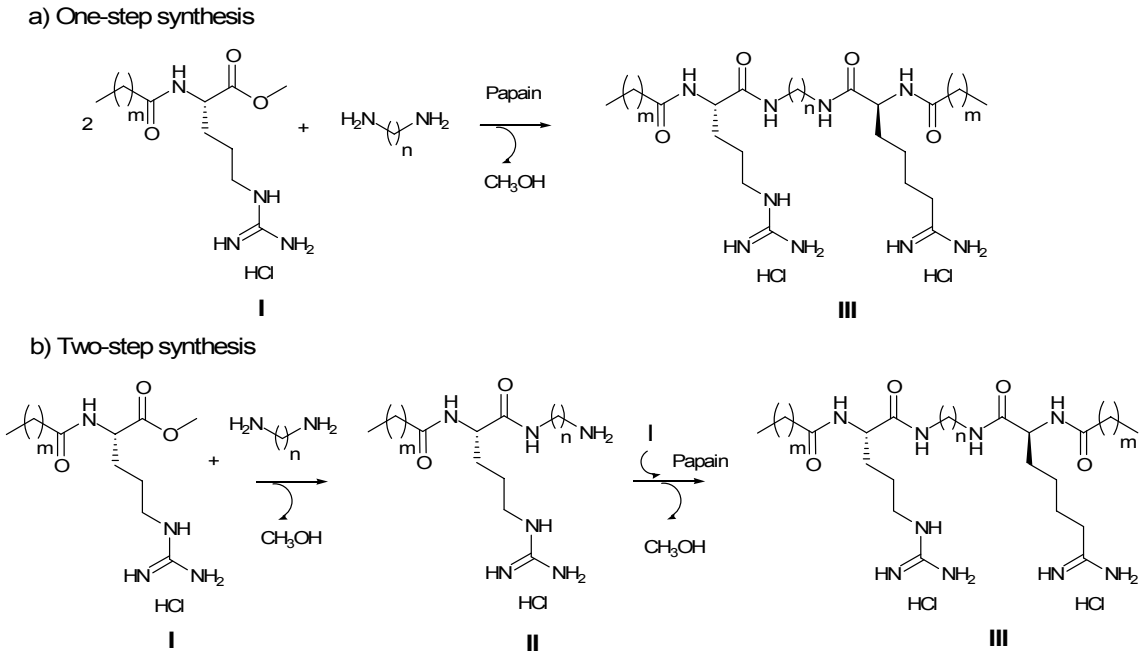

Fig. 9. Chemoenzymatic strategies for the synthesis of arginine-based gemini surfactants: (**I**) N^{α}-acyl-L-arginine methyl ester hydrochloride, (**II**) N^{α}-acyl-L-arginine(ω-aminoalkyl)amide hydrochloride, (**III**) bis(N^{α}-acyl-L-arginine)-α,ω-alkanediamide dihydrochloride.

Synthesis of arginine glyceride conjugates

As shown in Figure 10, arginine glyceride conjugates have been prepared in our group by chemical methods or using hydrolases such as, proteases and lipases.[24] The first step consisted of the selective protease-catalysed esterification of one the primary hydroxyl groups of the glycerol with the carboxylic group of the *N*-protected amino acid.

The second step was the acylation of the free hydroxyl groups of the glyceryl moiety with fatty acid using lipases as catalyst. Novozyme and Lipozyme can be successfully used as biocatalyst showing a high

regioselectivity towards the primary hydroxyl group of the amino acid glyceryl ester derivative.

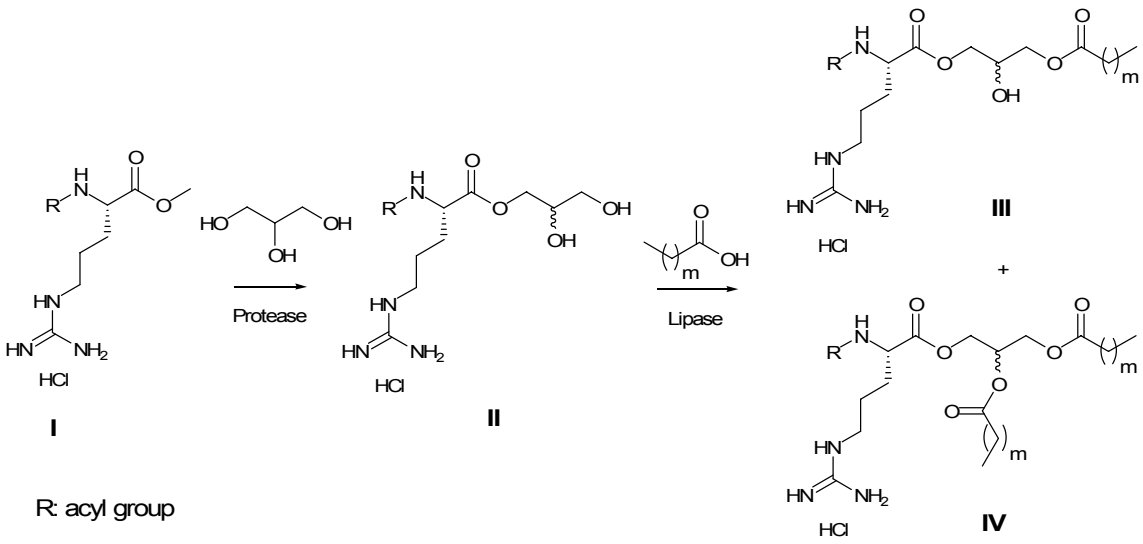

Fig. 10. Chemoenzymatic strategy for the synthesis of arginine glycerolipid conjugates: (**I**) N^{α}-acyl-L-arginine methyl ester hydrochloride, (**II**) 1-*O*-(N^{α}-acyl-L-arginyl)-*rac*-glycerol hydrochloride, (**III**) 1-acyl-3-*O*-(N^{α}-acyl-L-arginyl)-*rac*-glycerol hydrochloride and (**IV**) 1,2-diacyl-3-*O*-(N^{α}-acyl-L-arginyl)-*rac*-glycerol hydrochloride.

Synthesis of arginine-based bola-amphiphiles

To the best of our knowledge there are not reports about the preparation of arginine-based bola-amphiphiles. In this thesis, novel bis(phenylacetylarginine) derivatives with bola-amphiphile like structure have been prepared by a chemoenzymatic methodology in order to investigate their antimicrobial activity.

Interestingly, Pavlíková *et al.*[31] have reported QSAR studies between structure, aggregation properties and antimicrobial activity of quaternary ammonium bola-amphiphiles. They concluded that the lipophilicity contribution of the extending spacer chain to the hydrophilic lipophilic balance (HLB) of the molecules plays a key role in the antimicrobial activity.

Physico-chemical and biological properties of arginine-based surfactants

Critical micellar concentration (CMC):

Surfactants, when present at low concentrations in solution, are adsorbed onto surfaces or interfaces in an oriented fashion with a consequent decrease in the surface tension of the solvent system. In the bulk of the solution, they form aggregates of various sizes and shapes (spheres, ellipsoids or cylinders), commonly known as micelles. Aggregation occurs at a critical concentration, called critical micellar concentration (CMC)

Single chain arginine-based surfactants have CMC values *ca* 1-10 mM and these values decrease linearly as the number of the methylene groups in the alkyl chain increases.[27] Gemini arginine-based surfactants, bis(Args), show CMC values 2-3 orders of magnitude lower than the corresponding single chain surfactants. As expected, the CMC decreases when the number of methylene groups in the spacer chain increases.[21,32,33] Therefore, gemini surfactants can produce lower surface tensions than single chain surfactants at the same concentration. Diacylglycerol arginine-based surfactants show CMC in the range of 5-0.25 mM. Comparing these values with those of natural phospholipids such as lecithins with the same alkyl chain length, the CMC of the new compounds are one order of magnitude higher due to the better solubility properties of their hydrophilic head group.[22]

Antimicrobial activity:

Arginine-based surfactants show antimicrobial activity against broad spectrum of bacteria. Essential structural factors for their antimicrobial activity include both the length of the fatty residue and the presence of the protonated guanidine function. Interestingly, dimerization enhanced the antimicrobial activity for the gemini surfactants compared with single chain surfactants.[34] In general, the correlation between the alkyl chain length and the antimicrobial activity was not linear. Among the arginine-based

surfactants synthesised in our group, bis(N^{α}-caproyl-L-arginine)-1,3-propanediamide dihydrochloride, $C_3(CA)_2$ (Figure 11), showed the most potent antimicrobial activity against both Gram-positive and Gram-negative bacteria.[34,35]

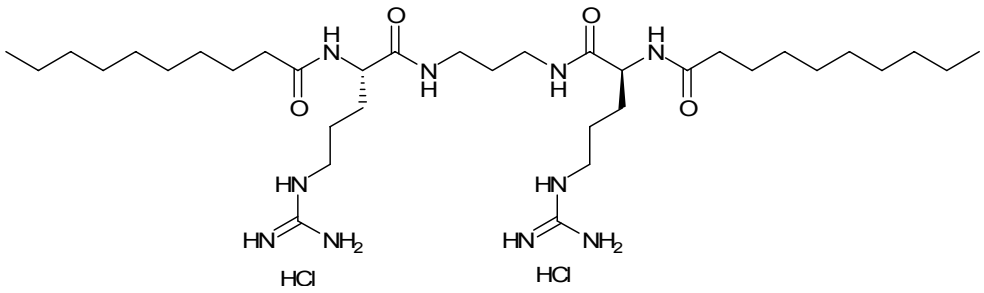

Fig. 11. Structure of $C_3(CA)_2$.

Diacylglycerol arginine-based surfactants also possess antimicrobial activity. The maximum activity corresponds to the compound with six methylene groups in the alkyl chain and their activity decreases with increasing alkyl chain length.[22]

Toxicity:

Single chain arginine-based surfactants showed low haemolytic activity and they can be considered non-haemolysing agents. Besides, according to their haemolytic activity and the *in vivo* eye irritation Draize test, these linear surfactants are classified as non irritant to eyes.[27] Bis(Args) were classified as non irritant or moderate irritant, depending on their hydrophobicity.[36] The potential ocular irritation also indicates that diacylglycerol arginine-based surfactants are moderate irritants such as betaine, in contrast to other commercially available surfactants such as SDS, benzalkonium chloride, cetyltrimethylammonium bromide.[22]

Biodegradability :

Furthermore, single chain arginine-based surfactants can be considered biodegradable.[27] However, bis(Args) showed lower

biodegradation rate than that of the single-chain arginine-based surfactants due to their higher hydrophobicity.[34]

In general, arginine-based surfactants constitute an interesting alternative to quaternary ammonium compounds, (QACs) because the last ones have a poor chemical and biological degradability due to their chemical stability and therefore, they constitute a risk of toxicity to aquatic organisms.

1.3. Iminocyclitols

During the last years our group has also focused its attention in the chemoenzymatic preparation of iminocyclitols as potential inhibitors of glycosidases and glycosyltransferases. It has been reported that these compounds and their alkyl derivatives possess antimicrobial activity.[37-39] However, to date very few studies have assessed their antimicrobial activity. In the frame of this work, novel *N*-alkylated iminocyclitol derivatives have been prepared to investigate their possible antimicrobial activity.

1.3.1. Structure and biological activity of iminocyclitols

Iminocyclitols, also called iminosugars or azasugars, are naturally occurring polyhydroxylated alkaloids. These compounds mimic the structures of sugars in which the ring oxygen is replaced by nitrogen. Iminocyclitols are classified into different structures. Among them, the most common are polydroxylated pyrrolidines, piperidines, pyrrolizidines and indolizidines (Figure 12).

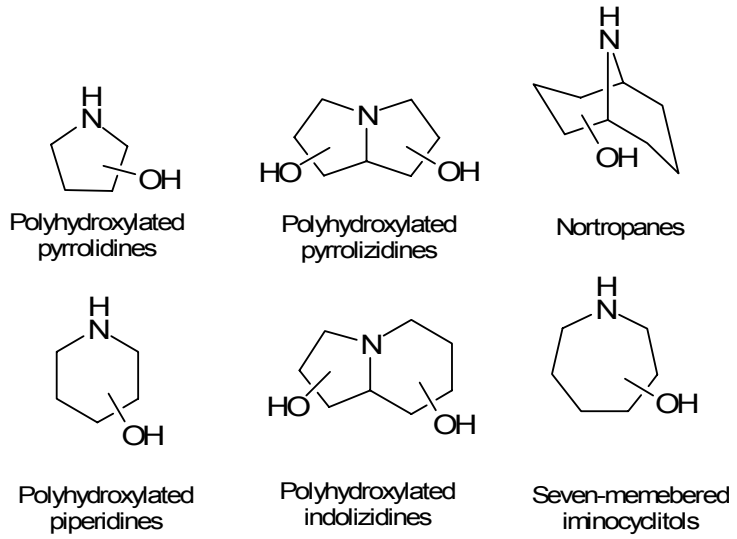

Fig. 12 Basic scaffolds of iminocyclitols.

Polyhydroxylated compounds such as oligosaccharides, complex carbohydrates and their lipid and protein conjugates, are molecules of paramount importance in biochemical recognition processes such as cellular adhesion, viral infections, cellular differentiation, metastasis and numerous signal transduction events.[40] As a consequence, the enzymes involved in their synthesis or degradation namely glycosyltransferases and glycosidases, respectively, are targets for inhibition or activation[41] as they are involved in metabolic alterations and diseases such as type diabetes Mellitus, hepatitis B and C, glycosphingolipid storage disorders (such as Gaucher disease), cystic fibrosis, colon-rectal cancer or viral infections.[42-46]

Some iminocyclitols have found to be potent inhibitors of glycosidades and glycosyltransferases. It has been suggested that they bind specifically to the active site of these enzymes mimicking the corresponding natural substrate.[47] From the mechanistic point of view, protonated iminocyclitols may mimic the oxonium ion transition state of sugar transfer reactions in both glycosidases and glycosyltransferases.[48,49] Therefore, these compounds are potential drugs for the treatment of a wide range of diseases.

Nojirimycin (Figure 13) was discovered in 1966 as the first natural glucose mimic. It was shown to be a potent inhibitor of α- and

ß-glucosidases from various sources. Since then, over 100 glycosidase inhibitors have been isolated from plants and micro-organisms. Some examples are *N*-butildeoxynojirimycin (a glucosidases' inhibitor)[50,51], swainsonine (a Golgi α-mannosidase II inhibitor)[52,53], and isofagomine (a glycogen phosphorylase and ß-glucosidase inhibitor)[54,55] which are promising anti-HIV, anticancer and antidiabetic chemotherapeutic agents, respectively (see structures in Figure 13).

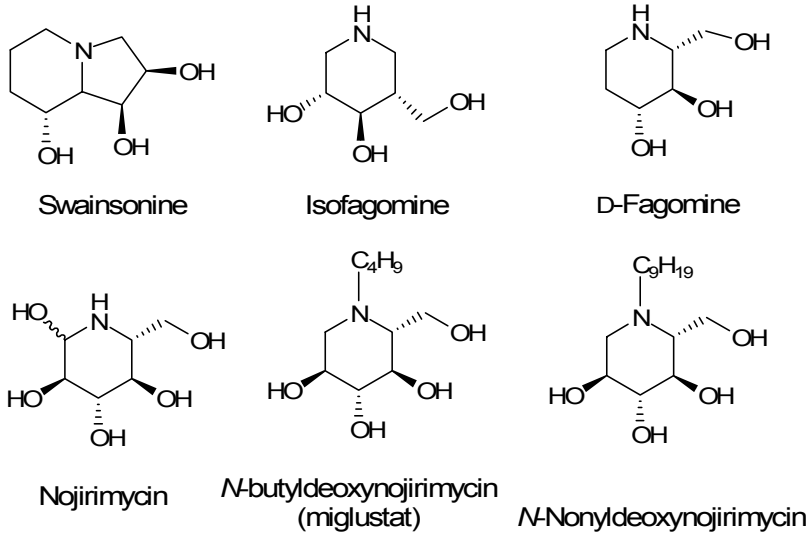

Fig. 13 Structure of some iminocyclitols.

The interest in the iminocyclitols has recently increased due to their potential application in a new concept in drug research for the treatment of metabolic disorders. These disorders are provoked by small changes in the amino acid sequence of the enzyme, due to mutations on the gene encoding the protein, which leads to an incorrect three-dimensional structure of the enzyme and therefore its loss of functionally. The new strategy consists of increasing the fraction of the correctly folded variant protein encoded by specific chemical chaperones (*i.e.* small molecules whose function is to assist a protein to properly fold and enter normal processing pathway). Recently, Sawkar *et al.*[56] have reported that *N*-nonyldeoxynojirimycin (Figure 13) increased two-fold the activity of N307S ß-glucosidase, indicating that this iminocyclitol may be clinically useful against the Gaucher disease. It is also

remarkable that treatment with miglustat (Figure 13) improves key clinical features of type I Gaucher disease after 1 year of treatment.[57]

Among the iminocyclitols, D-fagomine (Figure 13) has attracted our attention due to their properties and relative simple structure. D-fagomine is a polyhydroxylated piperidine which was firstly isolated from buckwheat seeds (*Fagopyrum esculentum* Moench)[58] and later from *Castanospermum australe*[59], dry *Xanthocercis zambesiaca* leave[60] and *Morus bombycis* leaves.[61] It has been reported that D-fagomine has activity against mammalian gut α-glucosidase and ß-galactosidase.[60] More recently, Nojima *et al.*[62] have reported that D-fagomine produced an antihyperglycemic effect on streptozotocin-diabetic mice and promotes glucose-induced insulin secretion. Moreover, Iqbal *et al.*[63] have assessed its allelopathic potential and their results suggest that this iminosugar affects the growth or germination of different plant species.

The antimicrobial activity of D-fagomine has not been reported previously, although it has been shown that similar iminocyclitols inhibit the bacterial growth. Segraves *et al.*[37] have isolated *C*-alkylated 3,4-di-*epi*-fagomines from a *Batzella* sp. sponge. These azasugars were tested against *Staphylococcus epidermidis* and they showed high antimicrobial action. Maddry *et al.*[38] have reported the preparation of *C*-alkylated polyhydroxylated pyrrolidone as aza analogs of arabinose. These iminosugars showed moderated antimicrobial activity over *Mycobacterium tubercolisis,* depending on the alkyl chain length. The mechanism of action is unclear but these results suggest that they could be inhibitors of cell wall biogenesis, in particular, of arabinotransferases.

1.3.2. Chemoenzymatic synthesis of iminocyclitols

Chemical synthetic approaches of iminocyclitols and its derivatives involve cumbersome protection-deprotection reactions, quiral

starting materials and moderate global yields are achieved.[64-66] As example, recent syntheses of D-fagomine and other stereoisomers have been described starting from quiral D-serine-derived Garner aldehyde in 6-7 steps with global yields around 12 %.[67,68]

In contrast, chemoenzymatic approaches afford effective and selective synthetic methodologies for the preparation of iminocyclitols from simple and achiral starting materials. Enzymatic reactions, being mild and selective, produce fewer impurities than other methods, thus facilitating the product purification and improving global yields. This is very attractive when dealing with multifunctional molecules, because cumbersome protection-deprotection strategies can be circumvented. Moreover, the presence of hazardous by-products, formed under strong chemical conditions, and potentially toxic starting materials in the product formulations is avoided. Many of these approaches to obtain iminocyclitols are based on the use of dihydroxyacetone phosphate (DHAP) dependent aldolases which catalyze the aldol additions between DHAP and aldehydes with fine control of the absolute configuration of the newly formed stereogenic centres.

DHAP-aldolases tolerate a broad range of aldehydes but they are highly specific for their donor substrate. The aldolization generates two quiral centres and consequently, four possible diasteromeric products can be generated. Nature has evolved four stereochemically complementary DHAP-aldolases (Figure 14) which allow the formation of all four possible diasteromeric adducts. The aldol addition proceeds with complete stereospecificity with respect to the configuration on carbon 3 and in some instances, with slightly decreased specificity on carbon 4.[69]

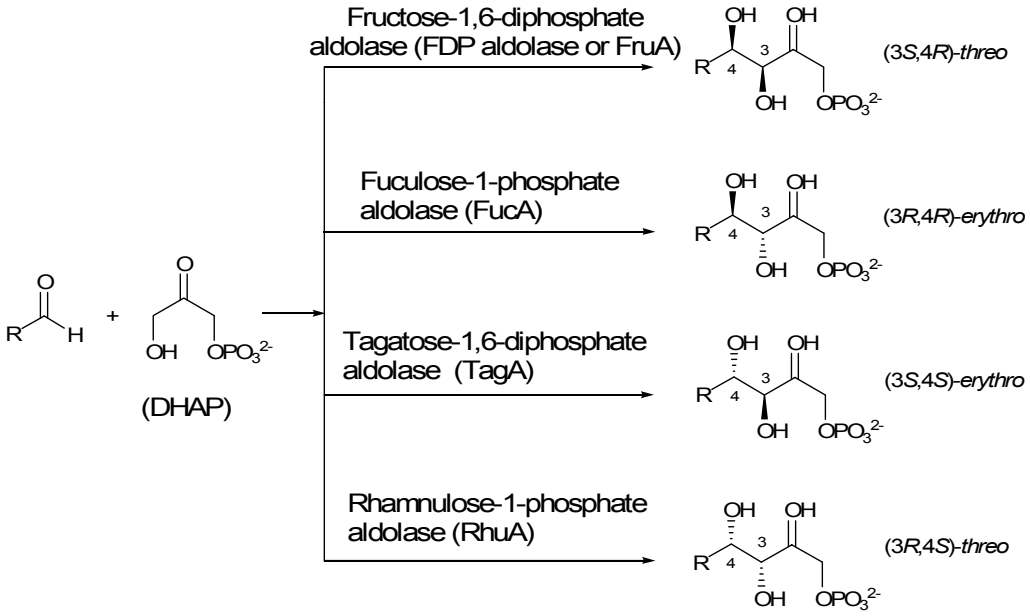

Fig. 14. Complementary stereochemistry of DHAP- aldolases.

The chemoenzymatic preparation of iminocyclitols has been reported using azide aldehydes and *N*-Cbz-amino aldehydes as starting materials (Figure 15). In our group many iminocyclitols have been successfully synthesised from *N*-Cbz-amino aldehydes using DHAP-dependent aldolase as biocatalysts.[70,71]

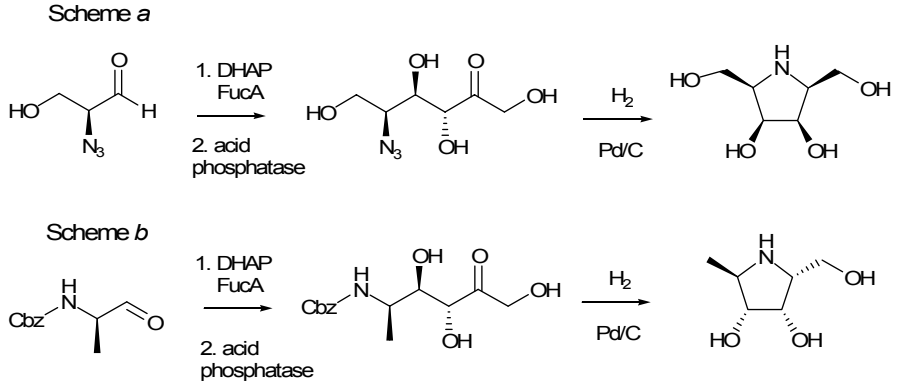

Fig. 15. Examples of synthesis of polyhydroxylated pyrrolidines using azide aldehydes (Wang *et al.*[72]) and *N*-Cbz-amino aldehydes (Espelt *et al.*[71]) as starting materials and Fuculose-1-phosphate aldolase (FruA) as biocatalyst.

One of the drawbacks of these approaches is the preparation and availability of the reagent DHAP. Jung *et al.* reported the chemical synthesis of DHAP involving 6 steps in 60% overall yield.[73] Recently, a methodology has been reported for synthesizing DHAP in three steps with

an overall yield of 74 %.[74] Alternatively, enzymatic methods to generate DHAP, which can be coupled with the aldol reaction, have also been described.[75-78] However, some limitations arising from the lack of compatibility of conditions between the coupled enzymatic reactions and the product separation and purification have been observed.[79]

Another approach is to use a mixture of DHA and a small amount of inorganic arsenate to replace DHAP. DHA reacts in solution with inorganic arsenate spontaneously to form dihydroxyacetone arsenate, which mimics DHAP and is accepted by fructose-1,6-diphosphate aldolase (FDP aldolase).[80] However the toxicity of arsenate, complications during the purification of the aldol adduct and low yields limit the attractiveness of this method.

Fructose-6-phosphate aldolase (FSA): an alternative to fructose-1,6-diphosphate aldolase (FDP aldolase)

A promising alternative to FDP aldolase is the novel fructose-6-phosphate aldolase (FSA). This recombinant enzyme was firstly cloned, overexpressed in *E. coli*, purified and characterized by Schürmann *et al*.[81,82] It as been reported that FSA catalyses the cleavage and formation of fructose 6-phosphate (Figure 16).[81] Consequently, the most striking advantage of FSA is that it uses the inexpensive and readily available dihydroxyacetone (DHA) as nucleophile. However, to date the synthetic applications of this novel enzyme have not been investigated yet. Recently, Schürmann *et al*.[83] have reported the possible aldol addition of DHA onto small aldehydes catalyzed by FSA although chemical data as yields and stereoselective were not assessed. In the present work, FSA has been employed to prepare D-fagomine and some of its *N*-alkylated derivatives.

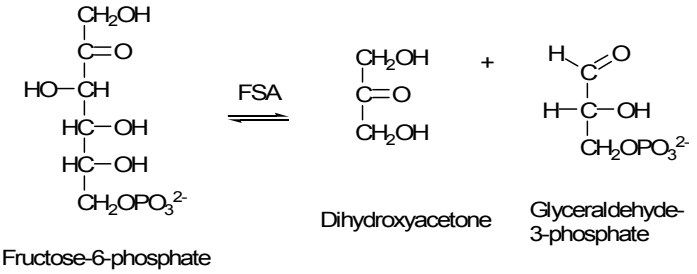

Fig. 16 Cleavage or formation of fructose 6-phosphate catalysed by FSA.

1.4. Techniques employed to study the interaction of biocides with membrane models

The perturbation of lipid membranes by membrane-active agents such as amphiphilic compounds is governed mainly by physico-chemical processes. Hence, the study of the interaction of cationic biocides with membrane models can provide valuable information for understanding the mechanism of action of these molecules. The ultimate goal of theses studies is to provide the basis for a rational design of new and improved antimicrobial agents based on the physico-chemical properties of the molecule.

Liposomes are vesicles constituted by phospholipid bilayers and constitute a simple biomembrane model (Figure 17). Multilamellar vesicles (MLV) are formed when thin lipid films are dispersed in excess water by vigorous mixing. They form structures composed by a large number of concentric bilayers, which are separated by a water layer. The vesicles can be downsized by a variety of techniques. Small unilamellar vesicles (SUV, mean diameter 15-50 nm) can be obtained by sonication and large unilamellar vesicles (LUV, mean diameter 120-140 nm) by extrusion.

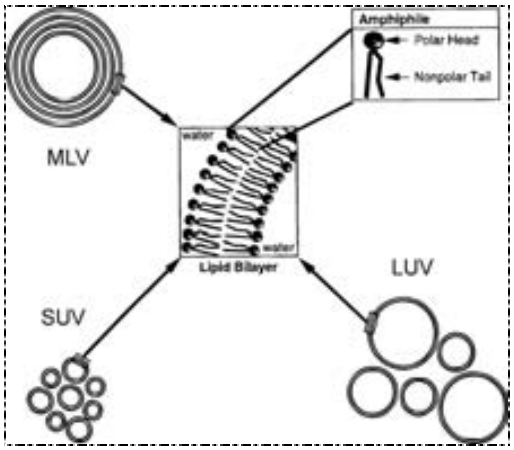

Fig. 17. Scheme of the different liposome structures.

Lipid multilamellar vesicles are suitable membrane models for studying interactions of biologically active molecules with lipid membranes Consequently, liposomes have been widely used to investigate the interaction of phospholipids with antimicrobial agents which act on the plasma membrane structure. However, they suffer from several limitations. For instance, the range over which the lipidic composition can be varied without modifying the surface curvature and phase state is limited. Besides, the degree of lipid packing is not uniform along the bilayer[84,85] and the physical state of compositionally identical bilayer dispersions depends on the method of preparation.[85] Moreover, some lipids may not form stable multilamellar vesicles suitable for DSC studies. Lipid monolayers can overcome these limitations being considered as an excellent model system to study the interactions of active compounds with different lipid compositions at the air/water interface.

Many natural antimicrobial peptides as gramadicin A, melittin, magainin and defensin A have a small molecular weight and cationic charges (*i.e.* they possess basic amino acids). Their amphipathic character makes them surface-active products. The killing event for bacteria is the permeabilization of the cytoplasmic membrane, generally induced by the formation of channels. For this reason, the monolayer technique is suitable

for studying their physico-chemical and biological properties as well as their interaction with lipid monolayers.[84]

1.4.1. Differential scanning calorimetry (DSC)

DSC is a technique for measuring the energy necessary to establish a nearly zero temperature difference between a substance and inert reference material, as the two specimens are subjected to identical temperature regimes in an environmental heated or cooled at a controlled rate. This calorimetric technique has been applied extensively to the study of thermal behaviour of lipids in biological membranes. 1,2-dipalmitoylphosphatidyl-choline (DPPC) is a zwitterionic phospholipid widely used to prepare lipid vesicles (Figure 18).

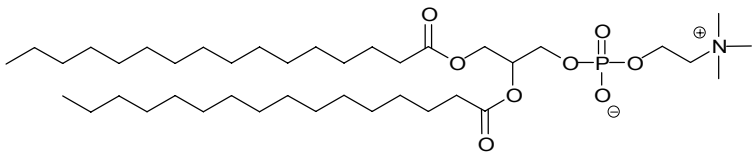

Fig. 18. Structure of 1,2-dipalmitoylphosphatidylcholine (DPPC).

Analysis of multilamellar vesicles (MLVs) of lipids with bulky polar heads (*e.g.* DPPC) by DSC is characterized by two-phase transitions (Figure 19). First, a pretransition around 35 °C related with the alkyl chain tilt and second, the main transition around 41 °C between an ordered gel state ($L_{\beta'}$ phase) and a disordered liquid-crystalline state (L_{α} phase).[86-88]

The study of the main thermotropic phase transition of MLVs by DSC represents a simple and precise method to investigate the influence of bioactive products on lipid membranes. The structural change associated with this transition is the *trans-gauche* isomerization of the acyl-chains of the lipid molecules. The average number of *gauche* conformers is related to the bilayer fluidity.[86] The presence of compounds susceptible of interacting with the phospholipid molecules may cause perturbations, which can

contribute to disturb the fluidity of the membrane. Two parameters related with the phase transition were studied: the phase transition temperature (T_m) and the width at half-height of the heat absorption peak ($\Delta T_{1/2}$).

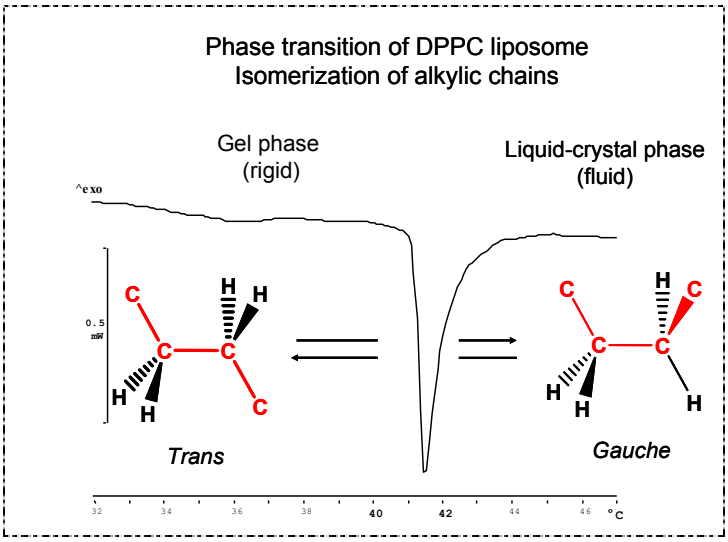

Fig. 19. DSC curve corresponding to the phase transition of DPPC multilamellar vesicles.

The phase transition temperature (T_m, also called lipid chain melting temperature) is defined as the temperature at which the substance undergoing the transition is half converted). T_m is characteristic for each lipid and it depends on the fatty acid chain length, the degree of unsaturation, and the polar head group structure. The effect of additives distributed inside the phospholipid bilayers may induce a decrease of T_m, indicating that the additive is interacting with polar heads of the phospholipid molecules.

Liposomes are characterized by a reversible transition over a narrow temperature range, from 0.2 to 1.0°C, for pure lipid suspensions. The sharpness of the phase transition is often expressed as the temperature width at half-height of the absorption peak, $\Delta T_{1/2}$. The transition width, $\Delta T_{1/2}$, is a measure of the cooperativity of the phase transition, *i.e.* the number of phospholipids undergoing a simultaneous *trans-gauche* transition.[86] The widening of the transition width induced by additives may be interpreted as the additive molecules incorporated in the membrane

tending to disrupt the interaction between lipid molecules, responsible for the cooperativity.[89]

1.4.2. Fluorescence spectroscopy: ANTS/DPX leakage assay

Leakage of encapsulated material in large unilamellar vesicles (LUV) can be assessed using the fluorescence spectroscopy. Consequently, this technique also allows studying the interaction of biocides with phospholipid membranes.

The encapsulated material are the fluorochrome 8-aminonaphtalene-1,3,6-trisulfonic acid (ANTS) and its quencher *N,N'-p*-xylenebis(pyridinium) bromide (DPX). Thus, the dequenching of co-encapsulated ANTS and DPX resulting from the dilution is monitored on a spectrofluorometer, with the maximum of fluorescence intensity corresponding to 100 % leakage. Hence, this assay allows measuring the increase of the fluidity of DPPC-LUVs caused by solutes at different molar fraction (Figure 20).

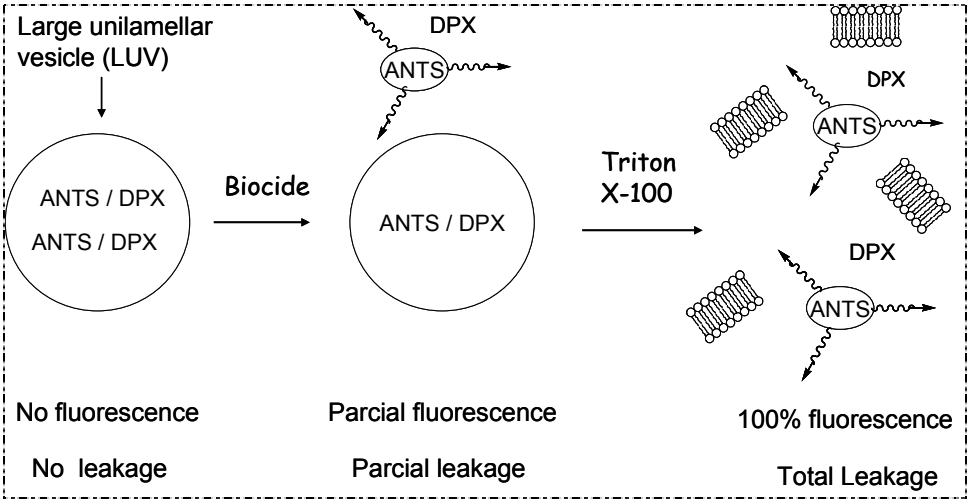

Fig. 20. Scheme of the ANTS/DPX leakage assay measured by the fluorescence emitted by the fluorochrome ANTS.

1.4.3. Langmuir film balance

The interaction of solutes with phospholipid monolayers can be studied using a Langmuir film balance. This instrument enables to control the molecular density (area) of a floating monolayer at the air/water interface, while simultaneously measure the surface pressure.

The interaction of membrane-active agents with phospholipid monolayers can be studied using a Langmuir film balance. Depending on the charge of the polar head, they can be zwitterionic (*e.g.* DPPC) or anionic phospholipids (*e.g.* 1,2-dipalmitoyl-*sn*-glycero-3-[phospho-*rac*-(1-glycerol)] sodium salt (DPPG, Figure 21). These lipids can be also a mixture of phospholipids such as a total lipid extract from *Escherichia coli*. The last one was employed in the present work because it is a more complex biomembrane model than that formed by pure lipids.

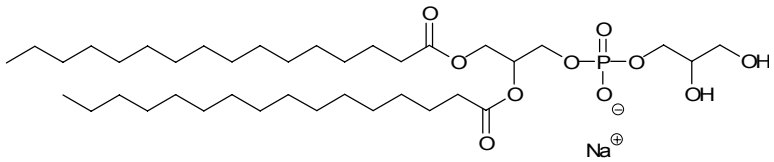

Fig. 21. Structure of 1,2-dipalmitoyl-*sn*-glycero-3-[phospho-*rac*-(1-glycerol)] sodium salt DPPG, an anionic lipid.

Two different experiments can be performed: kinetic penetration at constant area and compression isotherms. These techniques allow assessing the ability of the compounds to insert into the monolayer.

Kinetic penetration at constant area

This experiment consists of spreading a phospholipid monolayer on the air-liquid interface of a Teflon trough (Figure 22). The surface area is constant, achieving an initial surface pressure. Then, different volumes of a concentrated compound solution are injected in the buffered subphase solution and the increase in surface pressure is measured by a Wilhelmy

plate connected to the Langmuir film balance. Consequently, the term "monolayer penetration" is used to describe the interaction of an insoluble monolayer spread at the air/water interface with a soluble active compound in the aqueous phase. This interaction can be measured maintaining the film area constant and to measuring the surface pressure changes on adding the penetrating compound in the subphase. The parameters that must be taken into account are:

a) the initial pressure of the lipid film (π_0): it reflects the packing of the lipids in the monolayer at the air/water interface with a soluble active compound in the aqueous phase. However, in order to compare the solute penetration in various lipid monolayers, it is better to choose the lipid density as the lipid packing parameter.

b) the concentration of the solute in the subphase.

c) the exclusion density (σ_{ex}), that is the lipid density at which the solute no longer penetrates.

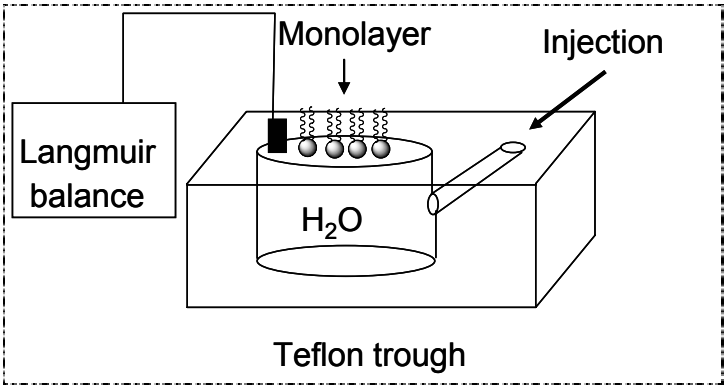

Fig. 22. System employed to perform the kinetics penetration at constant area.

Compression isotherms

This experiment consists of spreading a phospholipid monolayer on the aqueous subphase. Then, the monolayer is compressed with a barrier and the increase of surface pressure and the mean molecular area

(molecular density) are continuously monitored measured during the compression using the Langmuir film balance. Pure phospholipid monolayer shows characteristic compression isotherms and deviations from this isotherm can be observed when solutes are present in the subphase. These effects allow gaining insight into the interaction lipid-solute.

Initially, phospholipid monolayers are spread at the air-water interface and their molecules are expanded, resembling a gaseous state (see Figure 23). In course of the film compression, there is a change in the molecular packing. The compression rate must be slow enough to ensure that changes occur under thermodynamic equilibrium conditions. Thus, the compression isotherm involves different orientation of the lipid molecules:
a) liquid-expanded films (L-E films are very compressible).
b) liquid-condensed films (L-C films, molecules begin to be close-packed).
c) solid film, characterized by a low compressibility.
On further compression the film collapses in a three-dimensial state at the collapse pressure (π_c).

Figure 23 shows the compression isotherm profile of DPPC. This profile shows the phase transition from liquid-expanded (L-E) to liquid-condensed (L-C) phases at 7 mN m^{-1} and 90 $Å^2$ mol^{-1} and the collapse pressure at 60 mN m^{-1} and 30 $Å^2$ mol^{-1} of molecular area.

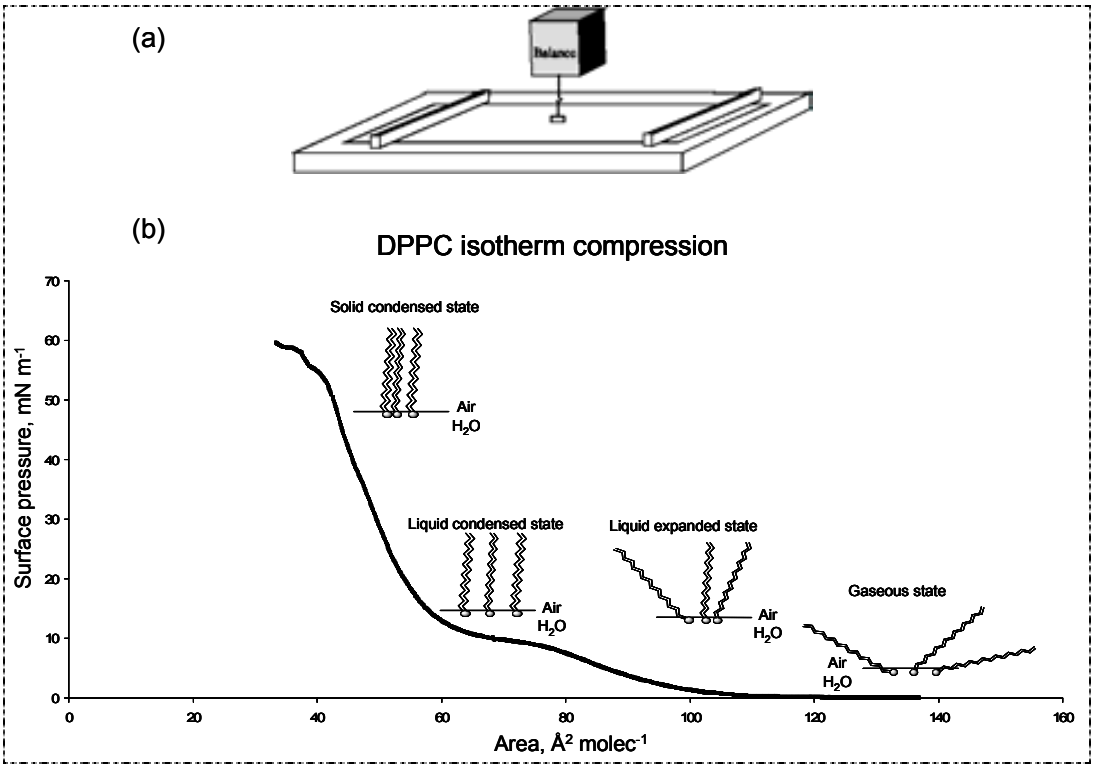

Fig. 23 (a) Langmuir film balance with a Wilhelmy plate electrobalance measuring the surface pressure and barriers for reducing the available surface area and (b) profile of compression isotherm of DPPC, showing the states and the orientation of DPPC molecules at the air-water interface.

1.5. Techniques employed to study the antimicrobial action

Elucidation of the mode of action of antimicrobial agents can be achieved by several techniques. In this thesis, the techniques employed have been determination of minimum inhibition concentration (MIC), flow cytometry (FC), viable cell counts, transmission electron microscopy (TEM) and atomic absorption spectrophotometry. All these techniques have limitations and therefore, it is convenient the use of complementary methods to achieve a better assessment of the antimicrobial action of biocides.

1.5.1. Minimum inhibitory concentration (MIC)

The minimum inhibitory concentration (MIC) is defined as the lowest concentration of the antimicrobial agent that results in inhibition of visible growth. Thus, the lower the MIC values, the higher antimicrobial activity. This assay can be performed in a 96-microwell plate (Figure 24), where each raw is inoculated with the tested micro-organism and each column contained different concentrations of the antimicrobial agent.

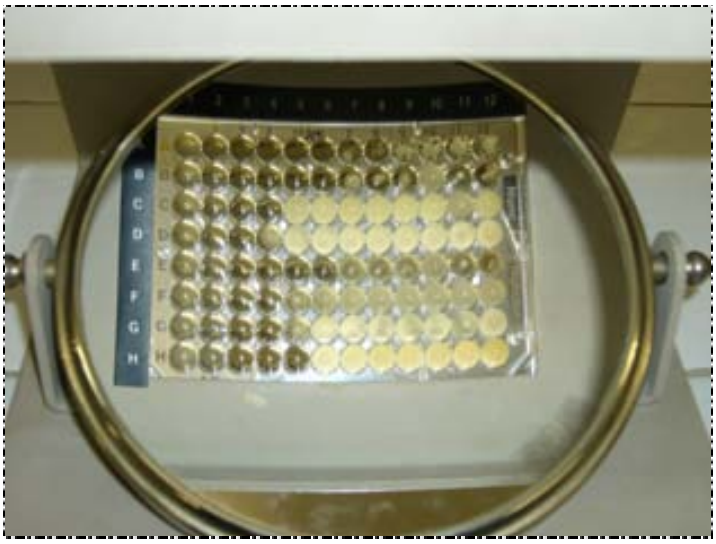

Fig. 24. Growth (turbidity) occurs in those wells with biocide concentrations below the MIC. Column number 12 was the negative control (*i.e.* inoculated medium in absence of biocide).

1.5.2. Flow cytometry (FC)

Flow cytometry (FC) is a technique for counting, examining and sorting microscopic particles suspended in a stream of fluid. It allows simultaneous multiparametric analysis of the physical and/or chemical characteristics of single cells flowing through an optical/electronic detection apparatus.

Flow cytometry (FC) can measure characteristics of single cells suspended in a flowing stream. A focussed beam of laser light hits the moving cell and light is scattered in all directions. Detectors receive the

pulses of scattered light and they are converted into a form suitable for computer analysis and interpretation. Properties of the cell, surface molecules or intracellular constituents, can also be accurately quantified if the cellular marker of interest can be labelled with a fluorescent dye. Each flow cytometer is usually able to detect different fluorochromes simultaneously, depending on its configuration (source: http://www.wehi.edu.au/cytometry/flowintrol.html).

Different fluorescent dyes have been described to evaluate the membrane integrity of cells. The fluorochromes Syto-13 and propidium iodide (PI) were employed in this thesis. The cell-permeant SYTO 13 green fluorescent nucleic acid stain exhibits bright, green fluorescence upon binding to nucleic acids of damaged and intact cells. PI is a popular red-fluorescent nuclear and chromosome counterstain. Since PI is not permeant to live cells, it is also commonly used to detect dead cells in a population. Thus, the dual staining can be used to discriminate between:

a) viable bacteria with intact plasma membrane, only stained by Syto-13.

b) damaged cells, stained by both Syto-13 and PI.

c) several damaged or dead cells, only stained by PI.

As example, Figure 25 shows fluorescence conferred by Syto-13 corresponding to intact *Staphylococcus aureus*.

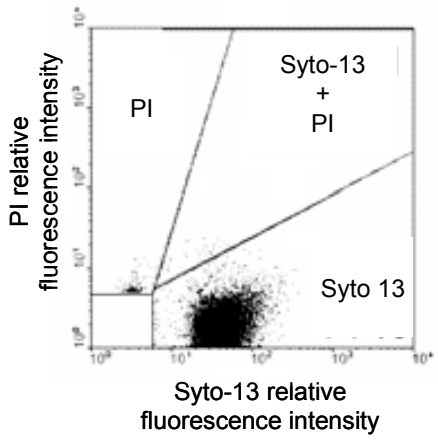

Fig. 25 Untreated *Staphylococcus aureus* (*i.e.* control) stained by Syto-13 and PI.

FC also allows the assessment of the perturbing effect on the membrane potential caused by biocides. In this work, bis-oxonol was used as fluorescent dye. Oxonols are anionic lipophilic dyes which are not extensively accumulated cytosolically by cells with an inside negative transmembrane potential. Therefore, bis-oxonol fluorescence increases with the strength of the biocide treatment, as it can be accumulated inside the cell when homeostatic conditions are lost and membrane potential decreases.[90]

1.5.3. Viable cell counts

Indirect viable cell counts, also called plate counts, involve plating out (spreading) a sample of a culture on a nutrient agar surface. The sample or cell suspension can be diluted in a nontoxic diluent (*e.g.* water or saline) before plating. If plated on a suitable medium, each viable unit grows and forms a colony. Each colony that can be counted is called a colony forming unit (cfu) and the number of cfu's is related to the viable number of bacteria in the sample.

Advantages of the technique are its sensitivity (theoretically, a single cell can be detected), and it allows for inspection and positive identification of the organism counted. Disadvantages are: (1) only living cells develop colonies that are counted; (2) clumps or chains of cells develop into a single colony; (3) colonies develop only from those organisms for which the cultural conditions are suitable for growth. The latter makes the technique virtually useless to characterize or count the total number of bacteria in complex microbial ecosystems such as soil or the animal rumen or gastrointestinal tract.

1.5.4. Transmission electronic microscopy (TEM)

This technique provides information about surface and intracellular changes on bacteria and therefore, it is a valuable tool to gain insight the effects caused on bacteria after exposure to biocides. TEM is performed on thin sections of bacteria that had been treated with the selected antimicrobial agents and it allows identifying damage to the cell membranes and cell contents, as well observing changes in cellular morphology after exposure to a biocide.[91-95]

1.5.5. Atomic absorption spectrophotometry

This technique provides accurate quantitative analyses for metals in solution. Absorbance values for unknown samples are compared to calibration curves prepared by running known samples.

The first signal of an increase in membrane permeability is usually provided by the leakage of potassium ions. Membrane-active agents release various cytoplasmatic constituents from treated cells. Thus, potassium leakage reflects changes in the membrane structure together with consequences on the viability of cells.[96] Here, we have assessed K^+ leakage from bacteria after exposure to biocides by atomic absorption spectrophotometry. This technique requires high number of bacterial cells (*ca* 10^9 cfu mL^{-1})[16] and a potassium-free buffer system whitout interfering ions (*e. g.* sodium) in the buffer.

References:

1. Morton, L. H. G.; Greenway, D. L. A.; Gaylarde, C. C.; Surman, S. B., Consideration of some implications of the resistance of biofilms to biocides. *Int. Biodeterior. Biodegrad.* **1998**, *41*, 247-259.

2. Fux, C. A.; Stoodley, P.; Hall-Stoodley, L.; Costerton, J. W., Bacterial biofilms: a diagnostic and therapeutic challenge. *Expert Rev. Anti Infect Ther.* **2003**, *1*, 667-683.
3. Russell, A. D., Assesssment of sporicidal efficacy. *Int. Biodeterior. Biodegrad.* **1998**, *41*, 281-287.
4. Poxton, I. R., Prokaryote envelope diversity. *J. Appl. Bacteriol. Symposium Supplement* **1993**, *74*, 1S-11S.
5. Madigan, M. T.; Martinko, J. M., *Brock Biology of Microorganisms*. 11 ed.; Pearson Prentice Hall: Upper Saddle River, 2006.
6. Denyer, S. P., Mechanisms of action of antibacterial biocides. *Int. Biodeterior. Biodegrad.* **1995**, *36*, 227-245.
7. Denyer, S. P.; Stewart, G. S. A. B., Mechanisms of action of disinfectants. *Int. Biodeterior. Biodegrad.* **1998**, *41*, 261-268.
8. Kabara, J. J., *Cosmetic and Drug Preservation: Principles and Practice*. New York, 1984.
9. McDonnell, G.; Russell, A., D., Antiseptics and disinfectants: activity and resistance. *Clin. Microbiol. Rev.* **1999**, *12*, 147-179.
10. Lohner, K.; Prenner, E. J., Differential scanning calorimetry and X-ray diffraction studies of the specificity of the interaction of antimicrobial peptides with membrane-mimetic systems. *Biochim. Biophys Acta: Biomembranes* **1999,** *1462*, 141-156.
11. Köhler, T.; Pechère, J.-C.; Plésiat, P., Bacterial antibiotic efflux systems of medical importance. *Cel. Mol. Life Sci.* **1999**, *56*, 771-778.
12. Wright, G. D., Mechanisms of resistance to antibiotics. *Curr. Opin. Chem. Biol.* **2003**, *7*, 563-569.
13. Russell, A. D., Mechanisms of bacterial resistance to biocides. *Int. Biodeter. Biodegradat.* **1995**, *36*, 247-265.
14. Langsrud, S.; Sidhu, M. S.; Heir, E.; Holck, A. L., Bacterial disinfectant resistance-a challenge for the food industry. *Int. Biodeter. Biodegradat.* **2003**, *51*, 283-290.
15. Gilbert, P.; Moore, L. E., Cationic antiseptics: diversity of action under a common epithet. *J. Appl. Bacteriol.* **2005**, *99*, 703-715.
16. Denyer, S. P.; Hugo, W. B., *Mechanisms of action of chemical biocides: their study and exploitation*. 1 ed.; Blackwell Scientific Publications: Oxford, 1991.
17. Daoud, N. N.; Dickinson, N. A.; Gilbert, P., Antimicrobial activity and physico-chemical properties of some alkyldimethylbenzylammonium chlorides. *Microbios* **1983**, *37*, 73-85.
18. Rodrigues, L.; Banat, I. M.; Teixeira, J.; Oliveira, R., Biosurfactants: potential applications in medidicine. *J. Antimicrob. Chemother.* **2006**, *57*, 609-618:
19. Singh, P.; Cameotra, S. S., Potential applications of microbial surfactants in biomedical sciences. *Trends Biotechnol.* **2004**, *22*, 142-146.
20. Clapés, P.; Infante, M. R., Amino acid-based surfactants: enzymatic synthesis, properties and potencial applications. *Biocatal. Biotransform.* **2002**, *20*, 215-233.
21. Pérez, L.; Torres, J. L.; Manresa, A.; Solans, C.; Infante, M. R., Synthesis, aggregation, and biological properties of a new class of gemini cationic amphiphilic compounds from arginine, bis(Args). *Langmuir* **1996**, *12*, 5296-5301.
22. Pérez, L.; Pinazo, A.; Vinardell, P.; Clapés, P.; Angelet, M.; Infante, M. R., Synthesis and biological properties of dicationic arginine-diglycerides. *New J. Chem.* **2002**, *26*, 1221-1227.

23. Pérez, L.; Infante, M. R.; Pons, R.; Morán, C.; Vinardell, P.; Mitjans, M.; Pinazo, A., A synthetic alternative to natural lecithins with antimicrobial properties. *Colloids Surf. B: Biointerfaces* **2004**, 35, 235-242.
24. Morán, C.; Infante, M. R.; Clapés, P., Synthesis of glycero amino acid-base surfactants. Part 1. Enzymatic preparation of *rac*-1-*O*-(*N*-acetyl-L-aminoacyl)glycerol derivatives. *J. Chem. Soc., Perkin Trans. 1* **2001**, 2063-2070.
25. Clapés, P.; Morán, C.; Infante, M. R., Enzymatic Synthesis of Arginine-Based Cationic Surfactants. *Biotechnol. Bioeng.* **1999**, *63*, 332-343.
26. Piera, E.; Infante, M. R.; Clapés, P., Chemoenzymatic synthesis of arginine-based gemini surfactants. *Biotechnol. Bioeng.* **2000**, *70*, 323-331.
27. Morán, C.; Clapés, P.; Comelles, F.; García, T.; Pérez, L.; Vinardell, P.; Mitjans, M.; Infante, M. R., Chemical Structure/Property Relationship in Single-Chain Arginine Surfactants. *Langmuir* **2001**, *17*, 5071-5075.
28. Infante, M. R.; García, J.; Erra, P.; Julia, R.; Prats, M., Surface activity molecules: preparation and properties of long chain N^{α}-acyl-L-α-amino-ω-guanidine alkyl acid derivatives. *Int. J. Cosmet. Sci.* **1984**, *6*, 275-282.
29. Infante, M. R.; Pinazo, A.; Seguer, J., Non-conventional surfactants from amino acids and glycolipids: Structure, preparation and properties. *Colloids Surf. A* **1997**, *123-124*, 49-70.
30. Piera, E.; Comelles, F.; Erra, P.; Infante, M. R., New alquil amide type cationic surfactants from arginine. *J. Chem. Soc., Perkin Trans. II* **1998**, 335-342.
31. Pavlíková, M.; Lacko, I.; Devínsky, F.; Mlynarcik, D., Quantitative relationships between structure and antimicrobial activity of quaternary ammonium bolaamphiphiles. *Collect. Czech. Chem. Commun.* **1995**, *60*, 1213-1229.
32. Pinazo, A.; Wen, X.; Pérez, L.; Infante, M. R.; Franses, E. I., Aggregation behavior in water of monomeric and gemini cationic surfactants derived from arginine. *Langmuir* **1999**, *15*, 3134-3142.
33. Pérez, L.; Pinazo, A.; Rosen, M. J.; Infante, M. R., Surface Activity Properties at Equilibrium of Novel Gemini Cationic Amphiphilic Compounds from Arginine, Bis(Args). *Langmuir* **1998**, *14*, 2307-2315.
34. Pérez, L.; García, M. T.; Ribosa, I.; Vinardell, M. P.; Manresa, A.; Infante, M. R., Biological properties of arginine-based gemini cationic surfactants. *Environ. Toxicol. Chem.* **2002**, *21*, 1279-1285.
35. Castillo, J. A.; Pinazo, A.; Carilla, J.; Infante, M. R.; Alsina, M. A.; Haro, I.; Clapés, P., Interaction of antimicrobial arginine-based cationic surfactants with liposomes and lipid monolayers. *Langmuir* **2004**, *20*, 3379-3387.
36. Mitjans, M.; Martínez, V.; Clapés, P.; Pérez, L.; Infante, M. R.; Vinardell, M. P., Low potential ocular irritation of arginine-based gemini surfactants ant their mixtures with nonionic and zwitterionic surfactants. *Pharmac. Res.* **2003**, *20*, 1697.
37. Segraves, N. L.; Crews, P., A Madagascar sponge Batzella sp. as a source of alkylated Iminosugars. *J. Nat. Prod.* **2005**, *68*, 118-121.
38. Maddry, J. A.; Bansal, N.; Bermudez, L. E.; Comber, R. N.; Orme, I. M.; Suling, W. J.; Wilson, L. N.; Reynolds, R. C., Homologated aza analogs of arabinose as antimycobacterial agents. *Bioorg. Med. Chem. Lett.* **1998**, *8*, 237-242.
39. Greimel, P.; Spreitz, J.; Stütz, A. E.; Wrodnigg, T. M., Iminosugars and Relatives as Antiviral and Potential Anti-infictives Agents. *Curr. Top. Med. Chem.* **2003**, *3*, 513-523.
40. Koeller, K. M.; Wong, C.-H., Emerging themes in medicinal glycoscience. *Nat. Biotechnol.* **2000**, *18*, 835-841

41. Kolter, T.; Wendeler, M., Chemical Chaperones-A New Concept in Drug Research. *ChemBioChem* **2003**, *4*, 260-264.
42. Asano, N., Akaloidal sugar mimetics: biological activities and therapeutical applications. *J. Enzym. Inhib.* **2000**, *15*, 215-234.
43. Asano, N., Glycosidase inhibitors: update and perspectives on practical use. *Glycobiology* **2003**, *13*, 93-104.
44. Wong, C.-H., *Carbohydrate-Based Drug Discovery*. Wiley-VCH: Weinheim, 2003; Vol. Volume 1.
45. Wong, C.-H., *Carbohydrate-Based Drug Discovery*. Wiley-VCH: Weinheim, 2003; Vol. Volume 2.
46. Fiaux, H.; Popowycz, F.; Favre, S.; Schutz, C.; Vogel, P.; Gerber, S.; Juillerat, L., Functionalized Pyrrolidines Inhibit alpha-Mannosidase Activity and Growth of Human Glioblastoma and Melanoma Cells. *J. Med. Chem.* **2005**, *48*, 4237-4246.
47. Asano, N.; Nash, R. J.; Molyneux, R. J.; Fleet, G. W. J., Sugar-mimic glycosidase inhibitors: natural occurrence, biological activity and prospects for therapeutic application. *Tetrahedron: Asymmetry* **2000**, *11*, 1645-1680.
48. Rye, C. S.; Withers, S. G., Glycosidase mechanisms. *Curr. Opin. Chem. Biol.* **2000**, 4, 573-580.
49. Qiao, L.; Murray, B. W.; Shimazaki, M.; Schultz, J.; Wong, C. H., Synergistic Inhibition of Human α-1,3-Fucosyltransferase V. *J. Am. Chem. Soc.* **1996**, *118*, 7653-7662.
50. Ratner, L.; Heyden, N. V.; Dedera, D., Inhibition of HIV and SIV infectivity by blockade of α-glucosidase activity. *Virology* **1991**, *181*, 180-192.
51. Naoki, A.; Haruhisa, K.; O., K.; Emiko, T.; M., K.; O., M.; Masanori, B., *N*-Alkylated Nitrogen-in-the-Ring Sugars: Conformational Basis of Inhibition of Glycosidases and HIV-1 Replication. *J. Med. Chem.* **1995**, *38*, 2349-2356.
52. Goss, P. E.; Baker, M. A.; Carver, J. P.; Dennis, J. W., Inhibitors of carbohydrate processing: A new class of anticancer agents. *Clin. Cancer Res.* **1995**, *1*, 935-944.
53. Tulsiani, D. R.; Harris, T. M.; Touster, O., Swainsonine inhibits the biosynthesis of complex glycoproteins by inhibition of golgi mannosidase II. *J. Biolg. Chem.* **1982**, *257*, 7936-7939.
54. Jakobsen, P.; Lundbeck, J. M.; Kristiansen, M.; Breinholt, J.; Demuth, H.; Pawlas, J.; Torres Candela, M. P.; Andersen, B.; Westergaard, N.; Lundgren, K.; Asano, N. i., Iminosugars: potential inhibitors of liver glycogen phosphorylase. *Bioorg. Med. Chem.* **2001**, *9*, 733-744.
55. Jespersen, T. M.; Dong, W.; Sierks, M. R.; Skrydstrup, T.; Lundt, I.; Mikael, B., Isofagomine, a Potent, New Glycosidase Inhibitor. *Angew. Chem. Int. Ed.* **1994**, *33*, 1778-1779.
56. Sawkar, A. R.; Cheng, W.-C.; Beutler, E.; Wong, C.-H.; Balch, W. E.; Kelly, J. W., Chemical chaperones increase the cellular activity of N370S β-glucosidase: A therapeutic strategy for Gaucher disease. *PNAS* **2002**, *99*, 15428-15433.
57. Elstein, D.; Hollak, C.; Aerts, J. M. F. G.; van Weely, S.; Maas, M.; Cox, T. M.; Lachmann, R. H.; Hrebicek, M.; Platt, F. M.; Butters, T. D.; Dwek, R. A.; Zimran, A., Sustained therapeutic effects of oral miglustat (Zavesca, *N*-butyldeoxynojirimycin, OGT 918) in type I Gaucher disease. *J. Inherit. Metab. Dis.* **2004**, *27*, 757-766.
58. Koyama, M.; Sakamura, S., The structure of a new piperidine derivative from buckwheat seeds (*Fagopyrum esculentum* Moench). *Agric. Biolog. Chem.* **1974**, *38*, 1111-1112.

59. Molyneux, R. J.; Benson, M.; Wong, R. Y.; Tropea, J. E.; Elbein, A. D., Australine, a Novel Pyrrolizidine Alkaloid Glucosidase Inhibitor from Castanospermum australe. *J. Nat. Prod.* **1988**, *51*, 1198-1206.
60. Kato, A.; Asano, N.; Kizu, H.; Matsui, K.; Watson, A. A.; Nash, R. J., Fagomine Isomers and Glycosides from *Xanthocercis zambesiaca*. *J. Nat. Prod.* **1997**, *60*, 312-314.
61. Asano, N.; Tomioka, E.; Kizu, H.; Matsui, K., Sugars with nitrogen in the ring isolated from the leaves of Morus bombycis. *Carbohydr. Res.* **1994**, *253*, 235-245.
62. Nojima, H.; Kimura, I.; Chen, F.-J.; Sugihara, Y.; Haruno, M.; Kato, A.; Asano, N., Antihyperglycemic Effects of *N*-Containing Sugars from *Xanthocercis zambesiaca*, *Morus bombycis*, *Aglaonema treubii*, and *Castanospermum australe* in Streptozotocin-Diabetic Mice. *J. Nat. Prod.* **1998**, *61*, 397-400.
63. Iqbal, Z.; Hiradate, S.; Noda, A.; Isojima, S.-I.; Fujii, Y., Allelopathy of buckwheat: Assessment of allelopathic potential of extract of aerial parts of buckwheat and identification of fagomine and other related alkaloids as allelochemicals. *Weed Biol. Manag.* **2002**, *2*, 110-115.
64. Pandey, G.; Kapur, M., A general strategy towards the synthesis of 1-N-iminosugar type glycosidase inhibitors: demonstration by the synthesis of - as well as - glucose type iminosugars (isofagomines). *Tetrahedron Lett.* **2000**, *41*, 8821-8824.
65. Goujon, J.-Y.; Gueyrard, D.; Compain, P.; Martin, O. R.; Ikeda, K.; Kato, A.; Asano, N., General synthesis and biological evaluation of α-1-*C*-substituted derivatives of fagomine (2-deoxynojirimycin-α-*C*-glycosides). *Bioorg. Med. Chem.* **2005**, *13*, 2313-2324.
66. Murray, A. J.; Parsons, P. J., A Convenient Approach to (-)-8-*epi*-Swainsonine *Synlett* **2006**, 1443-1445.
67. Banba, Y.; Abe, C.; Nemoto, H.; Kato, A.; Adachi, I.; Takahata, H., Asymmetric synthesis of fagomine and its congeners. *Tetrahedron Asymm.* **2001**, *12*, 817-819.
68. Takahata, H.; Banba, Y.; Ouchi, H.; Nemoto, H.; Kato, A.; Adachi, I., Asymmetric Synthesis of the Four Possible Fagomine Isomers. *J. Org. Chem.* **2003**, *68*, 3603-3607.
69. Faber, K., *Biotransformations in Organic Chemistry*. 5th ed.; Springer: Heidelberg, 2004.
70. Espelt, L.; Parella, T.; Bujons, J.; Solans, C.; Joglar, J.; Delgado, A.; Clapés, P., Stereoselective aldol additions catalyzed by dihydroxycetona phosphate-dependent aldolases in emulsion systems: preparations and structural characterization of linear and cyclic iminopolyols from aminoaldehydes. *Chem. Eur. J.* **2003**, *9*, 4887-4899.
71. Espelt, L.; Bujons, J.; Parella, T.; Calveras, J.; Joglar, J.; Delgado, A.; Clapés, P., Aldol additions of dihydroxyacetone phosphate to *N*-Cbz-amino aldehydes catalyzed by L-fuculose-1-phosphate aldolase in emulsion systems: inversion of stereoselectivity as a function of the acceptor aldehyde. *Chem. Eur. J.* **2005**, *11*, 1392-1401.
72. Wang, Y.-F.; Yoshikazu, T.; Wong, C.-H., Remarkable Stereoselectivity in the Inhibition of α-Galactosidase from Coffee Bean by a New Polyhydroxypyrrolidine Inhibitor. *Angew. Chem. Int. Ed.* **1994**, *33*, 1242-1244.
73. Jung, S.; Jeong, J.; Miller, P.; Wong, C. H., An Efficient Multigram-Scale Preparation fo Dihydroxyacetone Phosphate. *J. Org. Chem.* **1994**, *59*, 7182-7184.
74. Meyer, O.; Ponaire, S.; Rohmer, M.; Grosdemange, C., Lewis Acid Mediated Regioselective Ring Opening of Benzylglycidol with Dibenzyl Phosphate: Short and Attractive Synthesis of Dihydroxyacetone Phosphate. *Org. Lett.* **2006**, *8*, 4347-4350.
75. Fessner, W. D.; Sinerius, G., Enzymes in organic synthesis. 7. Synthesis of dihydroxyacetone phosphate (and isosteric analogs) by enzymic oxidation: sugars from glycerol. *Angew. Chem. Int. Ed.* **1994**, *33*, 209-212.

76. Charmantray, F.; El Blidi, L.; Gefflaut, T.; Hecquet, L.; Bolte, J.; Lemaire, M., Improved Straightforward Chemical Synthesis of Dihydroxyacetone Phosphate through Enzymatic Desymmetrization of 2,2-Dimethoxypropane-1,3-diol. *J. Org. Chem.* **2004**, *69*, 9310-9312.
77. Sánchez, I.; García, J. F.; Bastida, A.; García-Junceda, E., Multienzyme system for dihydroxyacetone phosphate-dependent aldolase catalyzed C-C bond formation from dihydroxyacetone. *Chem. Com.* **2004**, 1634-1635.
78. van Herk, T.; Hartog, A. F.; Schoemaker, H. E.; Wever, R., Simple Enzymatic *in situ* Generation of Dihydroxyacetone Phosphate and Its Use in a Cascade Reaction for the Production of Carbohydrates: Increased Efficiency by Phosphate Cycling. *J. Org. Chem.* **2006**, *71*, 6244-6247.
79. Fessner, W.-D.; Walter, C., Enzymic C-C bond formation in asymmetric synthesis. *Top. Curr Chem.* **1996**, *184*, 97-194.
80. Drueckhammer, D. G.; Durrwachter, J. R.; Richard, L. P.; Crans, D. C.; Daniels, L.; Wong, C. H., Reversible and *in situ* formation of organic arsenates and vanadates as organic phosphate mimics in enzymatic reactions: mechanistic investigation of aldol reactions and synthetic applications. *J. Org. Chem.* **1989**, *54*, 70-77.
81. Schürmann, M.; Sprenger, G. A., Fructose-6-phosphate Aldolase Is a Novel Class I Aldolase from *Escherichia coli* and Is Related to a Novel Group of Bacterial Transaldolases. *J. Biolog. Chem.* **2001**, *276*, 11055-11061.
82. Thorell, S.; Schürmann, M.; Sprenger, G. A.; Schneider, G., Crystal Structure of Decameric Fructose-6-Phosphate Aldolase from *Escherichia coli* Reveals Inter-subunit Helix Swapping as a Structural Basis for Assembly Differences in the Transaldolase Family. *Journal of Molecular Biology* **2002**, *319*, 161-171.
83. Schürmann, M.; Sprenger, G. A., Fructose 6-phosphate aldolase and 1-deoxy-D-xylulose 5-phosphate synthase from *Escherichia coli* as tools in enzymatic synthesis of 1-deoxysugars. *J. Mol. Catal. B: Enzymatic* **2002**, *19-20*, 247-252.
84. Maget-Dana, R., The monolayer technique: a potent tool for studying the interfacial properties of antimicrobial and membrane-lytic peptides and their interactions with lipid membranes. *Biochim. Biophys. Acta: Biomembranes* **1999**, *1462*, 109-140.
85. Brockman, H., Lipid monolayers: why use half a membrane to characterize protein-membrane interactions? *Curr. Opin. Struc. Biol.* **1999**, 9, 438-443.
86. Lo, Y.-L.; Rahman, Y.-E., Protein Location in Liposomes, A Drug carrier: A Prediction by Differential Scanning Calorimetry. *J. Pharmac. Sci.* **1995**, *804*, 805-814.
87. Pedersen, T. B.; Sabra, M. C.; Frokjaer, S.; Mouritsen, O. G.; Jorgensen, K., Association of acylated cationic decapeptides with dipalmitoylphosphatidylserine-dipalmitoylphosphatidylcholine lipid membranes. *Chemis. Phys. Lipids* **2001**, 113, 83-95.
88. Ramaswami, V.; Haaseth, R. C.; Matsunaga, T. O.; Hruby, V. J.; O'Brien, D. F., Opioid peptide interactions with lipid bilayer membranes. *Biochim. Biophys. Acta: Biomembranes* **1992**, *1109*, 195-202.
89. Inoue, T.; Iwanaga, T.; Fukushima, K.; Shimozawa, R., Effect of sodium octanoate and sodium perfluorooctanoate on gel-to-liquid-crystalline phase transition of dipalmitoylphosphatidylcholine vesicle membrane. *Chem. Phys. Lipids* **1988,** *46*, 25-30.
90. Comas, J.; Vives, J., Assessment of the effects of gramicidin, formaldehyde, and surfactants on *Escherichia coli* by flow cytometry using nucleic acid and membrane potential dyes. *Cytometry* **1997**, *29*, 58-64.
91. Claeson, P.; Radström, P.; Sköld, O., Bactericidal effect of the sesquiterpene *t*-cardinol on *Staphylococcus aureus*. *Phytother. Res.* **1992**, *6*, 94-98.

92. Yamaguchi, H.; Hirasawa, K.; Tanaka, T.; Shioiri, T.; Matsue, I., The inhibitory effect of chlorhexidine digluconate on dental plaque formation. *J. Periodontol.* **1981**, *52*, 630-638.
93. Malik, Z.; Ladan, H.; Nitzan, Y., Mesosomal structures and antimicrobial activity induced by hemin oxidation or porphyrin photodynamic sensitization in Staphylococci. *Curr. Microbiol.* **1988**, *16*, 321-328.
94. Shin, K.; Yamauchi, K.; Teraguchi, S.; Hayasawa, H.; Tomita, M.; Otsuka, Y.; Yamazaki, S., Antibacterial activity of bovine lactoferrin and its peptides against enterohaemorrhagic *Escherichia coli* O157:H7. *Lett. Appl. Microbiol.* **1998**, *26*, 407-411.
95. Rodríguez, E.; Seguer, J.; Rocabayera, X.; Manresa, A., Cellular effects of monochloride of L-arginine, *N*-lauroyl ethylester (LAE) on exposure to *Salmonella typhimurium* and *Staphylococcus aureus*. *J. Appl. Microbiol.* **2004**, *96*, 903-912.
96. Mlynarcik, D.; Sirotkova, L.; Devinsky, F.; Masarova, L.; Pikulikova, A.; Lacko, I., Potassium leakage from *Escherichia coli* cells treated by organic ammonium salts. *J. Basic Microbiol.* **1992**, *32*, 43-47.

2. OBJECTIVES

The main goal of the present thesis was to gain insight into the mode of antibacterial action of arginine-based surfactants to design novel antimicrobial agents with improved antibacterial activity.

As mentioned in the introduction, our group has prepared different series of arginine acid-based surfactants which have shown broad spectrum activity. It is believed that their main target may be the cytoplasmatic bacterial membrane. The initial goal of this thesis was to investigate their mode of action. With this aim, the following objectives were pursued:

1) To study the interaction between arginine-based surfactant and membrane models.

2) To assess the effects caused by a gemini arginine-based surfactant, $C_3(CA)_2$, on *Staphylococcus aureus* and *Escherichia coli*.

After these physico-chemical and microbiological studies, the third objective was:

3) To design novel bis(phenylacetylargine) derivatives, bis(PhAcArg), to enhance the antimicrobial action of the arginine-based surfactants synthesised thus far.

Finally, with the aim of looking for novel antimicrobial agents, the fourth objective was:

4) To synthesise D-fagomine and *N*-alkyl-D-fagomine derivatives to evaluate their antimicrobial activity.

3. RESULTS AND DISCUSSION

3.1. Interaction of antimicrobial arginine-based cationic surfactants with membrane models

Cationic surfactants such as hexadecyltrimethylammonium bromide (HTAB) and bisbiguanides such as chlorhexidine (CHX) possess broad antimicrobial activity. Their target is the cytoplasmic membrane, which is basically a bilayer of phospholipids where proteins are anchored (section 1.1.1., page 15). It is believed that arginine-based cationic surfactants such as LAM, $C_3(OA)_2$ and $C_3(CA)_2$, (Figure 1) should have the same target but to date their interaction with membrane models has not been investigated yet.

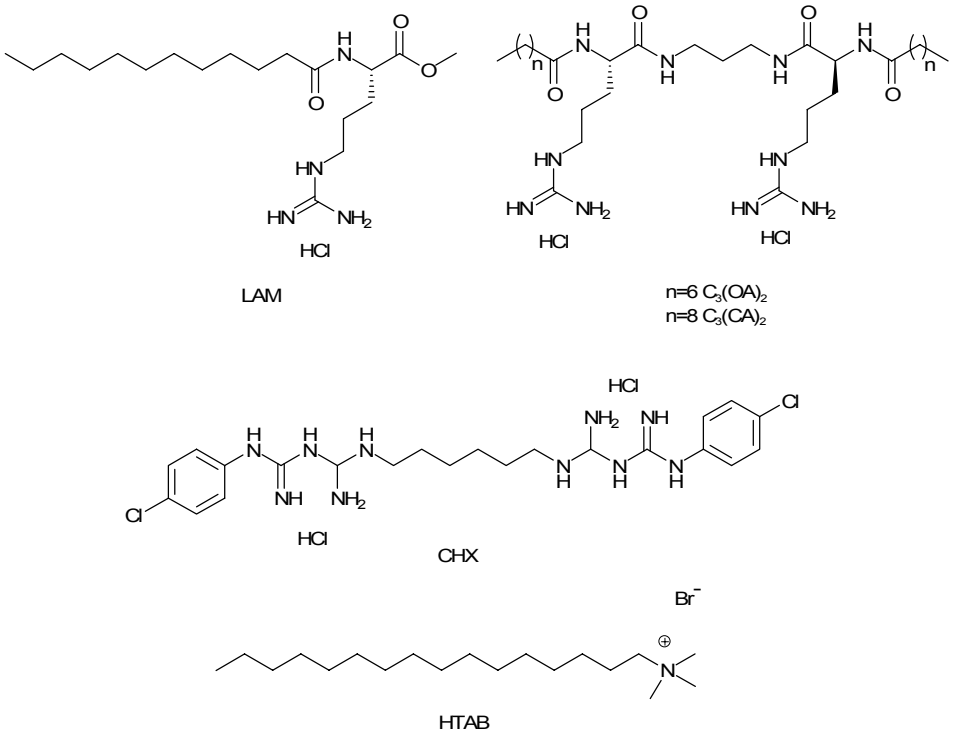

Fig. 1. Structures of the selected antimicrobial agents.

To gain insight into the physicochemical factors that determine the antimicrobial activity of arginine-based surfactants, their interaction with model lipid-membranes systems was investigated. The study also included HTAB and CHX for the sake of comparison. In this chapter, the antimicrobial activity and the physicochemical effects of these compounds on multilamellar vesicles (MLVs), large unilamellar vesicles (LUVs) and phospholipid monolayers are described in detail.

3.1.1. Antimicrobial activity

The minimum inhibitory concentration (MIC) values of LAM, $C_3(CA)_2$, $C_3(OA)_2$, HTAB and CHX against seven Gram-positive bacteria, eight Gram-negative bacteria and one yeast are summarized in Table 1.

Table 1. Minimum inhibitory concentration in mg L^{-1} of the selected compounds. In parenthesis, MICs values are expressed in μM.

Micro-organism	HTAB Mw 364.45	$C_3(OA)_2$ Mw 710.45	LAM Mw 406.99	$C_3(CA)_2$ Mw 767.92	CHX Mw 582.40
Gram-negative bacteria					
C. freundii	64 (18)	64 (90)	256 (628)	32 (42)	1 (2)
B. bronchiseptica	4 (1)	8 (11)	256 (628)	4 (5)	1(2)
P. aeruginosa	>256 (>70)	256 (359)	64 (157)	32 (42)	8 (14)
S. typhimurium	128 (35)	32 (45)	32 (79)	16 (21)	2 (4)
E. aerogenes	128 (35)	32 (45)	n.d.	16 (21)	8 (14)
S. faecalis	256 (70)	128 (179)	32 (79)	8 (10)	8 (14)
E. coli	32 (9)	16 (22)	32 (79)	8 (10)	2 (4)
K. pneumoniae	256 (70)	8 (11)	128 (314)	8 (10)	8 (14)
Gram-positive bacteria					
B. cereus	>256 (>70)	256 (359)	64 (157)	32 (42)	8 (14)
A. oxydans	2 (0,5)	32 (45)	64 (157)	16 (21)	1(2)
S. epidermidis	>256 (>70)	256 (359)	64 (157)	32 (42)	4 (7)
B. subtlis	64 (18)	16 (22)	256 (628)	16 (21)	4 (7)
S. aureus	2 (0.5)	16 (22)	64 (157)	2 (3)	0.5 (1)
M. luteus	1 (0.3)	8 (11)	256 (628)	4 (5)	1(2)
M. phlei	256 (70)	256 (359)	n.d.	16 (21)	8 (14)
Yeast					
C. albicans	1 (0,3)	8 (11)	64 (157)	2 (3)	0.5 (1)

The lower the MIC values the higher the antimicrobial activity. A cursory inspection of Table 1 shows that the MIC values for each compound depended exclusively on the bacterium but not on the nature of the outer membrane (*i.e.* Gram-positive or Gram-negative). The cell envelope of Gram-negative bacteria is

more complex than that of Gram-positive bacteria, but the presence of large amounts of negatively charged phospholipids and phosphatidylethanolamine (PE) is a common feature.[1] If MIC values are expressed in μg mL^{-1} the antimicrobial activity increased in the order of HTAB < $C_3(OA)_2$ < LAM < $C_3(CA)_2$ < CHX. To compare more precisely compounds with different molecular weight, MIC values were also expressed in μM instead of the typical mg L^{-1}. Then, the order is slightly different; LAM ≤ $C_3(OA)_2$ ≤ HTAB < $C_3(CA)_2$ < CHX. Remarkably, $C_3(CA)_2$ possessed lower MIC values than those of the commercial HTAB, for most of the micro-organisms assayed. In previous studies,[2,3] it has been shown that the optimum biological effect of single chain arginine-based surfactants was obtained with hydrocarbon alkyl moieties of 10 methylene groups (*i.e.* LAM). Pérez *et al.*[4] have reported that the minimum MIC values of the arginine-based gemini surfactants were obtained with the $C_n(CA)_2$ homologues. In this work, $C_3(CA)_2$ was the most active and for some micro-organisms similar to CHX. The results suggest that both the length of acyl chains and the positive charges, which determine the hydrophilic-lipophilic balance (HLB) of the molecule, are responsible for their membrane-disrupting properties.

3.1.2. Interaction of arginine-based surfactants with multilamellar vesicles

Analysis of multilamellar vesicles (MLVs) of lipids with bulky polar heads by differential scanning calorimetry (DSC) is characterized by two-phase transitions (Figure 2 curve a); a pretransition around 35 °C related with the alkyl chain tilt and the main transition around 41 °C between an ordered gel state ($L_{\beta'}$ phase) and a disordered liquid-crystalline state (L_{α} phase).[5-7]

The study of the main thermotropic phase transition of MLVs by DSC represents a simple and precise method to investigate the influence of bioactive products on lipid membranes. The structural change associated with this transition is the *trans-gauche* isomerization of the acyl-chains of the lipid

molecules. The average number of *gauche* conformers is related to the bilayer fluidity.[5] The presence of compounds susceptible of interacting with the phospholipid molecules may cause perturbations, which can contribute to disturb the fluidity of the membrane. Two parameters related with the phase transition were studied: the phase transition temperature (T_m), which corresponds to the gel to liquid-crystalline transition; and the width at half-height of the heat absorption peak ($\Delta T_{1/2}$), which is a measure of the cooperativity of this phase transition process.

The effect of the compounds on the main thermotropic phase transition parameters of MLVs of zwitterionic 1,2-dipalmitoylphosphatidylcholine (DPPC) was investigated with mixtures containing 0, 1, 2, 3, 4, 5, 10, 20, and 30 mol % of the tested compound. As example, Figure 2 depicts the DSC melting profiles of DPPC MLVs in the presence of different mol % of $C_3(CA)_2$. It is noteworthy that the addition of the product always caused the complete disappearance of the pretransition.

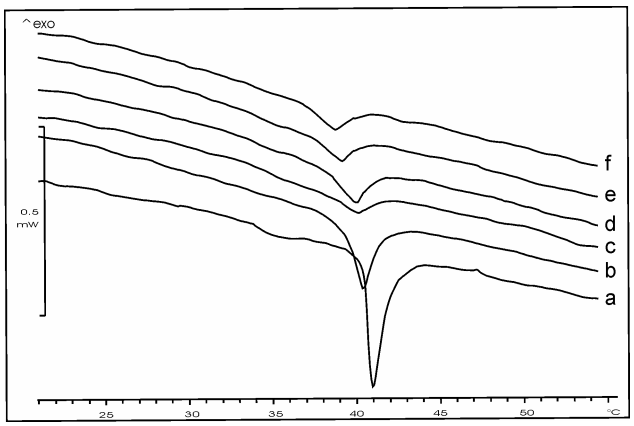

Fig. 2. DSC curves obtained with DPPC MLVs in presence of $C_3(CA)_2$. The molar percentage of $C_3(CA)_2$ were 0 % (a), 1 % (b), 2 % (c), 3 % (d), 4 % (e) and 5 % (f).

From the DSC curves thus obtained, the T_m (Figures 3a-b) and $\Delta T_{1/2}$ (Figures 5a-b) were plotted against the mol % of each product. As seen in Figures 3a-b, the higher the concentration of the product in the MLVs preparation, the lower the T_m values observed, except for HTAB.

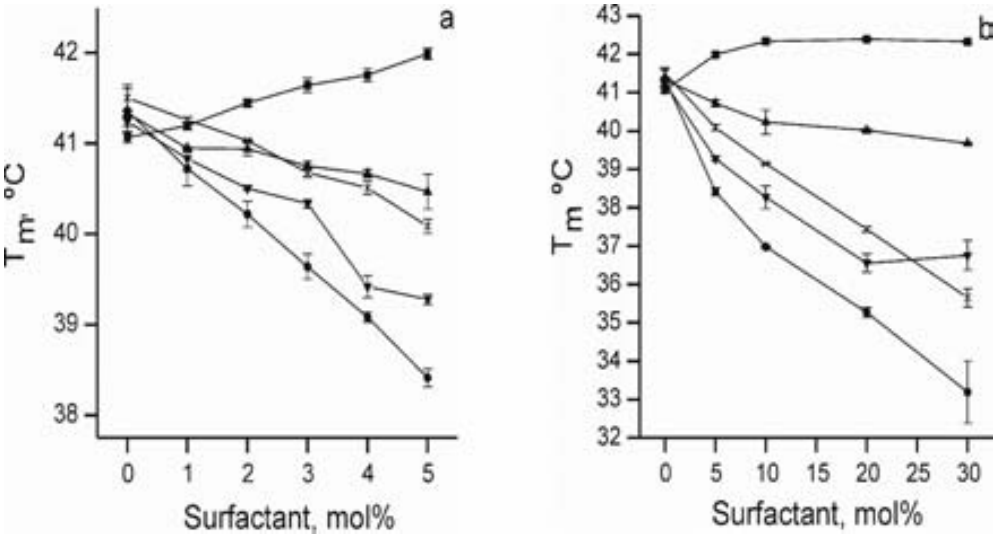

Fig. 3. The phase transition temperature (T_m) of DPPC MLVs as a function of the molar percentage of antimicrobial compound, in a concentration range (a) between 0 and 5 mol % and (b) between 0 and 30 mol %; LAM (X), $C_3(OA)_2$ (▲), $C_3(CA)_2$ (▼), HTAB (■) and CHX (●).

For the ideal case where the solute concentration in the lipid membrane is sufficiently low as in the present case, the depression of phase transition temperature is related to the solute concentration in the membrane by equation (1):

$$-\Delta T = \frac{RT_{m,0}^2}{\Delta H} \times x'_i \qquad (1)$$

where ΔH is the enthalpy change associated with the phase transition of pure lipid vesicles (*i.e.* 36.4 KJ mol^{-1} for DPPC MLVs), R is the gas constant, x'_i is the mole fraction of surfactants in the membrane, $T_{m,0}$ is the transition phase temperature of pure lipid vesicles (*i.e.* 314 K for DPPC MLVs) and $-\Delta T$ is T_m-$T_{m,0}$. Converting the number of moles to molar concentration for dilute solution with respect to both lipid and surfactant, equation (1) leads to equation (2)[8]:

$$-\Delta T = \frac{RT_{m,0}^2}{\Delta H} \times \frac{K}{55.5 + C_L K} C_A^0 \qquad (2)$$

where C_L and C_A^0 are the total concentration of the lipid and product in mol %, respectively, and K is the coefficient of surfactant between the bulk solution and the lipid membrane. Consequently, the partition coefficient K also reflects the interaction of the compound with the lipid molecules. The $-\Delta T = T_m$-$T_{m,0}$ values were plotted against the molar concentration of the compound in a range

between 0 to 3x10^{-4} M (*i.e.* 0-5 mol %) (Figure 4). In this concentration range, it was possible to estimate the partition coefficient (*K*) of the compound between the bulk solution and the lipid membrane, using equation (2) (Figure 4).

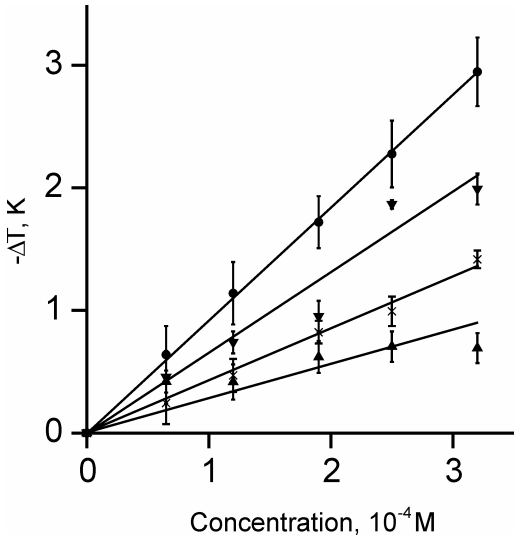

Fig. 4. The depression of the transition temperature $\Delta T = T_m - T_{m,0}$, of DPPC MLVs as a function of the molarity of the compound. Solid lines correspond to equation (1) fitted to the experimental data for the compounds LAM (X), $C_3(OA)_2$ (▲), $C_3(CA)_2$ (▼) and CHX (●).

From the slope of the straight lines thus obtained, the partition coefficients (*K*) were calculated and listed in Table 2. The results indicate that the partition of the compounds into the lipid membrane increased in the order $C_3(OA)_2$ < LAM < $C_3(CA)_2$ < CHX, in good agreement with their antimicrobial activity.

Table 2. Partition coefficient (*K*) of the selected compounds between the bulk solution and the DPPC MLVs calculated from the slopes of the linear regressions of Figure 4.

Compound	*K*
$C_3(OA)_2$	5.1 ± 1.0
LAM	10.8 ± 0.9
$C_3(CA)_2$	15.8 ± 1.2
CHX	22.5 ± 1.8

A different situation was observed for HTAB. Here, T_m increased in a concentration range between 0 and 5 mol %, whereas at higher concentration T_m was constant. This result may be explained considering the effect of *n*-alkanes, alcohols, fatty acids and tertiary alkyl ammonium salts on phospholipid phase transition behaviour.[9,10] Compounds with hydrocarbon chain length ≤ 10 intercalate into the hydrophobic core of the lipid bilayer, causing a void near the acyl hydrocarbon core. This void increases the ratio of *trans* to *gauche* conformers diminishing the stability of the lamellar gel phase and, therefore, decreasing T_m. On the other hand, the longer the alkyl chain (> 12 carbons) of the compound the smaller the void formed, causing less disruption of the packing of the phospholipid acyl chains. This increases the van der Waals interactions and therefore produces a small increase of T_m.[7] The behaviour of HTAB followed this latter trend, whereas the rest of the compounds under study performed as the shorter hydrocarbon alkyl chains.

To confirm these observations, dodecyltrimethylammonium bromide (DTAB), bearing a shorter alkyl chain than that of HTAB was also studied at concentrations ranging from 0 to 20 mol % (see Figure S.2.8., page 91). Here, the DSC analyses showed a decrease of 0.3 ^oC mol $\%^{-1}$ of the phase transition temperature, suggesting the formation of voids in the hydrophobic core.

The transition width at half-height of the heat absorption peak ($\Delta T_{1/2}$) is a measure of the cooperativity of the lipid molecules during the gel to liquid crystalline transition. The broadening of the endothermic peaks indicates that compounds were incorporated into the DPPC MLVs, disrupting the correlation between lipid molecules (*i.e.* cooperativity).[11] Both $C_3(CA)_2$, and CHX increased this parameter in the concentration range studied, whereas LAM had small effect up to 5 mol % but increased linearly between 5 to 30 mol % (Figures 5a-b).

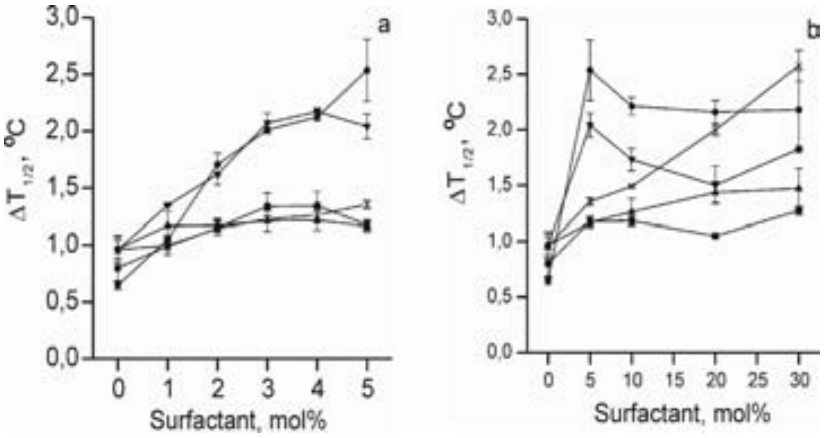

Fig. 5. The transition width ($\Delta T_{1/2}$) of DPPC MLVs as a function of the molar percentage of antimicrobial compound in concentration range (a) between 0 and 5 mol % and between (b) 0 and 30 mol %; LAM (X), $C_3(OA)_2$ (▲), $C_3(CA)_2$ (▼), HTAB (■) and CHX (●).

To better correlate both T_m and the cooperativity, $\Delta T_{1/2}$ was plotted against the $-\Delta T$ values ($-\Delta T = T_m - T_{m,0}$, where $T_{m,0}$ corresponds to T_m of pure DPPC MLVs, Figure 6). HTAB was not considered here since this compound increased the T_m of the DPPC MLVs. The results may be fitted to a linear equation in accordance with a previous work.[8] Since $-\Delta T$ is directly proportional to the mole fraction of the compound into the lipid membrane, this plot reflects the extension of the perturbation of the lipid membrane by the product: the higher the slope of the straight line the larger the perturbation of the MLVs. An inspection of the slopes for each compound, depicted in Figure 6, revealed that both CHX and $C_3(CA)_2$ caused the largest effect on the DPPC MLVs.

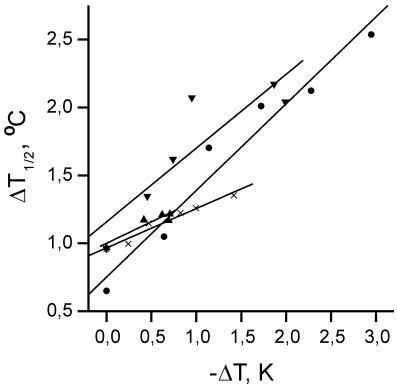

Fig. 6. Correlation between the transition width ($\Delta T_{1/2}$) and the depression of the transition temperature $-\Delta T = T_m - T_{m,0}$ of DPPC MLVs in the presence of LAM (X), $C_3(OA)_2$ (▲), $C_3(CA)_2$ (▼) and CHX (●).

Considering that for most cationic antimicrobial compounds the mechanism of action is similar,[12] their activity on the lipid bilayer depended on the charge of the polar head and on both the structure and hydrophobicity of the lipophilic moiety: LAM has only one charged polar group whereas $C_3(CA)_2$ has two polar groups per molecule and was more hydrophobic than $C_3(OA)_2$. As indicated above, the hydrophobicity of the side chain in $C_3(OA)_2$, was analogous to that of the CHX (log$P$ = 2.8).[13] The differences observed between these two products stressed the importance of the structure of the lipophilic moiety in the antimicrobial activity.

The variation of the enthalpy transition of DPPC bilayers caused by the solutes could not be measured with good precision. The instrument used was a conventional calorimeter and the scanning rate was 5 °C min^{-1}. It appears that lower scanning rate is required to achieve reproducible values of ΔH.[5] To confirm this observation the variation of the enthalpy transition of pure DPPC bilayers were measured with a micro-calorimeter (Micro DSC III, Setaram) at 0.5°C min^{-1}. The variation of the enthalpy transition was measured with good precision but the volume of sample required (60 μL) was higher than with the conventional calorimeter (30 μL).

In summary, the thermotropic variables of DPPC MLVs correlated well with the antimicrobial activity of the compounds under study. The most potent antimicrobial compounds, $C_3(CA)_2$ and CHX, showed the highest partition into the lipid membrane (*i.e.* the highest K values) and the greatest widening of the transition width ($\Delta T_{1/2}$) with the decrease of the transition temperature (T_m).

3.1.3. Interaction of $C_3(CA)_2$ and CHX with unilamellar lipid vesicles

Previously, the gemini surfactant $C_3(CA)_2$ and the antiseptic CHX displayed high interaction with DPPC MLVs. At this point, our interest was focused on the assessment of the ability of $C_3(CA)_2$ to increase the fluidity of DPPC vesicles using another different technique. With this aim, leakage assays of encapsulated material in large unilamellar vesicles (LUVs) caused by $C_3(CA)_2$

were performed. For the sake of comparison, the effect caused by CHX was also studied.

The ANTS fluorescent dye and the DPX quencher were co-encapsulated in DPPC LUVs. The effect of $C_3(CA)_2$ and CHX on the release of encapsulated content was monitored by dequenching of the ANTS. Figure 7 shows the fluorescence curves of LUVs aliquots after different additions from concentrated solutions of $C_3(CA)_2$ and CHX. Finally, Triton X-100 was added to the LUV suspension in order to dissolve the vesicles and to obtain the maximum fluorescence intensity.

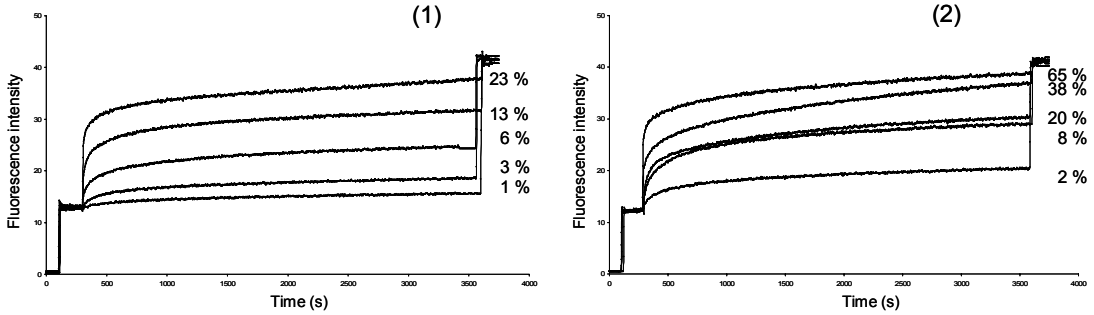

Fig. 7. Curves of fluorescence intensity of DPPC-LUVs containing fluorescent dyes in presence of (1) $C_3(CA)_2$ and (2) CHX at different mole fractions.

The ANTS-DPX leakage from DPPC LUVs induced by $C_3(CA)_2$ and CHX was calculated from the curves shown in Figure 7. Thus, the percentage of leakage was calculated using equation (3):

$$\% \text{ Leakage} = \frac{F_f - F_0}{F_{100} - F_0} \times 100 \qquad (3)$$

where:

F_f is the fluorescence intensity after adding the solute, F_0 is the initial fluorescence and F_{100} is the fluorescence after the addition of Triton X-100.

As shown in Figure 8, $C_3(CA)_2$ showed higher ability than CHX to release the encapsulated material from DPPC LUVs. As example, the 50 % of leakage was achieved with 8 mol % of $C_3(CA)_2$ while 29 mol % of CHX was required to achieve the same percentage of leakage. Although both compounds are cationic

amphiphiles, the excellent surfactant properties of $C_3(CA)_2$ could enhance its interaction with DPPC LUVs.

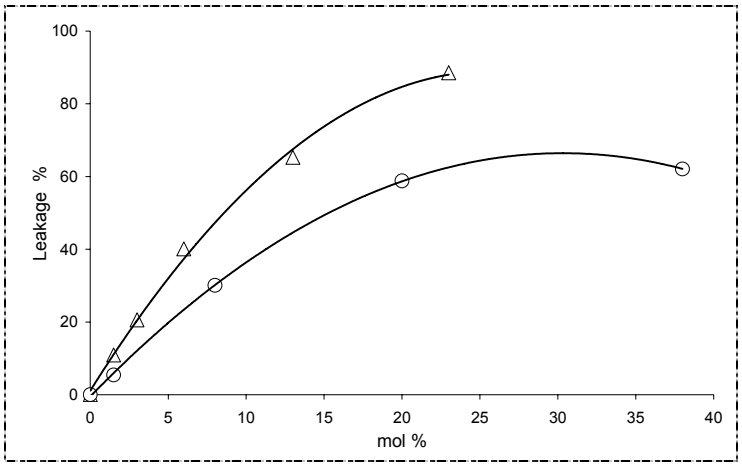

Fig. 8. Leakage percentage of encapsulated ANTS-DPX from DPPC LUVs in presence of $C_3(CA)_2$ (Δ) and CHX (O).

3.1.4. Interaction of arginine-based surfactants with lipid monolayers

As demonstrated thus far, lipid multilamellar vesicles are suitable membrane models for studying interactions of biologically active molecules with lipid membranes. However, they suffer from several limitations. For instance, the range over which the lipid composition can be varied without modifying the surface curvature and phase state is limited. Besides, the degree of lipid packing is not uniform along the bilayer[14,15] and the physical state of compositionally identical bilayer dispersions depends on the method of preparation.[15] Moreover, some lipids may not form stable multilamellar vesicles suitable for DSC studies. Lipid monolayers can overcome these limitations being considered as an excellent model system to study the interactions of active compounds with different lipid compositions at the air/water interface. Consequently, phospholipid monolayer is another membrane model widely used to study the interaction of membrane-active agents with phospholipids.

Here, three different phospholipids were employed to investigate their interaction with the selected compounds. DPPC and DPPG as zwitterionic and anionic phospholipids, respectively, and a total lipid extract from *Escherichia*

coli were also employed. The interaction between the tested compounds and the phospholipid monolayers was studied carrying out kinetic penetrations and compression isotherms. Before, it was necessary to determine the optimal compound concentration. With this purpose, the surface activity of the compounds was measured.

Surface activity

The surface activity or accumulation at the air/water interface of the selected compounds was assessed. To this end, different volumes of concentrated solutions of LAM, $C_3(CA)_2$, $C_3(OA)_2$, HTAB and CHX were injected into the PBS subphase and the pressure increases were recorded as a function of time. On increasing the amount of the tested compounds the surface pressure increased up to a saturation surface pressure. Figure 9a is an example of the pressure curves obtained for different concentrations of $C_3(CA)_2$. Here, at the lowest concentration assayed the maximum surface pressure was not achieved even after 60 min due to its high aqueous solubility (see Figures S.9.a. for other compounds in pages 92-96). From these plots, the curves of the surface pressure as a function of the product concentration were obtained (see Figure 9b as example and Figures S.9.b for other compounds in pages 92-96).

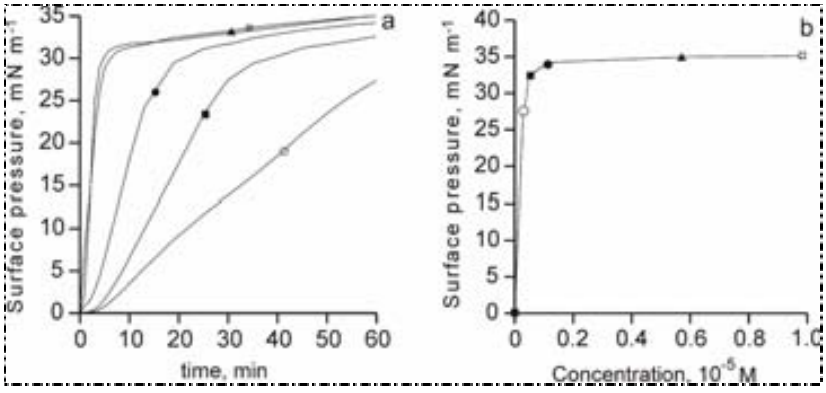

Fig. 9. (a) Surface activity of $C_3(CA)_2$ as a function of time at different concentrations: $1x10^{-5}$ M (□), $5.7x10^{-6}$ M (▲), $1.1x10^{-6}$ M (●), $5.7x10^{-7}$ M (■) and $2.9x10^{-7}$ M (○) and (b) surface pressure increases as a function of $C_3(CA)_2$ concentration.

Surface pressure at the saturation point for the compounds under study is summarized in Table 3. The results obtained may be explained considering the number of methylene groups in the hydrophobic side chains in relation with the polar head. HTAB, with an aliphatic chain of 14 methylene groups, gave a surface pressure higher than that of LAM with 10 methylene groups. Similarly, the two side chains attached to the central unity of $C_3(CA)_2$ account for a total of 16 methylene groups, thus explaining the remarkable surface activity of this compound. Compared to $C_3(CA)_2$, the lower ability of $C_3(OA)_2$ to accumulate at air-water interface may be related to its shorter side chains.

Finally, CHX showed low capacity to diminish surface tension, as expected from the inclusion of a chlorobenzene unit instead of a long aliphatic side chain. The lipophilicity (octanol/water partition coefficient (log*P*)) of the side chain in $C_3(OA)_2$, which was estimated[13] to be around 3.5 is close to the lipophilicity of the side chain of CHX (*i.e.*, chlorobenzene) (log*P* = 2.8), explaining their similar surface activity.

The surface activity data provided information on the suitable concentration of each compound that should be used in the bulk subphase for the experiments on the interaction with phospholipid monolayers (*i.e.* penetration kinetics and compression isotherms). This optimal concentration was the one that gave the *ca.* 80 % of the maximum surface pressure (80 % saturation concentration). In all cases, this concentration was ~ $3x10^{-5}$ M, except for $C_3(CA)_2$; 10^{-6} M. This result indicates the excellent surface properties of $C_3(CA)_2$ (see Table 3). Under these conditions, both the saturation of the product in the trough and the formation of domains were avoided.[16] The optimal concentrations for each product, calculated from pressure/concentration curves fell well below their respective critical micelle concentrations (CMC).

Table 3. Surface pressure at saturation concentration, at *ca.* 80 % saturation concentration and the CMC for each antimicrobial compound.

Product	Saturation conc. / M	Surface pressure / mN m^{-1}	80% saturation conc. / M	Surface pressure[a] / mN m^{-1}	CMC[b] /M
LAM	$4.5x10^{-5}$	29.3	$3.6x10^{-5}$	22.4	$60.0x10^{-4}$ [c]
$C_3(OA)_2$	$11.0x10^{-5}$	19.7	$3.4x10^{-5}$	15.5	$7.0\ x10^{-4}$ [d]
$C_3(CA)_2$	$0.6\ x10^{-5}$	34.2	$0.1x10^{-5}$	24.3	$0.3\ x10^{-4}$ [d]
HTAB	$4.1\ x10^{-5}$	31.9	$3.7x10^{-5}$	27.2	$10.0\ x10^{-4}$ [e]
CHX	$17.0\ x10^{-5}$	18.0	$4.0x10^{-5}$	16.8	$100.0\ x10^{-4}$ [f]

[a]Approximate values corresponding to 80 % saturation concentration, [b]At 25°C, [c]Reference[17], [d]CMC were measured in water at 25 °C using a tensiometer (Krúss K-12) with a Wilhelmy plate, [e]Reference[18], [f]Reference[19]

Penetration kinetics at constant area

The interaction of the selected products with monolayers of DPPC, DPPG and *E. coli* total lipid extract was studied first by analyzing the penetration kinetics at constant area. We chose both zwitterionic DPPC and anionic DPPG phospholipids to compare the effect of the electrostatic interaction with the cationic compounds. It is noticeable that negatively charged phospholipids are the major components of bacterial membranes, whereas zwitterionic lipids are of mammalian membranes.[20]

E. coli total lipid extract was also investigated because it resembles a real biomembrane closer than pure lipids. The concentration of each compound in the subphase was the corresponding at *ca.* 80 % saturation concentration (Table 3). Figures 10a-c depict the surface pressure increases ($\Delta\pi$) 30 min after injection of the compounds in the subphase *versus* the initial lipid pressure (π_0) of 5, 10, 20 and 32 mN m^{-1} of DPPC, DPPG and *E. coli* lipid extract monolayers.

From these results, the exclusion density (σ_{ex}) was determined as previously described by Maget-Dana *et al.*[14] The plots of the pressure increases as a function of the initial densities of the lipids, gave straight lines of negative

slope. The intercept of these lines with the X-axis defines the monolayer σ_{ex}. This parameter indicates the lipid film density at which the compound no longer penetrates and it is useful for comparing the relative penetration of a compound in various lipid monolayers. The calculated values of σ_{ex} for each antimicrobial compound are summarized in Table 4.

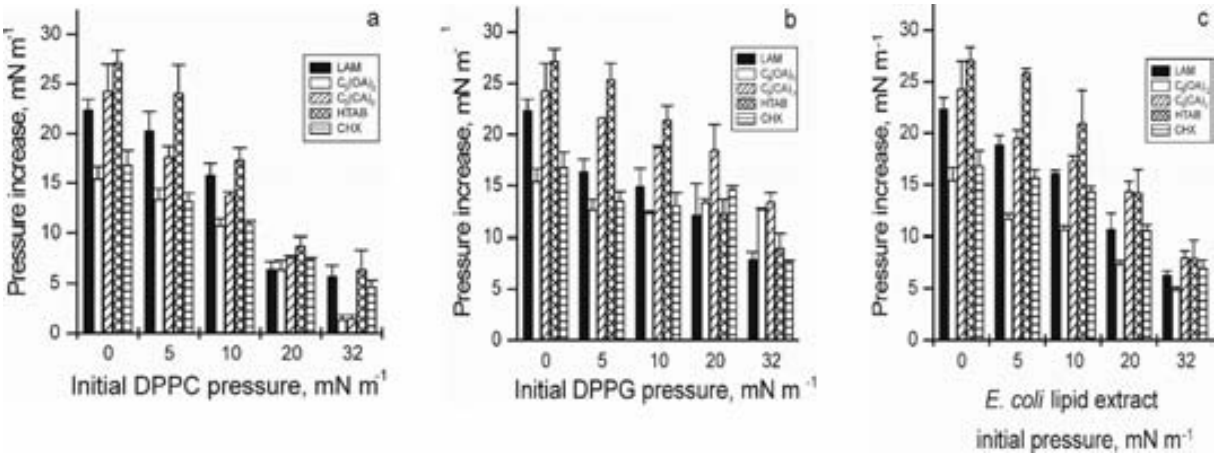

Fig. 10a-c. Surface pressure increases ($\Delta\pi$) 30 min after injection of the compounds in the subphase versus the initial lipid pressure (π_0) of 5, 10, 20 and 32 mN m^{-1} of DPPC, DPPG and *E. coli* lipid extract monolayers.

As a general trend, the higher the initial monolayer pressure, the lower the pressure increase, because of the increasing packing density of the lipid molecules. Moreover, the σ_{ex} values (see Table 4 and Figures S.10 in pages 97-98) show that the compounds incorporate better into the anionic DPPG monolayer than into zwitterionic DPPC.

For DPPC monolayers (see Fig. 10a and Fig. S.10.1 in page 97), the pressure increases raised in the order $C_3(OA)_2 \approx$ CHX < $C_3(CA)_2$ < LAM < HTAB indicating a low penetration capacity of gemini compounds. Here, it appears that the differences between gemini and single chain structures arise mostly from steric hindrance.

For DPPG monolayers (see Fig. 10b and Fig. S.10.2. in page 97) at π_0 = 5 and 10 mN m^{-1}, the highest pressure increases were observed for HTAB and $C_3(CA)_2$, whereas at π_0 = 32 mN m^{-1} $C_3(CA)_2$ and $C_3(OA)_2$ were the most active

compounds. According to σ_{ex} (Table 4) the incorporation of the compounds into the DPPG monolayer was higher for the gemini compounds than that for the single chain surfactants. This reflects that electrostatic interactions are predominant over the steric effects between the DPPG and the surfactant. Both, $C_3(CA)_2$ and $C_3(OA)_2$ have two positive charges per molecule against one of LAM and HTAB. CHX had lower interaction than that of arginine-based gemini surfactants, despite of having also two positive charges. This may be due to the lack of the long lineal hydrophobic chains and therefore, a different conformation may presumably be adopted at the air/water interface.

The penetration of the compounds in *E. coli* lipid extract monolayers at π_0 = 32 mN m^{-1} (see Figure 10c and Figure S.10.3. in page 98) was between that found in DPPC and DPPG. The surface pressure increase at π_0 = 32 mN m^{-1} raised in the order $C_3(OA)_2$ < LAM < CHX < $C_3(CA)_2$ ≈ HTAB but the differences between the most active antimicrobials CHX and $C_3(CA)_2$ were small. The σ_{ex} values (Table 4) indicated, however, that the incorporation of the products into this monolayer was lower than that with either DPPC or DPPG.

Table 4. Exclusion density (σ_{ex}) of the tested compounds in DPPC, DPPG and *E. coli* total lipid extract monolayers.

Product	σ_{ex} DPPC / molec nm^{-2}	σ_{ex} DPPG / molec nm^{-2}	σ_{ex} *E. coli* extract/ molec nm^{-2}
LAM	2.4 ± 0.2	3.0 ± 0.6	1.8 ± 0.1
$C_3(OA)_2$	2.3 ± 0.1	9.2 ± 0.5	1.8 ± 0.1
$C_3(CA)_2$	2.2 ± 0.1	4.5 ± 0.6	1.9 ± 0.1
HTAB	2.4 ± 0.1	2.9 ± 0.1	1.8 ± 0.2
CHX	2.6 ± 0.1	3.4 ± 0.2	2.1 ± 0.2

The exclusion pressure was calculated by plotting the pressure increases as a function of the initial pressure of the lipid monolayers and following the procedure used for the estimation of the exclusion density. Interestingly, the exclusion pressure in the *E. coli* monolayer was ≥ 35 mN m^{-1} for all the tested compounds. Considering that the packing density of biological membranes is around 32 mN m^{-1}, the studied compounds may insert into biomembranes.[21,22]

Compression isotherms of lipid monolayers

The shape of the compression isotherm shows the extent to which the compound is forced into the bulk subphase. If the products desorbed completely as the film was compressed, the resulting isotherm would match that to pure phospholipid. Thus, any deviation from that can be attributed to incomplete desorption of the antimicrobial.[23] Therefore, an interaction is thus expected to occur between the product and the phospholipid.

The isotherms taken from pure DPPC and DPPG (Figures 11a-b) showed the well-known phase transition from liquid-expanded (LE) to liquid-condensed (LC) phases around 7 mN m^{-1} and 90 $Å^2$ mol^{-1} of molecular area.[24] The *E. coli* total lipid extract isotherm (Fig. 11c) did not show the LE-LC transition, presumably because it was a mixture of three different phospholipids and contained a 17 % w/w of other unidentified compounds. The interaction of tested compounds with the lipid monolayers was investigated as the influence in the compression isotherms of DPPC, DPPG and *E. coli* lipid extract.

The compression isotherms obtained after spreading DPPC, DPPG and *E. coli* lipid extract on the subphases containing the compounds under study are depicted in Fig. 11a, 11b and 11c, respectively. The compound concentration was $4x10^{-5}$ M (*i.e.* ~80 % saturation concentration), except for $C_3(CA)_2$ (Figures 12a-c). Here, the 80 % saturation concentration corresponded to *ca.* $1x10^{-6}$ M, owing to its higher surface pressure (Table 3). Therefore, for the sake of clarity, the results obtained with $C_3(CA)_2$ were plotted separately.

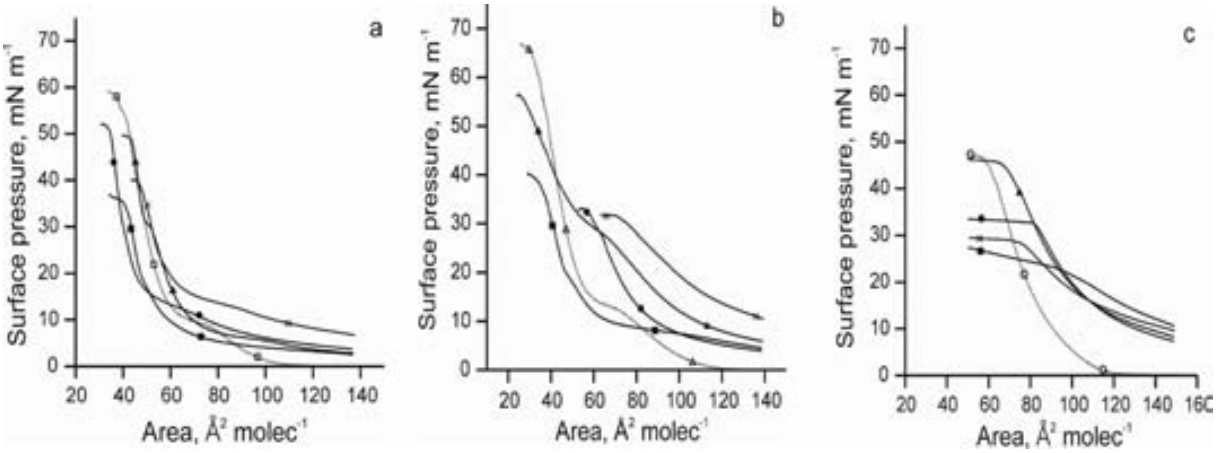

Fig. 11. Compression isotherms of (a) DPPC (□), (b) DPPG (Δ) and (c) *E coli* total lipid extract (○) monolayers (doted lines) spread on subphases containing LAM (X), $C_3(OA)_2$ (▲), HTAB (■) and CHX (●) at *ca.* 80 % saturation concentration (*ca.* $4x10^{-5}$ M).

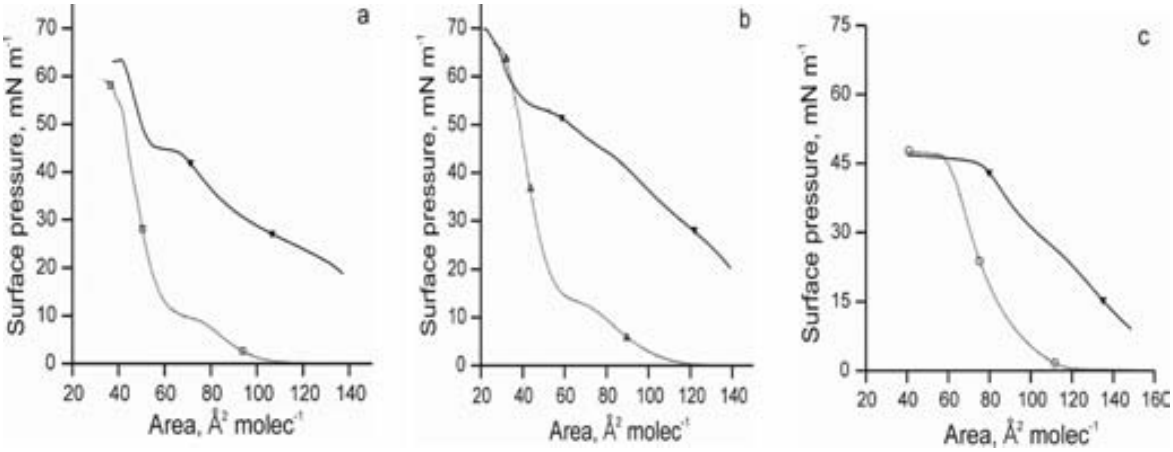

Fig. 12. Compression isotherms of (a) DPPC (□), (b) DPPG (Δ) and (c) *E coli* total lipid extract (○) monolayers (doted lines) spread on subphases containing $C_3(CA)_2$ (▼) at *ca.* 80% saturation concentration (*ca.* 10^{-6} M).

Analysis of the isotherms revealed that all the surfactants showed an immediate surface pressure increase at the onset of compression, due to its intrinsic adsorption at the air-water interface. We tried to reduce this effect by decreasing the product concentration in the subphase. However, a similar effect was noticed in experiments conducted at $1x10^{-5}$ M and $3x10^{-6}$ M corresponding to 20 % and 5 % saturation concentration, respectively, and $3x10^{-7}$ M and $5x10^{-8}$ M for $C_3(CA)_2$ (see Figures S.11. and S.12. in pages 98-105). Analogous findings were obtained with neutral surfactants such as nonoxynol-9 and C31G (equimolar mixture of C14 amine oxide and C16 alkyl betaine).[16]

The presence of the compounds in the subphase shifted the lipid monolayers to higher area/molecular values (*i.e.* expansion effect) compared to isotherms obtained in the absence of product. This effect was reflected as a decrease in the compressibility moduli (C_s^{-1}) of the monolayer, calculated using equation (4)[25] and summarized in Table 5.

$$C_s^{-1} = -A(\partial\Pi/\partial A)_T \qquad (4)$$

where A is the molecular area and Π is the surface pressure.

Table 5. Compressibility moduli (C_s^{-1}) of DPPC, DPPG and *E. coli* lipid extract monolayers spread in the presence, at *ca.* 80% saturation concentration, or absence of cationic compounds.

Π (mN/m)	Subphase PBS	Subphase LAM	Subphase $C_3(OA)_2$	Subphase $C_3(CA)_2$	Subphase HTAB	Subphase CHX
			DPPC			
10	6	14	24		42	21
20	89	47	91	51	89	65
30	138	113	40	25	128	115
40	154	35	197	48	2	138
50	115			72		66
60	16			66		
			DPPG			
10	39	21	25			
20	58	38	56	82	14	33
30	91	30	36	75	41	75
40	116		41	32	44	45
50	110			22	8	
60	38			37		
			E. coli extract			
10	45	16	16	69	48	36
20	90	36	40	53	34	51
30	83	1	73	38		75
40	96		40	64		

For HTAB, CHX and $C_3(OA)_2$ a shift towards lower values of area/molecule appeared in the DPPC or DPPG compression isotherm (Figure 11a-b). This indicates an ejection of the product and lipid molecules from the monolayer to the subphase, probably by the formation of mixed micelles. $C_3(CA)_2$ always produced an expansion of the lipid monolayers regardless on the pressure and type of phospholipid, indicating the insertion of the surfactant into the monolayer (Figures 12a-c).

The collapse pressure and the variation of the LE-LC phase transition were a function of both the compound and the lipid. Overall, the higher the concentration of the compound in the subphase, the lower the collapse pressure observed (Table 6).

Table 6. Collapse pressure (mN m^{-1}) of DPPC, DPPG and *E. coli* total lipid extract monolayers at *ca.* 80, 20 and 5 % saturation concentration of the antimicrobial compounds at the subphase.

	DPPC (60 mN m^{-1})[a]			DPPG (67 mN m^{-1})[a]			*E.coli extract* (48 mN m^{-1})[a]		
Product	80 %	20 %	5 %	80 %	20 %	5 %	80 %	20 %	5 %
LAM	40	59	61	32	57	57	30	44	46
$C_3(OA)_2$	49	55	65	56	61	67	46	47	49
$C_3(CA)_2$	63	63	60	70	71	70	47	47	48
HTAB	36	53	63	40	43	58	28	40	46
CHX	52	60	63	32	39	43	34	43	46

[a]Collapse pressure of the pure lipid monolayer.

Moreover, the LE-LC phase transition pressure tended to increase or disappear on increasing the product concentration. CHX abolished the LE-LC transition and reduced the collapse pressure regardless on the concentration, especially in DPPG monolayers. On the other hand, $C_3(CA)_2$ did not reduce the collapse pressure and the LE-LC transition shifted to higher pressures. Here, $C_3(CA)_2$ may hinder the reorientation of the alkyl chain of the lipids from horizontal to vertical position.[26]

The effects observed on the monolayer such as expansion, collapse pressure decrease and LE-LC phase transition modification reflect a clear destabilization of the monolayer packing by the compounds under investigation. As shown in Figures 11a-b and 12a-b, all these perturbing effects were more important in DPPG than in DPPC, as a result of the electrostatic interactions in agreement with the previous results on penetration kinetics.

The expansion of the DPPC and DPPG monolayers increased in the order $C_3(OA)_2$ < LAM ≈ HTAB ≈ CHX < $C_3(CA)_2$ and the collapse pressure decreased in the order $C_3(CA)_2$ > $C_3(OA)_2$ > LAM ≈ HTAB ≈ CHX. The expansion of the *E. coli* lipid extract monolayers increased in the order $C_3(OA)_2$ ≈ LAM ≈ CHX < HTAB < $C_3(CA)_2$ and the collapse pressure decreased in the order $C_3(CA)_2$ ≈ $C_3(OA)_2$ > LAM ≈ HTAB ≈ CHX. Consequently, the compounds with the highest antimicrobial activity caused a large expansion of the lipid monolayer or a large decrease in its collapse pressure together with a strong suppression of the LE-LC phase transition.

In summary, the penetration kinetics studies indicate that the antimicrobials incorporated better into anionic DPPG than into zwitterionic DPPC lipid monolayers. Here, mostly electrostatic forces governed the lipid-antimicrobial interaction. Concerning the compression isotherms, the highest expansion of the lipid monolayer was observed with the most active antimicrobial derived from arginine $C_3(CA)_2$, but this compound did not reduce the collapse pressure On the other hand, CHX reduced the collapse pressure and strongly suppressed the LC-LE phase transition. From the results obtained with lipid monolayers, a relation between the physicochemical properties with the antimicrobial activity was unclear.

References:

1. Lohner, K.; Prenner, E. J., Differential scanning calorimetry and X-ray diffraction studies of the specificity of the interaction of antimicrobial peptides with membrane-mimetic systems. *Biochim. Biophys. Acta: Biomembranes* **1999**, *1462*, 141-156.
2. Morán, C.; Clapés, P.; Comelles, F.; García, T.; Pérez, L.; Vinardell, P.;

Mitjans, M.; Infante, M. R., Chemical Structure/Property Relationship in Single-Chain Arginine Surfactants. *Langmuir* **2001**, *17*, 5071-5075.
3. Infante, M. R.; Pinazo, A.; Seguer, J., Non-conventional surfactants from amino acids and glycolipids: Structure, preparation and properties. *Colloids Surf. A* **1997**, *123-124*, 49-70.
4. Pérez, L.; García, M. T.; Ribosa, I.; Vinardell, M. P.; Manresa, A.; Infante, M. R., Biological properties of arginine-based gemini cationic surfactants. *Environ. Toxicol. Chem.* **2002**, *21*, 1279-1285.
5. Lo, Y.-L.; Rahman, Y.-E., Protein Location in Liposomes, A Drug carrier: A Prediction by Differential Scanning Calorimetry. *J. Pharm. Sci.* **1995**, *804*, 805-814.
6. Pedersen, T. B.; Sabra, M. C.; Frokjaer, S.; Mouritsen, O. G.; Jorgensen, K., Association of acylated cationic decapeptides with dipalmitoylphosphatidylserine-dipalmitoylphosphatidylcholine lipid membranes. *Chem. Phys. Lipids* **2001**, *113*, 83-95.
7. Ramaswami, V.; Haaseth, R. C.; Matsunaga, T. O.; Hruby, V. J.; O'Brien, D. F., Opioid peptide interactions with lipid bilayer membranes. *Biochim. Biophys. Acta: Biomembranes* **1992**, *1109*, 195-202.
8. Inoue, T.; Miyakawa, K.; Shimozawa, R., Interaction of surfactants with vesicle membrane of dipalmitoylphosphatidylcholine. Effect on gel-to-liquid-crystalline phase transition of lipid bilayer. *Chem. Phys. Lipids* **1986**, *42*, 261-270.
9. Lohner, K., Effects of small organic molecules on phospholipid phase transitions. *Chem. Phys. Lipids* **1991**, *57*, 341-362.
10. McIntosh, T. J.; Simon, S. A.; MacDonald, R. C., The organization of n-alkanes in lipid bilayers. *Biochim. Biophys. Acta: Biomembranes* **1980**, *597*, 445-463.
11. Inoue, T.; Iwanaga, T.; Fukushima, K.; Shimozawa, R., Effect of sodium octanoate and sodium perfluorooctanoate on gel-to-liquid-crystalline phase transition of dipalmitoylphosphatidylcholine vesicle membrane. *Chem. Phys. Lipids* **1988**, *46*, 25-30.
12. McDonnell, G.; Russell, A., D., Antiseptics and disinfectants: activity and resistance. *Clin. Microbiol. Rev.* **1999**, *12*, 147-179.
13. Leo, X. A.; Hansch, C.; Elkins, D., Partition coefficients and their uses *Chem. Rev.* **1971**, *71*, 525.
14. Maget-Dana, R., The monolayer technique: a potent tool for studying the interfacial properties of antimicrobial and membrane-lytic peptides and their interactions with lipid membranes. *Biochim. Biophys. Acta: Biomembranes* **1999**, *1462*, 109-140.
15. Brockman, H., Lipid monolayers: why use half a membrane to characterize protein-membrane interactions? *Curr. Opin. Struct. Biol.* **1999**, *9*, 438-443.
16. McConlogue, C. W.; Vanderlick, T. K., Monolayers with one component of variable solubility: studies of lysophosphocholine/DPPC mixtures. *Langmuir* **1998**, *14*, 6556 -6562
17. Pinazo, A.; Wen, X.; L., P.; R., I. M.; Franses, E. I., Aggregation behavior in water of monomeric and gemini cationic surfactants derived from arginine. *Langmuir* **1999**, *15*, 3134-3142.
18. Fang, L.; Li, G.-Z.; Wang, H.-Q.; Xue, Q.-J., Studies on cetyltrimethylammonium bromide (CTAB) micellar solution and CTAB reversed

microemulsion by ESR and 2H NMR. *Colloids Surf. A:* **1997**, *127*, 89-96.
19. Heard, D. D.; Ashworth, R. W., The colloidal properties of chlorhexidine and its interaction with some macromolecules. *J. Pharm. Pharmacol.* **1968**, *20,* 505-512.
20. Oren, Z.; Hong, J.; Shai, Y., A repertoire of novel antibacterial diastereomeric peptides with selective cytolytic activity. *J. Biol. Chem.* **1997**, *272*, 14643-14649.
21. Demel, R. A.; Peelen, T.; J., S. R.; De Kruijff, B.; Kuipers, O. P., Nisin Z, mutant nisin Z and lacticin 481 interactions with anionic lipids correlate with antimicrobial activity. A monolayer study. *Eur. J. Biochem.* **1996**, *235*, 267-274.
22. Marsh, D., Lateral pressure in membranes. *Biochim. Biophys Acta:* **1996**, *1286*, 183-223.
23. McConlogue, C. W.; Malamud, D.; Vanderlick, T. K., Interaction of DPPC monolayers with soluble surfactants: electrostatic effects of membrane perturbants. *Biochim. Biophys. Acta: Biomembranes* **1998**, *1372*, 124-134.
24. Sospedra, P.; Espina, M.; Gomara, M. J.; Alsina, M. A.; Haro, I.; Mestres, C., Study at the Air/Water Interface of a Hepatitis A *N*-Acetylated and *C*-Amidated Synthetic Peptide (AcVP3(110-121)-NH2): II. Miscibility in Lipid Monolayers. *J. Colloid Interface Sci.* **2001**, *244*, 87-96.
25. Sospedra, P.; Espina, M.; Alsina, M. A.; Haro, I.; Mestres, C., Study at the Air/Water Interface of a Hepatitis A *N*-Acetylated and *C*-Amidated Synthetic Peptide (AcVP3(110-121)-NH2): I. Surface Activity and Insertion in Lipid Monolayers. *J. Colloid Interface Sci.* **2001**, *244*, 79-86.
26. Miñones Jr., J.; Dynarowicz-Latka, P.; Conde, O.; Miñones, J.; Iribarnegaray, E.; Casas, M., Interactions of amphotericin B with saturated and unsaturated phosphatidylcholines at the air/water interface. *Colloids Surf. B:* **2003**, *29*, 205-215.

3.1.5. Supplemenray information

Fig. S.2.1. Differential scanning calorimetry (DSC) curves obtained with DPPC-LAM systems. Molar percentage of LAM ranged from 0 to 30 %.

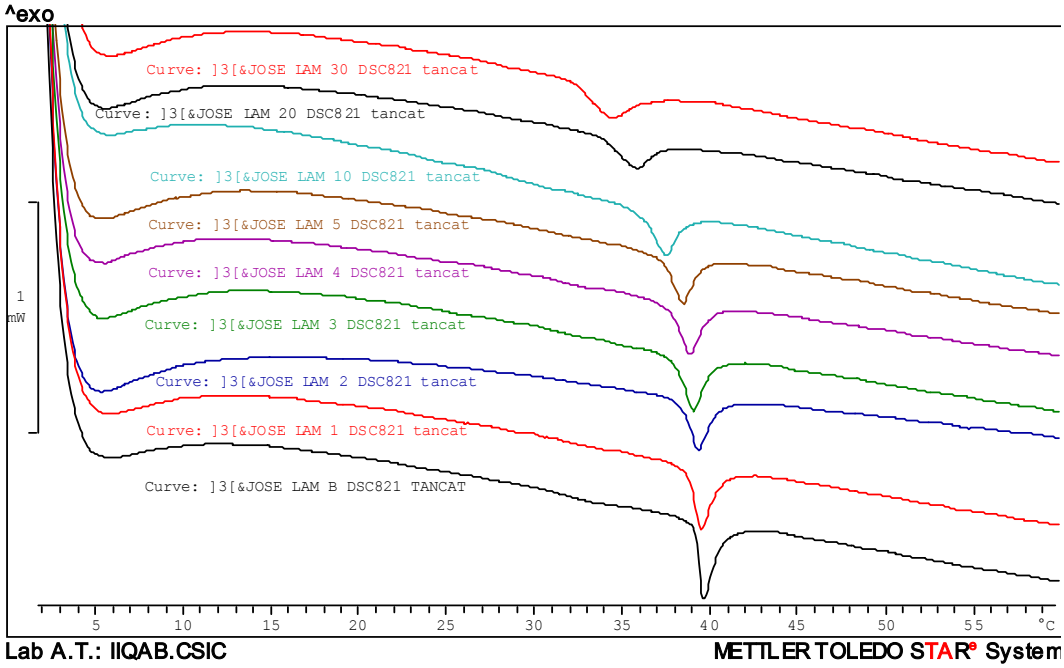

Fig. S.2.2. Differential scanning calorimetry (DSC) curves obtained with DPPC-$C_3(OA)_2$ systems. Molar percentage of $C_3(OA)_2$ ranged from 0 to 5 %.

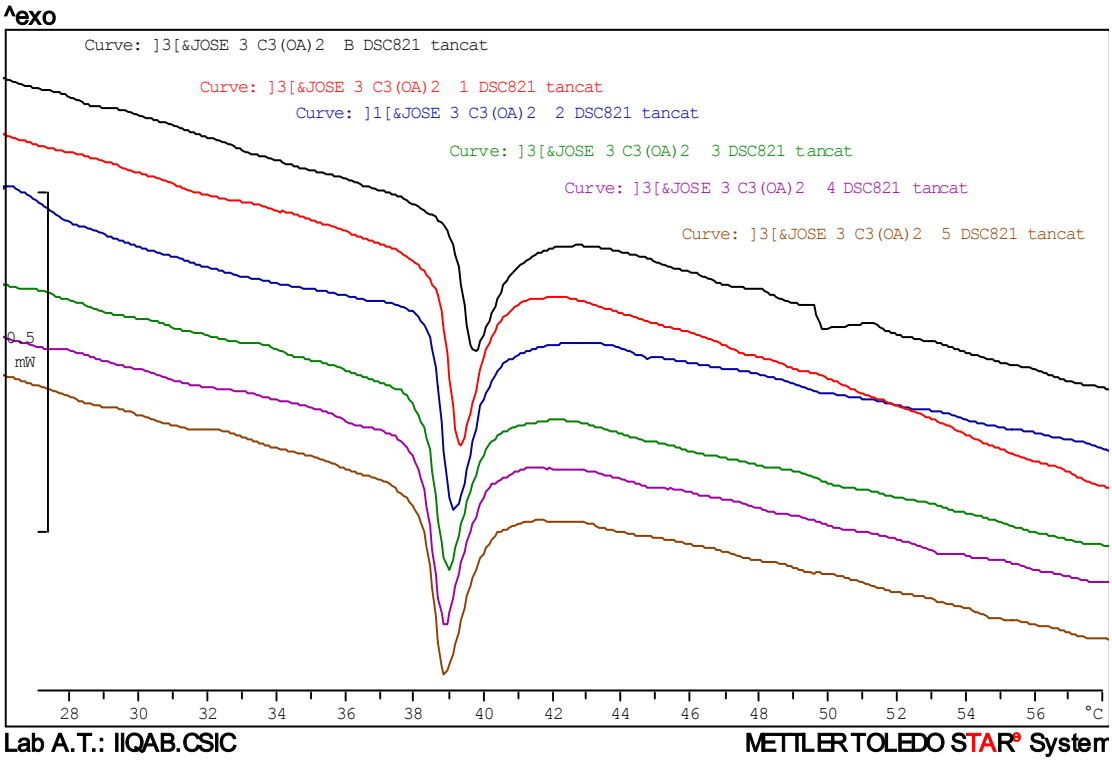

Fig. S.2.3. Differential scanning calorimetry (DSC) curves obtained with DPPC-$C_3(OA)_2$ systems. Molar percentage of $C_3(OA)_2$ ranged from 0 to 30 %.

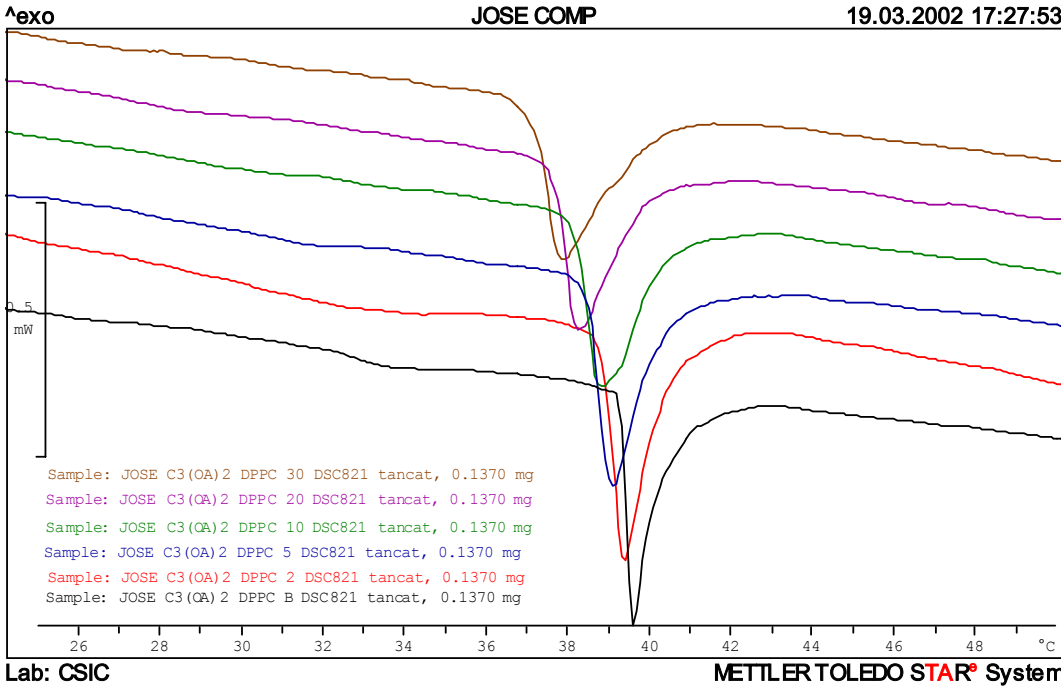

Fig. S.2.4. Differential scanning calorimetry (DSC) curves obtained with DPPC-$C_3(CA)_2$ systems. Molar percentage of $C_3(CA)_2$ ranged from 0 to 5 %.

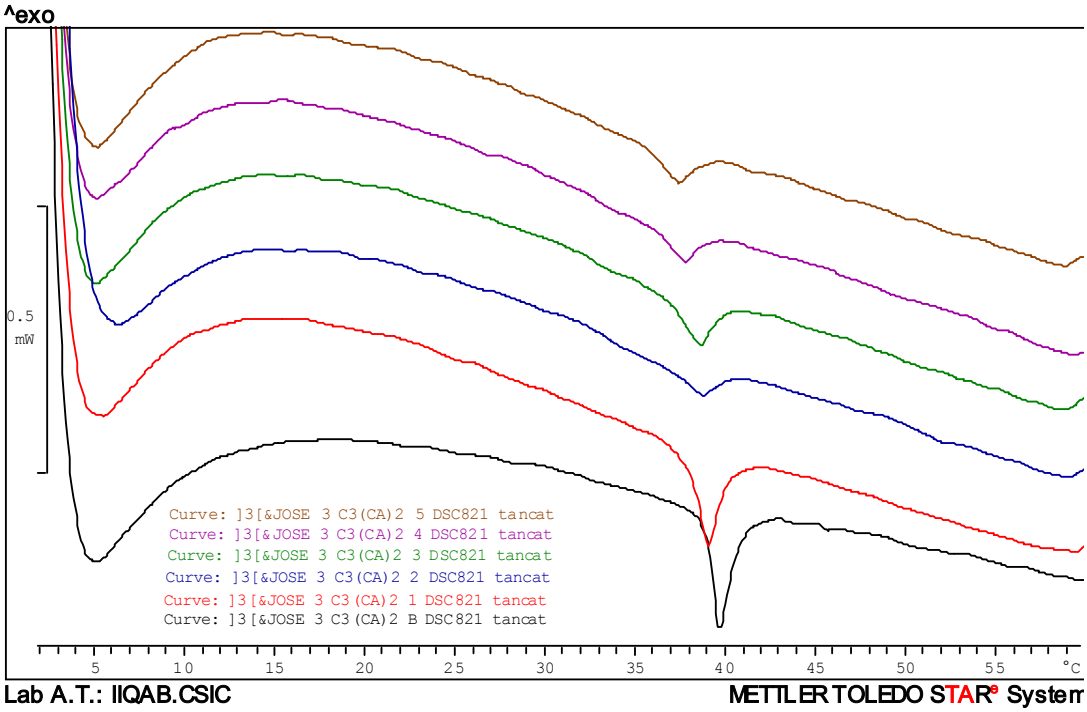

Fig. S.2.5. Differential scanning calorimetry (DSC) curves obtained with DPPC-$C_3(CA)_2$ systems. Molar percentage of $C_3(CA)_2$ ranged from 0 to 30 %.

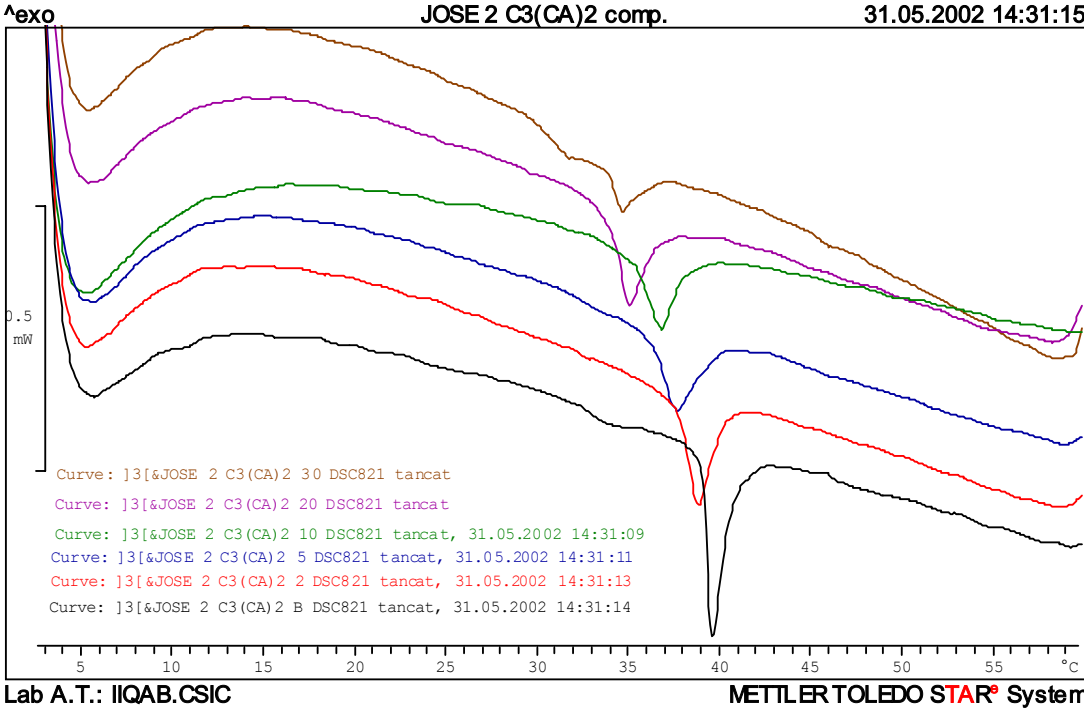

Fig. S.2.6. Differential scanning calorimetry (DSC) curves obtained with DPPC-HTAB systems. Molar percentage of HTAB ranged from 0 to 30 %.

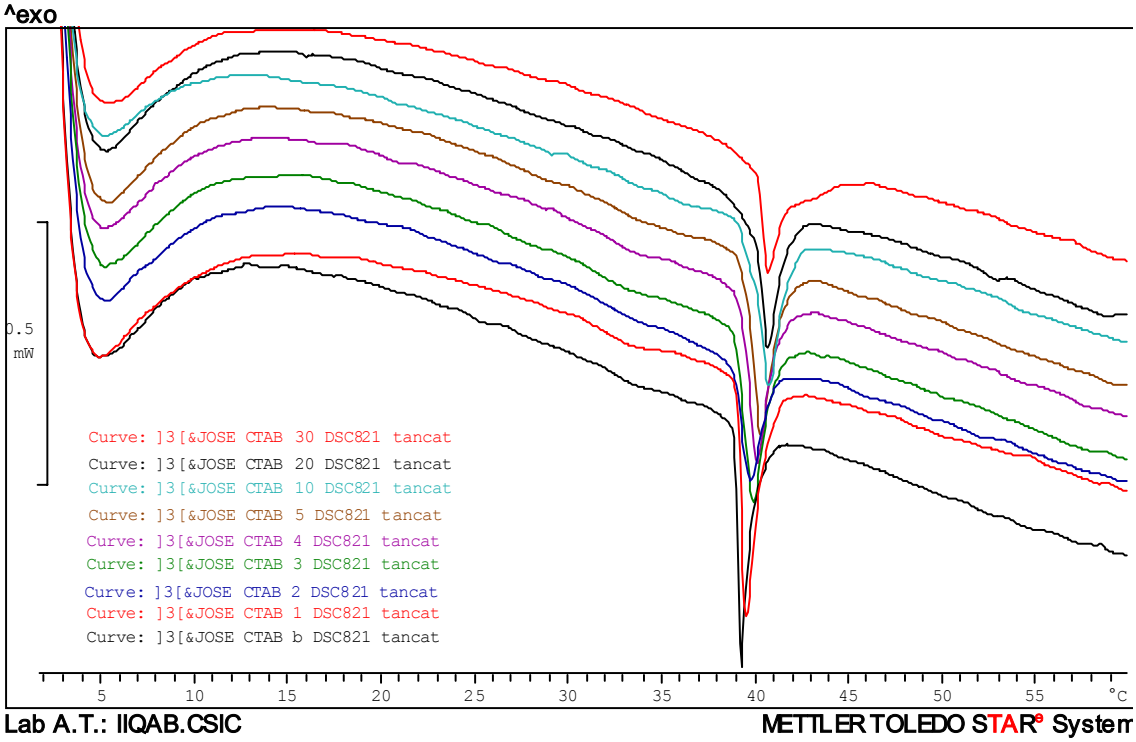

Fig. S.2.7. Differential scanning calorimetry (DSC) curves obtained with DPPC-$C_3(OA)_2$ systems. Molar percentage of CHX ranged from 0 to 30 %.

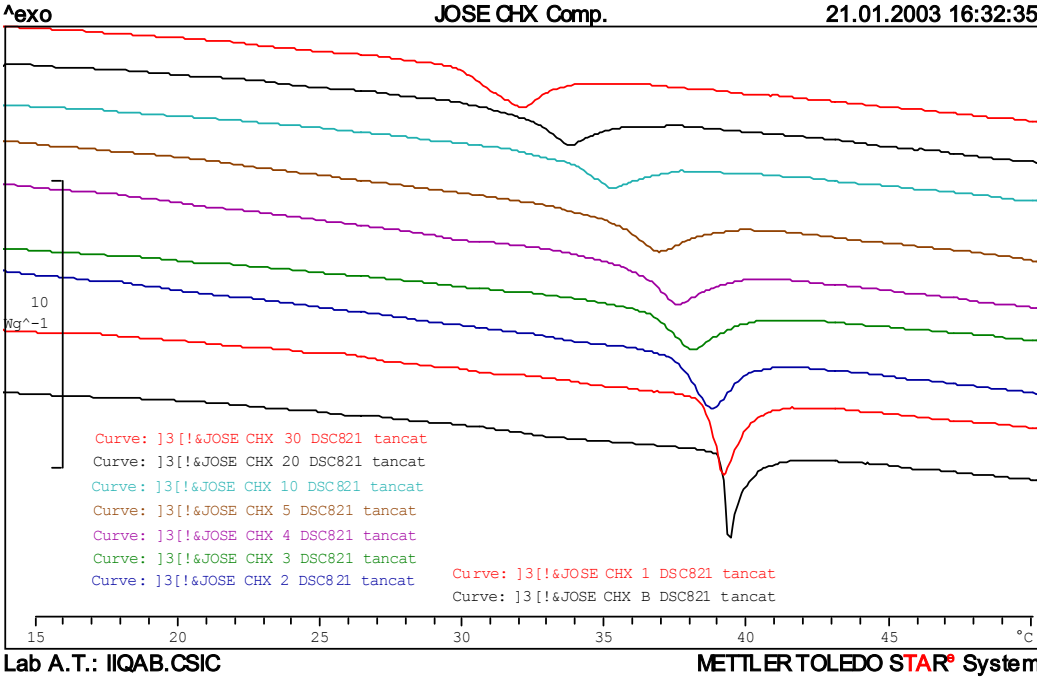

Fig. S.2.8. Differential scanning calorimetry (DSC) curves obtained with DPPC-DTAB systems. Molar percentage of DTAB ranged from 0 to 20 %.

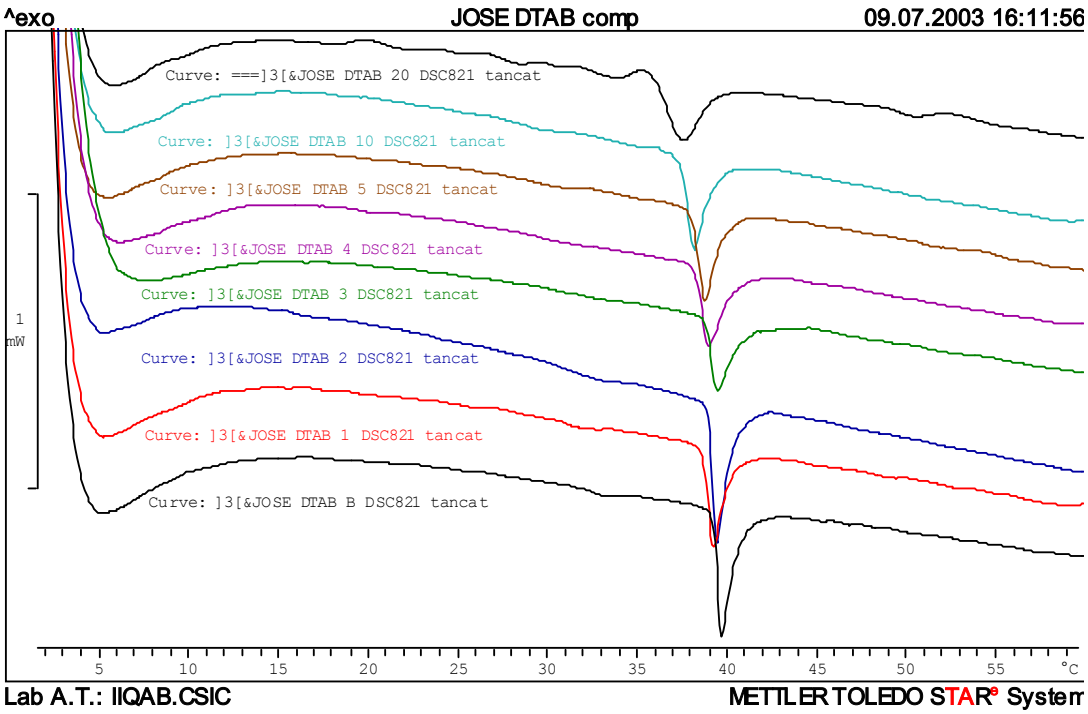

Fig. S.9.1.(a) Surface activity of LAM as a function of time at different concentrations (Note: 1 E-5 M = 10^{-5} M).

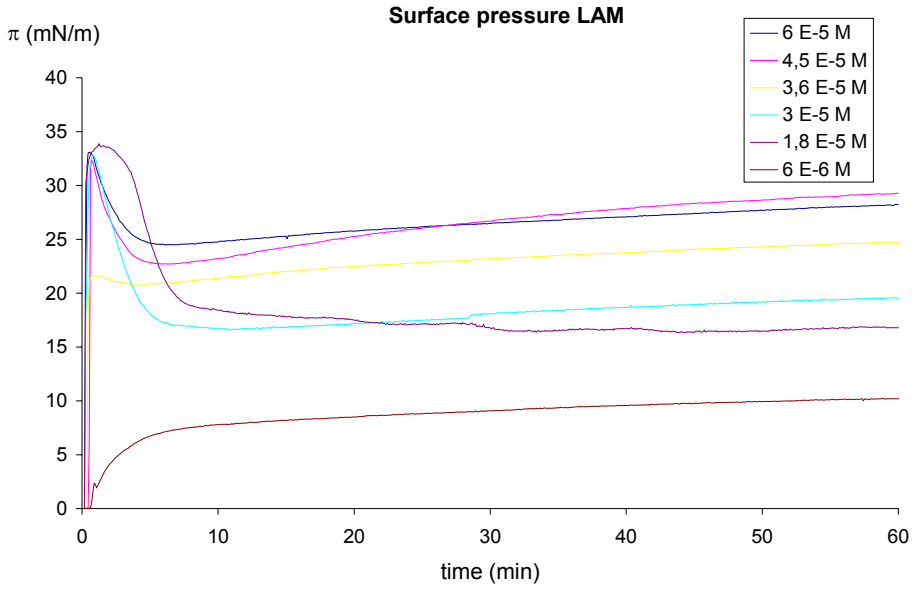

Fig. S.9.1.(b) Surface pressure increases as a function of LAM concentration.

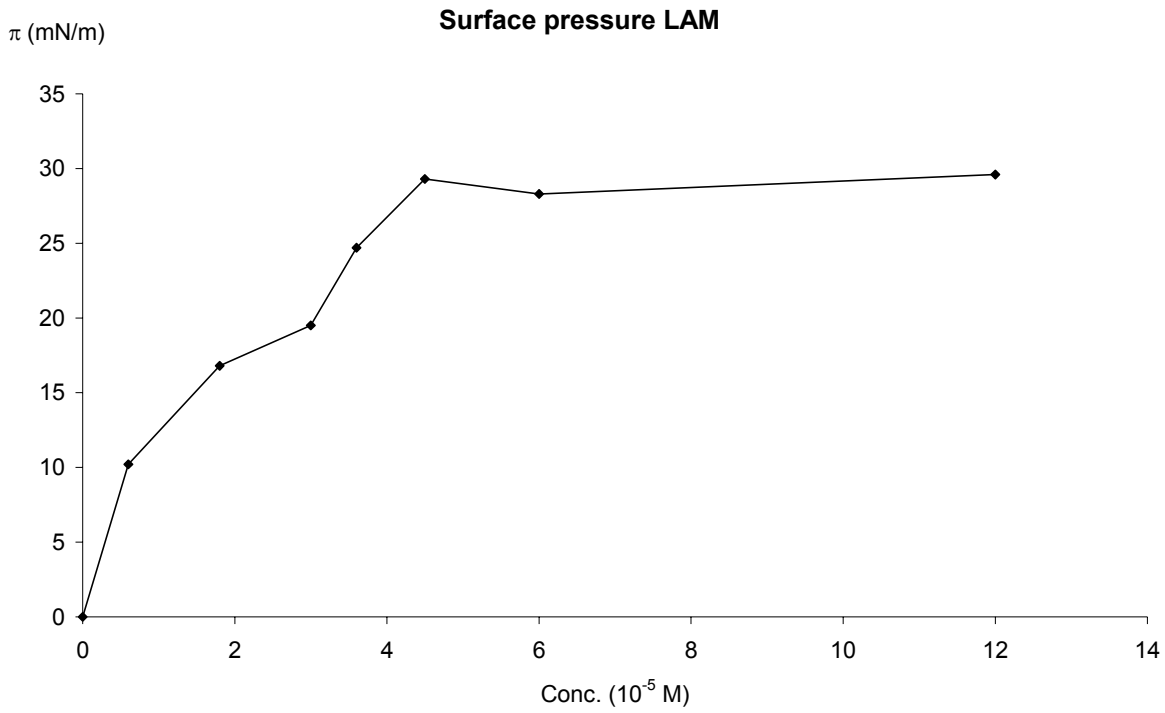

Fig. S.9.2.(a) Surface activity of $C_3(OA)_2$ as a function of time at different concentrations (Note: 1 E-5 M = 10^{-5} M).

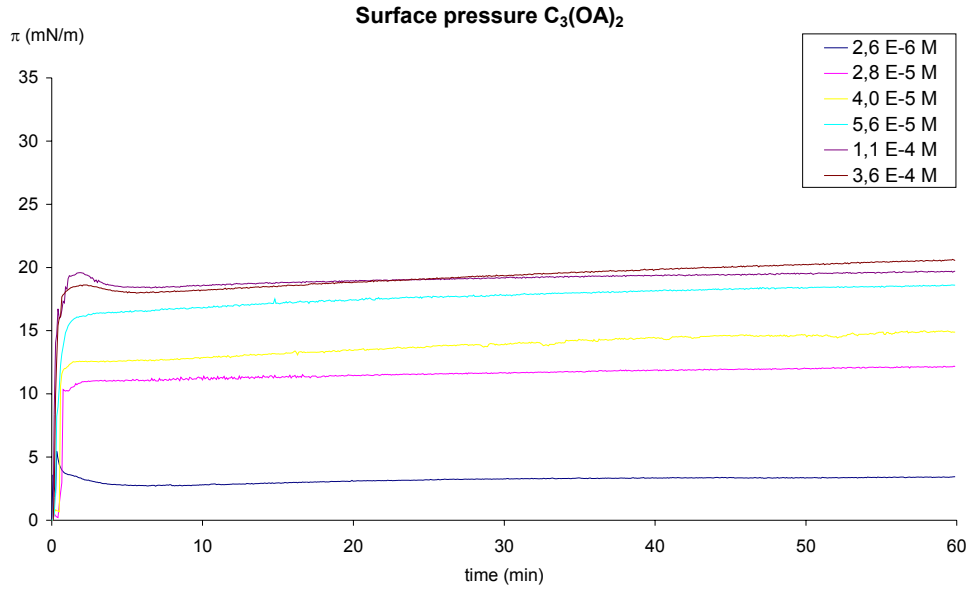

Fig. S.9.2.(b) Surface pressure increases as a function of $C_3(OA)_2$ concentration.

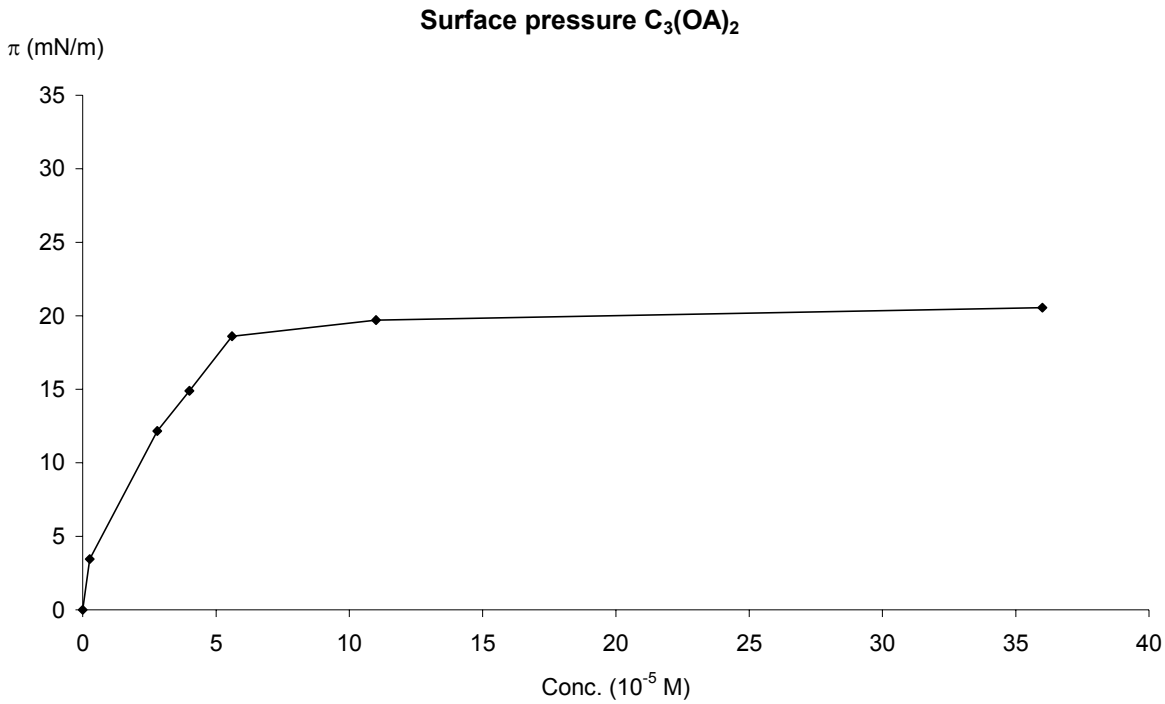

Fig. S.9.3.(a) Surface activity of $C_3(CA)_2$ as a function of time at different concentrations (Note: 1 E-5 M = 10^{-5} M).

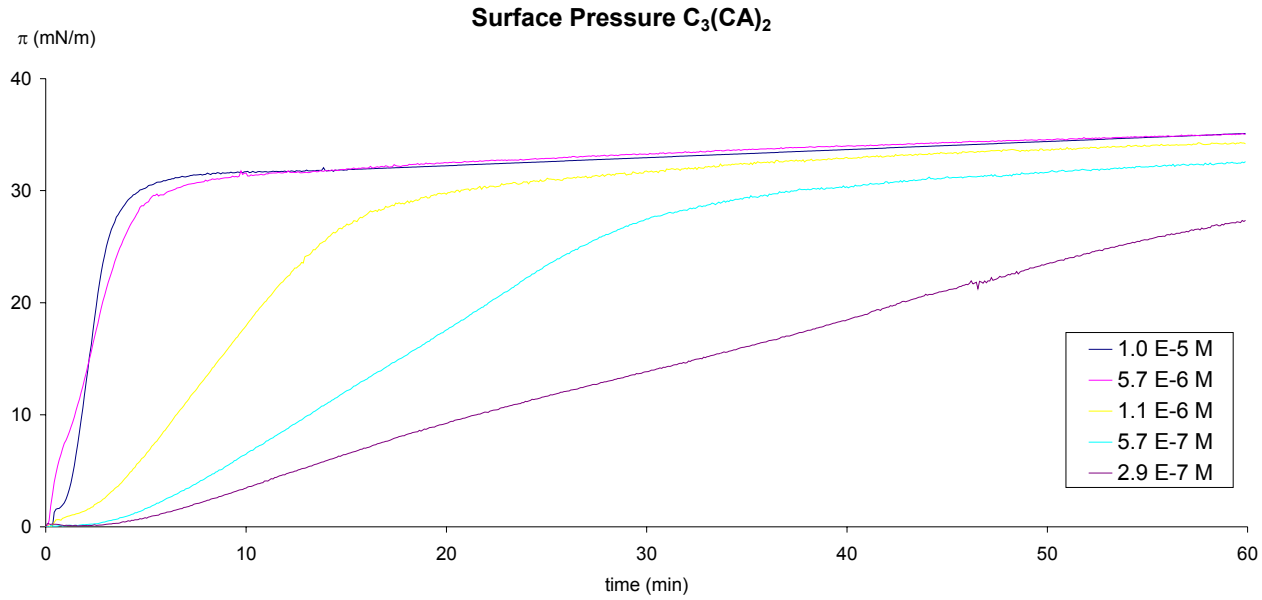

Fig. S.9.3.(b) Surface pressure increases as a function of $C_3(CA)_2$ concentration.

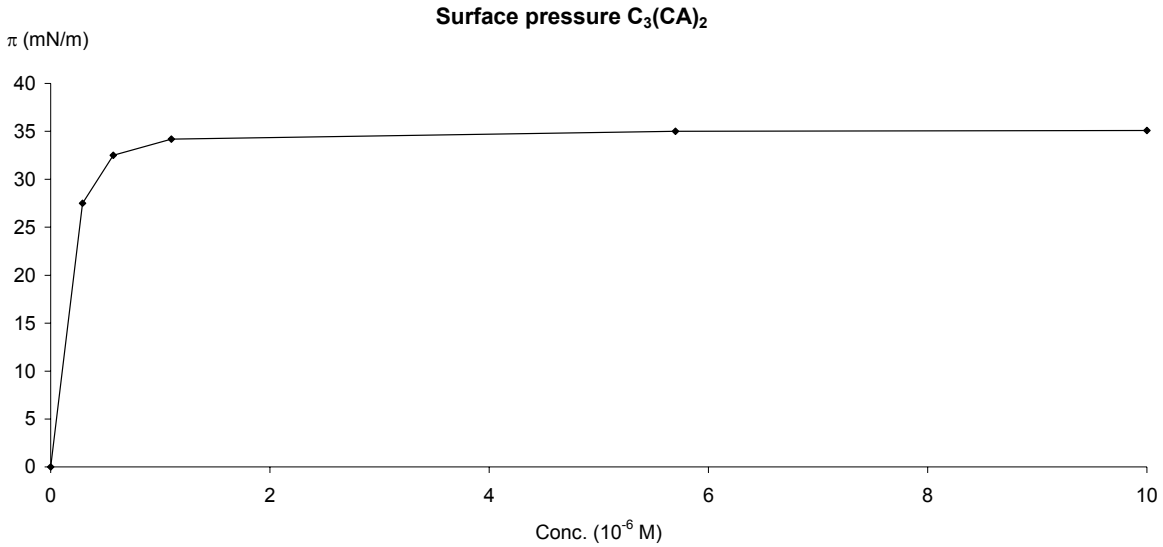

Fig. S.9.4.(a) Surface activity of HTAB as a function of time at different concentrations (Note: 1 E-5 M = 10^{-5} M).

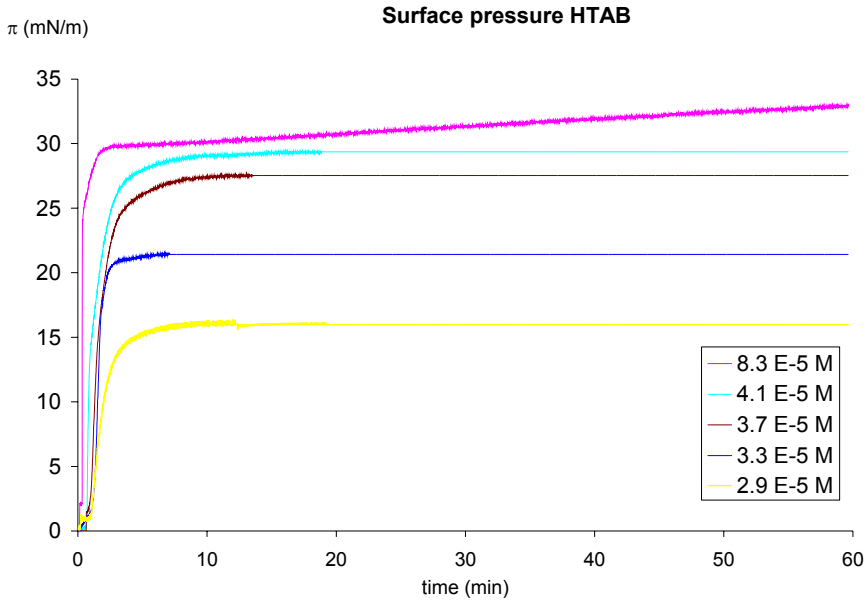

Fig. S.9.4.(b) Surface pressure increases as a function of HTAB concentration.

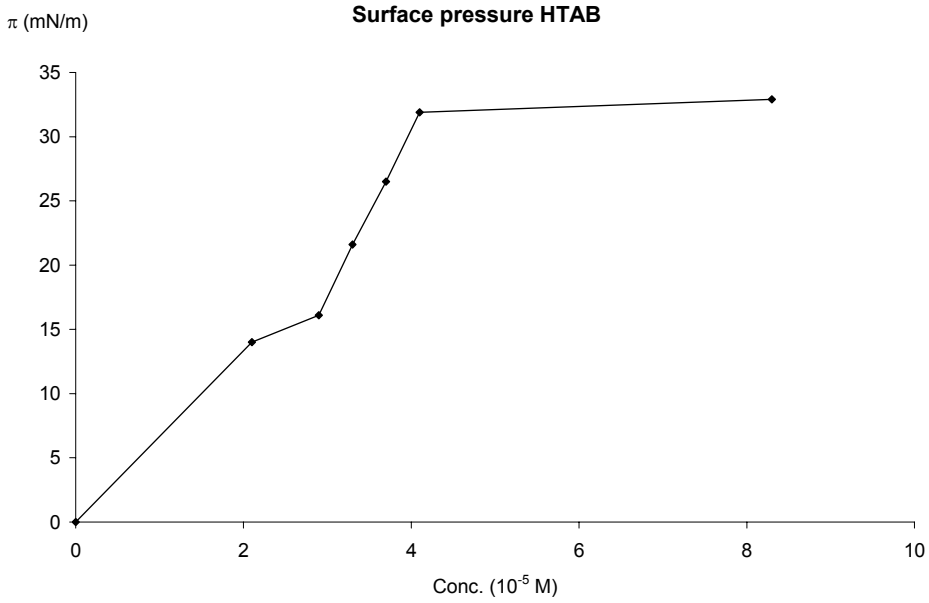

Fig. S.9.5.(a) Surface activity of CHX as a function of time at different concentrations (Note: 1 E-5 M = 10^{-5} M).

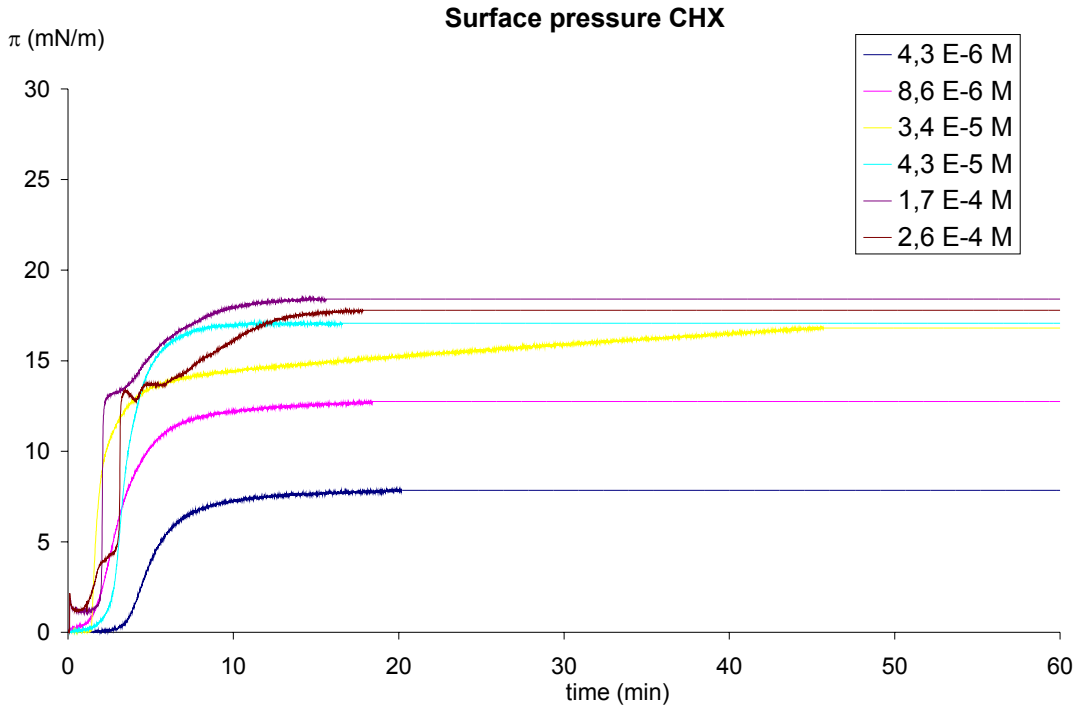

Fig. S.9.5.(b) Surface activity of CHX as a function of time at different concentrations.

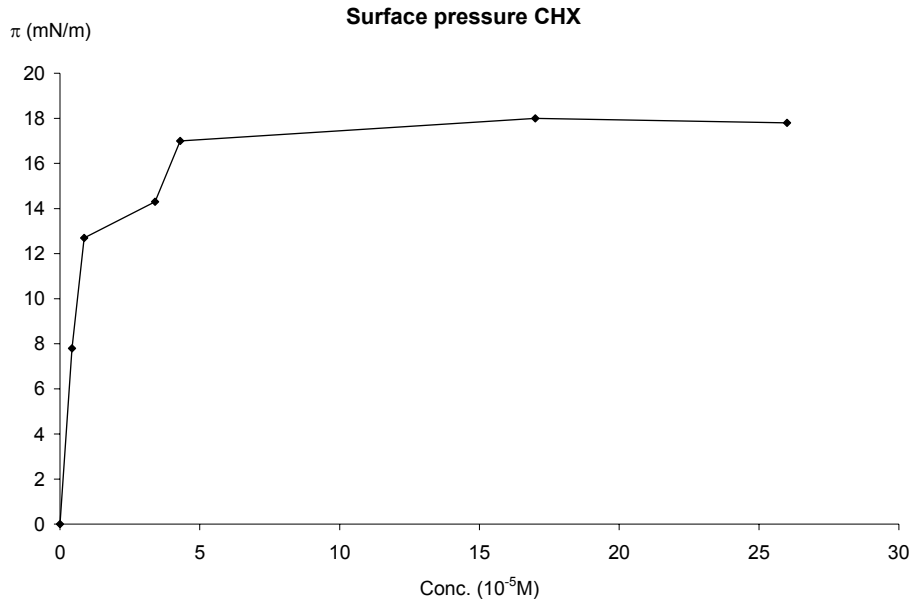

Fig. S.10.1. Pressure increases as a function of the initial density of the DPPC monolayer for each compound at 80% saturation concentration.

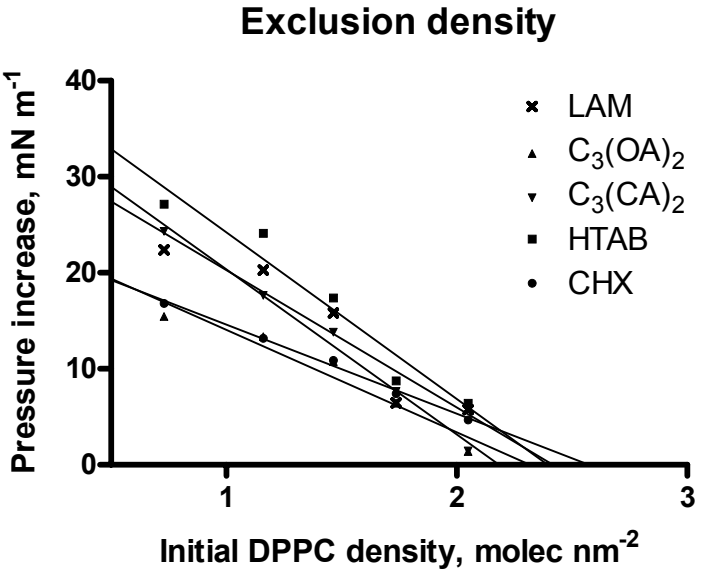

Fig. S.10.2. Pressure increases as a function of the initial density of the DPPG monolayer for each compound at 80% saturation concentration.

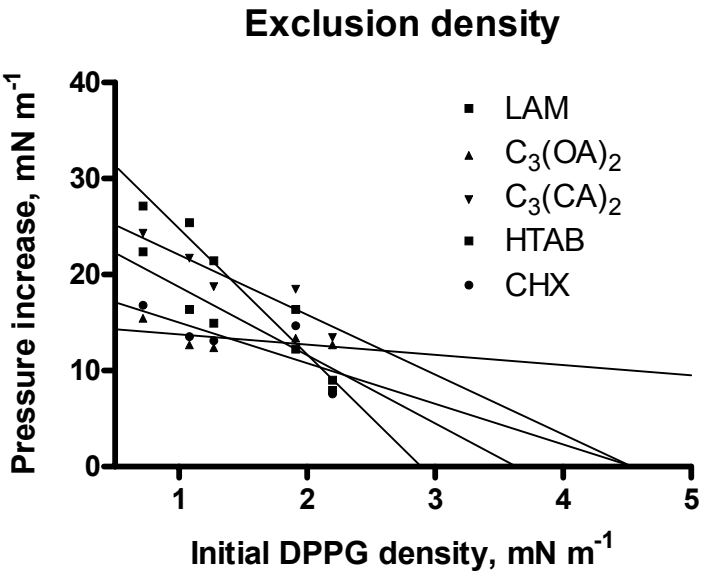

Fig. S.10.3. Pressure increases as a function of the initial density of the *E. coli* lipid extract monolayer for each compound at 80% saturation concentration.

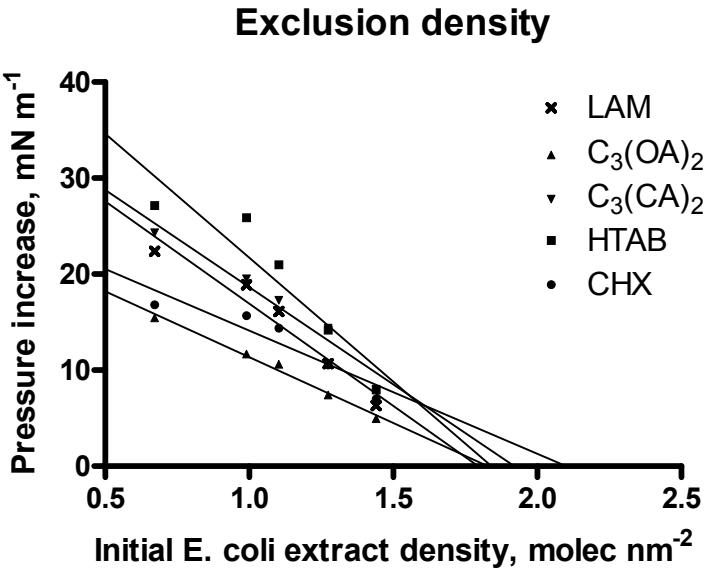

Fig. S.11.1 Compression isotherms of DPPC monolayer spread on subphases containing LAM at 80%, 20% and 5% saturation concentration.

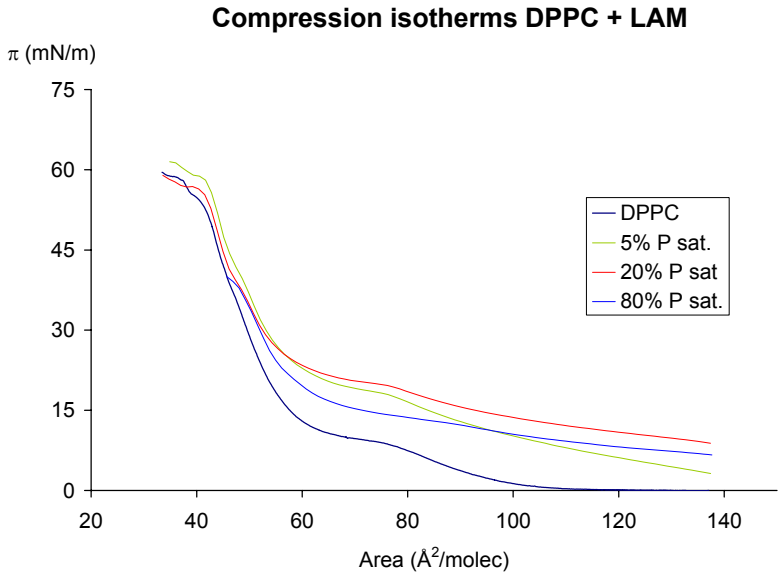

Fig. S.11.2. Compression isotherms of DPPC monolayer spread on subphases containing $C_3(OA)_2$ at 80%, 20% and 5% saturation concentration.

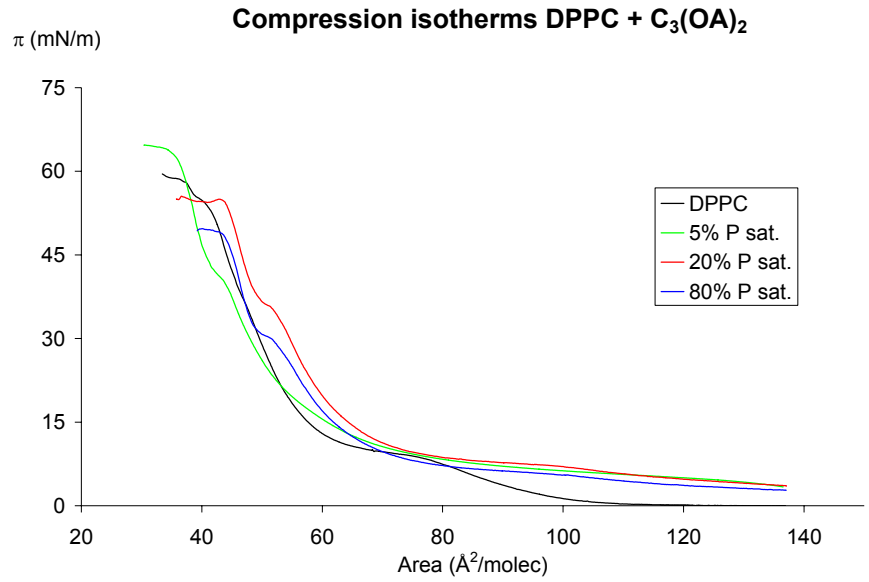

Fig. S.11.3. Compression isotherms of DPPC monolayer spread on subphases containing HTAB at 80%, 20% and 5% saturation concentration.

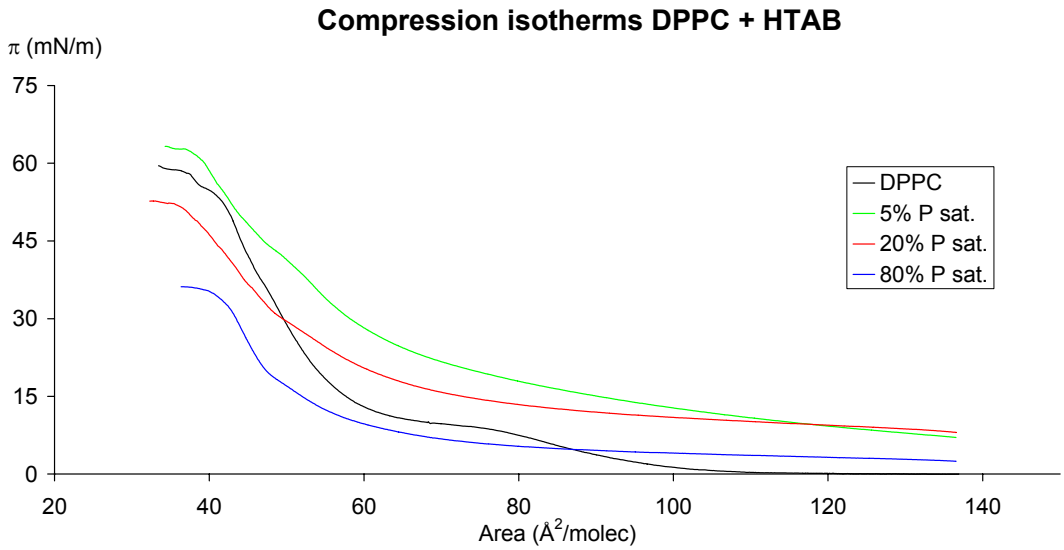

Fig. S.11.4. Compression isotherms of DPPC monolayer spread on subphases containing CHX at 80%, 20% and 5% saturation concentration.

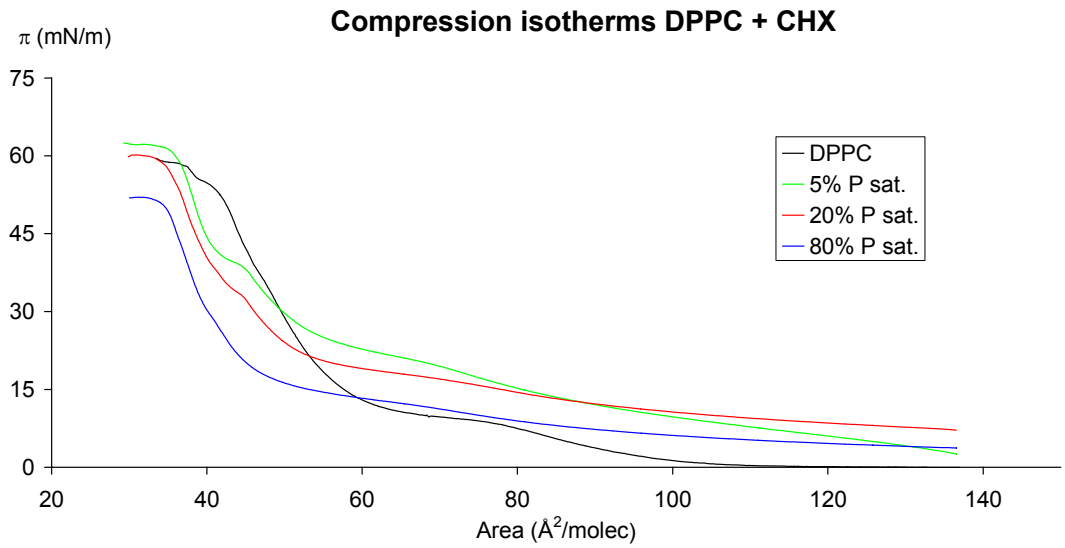

Fig. S.11.5. Compression isotherms of DPPG monolayer spread on subphases containing LAM at 80%, 20% and 5% saturation concentration.

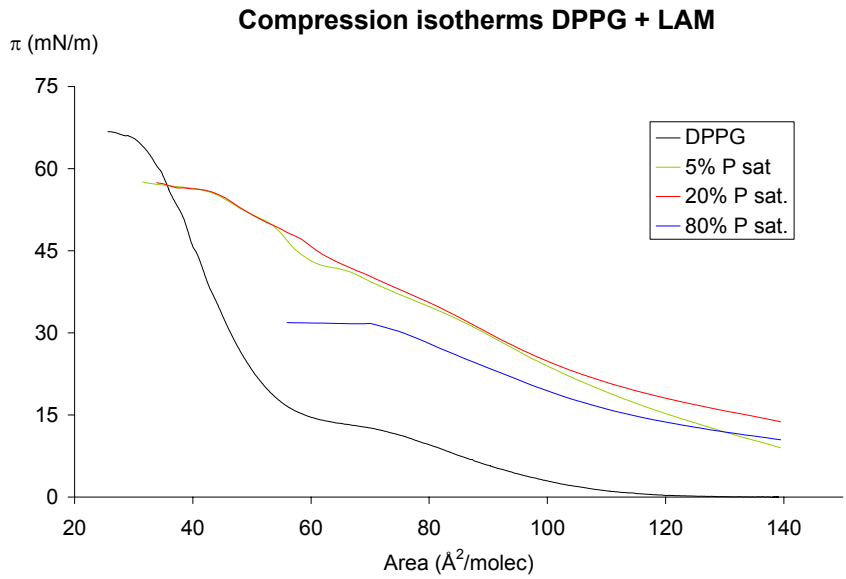

Fig. S.11.6. Compression isotherms of DPPG monolayer spread on subphases containing $C_3(OA)_2$ at 80%, 20% and 5% saturation concentration.

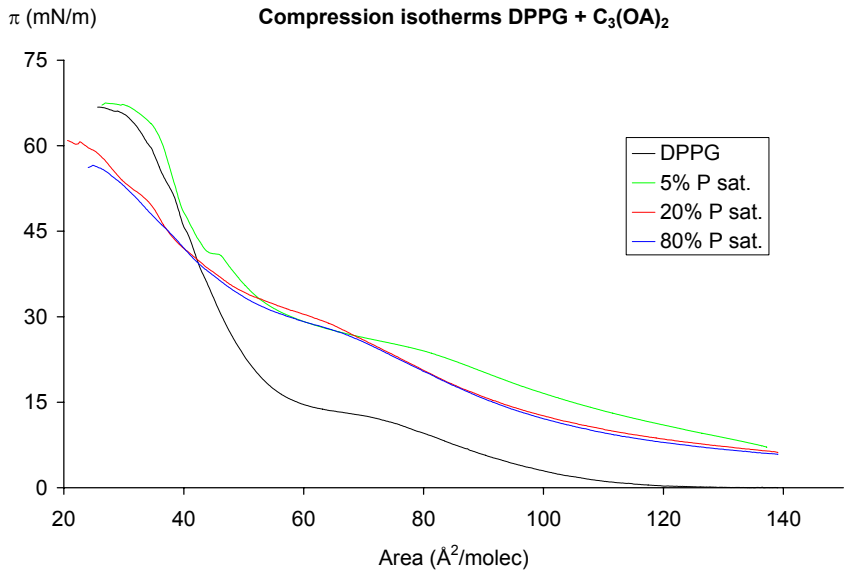

Fig. S.11.7. Compression isotherms of DPPG monolayer spread on subphases containing HTAB at 80%, 20% and 5% saturation concentration.

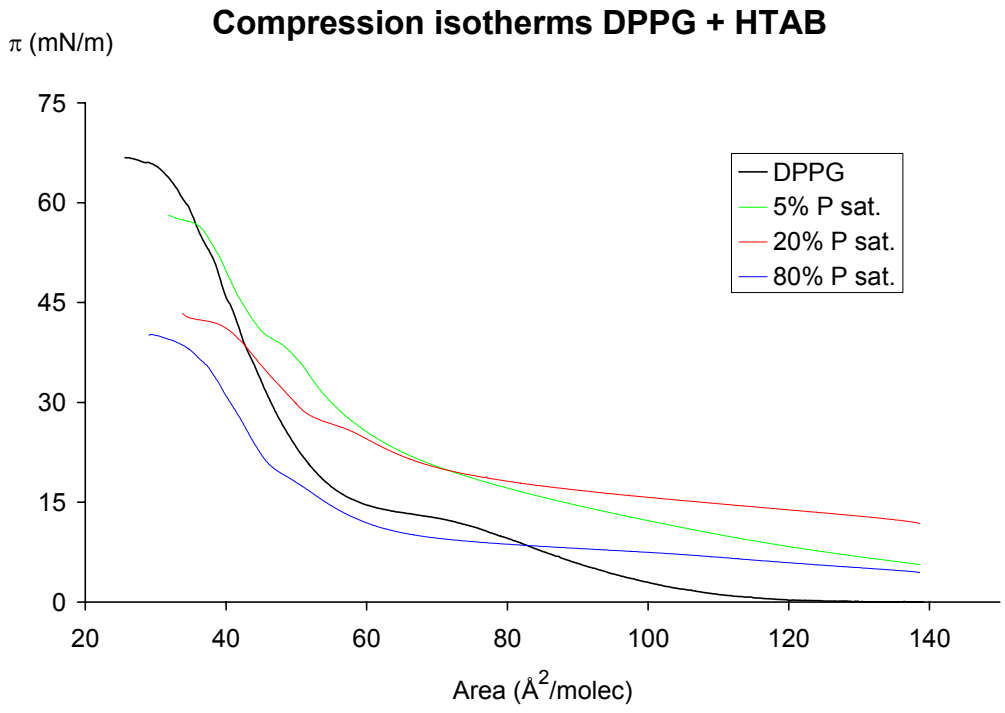

Fig. S.11.8. Compression isotherms of DPPG monolayer spread on subphases containing CHX at 80%, 20% and 5% saturation concentration.

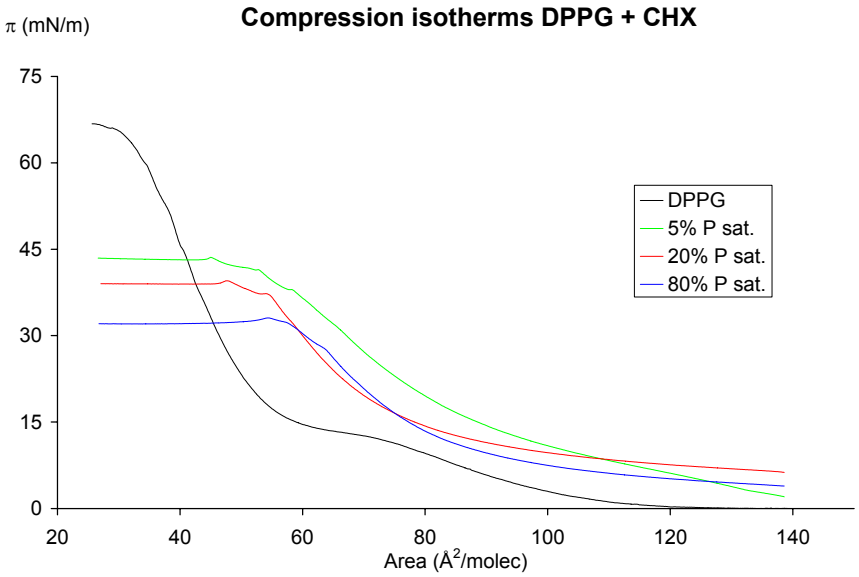

Fig. S.11.9. Compression isotherms of *E. coli* lipid extract monolayer spread on subphases containing LAM at 80%, 20% and 5% saturation concentration.

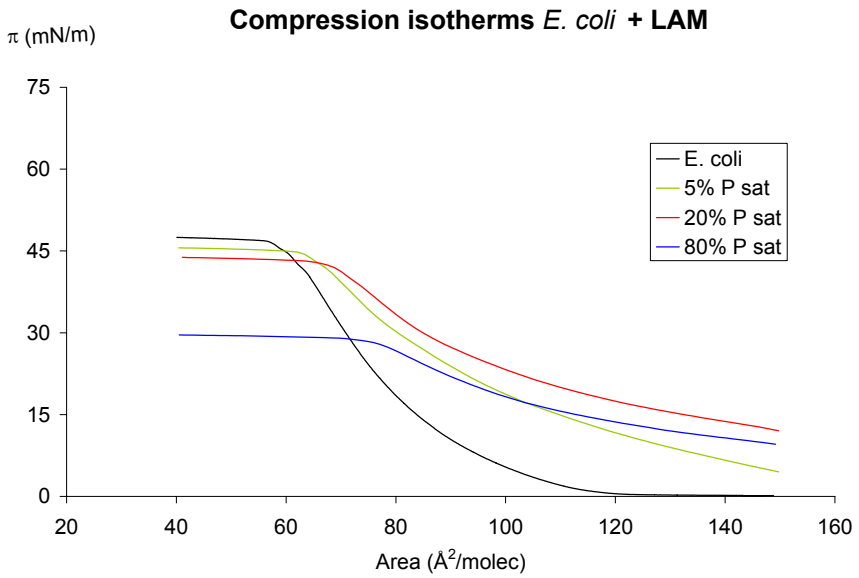

Fig. S.11.10. Compression isotherms of *E. coli* lipid extract monolayer spread on subphases containing $C_3(OA)_2$ at 80%, 20% and 5% saturation concentration.

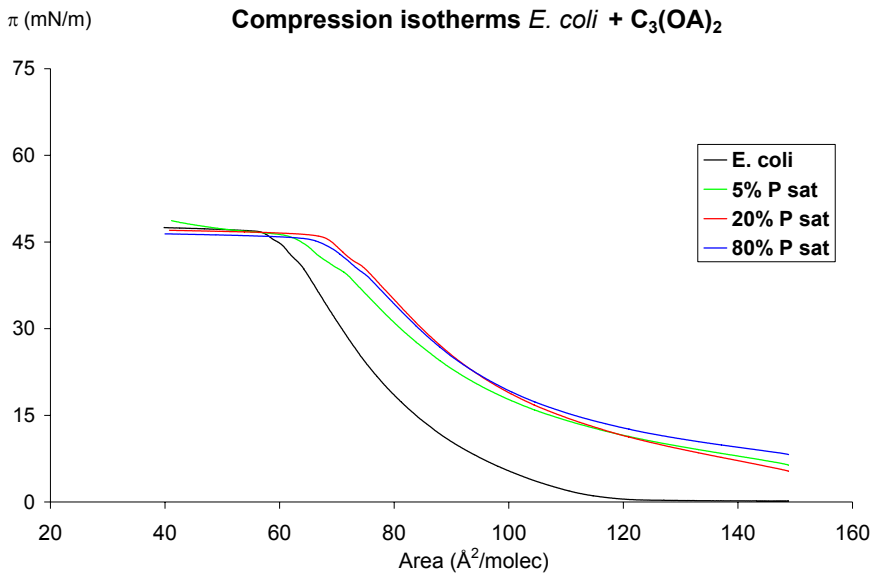

Fig. S.11.11. Compression isotherms of *E. coli* lipid extract monolayer spread on subphases containing HTAB at 80%, 20% and 5% saturation concentration.

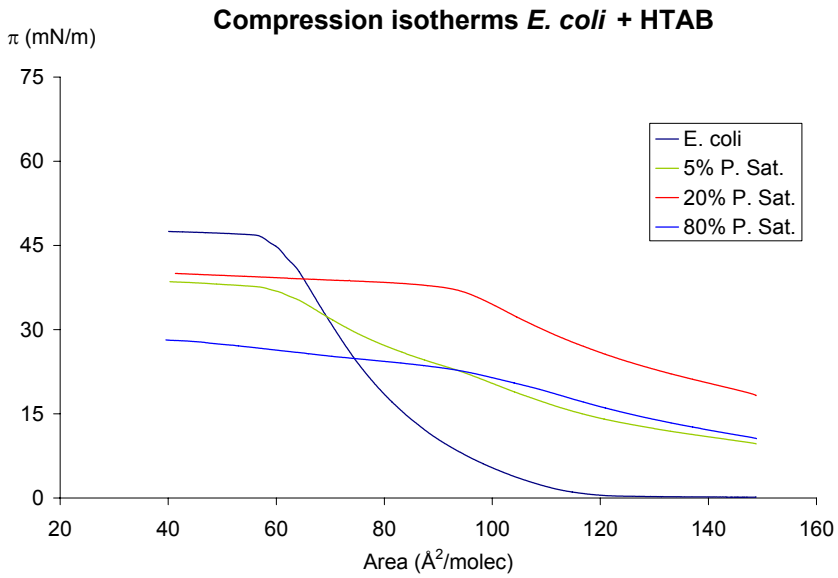

Fig. S.11.12. Compression isotherms of *E. coli* lipid extract monolayer spread on subphases containing CHX at 80%, 20% and 5% saturation concentration.

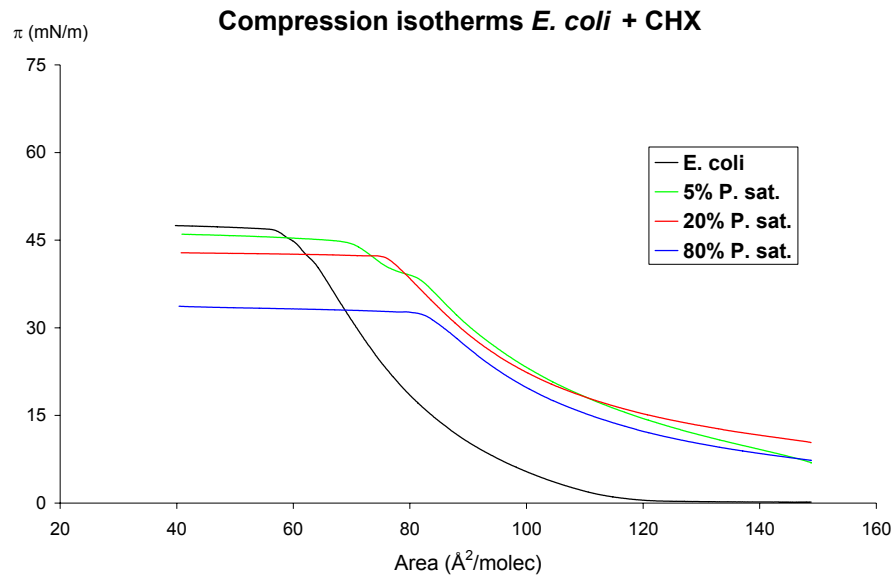

Fig. S.12.1. Compression isotherms of DPPC monolayer spread on subphases containing $C_3(CA)_2$ at 80%, 20% and 5% saturation concentration.

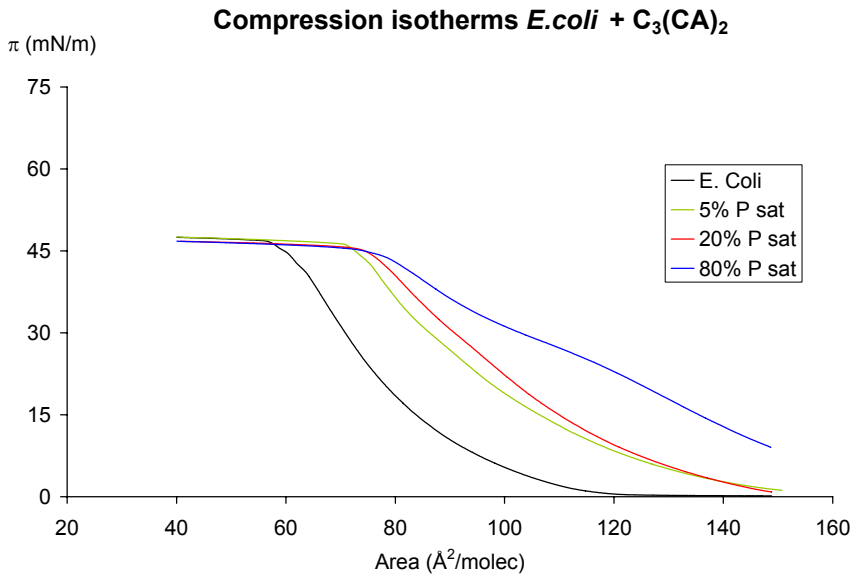

Fig. S.12.2. Compression isotherms of DPPG monolayer spread on subphases containing $C_3(CA)_2$ at 80%, 20% and 5% saturation concentration.

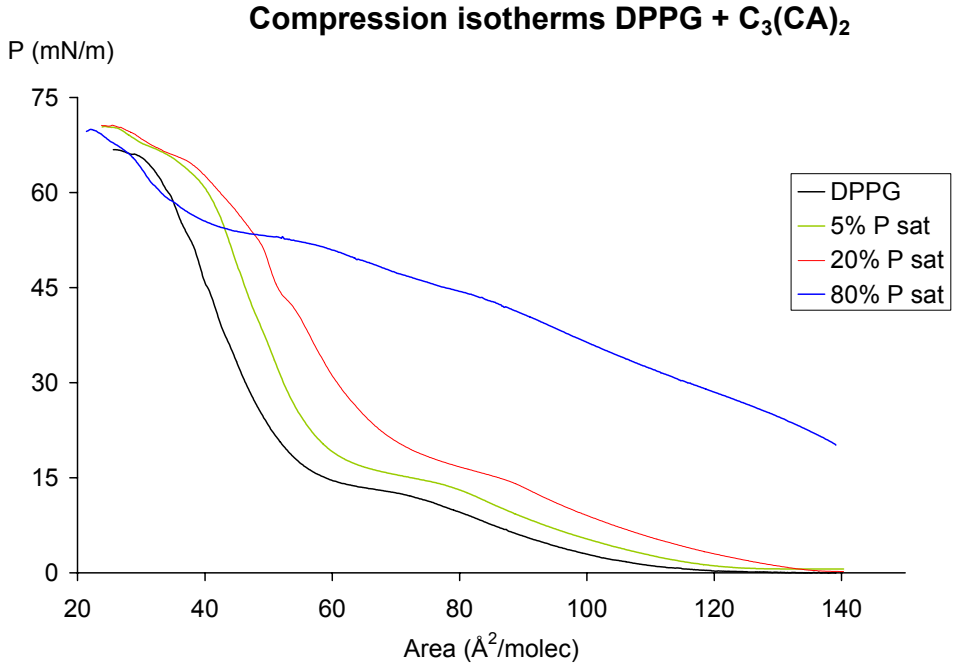

Fig. S.12.3. Compression isotherms of *E.coli* lipid extract monolayer spread on subphases containing $C_3(CA)_2$ at 80%, 20% and 5% saturation concentration.

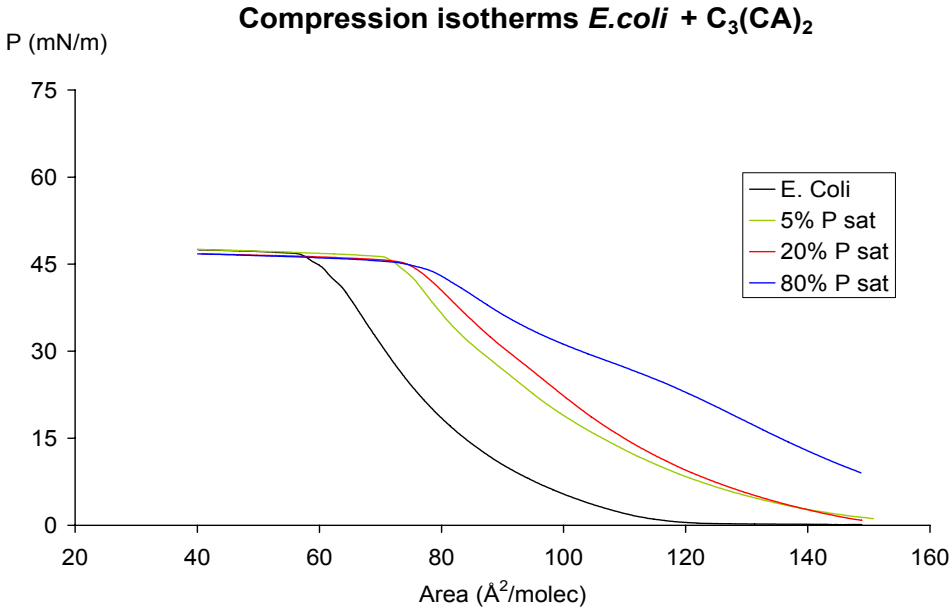

3.2. Comparative study of antibacterial activity of $C_3(CA)_2$ and CHX against *Staphylococcus aureus* and *Escherichia coli*

Among the arginine-based surfactants synthesised in our laboratory, bis(N^{α}-caproyl-L-arginine)-1,3-propanediamide dihydrochloride, $C_3(CA)_2$, (Figure 1) is a novel gemini (double-chain/double-polar head) compound which shows antimicrobial activity against a wide range of Gram-positive and Gram-negative bacteria. In the previous section, this surfactant showed high interaction with biomembrane models suggesting that the cytoplasmic membrane may be its main target.

At this point, our aim was to gain insight into its mode of the antimicrobial action. To this end, its effects on *Staphylococcus aureus* and *Escherichia coli* were compared with those caused by the commercial and widely known antiseptic, chlorhexidine dihydrochloride, CHX. (Figure 1). These effects were assessed using different techniques: flow cytometry, viable cell counts, transmission electronic microscopy and atomic absorption spectrophotometry. All these techniques have limitations and therefore, it is convenient the use of complementary methods to achieve a better assessment of the antimicrobial action of microbicides.

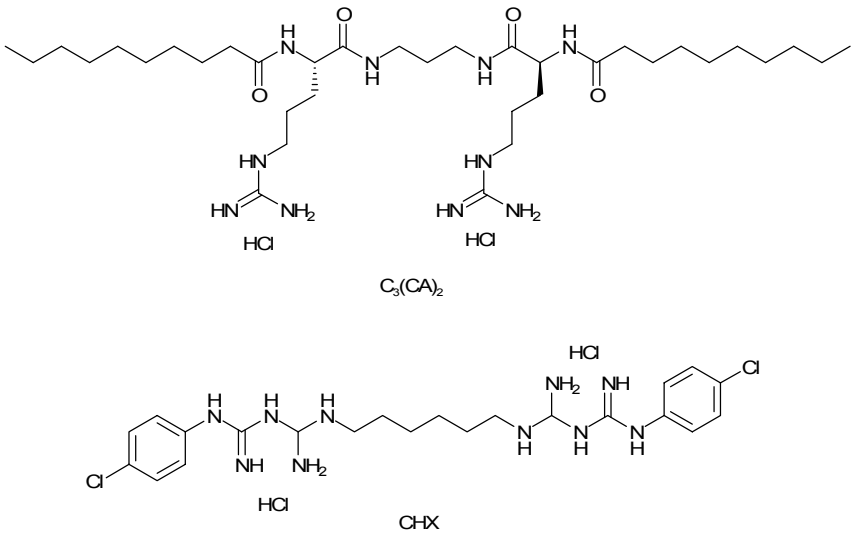

Fig. 1. Structures of the selected antimicrobial compounds.

The selected bacteria were *S. aureus* and *E. coli* as models of Gram-positive and Gram-negative bacteria, respectively. Both micro-organisms have been widely studied by flow cytometry[1-3] and by microscopy electronic transmission.[4-7] Hence, comparative studies and interpretation of the results were facilitated and conclusions drawn are better supported.

To study the effect of the antimicrobial agents on the bacterial population, two concentrations were selected on the basis of the minimum inhibitory concentrations (MIC): one concentration was 50 % greater than the corresponding MIC (3/2 MIC) and the second one was 50 % lower than the MIC (1/2 MIC) (see Table 1). As shown in the previous section, the (MIC) of $C_3(CA)_2$ and CHX against *Staphylococcus aureus* were 2 mg L^{-1} and 0.5 mg L^{-1}, respectively, and against *Escherichia coli* were 8 mg L^{-1} and 2 mg L^{-1}, respectively. The concentrations of the surfactant, $C_3(CA)_2$, were always lower than the corresponding critical micellar concentration (*i.e.* $3x10^{-5}$ M).[8]

Table 1. Minimum inhibitory concentrations in mg L^{-1} and the antimicrobial concentration tested.

	S. aureus			*E. coli*		
Product	1/2 MIC	MIC	3/2 MIC	1/2 MIC	MIC	3/2 MIC
$C_3(CA)_2$	1	2	3	4	8	12
CHX	0.25	0.5	0.75	1	2	3

3.2.1. Flow cytometry analyses and viability reduction

To assess the effect of $C_3(CA)_2$ and CHX on bacterial populations, flow cytometry (FC) analyses were performed using dual staining of cells with Syto-13 and propidium iodide (PI). Syto-13 is a nucleic acid stain which penetrates all types of cellular membranes and PI is a nucleic acid stain not taken up by intact cells.[9] Three types of stained cells could be observed after the treatment: cells stained with Syto-13 (intact cells), double-stained

cells PI/Syto-13 (partially damaged cells) and stained cells with PI (severely damaged cells). Consequently, the fluorochromes PI and Syto-13 were chosen because of their potential ability to distinguish between intermediate states of dead and live cells; PI confers fluorescence on cells which have lost their membrane integrity, whereas Syto-13 confers fluorescence on intact cells. To validate the FC results and to examine the putative relation between cell damage and cell viability, viable cells counts were determined after exposure to the microbicides.

The results with *S. aureus* are shown in Figure 2 and Table 2. The control population was mainly stained with Syto-13 (99±1 %). After 30 min of contact with 3 mg L^{-1} (3/2 MIC) of $C_3(CA)_2$, 95±1 % of the cells were stained with Syto-13, 2±1 % were double stained and 3±1 % were stained with PI, indicating slight damage caused by $C_3(CA)_2$. Varying the $C_3(CA)_2$ concentration did not alter the proportion of damaged cells (Table 2). Likewise, cell counts on plates did not change substantially with biocide concentration; viable cells dropped from 79±10 % at 1 mg L^{-1} (1/2 MIC) to 69±6 % at 3 mg L^{-1} (3/2 MIC).

When *S. aureus* was treated with 0.75 mg L^{-1} (3/2 MIC) of CHX (Figure 2), 11±4 % partially damaged (double stained), and 15±1 % severely damaged cells (PI stained cells) were seen. Decreasing the biocide concentration from 3/2 to 1/2 MIC did not affect the proportion of partially damaged cells, since double-stained cells only decreased from 11±4 to 5±1 % (Table 2). These results agree with the cell counts, where varying biocide concentration caused only a slight effect on cell viability.

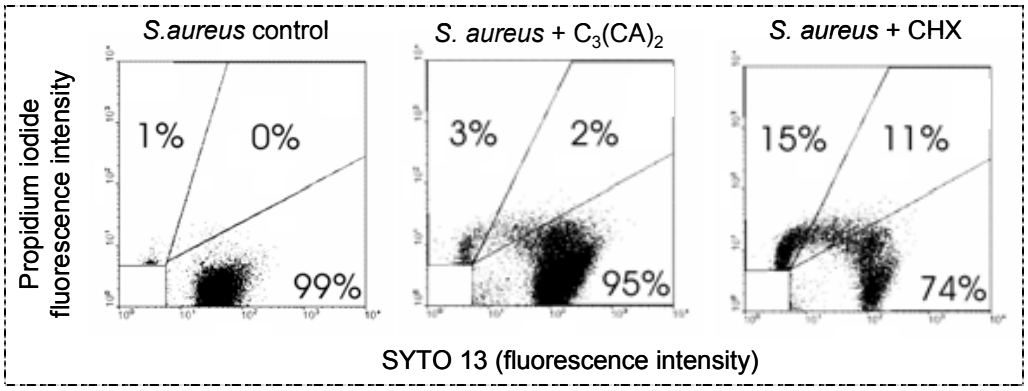

Fig. 2. Dual staining of *S. aureus* with PI and Syto-13 after exposure to $C_3(CA)_2$ and CHX. Time of contact was 30 min and antimicrobial concentration was 3/2 MIC.

Table 2. Effect of the antimicrobials on *S. aureus* after a dual stain with PI and Syto-13, and viability reduction by plate counts.

Sample	Conc. mg L^{-1}	Syto-13 (%)	PI+Syto 13 (%)	PI (%)	Cfu/mL (10^6)	Viability reduction (%)
Control	---	99±1	0	1±1	4.8±1.3	---
$C_3(CA)_2$	1	93±3	4±1	3±2	3.8±1.3	21±10
$C_3(CA)_2$	3	95±1	2±1	3±1	3.3±0.6	31±6
CHX	0.25	80±7	5±1	14±4	3.8±3.3	21±13
CHX	0.75	74±8	11±4	15±1	3.4±2.1	29±9

Time of contact was 30 min. Data are given as the mean ± SEM of three separate experiments.

A different pattern was observed in *E. coli* populations when they were treated with $C_3(CA)_2$ and CHX (Figure 3 and Table 3). The control population showed 91±4 % of intact cells (stained by Syto-13). After treatment with 12 mg L^{-1} (3/2 MIC) of $C_3(CA)_2$, a dramatic decrease in intact cells was detected, only 5±1 % of the population retained Syto-13 whereas 77±10 % were severely damaged (stained by PI), and the remaining 18±3 % were partially damaged (double stained, Figure 3). At 4 mg L^{-1} (1/2 MIC) of $C_3(CA)_2$, 42 % (PI and PI + Syto-13) of the population showed signs of damage and the reduction in viability was 77±1 % (Table 3).

Three sub-populations could clearly be observed (Figure 3) when *E. coli* cultures were treated with CHX at 3/2 MIC: 63±5 % remained intact

(Syto-13); 21±2 % showed partial damage (double stained); and 16±3 % of cells were severely damaged (stained by PI). As presented in Table 3, variation of CHX concentration did not appear to have any effect as observed by FC; the population stained by Syto-13 decreased from 67±5 to 63±5 %. However, the viability reduction changed significantly with CHX concentration, from 44±1 to 61±1 %.

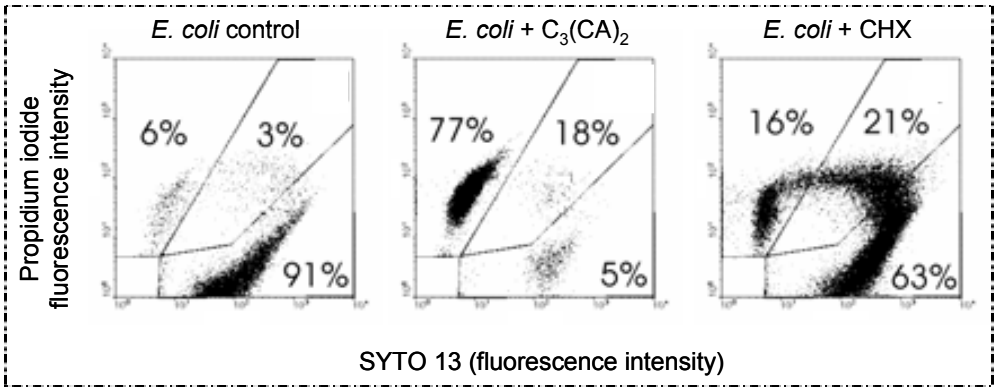

Fig. 3. Dual staining of *E. coli* with PI and Syto-13 after exposure to $C_3(CA)_2$ and CHX. Time of contact was 30 min and antimicrobial concentration was 3/2 MIC.

Table 3. Effect of the antimicrobials on *E. coli* after a dual stain with PI and Syto-13, and viability reduction by plate counts.

Sample	Conc. (mg L^{-1})	Syto-13 (%)	PI+Syto-13 (%)	PI (%)	Cfu/mL (10^6)	Viability reduction (%)
Control	---	91±4	3±1	6±3	2.5±1.5	---
$C_3(CA)_2$	4	58±11	15±2	27±3	0.6±0.3	77±1
$C_3(CA)_2$	12	5±1	18±3	77±10	0.1±0.1	95±1
CHX	1	67±5	13±2	20±3	1.4±0.8	44±1
CHX	3	63±5	21±2	16±3	1.0±0.4	61±1

Time of contact was 30 min. Data are given as the mean ± SEM of three separate experiments.

Membrane potential

Membrane depolarization was measured by determining the relative fluorescence intensity of bis-oxonol labeling using FC. The fluorochrome bis-oxonol is an anionic lipophilic dye which does not accumulate to any

great extent in cells with a negative transmembrane potential, and fluorescence increases as membrane potential decreases.[2] As shown in Figure 4, the negative controls (*i.e.* cell suspensions in absence of microbicides) emitted the minimum relative fluorescence intensity (Figures 4a and 4e) in the range M1 (0-350 fluorescence units (FU)), showing no significant depolarization of the cytoplasmic membrane. Thus, we considered that the range M1 corresponds to undamaged cells. As expected, the positive control (*i.e.* bacteria that underwent a thermal shock at 70 °C for 30 min) showed the maximum relative fluorescence intensity (Figures 4d and 4h). We considered the range M2 (between 350-1024 FU) as damaged and dead cells.

The effect of $C_3(CA)_2$ on *S. aureus* showed a bimodal profile (Figure 4b) with two distinct populations of cells: almost 50 % of the population emitted fluorescence in the region of non-damaged cells; while the rest emitted in the region of the dead cells. A different pattern was observed on exposure of *E. coli* to $C_3(CA)_2$ (Figure 4f); 84 % of cells were damaged or dead (increased fluorescence); and 16 % remained intact. When cells were exposed to CHX, a bimodal pattern was observed (*i.e.* 49 % intact and 51 % damaged cells) with *E. coli* (Figure 4h), whereas, for the most part, *S. aureus* was undamaged (Figure 4d).

$C_3(CA)_2$ and the comparator molecule, CHX, changed the polarity of the cell membrane bilayer of the bacteria due to similar effects on membrane depolarization were observed. However, both compounds showed different bacterial selectivity, suggesting a different mode of action; $C_3(CA)_2$ has a concentration dependent microbicidal effect on *E. coli*, but has little effect on *S. aureus*; whereas CHX has little effect on *E. coli*, and does cause some damage (though not loss of viability) to *S. aureus*. It is remarkable that the existence of sub-populations with different degree of damage suggests reversible damage or even, the presence of viable and non-viable organisms.

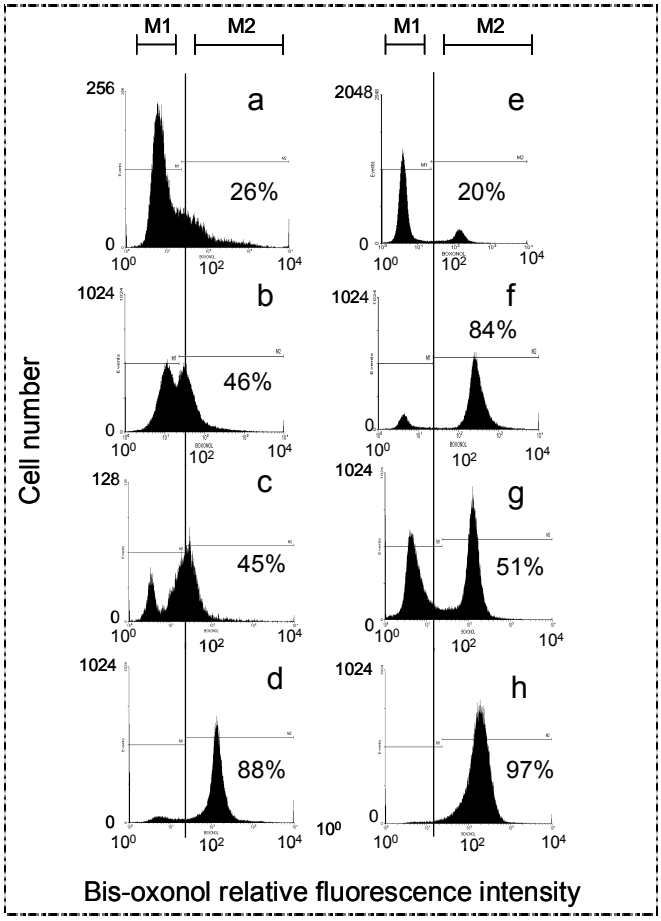

Fig. 4. Effect on the transmembrane potential of *S. aureus* and *E. coli* caused by exposure to $C_3(CA)_2$ and CHX, shown by bis-oxonol staining. The relative fluorescence intensities within the M1 regions were taken as live cells, and those within the M2 regions were take as dead cells (logarithmic scale). Untreated *S. aureus* control (a), *S. aureus* treated with $C_3(CA)_2$ (b), *S. aureus* treated with CHX (c), *S. aureus* heated at 70 °C (d), untreated *E. coli* control (e), *E. coli* treated with $C_3(CA)_2$ (f), *E. coli* treated with CHX (g), *E. coli* heated at 70 °C (h). In all cases, time of contact was 30 min and antimicrobial concentration was 3/2 MIC.

A lack of correlation between the membrane damaging action and cell viability seen for *S. aureus* suggests that membrane perturbation may be an important step in cell death, but is not necessarily a lethal event. Recently, Rodríguez *et al.* have reported the antimicrobial effects caused by N^{α}-lauroyl-L-arginine methyl ester on two bacteria.[10] The results also indicated that membrane perturbation caused by this arginine-based surfactant and recovering of cells on agar is not always directly related.

This may be due to technical factors such as the conditions for recovery of cells; or that membrane perturbation does not necessarily lead to dissolution of the proton motive force and cell death.[3,11,12] It is notable that two different populations (about 50 %) were registered using the bis-oxonol dye. This result points out the presence of sub-populations with different degrees of damage, suggesting reversible damages or even it could represent viable and nonviable organisms.[1]

The FC labels (*i.e.* Syto-13, PI and bis-oxoxonol) in combination with cell viability assays demonstrated marked differences between the microbicides in their action on the bacterial cells: when *E. coli* was exposed to $C_3(CA)_2$, 84 % showed loss of membrane potential, 27 to 77 % of cells showed membrane damage and 77 to 95 % loss of cell viability, depending on the concentration of $C_3(CA)_2$ used.

3.2.2. Transmission electronic microscopy (TEM)

This technique is a potent and useful tool to investigate the morphological damages caused on micro-organisms by microbicides and previous studies have reported the morphological effects of antimicrobials agents on *S. aureus*[5,7] and *E. coli*.[6] Here, Figure 5 shows micrographs of *S. aureus* and *E. coli* after exposure to $C_3(CA)_2$ and CHX. In all cases, the microbicides concentrations were 3/2 MIC and time of contact was 30 min.

TEM micrographs showed *S. aureus* populations with different extent of damage after $C_3(CA)_2$ and CHX treatments, in good agreement with FC analyses. In both cases intact cells, damaged and severely damaged cells were observed. Cells with white spots indicated a change in cytoplasm consistency, suggesting that a certain degree of membrane permeabilization occurred. The formation of mesosomes (*i. e.* convoluted invaginations of the cytoplasmic membrane in some bacterial cells) near the cytoplasmic

membrane was also observed, especially caused by $C_3(CA)_2$. The presence of ghost cells suggested that leakage of the cell cytoplasmic contents occurred as a result of gross cell alterations.

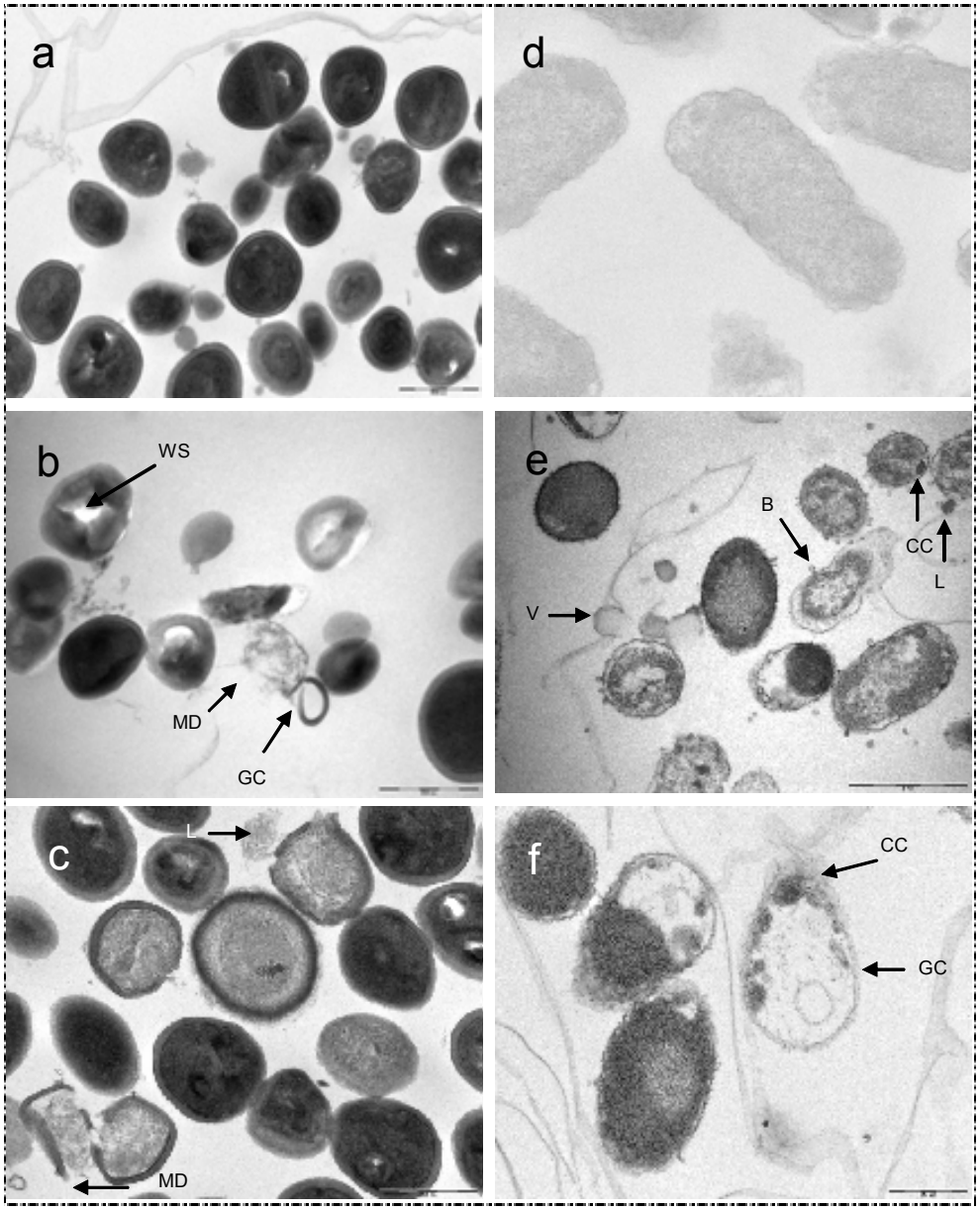

Fig. 5. Micrographs obtained by TEM. In all cases, time of contact was 30 min and microbicide concentration was 3/2 MIC. *S. aureus*: a) untreated control, b) $C_3(CA)_2$ (3 mg L^{-1}), c) CHX (0.75 mg L^{-1}). *E. coli*: d) untreated control, e) $C_3(CA)_2$ (12 mg L^{-1}), f) CHX (3 mg L^{-1}). Key to arrows: B, blebbling; CC: cytoplasmic coagulation; L, leakage; MD, membrane damage; V, empty vesicles; GC, ghost cells, WS, white spot.

TEM micrographs also showed *E. coli* populations with different extent of damage after $C_3(CA)_2$ and CHX treatments. Cytoplasmic coagulation was observed, evidenced by dark areas in the cells. Similar intracytoplasmic black spots have been reported in *E. coli* heat-treated cells.[13] Disruption of the cytoplasmic membrane was also observed, especially for $C_3(CA)_2$-treated *E. coli*, confirming membrane damage. Again, ghost cells were observed as result of gross cell alterations. The most striking ultrastructural effect observed in *E. coli* was the formation of vesicles blebbing out from the outer membrane in presence of $C_3(CA)_2$, similar to those reported for benzalkonium chloride-treated *Psuedomonas aeruginosa*.[14] TEM micrographs show that CHX caused intracytoplasmic changes in *E. coli* but low effect on the membrane integrity of *E. coli*, shown by PI and Syto-13 labelling, was observed. In good agreement, a moderate effect on *E. coli* membrane potential (51 % depolarization) and on cell viability (61 % reduction) were also observed.

3.2.3. Potassium leakage

Potassium ion (K^+) leakage reflects an increase of permeability of the cytoplasmic membrane and therefore, it is a first indication of membrane damage in micro-organisms.[15-17] Here, intracellular potassium leakage resulting from exposure to $C_3(CA)_2$ and CHX of *S. aureus* and *E. coli* at the corresponding 3/2 MIC was measured (Table 4). The negative blank was the K^+ leakage measured from the bacterial suspensions in absence of the antimicrobial agents. The positive blank was the K^+ released from the bacterial suspensions heated at 70°C for 30 min in absence of the antimicrobial agents.

Table 4 shows the percentage of K^+ leakage caused by both antimicrobial agents. This percentage was calculated as the ratio of net to total amount of K^+ released. The effect of $C_3(CA)_2$ and CHX on *S. aureus* leaked low amount of K^+. However, this result is in disagreement with the

membrane damage observed by FC analyses and TEM micrographs. Here, a possible explanation could be that the formation of white spots and ghost cells might be too few to provide a reading of potassium leakage as measured with atomic absorption spectrophotometry. Indeed, this methodology involves the use of a large number of cells.[18] Contrarily, the experiments with *E. coli* showed that both antimicrobial treatments leaked high amount of K^+. It is noteworthy that $C_3(CA)_2$ leaked similar amount of K^+ than the positive control. Thus, it seems that the amount of potassium leaked depends strongly on the nature of the micro-organism, rather than the nature of the membrane active agent.

Table 4. Potassium ion leakage.

Compound	*S. aureus* (ppm/10^3)	*S. aureus* (%)[a]	*E. coli* (ppm/10^3)	*E. coli* (%)[a]
Negative blank	363 ± 75	--	769 ± 42	--
Positive blank	509 ± 29	--	918 ± 33	--
$C_3(CA)_2$	401 ± 32	26	951 ± 52	>100
CHX	375 ± 63	8	889 ± 42	81

[a] The percentage of K^+ leakage was the ratio of net to total amount of K^+ released. In all cases, time of contact was 30 min and antimicrobial concentration was 3/2 MIC.

Finally, $C_3(CA)_2$ and CHX induce similar types of damage to *S. aureus* and *E. coli,* though they differ in the extent of membrane depolarization and reduction of cell viability. These differences suggest that both compounds damage bacteria in a different way, and that the surfactant properties of $C_3(CA)_2$ and its ability to partition into the biological membrane from aqueous solution might be important characteristics in its microbicidal action.

References:

1. Suller, M. T. E.; Lloyd, D., Fluorescence monitoring of antibiotic-induced bacterial damage using flow cytometry. *Cytometry* **1999**, *35*, 235-241.
2. Comas, J.; Vives, J., Assessment of the effects of gramicidin, formaldehyde, and surfactants on *Escherichia coli* by flow cytometry using nucleic acid and membrane potential dyes. *Cytometry* **1997**, *29*, 58-64.
3. Sheppard, F. C.; Mason, D. J.; Bloomfield, S. F.; Gant, V. A., Flow cytometric analysis of chlorhexidine action. *FEMS Microbiol. Lett.* **1997**, *154*, 283-288.
4. Claeson, P.; Radström, P.; Sköld, O., Bactericidal effect of the sesquiterpene t-cardinol on *Staphylococcus aureus*. *Phytother. Res.* **1992**, *6*, 94-98.
5. Shimoda, M.; Ohki, K.; Shimamoto, Y.; Kohashi, O., Morphology of defensin-treated *Staphylococcus aureus*. *Infect. Immun.* **1995**, 63, 2886-2891.
6. Henk, W. G.; Todd, W. J.; Enright, F. M.; Mitchell, P. S., The morphological effects of two antimicrobial peptides, hecate-1 and melittin, on *Escherichia coli*. *Scanning Microsc.* **1995**, *9*, 501-507.
7. Friedrich, C. L.; Moyles, D.; Beveridge, T.; Hancock, R., Antibacterial action of structurally diverse cationic peptides on Gram-positive bacteria. *Antimicrob. Agents Chemother.* **2000**, 44, 2086-2092.
8. Castillo, J. A.; Pinazo, A.; Carilla, J.; Infante, M. R.; Alsina, M. A.; Haro, I.; Clapés, P., Interaction of antimicrobial arginine-based cationic surfactants with liposomes and lipid monolayers. *Langmuir* **2004**, *20*, 3379-3387.
9. Bunthof, C. J.; van Schalkwijk, S.; Meijer, W.; Abee, T.; Hugenholtz, J., Fluorescent method for monitoring cheese starter permeabilization and lysis. *Appl. Environm. Microbiol.* **2001**, *67*, 4264-4271.
10. Rodríguez, E.; Seguer, J.; Rocabayera, X.; Manresa, A., Cellular effects of monochloride of L-arginine, *N*-lauroyl ethylester (LAE) on exposure to *Salmonella typhimurium* and *Staphylococcus aureus*. *J. Appl. Microbiol.* **2004**, *96*, 903-912.
11. Comas, J.; Vives, J., Enumeration, viability and heterogeneity in *Staphylococcus aureus* cultures by flow cytometry. *J. Microbiol. Methods* **1998**, 32, 45-53.
12. Vives, J.; Lebaron, P.; Nebe, G., Current and future applications of flow cytometry in aquatic microbiology. *FEMS Microbiology Reviews* **2000**, *24*, 429-448.
13. Woo, I. S.; Rhee, I. K.; Park, H. D., Differential damage in bacterial cells by microwave radiation on the basis of cell wall structure. *Appl. Environm. Microbiol.* **2000**, *66*, 2243-2247.
14. Joynson, J. A.; Forbes, B.; Lambert, R. J. W., Adaptive resistance to benzalkonium chloride, amikacin and tobramycin: the effect on susceptibility to other antimicrobials. *J. Appl. Microb.* **2002**, *93*, 96-107.
15. Mlynarcik, D.; Sirotkova, L.; Devinsky, F.; Masarova, L.; Pikulikova, A.; Lacko, I., Potassium leakage from *Escherichia coli* cells treated by

organic ammonium salts. *J. Basic Microbiol.* **1992**, *32*, 43-47.
16. Lambert, P. A.; Hammond, S. M., Potassium fluxes, first indications of membrane damage in micro-organisms. *Biochem. Biophys. Res. Commun.* **1973**, *54*, 796-799.
17. Fitzgerald, K. A.; Davies, A.; Russell, A. D., Mechanism of action of chlorhexidine diacetate and phenoxyethanol singly and in combination against Gram-negative bacteria. *Microbios* **1992**, *70*, 215-230.
18. Codling, C. E.; Hann, A. C.; Maillard, J. Y.; Russell, A. D., An investigation into the antimicrobial mechanisms of action of two contact lens biocides using electron microscopy. *Cont. Lens Anterior Eye* **2005**, *28*, 163-168.

3.3. Chemoenzymatic synthesis and biological properties of bis(phenylacetylarginine) amphiphilic derivatives

In the previous sections, the interactions of bis(N^{α}-caproyl-L-arginine)-1,3-propanediamide dihydrochloride, $C_3(CA)_2$, and chlorhexidine dihydrochloride, CHX, with biomembrane models and its antibacterial action were studied. The results point out that the chemical structure of $C_3(CA)_2$ confer excellent physico-chemical properties to act as membrane-active agent toward bacteria. However, CHX showed lower MICs values than $C_3(CA)_2$ although this biguanide possess low surface activity. At this point, we endeavoured to design novel novel bis(phenylacetylarginine) derivatives with bola-amphiphile like structure to improve the antimicrobial action of $C_3(CA)_2$.

$C_3(CA)_2$ and CHX are both dicationic, and their positive charges are connected through a hydrocarbon spacer chain (Figure 1). As $C_3(CA)_2$ already has good antibacterial activity, we intended to keep structural changes in the molecule to a minimum. Hence, with the CHX structure in mind, we thought of substituting the two N^{α}-caproyl groups of $C_3(CA)_2$ with two N^{α}-phenylacetyl residues and to vary the length of the spacer alkyl chain. The spacer chain length modulates the hydrophobic-hydrophilic balance of the molecule, influencing on the interfacial properties and therefore, on the antimicrobial activity of the molecule.[1] Based on previous works[2,3] on dimeric arginine derivatives, alkylendiamine spacers of 6, 8, 10, 12, and 14 methylene groups were chosen as the most appropriate.

3.3.1. Chemoenzymatic synthesis

The design of the novel bis(PhAcArg) amphiphiles was based on a previous work of chemoenzymatic preparation of arginine-based gemini surfactants, bis(Args),[4] using papain deposited onto Celite (section 4.3.13., page 163) as biocatalyst. The synthetic pathway of bis(Args) surfactants is showed in section 1.2.1 (page 28). In that work, the one-step synthesis of gemini bis(Args) from the corresponding *N*-acyl-arginine methyl ester was planned but low yields were

obtained. Then, a two-step synthesis of bis(Args) was considered and satisfactory yields were achieved. Therefore, a similar two-step synthesis was planned to obtain the novel bis(PhAcArg) amphiphiles (Figure 1).

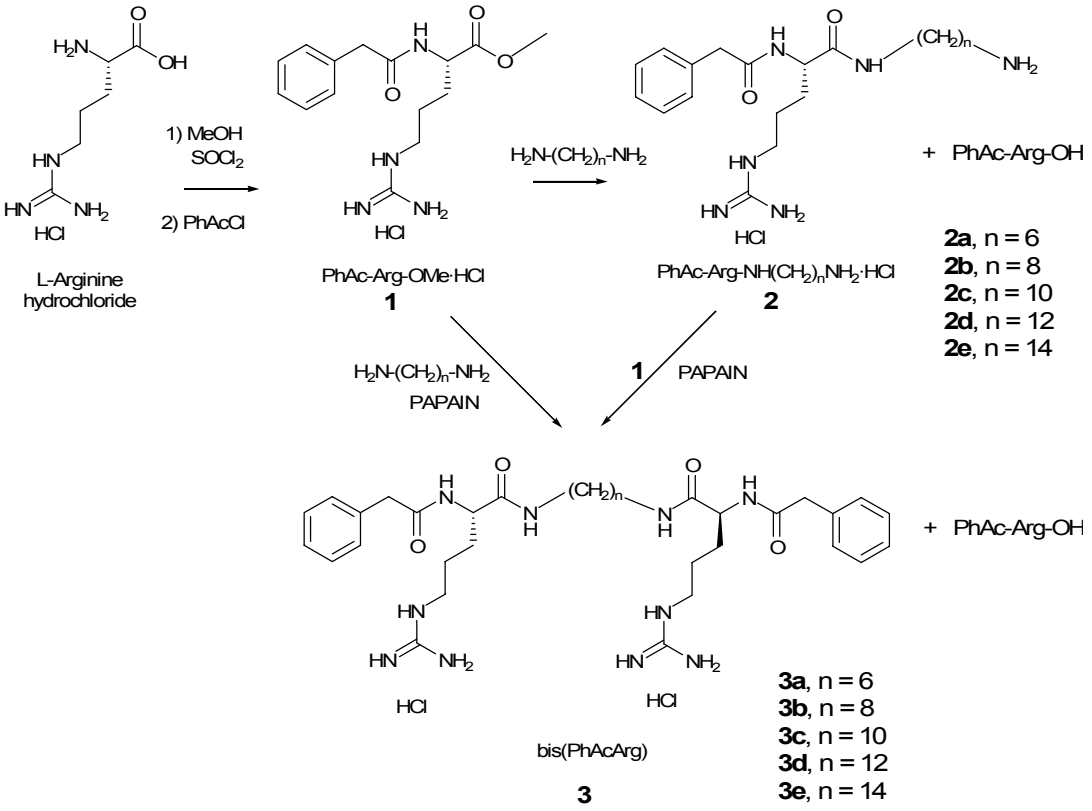

Fig. 1 Chemoenzymatic pathway of bis(PhAcArg) derivatives **3a-e**.

Firstly, the esterification of the α-carboxyl group of L-arginine (98 %) and acylation of the α-amine with phenylacetyl chloride (73 %) gave access to intermediate **1**. Then, the aminolysis of the α-methyl carboxylate group of **1** by one of the amino group of the α,ω-alkanediamine furnished compounds **2a-e**. This reaction took place without any catalyst in good yields (Table 1), using 5-7 eq. of diamine at temperature above the melting point of the corresponding diamine, which acted as solvent and reagent.

Compounds **3a-e** were then obtained by papain-catalysed amidation of **1** by **2** in ethanol/boric-borate buffer 0.1 M pH 8.2, 99.5/0.5, in good conversion (Table 2). The final purification steps (cation exchange chromatography followed by preparative HPLC) necessary to achieve highly pure products lead to moderate overall yields (21-27 %). The pure fractions were pooled and lyophilized to give

compounds **3a-d** (> 1 g, see isolated yields in Table 2) as white solids (NMR spectra in section 6.1., pages 195-199).

Table 1. Aminolysis of **1** by α,ω-alkanediamines of different lengths.

H_2N-(CH_2)n-NH_2	Temperature (°C)	PhAc-Arg-OH[a] (%)	Product **2**[a][b] (%)	Product **3**[a] (%)
n = 6	50	6	90	6
n = 8	55	9	85	9
n = 10	66	7	88	7
n = 12	72	6	87	6
n = 14	100	8	87	8

[a] Molar percentage conversion into the corresponding product with respect to PhAc-Arg-OMe (**1**) measured by HPLC of the crude reaction mixture using purified standards; reaction time: 2 h. [b] Isolated yields were not calculated, as a simple work-up was performed to remove excess diamine; therefore, the final product contained PhAc-Arg-OH and product **3**.

Table 2. Papain-catalyzed amide bond formation between **1** and **2**.

Product	Conversion[a] (%)	PhAc-Arg-OH[a] (%)	Isolated Yield (%)
3a	48	38	25
3b	48	29	21
3c	54	34	27
3d	58	25	26
3e	27	65	nr[b]

[a] Molar percentage conversion into the corresponding product with respect to PhAc-Arg-OMe (**1**), measured by HPLC from crude reaction mixture using purified standards; eeaction time: 72 h. 1.5 eq. **2** per mol PhAc-Arg-OMe. [b]No reaction.

The enzymatic amide bond formation failed for the reaction between **1** and 1,14-diaminotetradecane. Excess diamine from the previous step that had not been eliminated by simple washings appears to be responsible for the low reactions conversions. In fact, it had been observed that the diamines had a negative effect on papain activity by either acting as an inhibitor or modifying the enzyme ionization state due to the basicity of the product.[4]

To avoid the presence of an excess of diamine the formation of the bis(PhAcArg) in a one-pot enzymatic reaction, starting from the diamine and two equivalents of **1,** was undertaken. Interestingly, the new synthetic enzymatic

scheme furnished the bis(PhAcArg) in three steps, at room temperature and with reaction conversions similar to those obtained by the above described procedure (Table 3). Most importantly, this strategy allowed us to prepare the bis(PhAcArg) **3e** with 1,14-diaminotetradecane in 26 % isolated yield, comparable to those obtained with shorter spacer chain lengths

Table 3 Papain-catalyzed synthesis of **3** in one pot reaction.

Product	PhAc-Arg-OH[a] (%)	Product **2**[a] (%)	Product **3**[a] (%)
3a	13	16	55
3b	11	19	59
3c	11	17	55
3d	13	19	59
3e	10	20	37

[a] Molar percentage conversion into the corresponding product with respect to PhAc-Arg-OMe (**1**), measured by HPLC of the crude reaction mixture using purified standards; reaction time: 176 h; 1.1 equivalents of α,ω-alkanediamine per mol PhAc-Arg-OMe.

Figure 2 shows a HPLC chromatogram of a mixture of the novel bis(PhAcArg) derivatives **3a-e**. As it was expected, the higher lipophilicity of the compound, the higher retention time was measured by HPLC using a Lichrosphere 100 CN (propylciano) column.

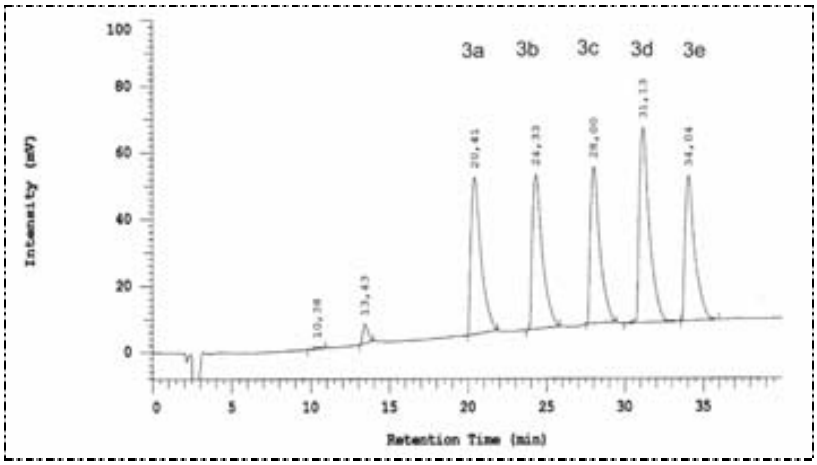

Fig. 2. Chromatogram of a mixture of bis(PhAcArg) **3a-e**. HPLC conditions: Lichrosphere 100 CN (propylcyano) column, 5 µm, 250x4 mm. Solvent A: H_2O 0.1 % TFA, Solvent B: ACN/H_2O 4:1 0.095 % TFA. Gradient: 10 to 70 % B in 40 min, P 127 bar, I 30 µl, F 1 mL min^{-1}, D 215 nm.

3.2.2. Biological properties

Antibacterial activity

Minimum inhibitory concentration (MIC) values for **3a-e**, $C_3(CA)_2$ and CHX against fifteen bacteria are summarised in Tables 4 and 5. For the sake of comparison, the MICs of $C_3(CA)_2$ and CHX also were assessed. To compare precisely compounds with different molecular weight MIC values were expressed in μM instead of the typical mg L^{-1}. For the novel bis(PhAcArg) **3**, the results indicated that there exists a clear effect of the spacer chain length on their antimicrobial properties. Overall, the lowest MIC values for the Gram-positive bacteria were achieved by **3d** (*i.e.* 12 methylene groups in the spacer chain), whereas **3e** (*i.e.* 14 methylene groups) showed the most potent inhibition of growth toward Gram-negative bacteria.

Gram-negative are generally more resistant than Gram-positive bacteria to the attack of antimicrobial agents. This can be explained by the different cell envelope structure of bacteria. Gram-negative bacteria possess an outer membrane composed mainly by lipopolysaccharides and porins which restricts the entrance of biocides and amphiphilic compounds.[5,6] The perturbation of this outer membrane requires a fine tuning of the hydrophobic-hydrophilic balance of the microbicide molecule.[7] Gram-positive bacteria possess a thick rigid and highly porous cell wall of peptidoglycans. Thus, small and hydrophilic molecules like penicillin can move through it without difficulty allowing an easy penetration of compounds into the cell.[8] Moreover, bacteria often possess efflux proteins located in the cytoplasm membrane acting as a protective mechanism against antimicrobial activity pumping out the antimicrobial molecules.[9,10]

Compared with $C_3(CA)_2$, compounds **3d**, and **3e** have an enhanced activity against Gram-positive and Gram-negative bacteria, respectively. The different antimicrobial efficiency of these compounds can be attributed to the combination of several physicochemical parameters: hydrophobicity, adsorption, aqueous solubility and transport in the test medium.

Table 4. Minimum inhibitory concentration in μM of **3a-e**, $C_3(CA)_2$ and CHX against Gram-positive bacteria.

Gram-positive bacteria	**3a**	**3b**	**3c**	**3d**	**3e**	$C_3(CA)_2$	CHX
Bacillus cereus var. mycoides	>323	>307	78	18	18	21	2
Staphyloccocus epidermidis	>323	19	39	2	36	10	2
Bacillus subtilis	>323	154	39	2	36	21	2
Staphyloccocus auerus	>323	77	19	5	36	3	1
Micrococcus luteus	>323	154	19	18	71	21	2
Enterococcus hirae	>323	>307	156	10	36	10	3
Mycobacterium phlei	>323	77	19	n.d.	n.d.	21	n.d.
Mycobacterium smegmatis	n.d.	n.d.	n.d.	n.d.	36	10	3

Table 5. Minimum inhibitory concentration in μM of **3a-e**, $C_3(CA)_2$ and CHX against Gram-negative bacteria.

Gram-negative bacteria	**3a**	**3b**	**3c**	**3d**	**3e**	$C_3(CA)_2$	CHX
Bordetella bronchiseptica	>323	154	39	37	36	5	2
Pseudomonas aeruginosa	>323	>307	>311	149	71	42	14
Salmonella typhimurium	>323	>307	>311	75	36	42	7
Enterobacter aerogenes	>323	>307	>311	149	18	42	14
Escherichia coli	>323	154	156	37	18	10	3
Klebsiella pneumoniae	>323	>307	>311	149	18	21	7
Serratia marcescens	>323	>307	>311	>298	>286	>333	7

As a measure of hydrophobicity, we estimated the logarithm of octanol-water partition coefficient (log*P*) of the compounds by using KowWin, software that is based on the atom/fragment contribution method developed at SRC (source: http://www.syrres.com). The estimated values are showed in Table 6. It is important to stress that these are estimated rather than experimental values.

Table 6. Estimated log*P* values of bis(PhAcArg) derivatives, $C_3(CA)_2$ and CHX.

Product	**3a**	**3b**	**3c**	**3d**	**3e**	$C_3(CA)_2$	CHX
log*P*	0.80	1.78	2.76	3.74	4.73	3.77	4.85

As expected, the log*P* increased on increasing the spacer chain length. Interestingly, the antimicrobial activity showed good correlation with log*P* of the bis(PhAcArg), in a good agreement with QSAR studies of biguanide biocides.[1,11] The most active compounds, including CHX, have an estimated log*P* value in a range between 3.74 and 4.85. It has been observed that the spacer chain length appears to modulate the lipophilicity of the molecule but it is not a key structural parameter for the antimicrobial activity.[1] The optimal length of the spacer chain will depend on the structure and nature of the polar heads as well as on the presence of other alkyl chains in the molecule.[2,12-14] Therefore, no individual structural moiety determined the antimicrobial activity by itself. It is the right combination of positive charges and hydrophobic groups which gave the adequate hydrophilic-lipophilic balance.[15,16]

The lowest MICs against Gram-positive and Gram-negative bacteria corresponded to **3d** and **3e**, respectively. Interestingly, these MIC values were moderately lower than that from $C_3(CA)_2$ and slightly higher than that from CHX. The optimal length of the spacer chain depends on the structure and nature of the polar head groups as well as on the presence of other alkyl chains in the molecule. Therefore, antibacterial activity cannot be determined by any given individual structural moiety alone. It is the right combination of positive charges and hydrophobic groups that provides the adequate hydrophilic-lipophilic balance.

Antifungal activity

It is known that exist more than 50000 species of fungi but only around 200 species cause disease in vertebrate animals and human beings. Fungi are basically classified in two groups: yeasts (unicellular micro-organisms with espheric or oval shape) and moulds (multicellular micro-organisms with filamentous shape) although numerous species are dimorphic (*i.e.* they can

change the morphology depending on the environmental conditions). Most pathogenic fungi are exogenous, yet the mycoses (*i. e.* infection caused by a fungus) with the highest incidence are caused by fungi that are part of the normal microbiota of the human body (opportunistic pathogens).[17] Bacterial infections are more numerous and virulent than mycosis, but antifungal chemotherapy is specially complicated due to the similarity of fungal cells with host cells. Moreover, the situation becomes more complicated because of the rapidly increasing number of immunocompromised patients and the emerging challenge of multidrug resistance.[18] In this work, the antifungal activity of bis(PhAcArg) **3a-e**, $C_3(CA)_2$ and CHX were assessed. Thus, the minimum inhibitory concentrations of the selected compounds toward 2 yeast and 6 molds were measured (Table 6).

Table 6. MICs values in μM of **3a-e**, $C_3(CA)_2$ and CHX against fungi.

Yeasts	**3a**	**3b**	**3c**	**3d**	**3e**	**$C_3(CA)_2$**	**CHX**
Candida albicans	>323	>319	312	149	143	166	55
Saccharomyces cerevisiae	>323	>319	156	149	143	166	28
Moulds							
Aspergillus repens	>323	319	78	19	36	5	7
Aspergillus niger	>323	>319	312	75	72	10	55
Penicillium chrysogenum	>323	>319	312	75	143	83	28
Cladosporium cladosporides	>323	160	78	37	18	5	7
Trichophyton mentagrophytes	>323	>319	312	149	72	21	14
Penicillium funiculosum	>323	160	78	19	18	21	7

Similarly to the antibacterial activity, the results for the novel bis(PhAcArg) **3** against fungi indicate that there exists a clear effect of the spacer chain length on the antimicrobial properties. The longer the spacer chain the higher the antifungal preservation capacity; compounds **3a** and **3b** did not show antimicrobial activity in the range tested, increasing the spacer chain did increase the antifungal effect (**3c-e**). However, $C_3(CA)_2$ and CHX are more potent

than compounds **3.** These results suggest again that the amphipathicity is the key parameter for the activity.

Compounds **3c**-**e**, $C_3(CA)_2$ and CHX showed both antibacterial and antifungal activity. Fungi are eukaryotic organisms and in many instances, antibacterial agents have no effect on them. An exception to this are the cationic biocides which main target are the bacterial cytoplasmatic and the fungal plasma membranes.[19-23]

The mechanism of action of some antifungal compounds is related to the inhibition of ergosterol biosynthesis among other metabolic pathways.[24] However, the mode of action of amphiphilic fungicides is still poorly understood. Some amphiphilic fungicides such as amphotericin B and nystatin, bind to ergosterol disrupting the membrane function, increasing its permeability and causing cell lysis.[13, 14] Pentamidine analogues (Figure 5) are dicationic aromatic compounds with equal or greater antifungal activity than that of fluconazole and amphotercin B.[25] The mitochondrion appears to be the primary cellular target of these compounds.[26]

Thus, the mode of antifungal action of **3c**-**e** could be mostly a perturbation of the plasma membrane, likely by binding to ergosterol, among other things. Furthermore, a potential effect on the mitochondrial processes might be also considered. Since this action requires the uptake of the compound through the membrane, an accurate lipophilic-hydrophilic balance of the molecule is also required.

Haemolytic effect and potential ocular irritation

In many instances, antimicrobial agents that kill or inhibit growing microbial cells may also be cytotoxic to others such as red blood cells. The determination of the haemolytic action of the compounds is a good measure to discriminate cytotoxic from non-cytotoxic compounds and also to asses the acute eye irritation potential.[27] Compounds **3a**, **3b,** and **3c** showed a low haemolytic

activity at the highest concentration tested and did not induce haemoglobin denaturation. Compounds, **3d**, **3e,** and CHX showed haemolytic activity and the results of haemolysis obtained at different concentrations are presented in a dose-response curve (Figure 3).

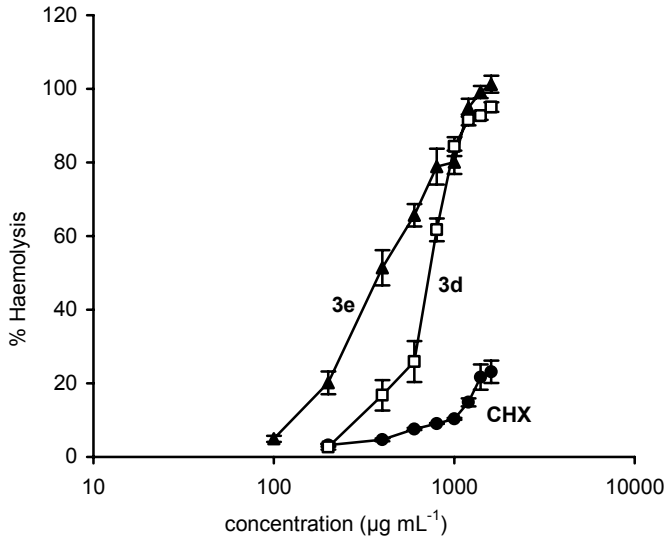

Fig. 3. Haemolysis induced by **3d** (open squares) and **3e** (black triangles) and CHX (black circles). Results are expressed as mean ± standard deviation of three experiments.

The values of the HC_{50} for **3d**, **3e**, and CHX are presented in Table 7 with the denaturation index (DI) and the lysis/denaturation ratio (L/D). From L/D ratio, CHX and **3d** can be considered as non-irritant to eyes, whereas **3e** was slightly irritant. Interestingly, CHX, **3d**, and **3e** were less irritant than $C_3(CA)_2$ which was found to be moderate irritant and more haemolytic.[28]

Table 7. Haemolytic data of **3d**, **3e** and CHX determined with human erythrocytes.

	3d	**3e**	CHX
HC_{50} (µg mL^{-1})[a]	1002 ± 81	366 ± 4	2525 ± 270
DI[b]	0	8 ± 1	0
L/D[c]	∞	46	∞
Classification	Non irritant	Slightly irritant	Non irritant

[a] Concentration giving 50 % haemolysis; values expressed as the mean ± standard deviation. [b] Denaturation index. [c] Lysis/denaturation ratio.

In the present study, CHX showed an HC_{50} higher than the reported in the literature using rabbit blood cells.[29] This should be attributed to both the different source of erythrocytes (*i.e.* from human and rabbit blood cells, respectively) and the different methodology employed.[30] The human erythrocytes have been proven to be more resistant than other species.[31] When the compounds were added to the erythrocyte suspension in an aqueous medium, they could first distribute between the erythrocyte membrane and the solution by adsorption until the equilibrium is reached. The interaction between the compound and erythrocyte membrane at sublytic concentration might be governed by the partition of the compound between the aqueous medium and the membrane. The partition is closely related to both the hydrophobicity of the compound and the ionic interaction. Haemolysis probably begins when the erythrocyte membranes are saturated with the molecules of the compound. Here, a good correlation (*i.e.* exponential relationship) was observed between the haemolysis induced by compounds **3a-e** at 1000 μg mL^{-1} and the number of methylenes of the spacer chain (Figure 4).

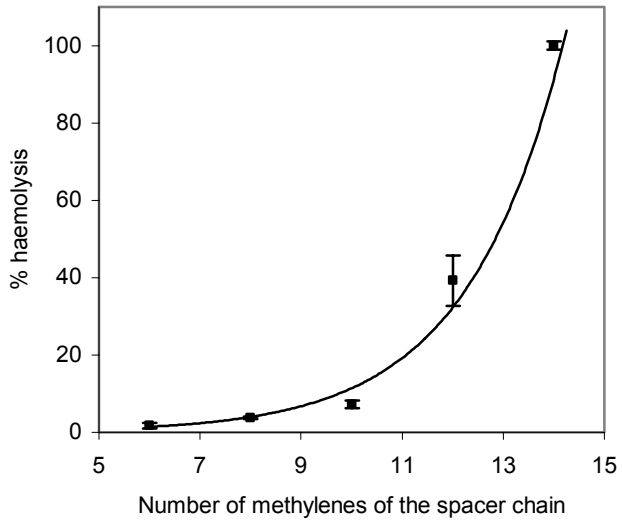

Fig. 4. Haemolytic activity of **3a-e** at 1000 μg mL^{-1} as a function of the methylene groups of the spacer chain. Results are expressed as mean ± standard deviation of three experiments. $R^2 = 0.986$ of the fitted curve.

The literature shows different examples on the relationship between haemolysis and the alkyl chain length of surfactants.[28,32-35] Overall, the longer

the alkyl chain length the higher the haemolytic activity within a family of structurally related compounds.

Despite the fact that the log*P* values of CHX, **3e**, and $C_3(CA)_2$ are comparable, CHX showed a lower haemolytic activity. It was observed that the interfacial activity of CHX was much lower than that of $C_3(CA)_2$, therefore, this may also be an important parameter to consider.[36] Again, the right combination of more than one parameter may explain the overall activity of the compounds.

Antileishmanial activity

Chemotherapy for parasitic infections such as leishmaniasis is still problematic as most of the drugs in use were developed over 40 years ago and suffer from drawbacks ranging from toxicity to the emergence of resistance. One example are aromatic diamidines such as pentamidine (Figure 5), which are effective agents for the treatment of protozoal infections.[37,38]

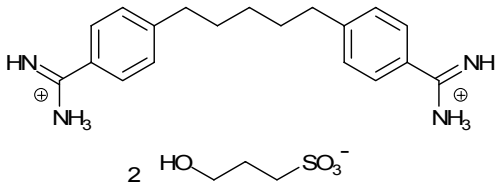

Fig. 5 Structure of pentamidine isethionate salt.

Due to the similar structure of the novel bis(PhAcArg) derivatives with pentamidine, we decided to assess their potential antileshmanial activity. (section 4.3.17., page 170) Initially, the chosen compounds were compounds **3a** and **3d-e**. Pentamidine isethionate salt was tested for the sake of comparison. The antileishmanial activity was measured on bases of the IC_{50} values (*i.e.* concentration of an inhibitor that is required for 50 % inhibition of the micro-organism). The results showed that **3a** did not significant show activity and **3d-e** showed lower activity than pentamidine (see Table 8).

Table 8. IC_{50} (μM)of compounds **3a**, **3d-e** and pentamidine toward *Leishmania infatum*.

Product	IC_{50} (μM) Average	Standard deviation
Pentamidine	22.0	1.3
3a	>800	---
3d	58.4	13.9
3e	45.0	7.9

In summary, novel bis(PhAcArg) derivatives were prepared by a facile chemoenzymatic methodology. The key step in the synthesis was the papain-catalysed amide bond formation between the N^{α}-phenylacetyl arginine methyl ester and the corresponding α,ω-alkanediamine. Replacement of the N^{α}-caproyl groups in the $C_3(CA)_2$ by N^{α}-phenylacetyl moieties lead to novel bis(PhAcArg) derivatives with enhanced antibacterial activity but lower antifungal activity than that of both $C_3(CA)_2$ and CHX. Their MICs values point out that the larger spacer alkyl chain, the more potent antimicrobial action. Therefore, we can conclude that the hydrophilic-lipophilic balance plays a key role in the antimicrobial activity of the novel bis(PhAcArg) derivatives, suggesting that these compounds act as membrane-active agent and their first target could be the bacterial cytoplasmic membrane and the fungal plasma membrane. Finally, the products showed low haemolytic activity against human erythrocytes and they did not show significant antileishmanial activity.

References:

1. Wernert, G. T.; Winkler, D. A.; Holan, G.; Nicoletti, G., Synthesis, biological activity, and QSAR studies of antimicrobial agents containing biguanides isosteres. *Austral. J. Chem.* **2004**, *57*, 77-85.
2. Pérez, L.; Torres, J. L.; Manresa, A.; Solans, C.; Infante, M. R., Synthesis, aggregation, and biological properties of a new class of gemini cationic amphiphilic compounds from arginine, bis(Args). *Langmuir* **1996**, *12*, 5296-5301.
3. Pérez, L.; Pinazo, A.; Rosen, M. J.; Infante, M. R., Surface Activity Properties at Equilibrium of Novel Gemini Cationic Amphiphilic Compounds

from Arginine, Bis(Args). *Langmuir* **1998**, *14*, 2307-2315.
4. Piera, E.; Infante, M. R.; Clapés, P., Chemoenzymatic synthesis of arginine-based gemini surfactants. *Biotech. Bioeng.* **2000**, *70*, 323-331.
5. Oros, G.; Cserhati, T.; Forgacs, E., Separation of the strength and selectivity of the microbiological effect of synthetic dyes by spectral mapping technique. *Chemosphere* **2003**, *52*, 185-193.
6. Rosen, M. J.; Fei, L.; Zhu, Y.-P.; Morrall, S. W., The relationship of the environmental effect of surfactants to their interfacial properties. *J. Surfactants Deterg.* **1999**, *2*, 343-347.
7. Infante, M. R.; Pinazo, A.; Seguer, J., Non-conventional surfactants from amino acids and glycolipids: Structure, preparation and properties. *Colloids Surf. A* **1997**, *123-124*, 49-70.
8. Patrick, G. L., *An introduction to Medicinal Chemistry*. 3ª ed.; Oxford University Press: New York, 2005; p 393.
9. Russell, A. D., Mechanisms of bacterial insusceptibility to biocides. *Am. J. Infect. Control* **2001**, *29*, 259-261.
10. Köhler, T.; Pechère, J.-C.; Plésiat, P., Bacterial antibiotic efflux systems of medical importance. *Cell. Mol. Life Sci.* **1999**, *56*, 771-778.
11. Warner, V. D.; Lynch, D. M.; Kim, K. H.; Grunewald, G. L., Quantitative structure-activity relationships for biguanides, carbamimidates, and bisbiguanides as inhibitors of *Streptococcus mutans* Nº. 6715. *J. Med. Chem.* **1979**, *22*, 359-366.
12. Pérez, L.; García, M. T.; Ribosa, I.; Vinardell, M. P.; Manresa, A.; Infante, M. R., Biological properties of arginine-based gemini cationic surfactants. *Environ. Toxicol. Chem.* **2002**, *21*, 1279-1285.
13. Menger, F. M.; Keiper, J., Gemini Surfactants. *Angew. Chem. Int. Ed.* **2000**, *39*, 1906-1920.
14. Massi, L.; Guittard, F.; Levy, R.; Duccini, Y.; Geribaldi, S., Preparation and antimicrobial behaviour of gemini fluorosurfactants. *Eur. J. Med. Chem.* **2003**, *38*, 519-523.
15. Tanzer, J. M.; Slee, A. M.; Kamay, B. A., Structural Requirements of Guanide, Biguanide, and Bisbiguanide Agents for Antiplaque Activity. *Antimicrob. Agents Chemother.* **1977**, *12*, 721-729.
16. Appelt, C.; Wessolowski, A.; Söderhäll, J. A.; Margitta, D.; Schmieder, P., Structure of the Antimicrobial, Cationic Hexapeptide Cyclo(RRWWRF) and Its Analogues in Solution and Bound to Detergent Micelles. *ChemBioChem* **2005**, *6*, 1654-1662.
17. Siqueira, J. F.; Sen, B. H., Fungi in endodontic infections. *Oral Surg. Oral Med., Oral Pathol. Oral Radiol. Endod* **2004**, *97*, 632-641.
18. Janiak, A. M.; Hoffmann, M.; Milewska, M. J.; Milewski, S., Hydrophobic derivatives of 2-amino-2-deoxy-glucitol-6-phosphate: A new type of -Glucosamine-6-phosphate synthase inhibitors with antifungal action. *Bioorg. Med. Chem.* **2003**, *11*, 1653-1662.
19. Massi, L.; Guittard, F.; Geribaldi, S.; Levy, R.; Duccini, Y., Antimicrobial properties of highly fluorinated bis-ammonium salts. *Int. J. Antimicrob. Agents* **2003**, *21*, 20-26.
20. Codling, C., Maillard, J. Y., Russell, D., Aspects of the antimicrobial mechanism of action of a polyquaternium and an amidoamine. *J. Antimicrob. Chemother.* **2003**, *51*, 1153-1158.

21. Togashi, I.; Gisusi, S.; Harada, A., Antifungal activity of commercial disinfectants against a benomyl-tolerant strain of *Trichoderma harzianum*. *J. Wood Sci.* **1998**, *44*, 414-416.
22. Tortorano, A. M.; Viviani, M. A.; Biraghi, E.; Rigoni, A. L.; Prigitano, A.; Grillot, R.; EBGA Network, In vitro testing of fungicidal activity of biocides against *Aspergillus fumigatus*. *J. Med. Microbiol.* **2005**, *54*, 955-957.
23. Codling, C. E.; Hann, A. C.; Maillard, J. Y.; Russell, A. D., An investigation into the antimicrobial mechanisms of action of two contact lens biocides using electron microscopy. *Cont. Lens Anterior Eye* **2005**, 28, 163-168.
24. Odds, F. C.; Brown, A. J. P.; Gow, N. A. R., Antifungal agents: mechanisms of action. *Trends Microbiol.* **2003**, 11, 272-279.
25. Del Poeta, M.; Schell, W. A.; Dykstra, C. C.; Jones, S.; Tidwell, R. R.; Czarny, A.; Bajic, M.; Bajic, M.; Kumar, A.; Boykin, D.; Perfect, J. R., Structure-In Vitro Activity Relationships of Pentamidine Analogues and Dication-Substituted Bis-Benzimidazoles as New Antifungal Agents. *Antimicrob. Agents Chemother.* **1998**, *42*, 2495-2502.
26. Ludewig, G.; Williams, J. M.; Li, Y.; Staben, C., Effects of pentamidine isethionate on *Saccharomyces cerevisiae*. *Antimicrob. Agents Chemother.* **1994**, *38*, 1123-1128.
27. Pape, W. J.; Pfannenbecker, U.; Hoppe, U., Validation of the red blood cell test system as in vitro assay for the rapid screening of irritation potential of surfactants. *Mol. Toxicol.* **1987**, *1*, 525-36.
28. Mitjans, M.; Martínez, V.; Clapés, P.; Pérez, L.; Infante, M. R.; Vinardell, M. P., Low potential ocular irritation of arginine-based gemini surfactants ant their mixtures with nonionic and zwitterionic surfactants. *Pharm. Res.* **2003**, *20*, 1697.
29. Ansel, H. C., Hemolysis of erythrocytes by antibacterial preservatives. IV. Hemolytic activity of chlorhexidine diacetate. *J. Pharm. Sci.* **1967**, *56*, 616-619.
30. Vives, M. A.; Infante, M. R.; Vinardell, M. P., Comparative study of the resistance of different erythrocytes to hemolysis by the surfactant lysine laurate. *J. Pharm. Sci.* **1997**, *3*, 601-604.
31. Udden, M. M.; Patton, C. S., Hemolysis and deformability of erythrocytes exposed to butoxyacetic acid, a metabolite of 2-butoxyethanol: I. Sensitivity in rats and resistance in normal humans. *J. Appl. Toxicol.* **1994**, *14*, 91-96.
32. Dufour, S.; Deleu, M.; Nott, K.; Wathelet, B.; Thonart, P.; Paquot, M., Hemolytic activity of new linear surfactin analogs in relation to their physico-chemical properties. *Biochim. Biophys. Acta: General Subjects* **2005**, *1726*, 87-95.
33. Galembeck, E.; Alonso, A.; Meirelles, N. C., Effects of polyoxyethylene chain length on erythrocyte hemolysis induced by poly[oxyethylene (n) nonylphenol] non-ionic surfactants. *Chem. Biolog. Interact.* **1998**, *113*, 91-103.
34. Dubnickova, M.; Bobrowska, M.; Soderstrom, T.; Iglic, A.; Hagerstrand, H., Gemini (dimeric) surfactant perturbation of the human erythrocyte. *Acta Biochim. Pol.* **2000**, *47*, 651-660.
35. Macián, M.; Seguer, J.; Infante, M. R.; Selve, C.; Vinardell, M. P., Preliminary studies of the toxic effects of nonionic surfactants derived from lysine. *Toxicology* **1996**, *106*, 1-9.
36. Castillo, J. A.; Pinazo, A.; Carilla, J.; Infante, M. R.; Alsina, M. A.; Haro, I.; Clapés, P., Interaction of antimicrobial arginine-based cationic surfactants with liposomes and lipid monolayers. *Langmuir* **2004**, *20*, 3379-3387.

37. Donkor, I. O.; Assefa, H.; Rattendi, D.; Lane, S.; Vargas, M.; Goldberg, B.; Bacchi, C., Trypanocidal activity of dicationic compounds related to pentamidine. *Eur. J. Med. Chem.* **2001**, *36*, 531-538.
38. Bell, C. A.; Cory, M.; Fairley, T. A.; Hall, J. E.; Tidwell, R. R., Structure-activity relationships of pentamidine analogs against Giardia lamblia and correlation of antigiardial activity with DNA-binding affinity. *Antimicrob. Agents Chemother.* **1991**, *35*, 1099-1107.

3.4. Chemoenzymatic synthesis and biological properties of D-fagomine and *N*-alkyl-D-fagomine derivatives

D-Fagomine, (2*R*,3*R*,4*R*)-2-hydroxymethylpiperidine-3,4-diol (Figure 1), is a naturally occurring iminosugar, which was first isolated from buckwheat seeds of *Fagopyrum esculentum* Moench,[1] with remarkable biological properties. This polyhydroxylated piperidine has inhibitory activity against mammalian intestinal α-, ß-glucosidase and α-, ß-galactosidase.[2, 3] Moreover, it appears to have a potent antihyperglycemic effect on streptozotocin-induced diabetic mice and promotes glucose-induced insulin secretion.[4, 5] Segraves *et al.* have found that *C*-alkylated 3,4-di-*epi*-fagomines from *Batzella* sp. sponge have a good antimicrobial activity against *Staphylococcus epidermidis*.[6]

In this chapter, D-fagomine and *N*-alkylated D-fagomine derivatives were prepared using the novel fructose-6-phosphate aldolase (FSA) and biological assays such as their antimicrobial activity against bacteria and fungi, inhibitory activity against glycosidases and their haemolytic activity were assessed.

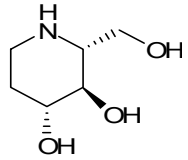

Fig. 1. Structure of D-fagomine.

3.4.1 Chemoenzymatic synthesis

D-Fagomine has been previously synthesized in our group with good diastereoselectivity (de 72 %).[7] The key step was the aldol addition of dihydroxyacetone phosphate (DHAP) to *N*-Cbz-3-amino-1-propanal catalyzed by using the commercial fructose-1,6-bis-phosphate aldolase from rabbit muscle, namely RAMA (Figure 2).

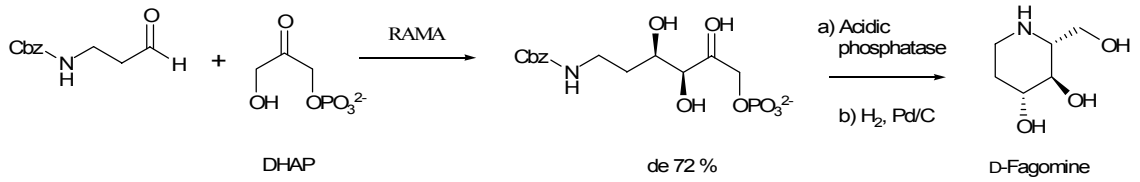

Fig. 2. Chemoenzymatic pathway of D-fagomine. RAMA catalyzed the aldol addition of DHAP to *N*-Cbz-3-aminopropanal.

In the present work, the key step was the stereoselective carbon-carbon bond formation between dihydroxyacetone (DHA) and *N*-Cbz-3-amino-1-propanal (Fig. 3). Here, the aldol addition was catalyzed by the novel fructose-6-aldolase (FSA). The cloning and overexpression in *E. coli* DH5α of the gene encoding FSA and the biochemical characterization was carried out for the first time by Schürmann *et al.*[8] These authors reported aldol additions of either DHA or hydroxyacetone to some hydroxyaldehydes for the synthesis of sugar derivatives.[9] Here, after growing and disrupting the *E. coli* cells, the enzyme was purified easily by a heat treatment at 75 °C during 40 min, centrifugation and lyophilisation of the supernatant to yield a pale brown powder with 1.7 U mg^{-1} (section 4.3.14., page 164). Further purification steps were not necessary since they were not crucial for the activity and stereoselectivity of the enzymatic aldol addition.

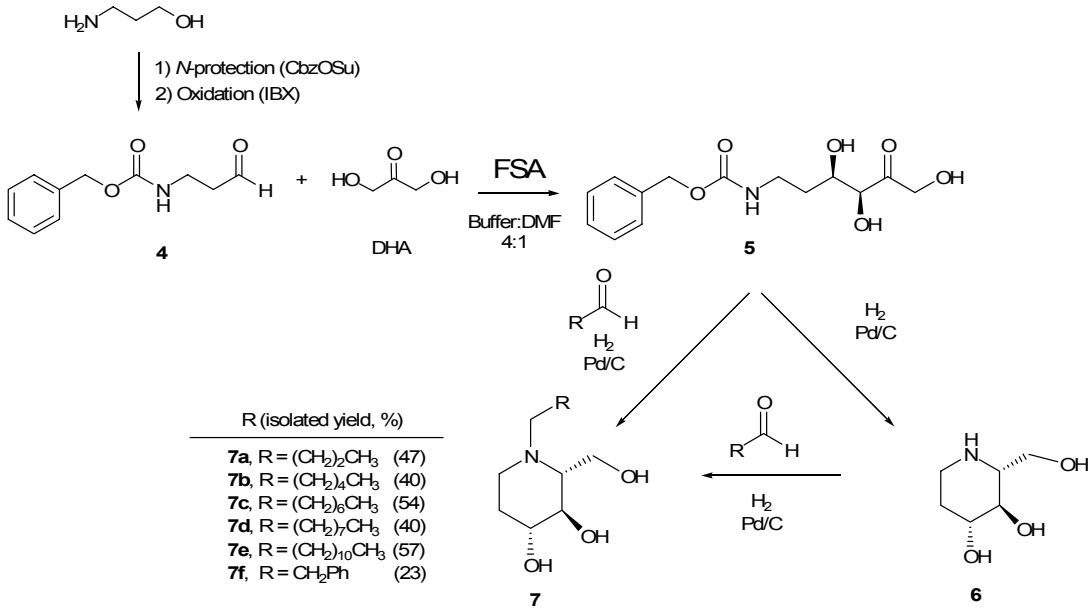

Fig. 3. Chemoenzymatic pathway of D-fagomine **6** and *N*-alkylated derivatives **7a-f**.

The FSA-catalyzed aldol addition between DHA and **4** was conducted at 4 ºC in boric-borate 50 mM pH 7 buffer containing 20 % v/v DMF, furnishing the aldol adduct **5** (isolated yield 69 %). The NMR spectra of the crude reaction showed small signals which corresponded to the minor diastereoisomer **8**. As shown in Figure 4, the low intensity of the signals and the overlapping with other signals made very difficult to quantify the diastereomeric ratio.

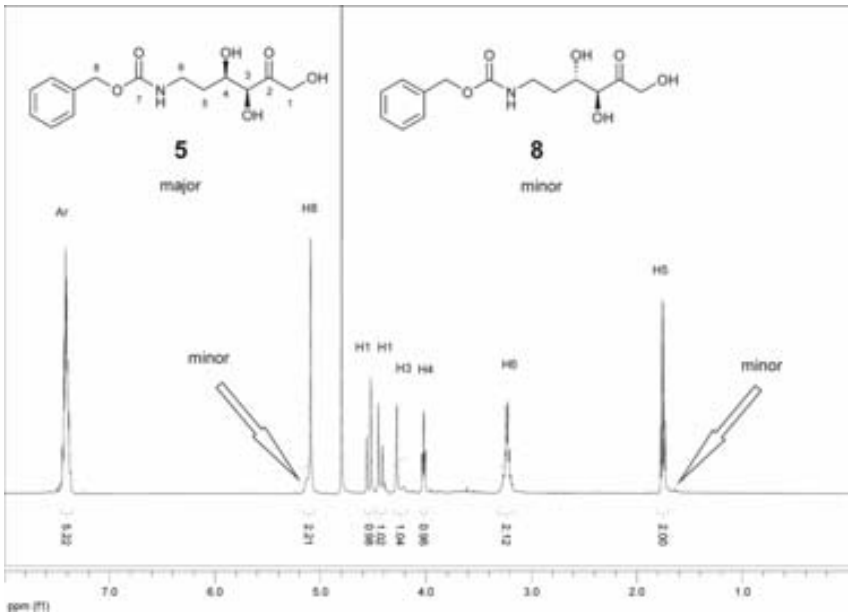

Fig. 4. ^{1}H-NMR spectrum of the FSA-catalyzed crude reaction between DHA and aldehyde **1**.

The formation of **8** was unequivocally assessed by comparing the NMR analyses of the adduct from the RAMA-catalyzed aldol addition of DHAP to *N*-Cbz-3-aminopropanal (Figure 5).[7] Based on mechanistic considerations of the DHAP-aldolases, it can be assumed that the absolute configuration at C-3 depends on the enzyme and it is conserved upon reaction with any acceptor. Consequently, the major diastereoisomer formed from the RAMA-catalyzed aldol addition of DHAP to *N*-Cbz-3-aminopropanal was (3*S*,4*R*)-6-[benzyloxy-carbonyl)amino]-5,6-dideoxy-1-*O*-phophonohex-2-ulose sodium salt **9** (de 72 %) (Figure 5). This ^{1}H-NMR spectrum also shows signals from the minor diastereoisomer (3*S*,4*S*) and other signals from the cyclic hemiaminal formed by spontaneous cyclation of the linear adduct.[7]

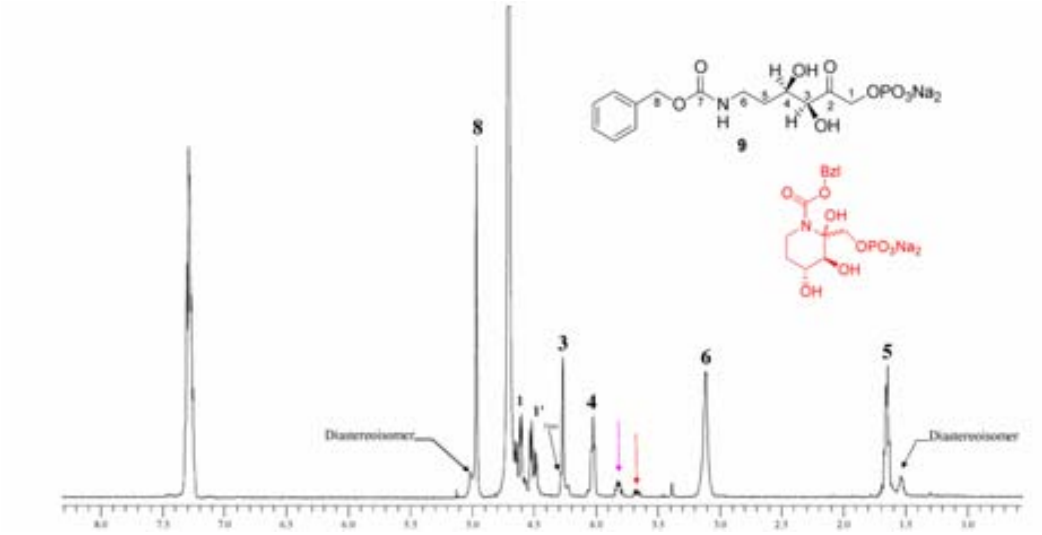

Fig. 5. ^{1}H-NMR spectrum of the RAMA-catalyzed crude reaction between DHAP and aldehyde **4**.

D-Fagomine **6** was obtained by selective catalytic reductive amination (H_2 50 psi, Pd/C) of **5** in 89 % isolated yield and diastereomeric ratio 93:7 (*i.e.* de 86 %) measured by NMR; $[\alpha]_D^{20}$ = +20.4 (*c* 1.0, H_2O) (lit[3] $[\alpha]_D^{20}$ = +19.5 (*c* 1.0, H_2O)). This positive value of the optical rotation indicates that the major compound was D-fagomine, discarding the formation of the corresponding enantiomer. Here, the aldol addition proceeds with complete stereospecificity with respect to the configuration on carbon 3 and in with slightly decreased specificity on carbon 4, involving the formation of D-2,4-di-*epi*-fagomine **10** as a minor diastereisomer (Figure 6).

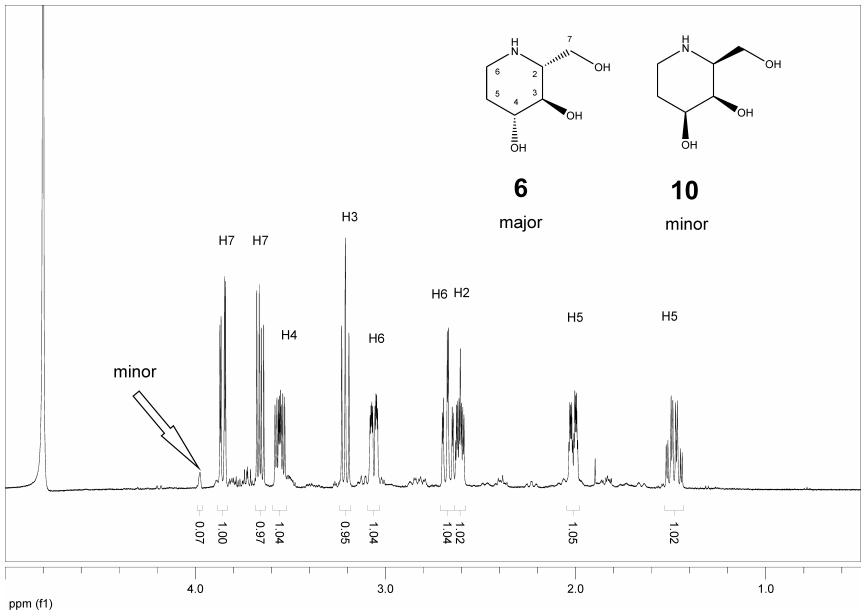

Fig. 6. ^{1}H-NMR spectrum of D-fagomine crude.

The inspection of the stereochemistry at the C-2 position for iminocyclitols revealed that the reductive amination of linear *N*-Cbz-aminopolyols with Pd/C is highly stereoselective, as reported previously by other authors.[10-13] Interestingly, it has been reported that in five- and six-membered ring systems, hydrogenation took place from the face opposite to the C-4 hydroxyl group, regardless of the stereoselectivity of the other substituents (Figure 7). Hence, the stereochemistry observed at C-2 was controlled by the configuration at C-4.[7, 14] During this hydrogenolysis, we also assumed that the stereochemistry at C-3 and C-4 is conserved and no epimerization occurred.[10, 12, 13] Thus, we can conclude that the analysis of the NMR spectrum of D-fagomine crude allows elucidating the stereoselectivity of the enzymatic reaction catalyzed by FSA (de 86 %).

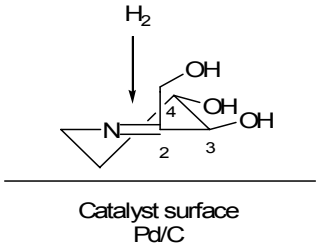

Fig. 7. Diastereoselectivity of the reductive amination for imine from aldol adduct **5**.

Further purification of the D-fagomine crude (24 mg) by cation exchange chromatography on CM-sepharose in NH_4^+ form, eluted isocratically with NH_4OH 0.01 M, gave an excellent separation of D-fagomine **6** (83 % recovery and de ≥ 99 %) and a minor diastereoisomer identified as D-2,4-di-*epi*-fagomine **10** (<1 mg) (see NMR spectra in section 6.1.). This minor diastereisomer arose from the *re*-face attack of the DHA-FSA complex on the aldehyde, similar to that found with D-fructose-1,6-bisphosphate aldolase.[7]

The reductive amination (H_2 50 psi, Pd/C) of different aldehydes in presence of D-fagomine gave the desired *N*-alkylated derivatives **7a-f** (Figure 3). These crude reactions were purified by silica column chromatography affording **7a-f** as unique diastereoisomers (isolated yields 40-50 %). Most interestingly, the reductive amination of butanal, octanal and nononal in the presence of the aldol adduct **5** also gave the iminocyclitols **7a** and **7c-d** as unique diastereoisomers

after purification by silica column chromatography (isolated yields 40-50 %). Thus, this one-pot reaction afforded the same stereoselectivity and similar isolated yields than that obtained from the former two step strategy (see NMR spectra in section 6.1.).

Synthetic advantages of FSA vs RAMA

It is remarkable that the use of FSA showed the following advantages *versus* the use of RAMA in the preparation of the aldol adduct **5**:

- FSA accepts DHA as donor, a simple starting material whereas RAMA requires DHAP as donor, an expensive reagent with low stability in aqueous solution at pH > 7.
- FSA affords the aldol adduct **5** while RAMA affords the same aldol adduct with a phosphate group, which can be cleaved using an acidic phosphatase.
- FSA affords the aldol adduct **5** with higher diastereoselectivity (de 86 %) than RAMA (de 72 %).

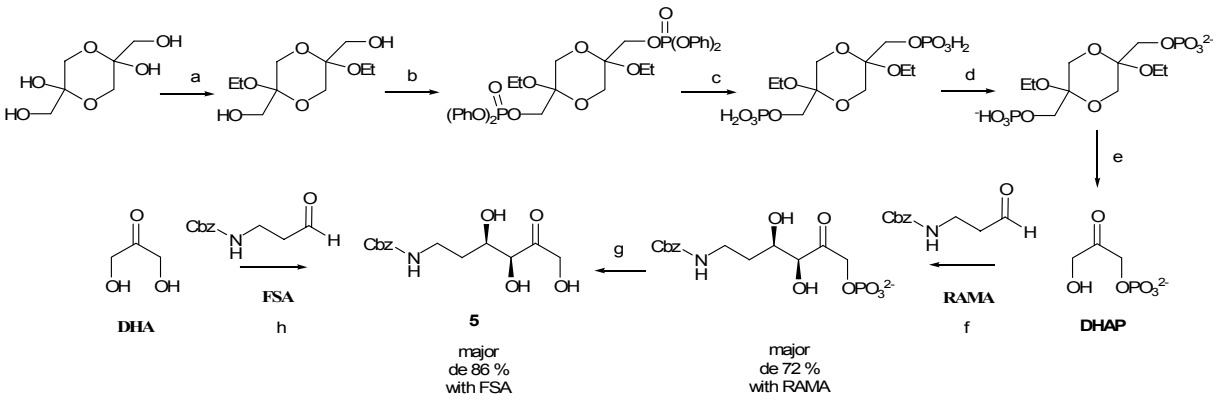

Fig. 8. Synthetic approaches of aldol adduct **5** using RAMA and FSA. Reagents: (a) $HC(OEt)_3$ in $EtOH/H_2SO_4$, (b) $Cl(O)P(OPh)_2$ in anhydrous pyridine, (c) H_2/PtO_2, (d-e) NaOH, acidic Dowex resin and then 65 °C, (f) buffer pH 7.0/ DMF 4:1, (g) acidic phosphatase, (h) buffer pH 7.0/ DMF 4:1.

Investigations of the synthetic abilities of FSA in organic synthesis will be studied in our group. We have found that this enzyme accepts, among others, *N*-Cbz-glycinal and *N*-Cbz-3-amino-2-hydroxypropanal, but α-alkyl branched *N*-Cbz-aminoaldehydes were not tolerated as substrates.

Reductive amination using $NaBCNH_3$

To the best of our knowledge, the preparation or isolation of iminocyclitol **11** has not been reported yet. We planned a synthetic approach shown in Figure 9 in order to obtain compound **11**. The ^{1}H-NMR of the hydrogenolysis crude showed that the *N*-deprotection was achieved successfully. Then, sodium cyanoborohydride was added to the mixture. The reaction crude was purified by flash chromatography on silica but the ^{1}H-NMR analyses showed that D-fagomine was formed as major compound.

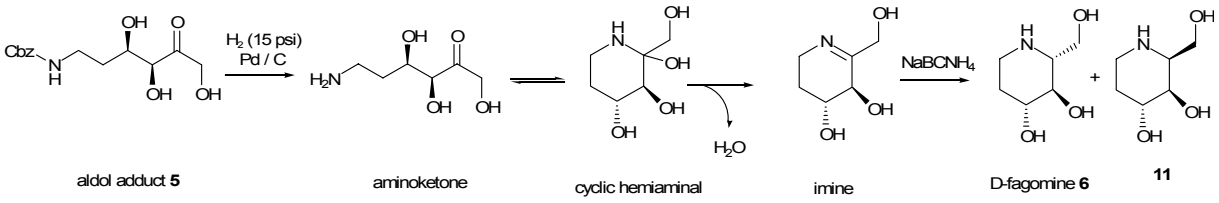

Fig. 9. Synthetic approach proposed to obtain diastereoisomer **11**.

3.4.2. Biological properties

Antimicrobial activity

The antimicrobial activity of D-fagomine **6** and the *N*-alkylated derivatives **7a-f** was measured on the basis the MIC values. Hence, all compounds were tested against 15 bacteria (8 Gram-positive and 7 Gram-negative bacteria) and 7 fungi (2 yeasts and 5 moulds) (see Table 1). Compounds **6**, **7a-d** and **7f** did not show activity at concentrations below 256 μg mL^{-1}, thus with much lower potency than that found for antiseptics such as cationic surfactants and biguanides.[15] Only compound **7e** showed moderate antimicrobial activity.

Interestingly, **7e** gave minimum inhibitory concentrations ranging from 32 to 64 μg mL^{-1} against most of the Gram-positive bacteria tested, whereas MICs of 128-256 μg mL^{-1} were observed for the Gram-negative bacteria. Compound **7e**

showed moderate antifungal activity. These results point out that iminocyclitols **6** and **7a-f** are highly hydrophilic compounds and higher lipophilicity is required to improve their antimicrobial action. In good agreement, Murata *et al.* have reported the antibacterial activity of five homologues of *N´*-alkyl-*N*-(2-aminoethyl)piperidines.[16] They found that the most potent agents are the tetradecyl and hexadecyl derivatives, showing MICs values around 2-40 μM against four bacteria. Consequently, it appears that *N*-alkyl-piperidines such as compounds **7a-f** target the cytoplasmatic membrane since their hydrophilic-lipophilic balance plays an important role, discarding more specific antimicrobial mechanisms as inhibition of bacterial enzymes, inhibition of DNA replication, etc.

Table 1. MICs in mg L^{-1} of *N*-dodecyl-D-fagomine **7e**.

Gram-positive bacteria	MIC	Gram-negative bacteria	MIC	Yeasts	MIC
Enterococcus hirae	32	*Salmonella typhimurium*	256	*Candida albicans*	>256
Mycobacterium smegmatis	128	*Bordetella bronchiseptica*	128	*Saccharomyces cerevisiae*	256
Staphylococcus aureus	64	*Pseudomonas aeuroginosa*	256	Moulds	
Bacillus subtlis	32	*Klebsiella pneumoniae*	256	*Aspergillus repens*	32
Bacillus cereus var. mycoides	32	*Escherichia coli*	128	*Penicillium chrysogenum*	256
Staphylococcus epidermidis	64	*Enterobacter aerogenes*	>256	*Cladosporium cladosporoides*	64
Micrococcus luteus	32	*Serratia marcescens*	>256	*Trichophyton mentagrophytes*	128
Micrococcus phley	64			*Penicillium funiculosum*	128

Inhibition of glucosidases

Since D-fagomine was reported to have inhibitory activity on α-glucosidase,[2, 3] different chemical modifications have been introduced to improve its activity and selectivity. Goujon *et al.* synthesized α-1-*C*-substituted derivatives with or without *N*-butyl group, which exhibited higher inhibitory activity than the parent compound against α-glucosidase from rice.[17] On the other hand, the substitution of the piperidine ring for an azepane ring decreased the inhibitory activity against both enzymes.[18]

Compounds **6** and **7a-f** were inhibitors of α-D-glucosidase from rice and ß-D-galactosidase from bovine liver (Table 2), whereas no inhibition was observed against ß-D-glucosidase from baker's yeast, ß-D-glucosidase from almond, α-D-mannosidase from jack beans and α-L-rhamnosidase from *Penicillium decumbens*. Interestingly, among the *N*-alkylated derivatives, **7d** and **7e** were the best inhibitors against α-D-glucosidase whereas **7e** was a good inhibitor for the ß-galactosidase. As shown in Table 2, the activity of **7a-f** against α-glucosidase increased with the aliphatic chain length up to 9 carbon atoms (**7d**). Rising the number of carbon atoms to 12 (**7e**) or including an aromatic moiety (**7f**) did not improve or caused a drastic decrease on the inhibitory activity, respectively. Kinetic studies indicated that active compounds behaved as competitive inhibitors of α-D-glucosidase from rice. These results suggested that **6** may interact with the subsite -1 of the two catalytic sites reported for α-glucosidase family II[19] and the *N*-alkyl substituent with a convenient length may fit into subsite +1, but not with the phenylethyl substitution. Inhibition of α-D-galactosidase from bovine liver by **6** and **7a-f** is also depicted in Table 2.

Table 2. Inhibition of glycosidases by compounds **6** and **7a-f**

Compound	α-D-glucosidase[a]		ß-D-galactosidase[b]	
	K_i (μM)[c]	IC_{50} (μM)	K_i (μM)[d]	IC_{50} (μM)
6	9.3	13.2	35.9	30.4
7a	126	151		NI[e]
7b	73.3	61.4		NI[e]
7c	27.3	35.3	242	203
7d	14.9	18.1	140	108
7e	16.4	20.7	9.3	6.0
7f	143	159	691	416

[a] From rice, [b] from bovine liver, [c] competitive inhibition, [d] non-competitive, [e] no inhibitor

For **7a-e,** the higher the hydrophobicity the lower the IC_{50} values, **7e** being the most active one. Inhibitory activity of **7e** was similar to that reported for the D-galacto isomer of **6**[20] and higher than that found for **6** or its α-1-*C*-ethyl

derivative.[21] Active compounds inhibited this enzyme in a non competitive manner, with a K_i value for **7e** 4-fold lower than that for **6**.

Cytotoxicity

Cytotoxicity of **6** and **7a**-**f** was estimated by determination of their haemolytic and protein denaturation effects on human erythrocytes.[22] The results showed that they did not have activity, with the exception of **7e**. The HC_{50} (*i.e.* concentration that induces the haemolysis of 50 % of the cells) for compound **7e** was 138±8 mg mL^{-1}, whereas the denaturation index (DI, *i.e.* hemoglobin denaturation induced by the compound) was 5±1. These values compare with commercial decylglucoside (HC_{50} 252±6 mg mL^{-1} and DI 14.2).[22]

As brief summary, the novel aldolase FSA allowed the preparation of D-fagomine in two steps from inexpensive and achiral starting materials such us DHA and *N*-Cbz-3-aminopropanal. *N*-dodecyl-D-fagomine **7e** elicited antibacterial, antifungal and activity with slight selectivity against Gram-positive bacteria, suggesting that these iminocyclitols target cytoplasmic membrane although higher lipophilicity is required to enhance their antimicrobial activity.

References:

1. Koyama, M.; Sakamura, S., Structure of a new piperdine derivative from buckwheat seeds (Fagopyrum esculentum). *Agr. Biol. Chem.* **1974**, *38*, 1111-1112.
2. Scofield, A. M.; Fellows, L. E.; Nash, R. J.; Fleet, G. W. J., Inhibition of mammalian digestive disaccharidases by polyhydroxy alkaloids. *Life Sci.* **1986**, *39*, 645-650.
3. Kato, A.; Asano, N.; Kizu, H.; Matsui, K.; Watson, A. A.; Nash, R. J., Fagomine Isomers and Glycosides from *Xanthocercis zambesiaca*. *J. Nat. Prod.* **1997**, *60*, 312-314.
4. Nojima, H.; Kimura, I.; Chen, F.-J.; Sugihara, Y.; Haruno, M.; Kato, A.; Asano, N., Antihyperglycemic Effects of *N*-Containing Sugars from *Xanthocercis zambesiaca*, *Morus bombycis*, *Aglaonema treubii*, and *Castanospermum australe* in Streptozotocin-Diabetic Mice. *J. Nat. Prod.* **1998**, *61*, 397-400.
5. Taniguchi, S.; Asano, N.; Tomino, F.; Miwa, I., Potentiation of glucose-induced insulin secretion by fagomine, a pseudo-sugar isolated from mulberry leaves. *Horm. Met. Res.* **1998**, *30*, 679-683.

6. Segraves, N. L.; Crews, P., A Madagascar sponge Batzella sp. as a source of alkylated Iminosugars. *J. Nat. Prod.* **2005**, *68*, 118-121.
7. Espelt, L.; Parella, T.; Bujons, J.; Solans, C.; Joglar, J.; Delgado, A.; Clapés, P., Stereoselective aldol additions catalyzed by dihydroxycetona phosphate-dependent aldolases in emulsion systems: preparations and structural characterization of linear and cyclic iminopolyols from aminoaldehydes. *Chem. Eur. J.* **2003**, *9*, 4887-4899.
8. Schürmann, M.; Sprenger, G. A., Fructose-6-phosphate Aldolase Is a Novel Class I Aldolase from *Escherichia Coli* and is Related to a Novel Group of Bacterial Transaldolases. *J. Biolog. Chem.* **2001**, *276*, 11055-11061.
9. Schürmann, M.; Sprenger, G. A., Fructose 6-phosphate aldolase and 1-deoxy-D-xylulose 5-phosphate synthase from *Escherichia coli* as tools in enzymatic synthesis of 1-deoxysugars. *J. Mol. Cat. B: Enzymatic* **2002**, *19-20*, 247-252.
10. Kajimoto, T.; Chen, L.; Liu, K. K. C.; Wong, C.-H., Palladium-mediated stereocontrolled reductive amination of azido sugars prepared from enzymic aldol condensation: a general approach to the synthesis of deoxy aza sugars
J. Am. Chem. Soc. **1991**, *113*, 6678-6680.
11. Liu, K. K. C.; Kajimoto, T.; Chen, L.; Zhong, Z.; Ichikawa, Y.; Wong, C. H., Use of dihydroxyacetone phosphate-dependent aldolases in the synthesis of deoxy aza sugars. *J. Org. Chem.* **1991**, *56*, 6280-9.
12. Takayama, S.; Martin, R.; Wu, J.; Laslo, K.; Siuzdak, G.; Wong, C. H., Chemoenzymatic Preparation of Novel Cyclic Imine Sugars and Rapid Biological Activity Evaluation Using Electrospray Mass Spectrometry and Kinetic Analysis. *J. Am. Chem. Soc.* **1997**, *119*, 8146-8151.
13. Pederson, R. L.; Wong, C.-H., An efficient asymmetric synthesis of ß-Hydroxyornithine. *Heterocycles* **1989**, *28*, 477-479.
14. Espelt, L.; Bujons, J.; Parella, T.; Calveras, J.; Joglar, J.; Delgado, A.; Clapés, P., Aldol additions of dihydroxyacetone phosphate to *N*-Cbz-amino aldehydes catalyzed by L-fuculose-1-phosphate aldolase in emulsion systems: inversion of stereoselectivity as a function of the acceptor aldehyde. *Chem. Eur. J.* **2005**, *11*, 1392-1401.
15. Castillo, J. A.; Pinazo, A.; Carilla, J.; Infante, M. R.; Alsina, M. A.; Haro, I.; Clapés, P., Interaction of antimicrobial arginine-based cationic surfactants with liposomes and lipid monolayers. *Langmuir* **2004**, *20*, 3379-3387.
16. Murata, Y.; Miyamoto, E.; Ueda, M., Antimicrobial and anti-plaque activity of *N'*-alkyl-*N*-(2-aminoethyl)piperidine against dental plaque bacteria. *J. Pharmac. Sci.* **1991**, *80*, 26-28.
17. Goujon, J.-Y.; Gueyrard, D.; Compain, P.; Martin, O. R.; Ikeda, K.; Kato, A.; Asano, N., General synthesis and biological evaluation of [α]-1-*C*-substituted derivatives of fagomine (2-deoxynojirimycin-[α]-*C*-glycosides). *Bioorg. Med. Chem.* **2005**, *13*, 2313-2324.
18. Li, H. Q.; Bleriot, Y.; Chantereau, C.; Mallet, J. M.; Sollogoub, M.; Zhang, Y. M.; Rodríguez, E.; Vogel, P.; Jímenez, J.; Sinay, P., The first synthesis of substituted azepanes mimicking monosaccharides: a new class of potent glycosidase inhibitors. *Org. Biomol. Chem.* **2004**, *2*, 1492-1499.
19. Kimura, A.; Lee, J.-H.; Lee, I.-S.; Lee, H.-S.; Park, K.-H.; Chiba, S.; Kim, D., *Carbohydr. Res.* **2004**, *339*, 1035-1040.
20. Asano, N.; Oseki, K.; Kizu, H.; Matsui, K., Nitrogen-in-the-Ring Pyranoses

and Furanoses: Structural Basis of Inhibition of Mammalian Glycosidases. *J. Med. Chem.* **1994**, *37*, 3701-3706.
21. Asano, N.; Nishida, M.; Miyauchi, M.; Ikeda, K.; Yamamoto, M.; Kizu, H.; Kameda, Y.; Watson, A. A.; Nash, R. J.; Fleet, G. W. J., Polyhydroxylated pyrrolidine and piperidine alkaloids from Adenophora triphylla var. japonica (Campanulaceae). *Phytochemistry* **2000**, *53*, 379-382.
22. Mitjans, M.; Martínez, V.; Clapés, P.; Pérez, L.; Infante, M. R.; Vinardell, M. P., Low potential ocular irritation of arginine-based gemini surfactants ant their mixtures with nonionic and zwitterionic surfactants. *Pharm. Res.* **2003**, *20*, 1697-1701.

4. EXPERIMENTAL SECTION

4.1. Materials

Arginine-based surfactants

N^{α}-Lauroyl-L-arginine methyl ester hydrochloride (LAM), bis(N^{α}-octanoyl-L-arginine)-1,3-propanediamide dihydrochloride ($C_3(OA)_2$) and bis(N^{α}-caproyl-L-arginine)-1,3-propanediamide dihydrochloride ($C_3(CA)_2$) were synthesized in our laboratory previously to this thesis.[1, 2]

Phospholipids

1,2-Dipalmitoyl-*sn*-glycero-3-phosphocholine (DPPC) and *E. coli* total lipid extract containing: 58 % of 1,2-diacyl-*sn*-glycero-3-phosphoethanolamine (DPPE), 15 % of 1,2-dipalmitoyl-*sn*-glycero-3-[phospho-*rac*-(1-glycerol)] sodium salt (DPPG), 10 % of cardiolipin and 17 % of other compounds, were purchased from Avanti Polar Lipids Inc. 1,2-Dipalmitoyl-*sn*-glycero-3-[phospho-*rac*-(1-glycerol)] sodium salt (DPPG) was purchased from Sigma.

Antimicrobial agents

Hexadecyltrimethyl ammonium bromide (HTAB) and chlorhexidine dihydrochloride were purchased from Sigma. Dodecyltrimethylammonium bromide (DTAB) was purchased from Aldrich.

Molecular dyes

Syto-13, propidium iodide (PI) and bis-1,3-dibutylbarbutiric acid (bis-oxonol) were supplied from Molecular Probes Europe BV (Leiden, the Netherlands).

Diamines

1,6-Diaminohexane and 1,8-diaminooctane were purchased from Merck. 1,10-Diaminodecane and 1,12-diaminododecane were obtained from Fluka.

Aldehydes

Butanal 99 %, hexanal 98 %, octanal 99 %, nonanal, 95 % dodecanal 92 % and phenylacetaldehyde 90 % were obtained from Aldrich. Dodecanal and phenylacetaldehyde were purified by flash column chromatography on silica using $CHCl_3$ and $CHCl_3$/hexane 1:1 as eluents, respectively.

Other reagants

N-(Benzyloxycarbonyloxy)succinimide, palladium over charcoal (10 % Pd), phenylacetyl chloride, oxalyl chloride and 1,12-dodecane-dicarboxylic acid were obtained from Aldrich. L-Arginine hydrochloride, lithium sodium hydride, 1,4-dithio-D,L-threitol (DTT), 3-amino-1-propanol and Celite-545 (particle size 26 μm, mean pore diameter 17.000 nm, specific surface area BET method 2.19 m^2 g^{-1}) were obtained from Fluka. Dihydroxyacetone and aluminium oxide 90 active neutral were purchased from Merck. Ammonia was obtained from Praxair. Bradford reagent was obtained from Sigma.

Solvents

Tetrahydrofuran and dichloromethane were distilled over sodium and CaH_2, respectively, before use. All other solvents and reagents were of analytical grade and were used without further purification. Ultra pure water, produced by a nanopure purification system coupled to a Milli-Q water purification system, resistivity 18.2 MΩ cm was used for the aqueous solutions.

4.2. Instruments

^1H NMR (500 MHz) spectra of compounds were recorded with a Varian Mercury-500 spectrometer and ^{13}C NMR (100 MHz) spectra with a Varian Mercury-400.

HPLC (Merck-Hitachi, Licrograph) with detector UV-vis. HPLC (Waters Prep LC 4000) with detector UV-vis.

Infrared spectra of compounds in KBr tablets were recorded with a Nicolet Avatar 360 FT-IR.

Elemental analyses were performed with an EA1108-Elemental analyzer by Servei de Microanàlisi Elemental at Instituto de Investigaciones Químicas y Ambientales (IIQAB-CSIC).

Specific rotations were measured with a Perkin Elmer Model 341 (Überlingen, Germany) polarimeter.

Mass spectra were obtained using MALDI-TOF spectroscopy with a VOYAGER-DE-RP at Universidad de Barcelona.

Melting point of 1,14-diaminotetradecane was determined with a Kofler apparatus.

Thermotropic phase transition variables of MLVs of DPPC were measured by a DSC 821E Mettler Toledo calorimeter.

Fluorescence measurements were done on a Perkin-Elmer (Beaconsfield, Bucks, UK) spectrofluorimeter LS 50.

Surface activity measurements were recorded using a Langmuir film balance Nima 516 using a circular Teflon trough (60.35 cm^2 and 70 mL of capacity) equipped with a Wilhelmy plate, made from chromatography paper (Whatman Chr 1) as the pressure sensor.

Compression isotherms were performed on a Langmuir film balance Nima 516 equipped with a rectangular Teflon trough (19.5x20 cm^2 and 250 mL of capacity).

A Coulter Epics Elite flow cytometer (Coulter Corp., Florida, USA) equipped with a 15 mW air-cooled 488 nm argon-ion laser (for Syto-13, PI and bis-oxonol excitation) was used. The green emission from Syto-13 and bis-oxonol was collected through a 525 nm band-pass filter. The red emission from PI was collected with a 675 nm band-pass filter. Although the maximum emission is in a shorter wavelength, the 675 nm band-pass filter was used in order to minimize interference with the strong fluorescence of Syto-13. Bacteria were counted using a Cytek Flow Module (Cytek Development, CA, USA) adapted to the flow cytometer. Forward, side-scatter and fluorescence signals were collected in logarithmic scale. A significant percentage of the bacterial population that can be detected by its Syto-13 fluorescence appears in the first channel of the scatter. Consequently, fluorescence is used to discriminate bacteria rather than scatter, thus obtaining a better resolution and decreasing the background. Data were analyzed with Elitesoft version 4.1 (Coulter Corporation, Florida, USA) and WinMDI version 2.8 software.

Cell suspensions were analyzed with a Multisizer II (Coulter) using a 30 μm aperture. Cell suspensions were diluted (1/1000) in 0.9 % NaCl previously passed through a 0.2 μm filter. Data were analysed by AccuComp software version 1.15 (Coulter).

Microscopy was performed with a Philips EM 30 (Eindhoven, Holland) microscope with an acceleration of 60 kV.

The potassium concentration in the supernatant was measured using an atomic absorption Philips PU9200X spectrophotometer (Philips Cambridge, UK).

A shot cell disrupter system (Constant Systems, Northans, UK) was used to disrupt *E. coli* cells employed for the overexpression of the FSA enzyme.

4.3. Methods

4.3.1. Preparation of multilamellar vesicles (MLVs)

Multilamellar vesicles (MLVs) of DPPC were prepared as follows. A standard solution of DPPC (4.4 mg mL^{-1}) in $CHCl_3$/MeOH 1:1 v/v was prepared and aliquoted (100 μL) in test tubs. Then, the solvent was removed under nitrogen steam while rotating the tube to form a thin film of lipid on the tube walls. The residual solvent was removed under vacuum. MLVs were obtained by hydrating the lipid film with 4-(2-hydroxy-ethyl)piperazine-1-ethanesulfonic acid (Hepes) buffer 5 mM pH 7.4 (100 μL), containing the corresponding amount of surfactant, followed by five alternative cycles of sonication (2 min) and heating at 60 °C (2 min).

4.3.2. Differential scanning calorimetry (DSC)

Hermetically sealed aluminum pans (40 μL nominal volume) were used. DSC runs were carried out with freshly liposome preparations. Pans were loaded with DPPC MLVs suspension (30 μL, corresponding to 0.13 mg of DPPC), and submitted to three heating/cooling cycles in a temperature range between 0 to 60 °C at a scanning rate of 5 °C min^{-1}. The data from the first scan were always discarded to avoid mixing artefacts. Experiments were carried out in triplicate.

4.3.3. Leakage of encapsulated material in LUVs

For the ANTS-DPX leakage assay, about 15 mg of DPPC were dissolved in $CHCl_3$/MeOH 2:1 (3 mL). The solvent was evaporated under vacuum at 55 °C affording a dry lipid film. Then, 2 mL of buffer solution (5 mM Hepes, 20 mM NaCl, pH 7.4, ~200 mOsm) containing ANTS (12.5 mM) and DPX (45 mM) was added to the dry lipid. This mixture was heated and sonicated to give a lipid suspension. The lipid suspension was sonicated for 10 min affording MLVs. The MLV suspension was frozen and

thawed 10 times to afford LUVs with the maximum possible entrapment of encapsulated ANTS/DPX. This preparation was extruded 10 times through two 100 nm pore-size polycarbonate filters (Nucleopore, Pleasanton, CA) in a high pressure extruder (Lipex, Biomembranes, Vancouver, Canada) above the transition temperature of DPPC (50 °C). Vesicles with encapsulated contents were separated from the media on a Sephadex G-75 column (Pharmacia, Uppsala, Sweden) equilibrated with isotonic buffer (5 mM Hepes, ~70 mM NaCl, pH 7.4, ~200 mOsm). Lipid concentration of the vesicles was determined by phosphate analysis described by Böttcher *et al.*[3] (see below). The vesicles' size (diameter ~0.1 μm) was determined from the measurement of the sample diffusion coefficient by photon correlation spectroscopy. Fluorescence measurements were done using 1-cm path-length quartz cuvettes with stirring and thermostatting at 25 °C. These measurements were performed by setting the ANTS emission at 520 nm as a function of time and the excitation at 355 nm. No leakage (0 % leakage) corresponded to the initial fluorescence from the LUV suspension (100 μM DPPC) while complete leakage (100 %) was the fluorescence value obtained after the addition of 10 % (v/v) Triton X-100. Experiments were conducted in duplicate.

Assessment of lipid concentration. The quantification of the lipid concentration involves the following procedure:

A calibration curve is carried out in duplicate using an initial solution of $NaH_2PO_4 \cdot H_2O$ 1 mM (0, 25, 50, 75 and 100 μL). The sample is added inside a tube in absence of phosphate ions. $HClO_4$ 70 % (0.4 mL) in glass tubs is heated at 205 °C for 45 min. The tubs are cooled and then, an aliquot (4 mL) of a molybdate solution ($[(NH_4)_6Mo_7O_{24} \cdot 4H_2O]$ (2.2 g, 3.93 mmol) in H_2SO_4 95 % (14.3 mL)) is added. After that, ascorbic acid 10 % w/w (0.5 mL) is added to the mixture. The mixture is shacked with vortex and heated at 80 °C for 20 min. The solutions acquire a blue-green colour. The absorbance is measured at λ 812 nm using a colorimeter.

4.3.4. Surface activity

Increasing volumes of an aqueous concentrate solution of surfactants in phosphate buffered saline (PBS) pH 7.4 were injected beneath the air/water surface and the pressure increases recorded during a period of 60 min. For each compound, the saturation concentration (*i.e.* the minimum concentration that gives the maximum surface pressure) was determined. Dimethyl sulfoxide (DMSO) was used to prepare the concentrated solution of CHX, due to its low aqueous solubility. Surface pressure was measured at 21±1 ºC with the accuracy of ±0.1 mN m^{-1}.

4.3.5. Penetration kinetics at constant area

The interactions of the selected compounds with lipid monolayers were determined with the same device described previously for the surface activity measurements. Lipid monolayers of DPPC, DPPG and *E. coli* total lipid extract were spread on PBS subphase from $CHCl_3$/MeOH 2:1 v/v solutions, at the required initial pressure: 5, 10, 20 and 32 mN m^{-1}. Then, the appropriate amount of the stock solution of each product was injected in the subphase. The final concentration of each compound was fixed according to their surface pressure curves (*i.e.* approximately 80 % of the saturation concentration). The pressure increases were recorded at 21±1 °C for 30 min, to ensure that the equilibrium was reached. The subphase was stirred continuously to ensure a homogeneous distribution. The experiments were performed in triplicate and the standard error was estimated in each case.

4.3.6. Compression isotherms

Fixed amounts of DPPC, DPPG, and *E. coli* lipid extract (50 µL solution of 1 mg phospholipids/mL in $CHCl_3$/MeOH 2:1 v/v, *ca.* $4x10^{16}$ lipid molecules) were spread on the aqueous subphase containing the product

under study at three different concentrations: 80 %, 20 % and 5 % of the saturation concentration. Then, the solvent was allowed to evaporate for at least 10 min. Films were compressed continuously with an area reduction rate of 12.9 $Å^2$ $molecule^{-1}$ min^{-1}. The experiments were performed in triplicate and the reproducibility was ± 1 $Å^2$ mol^{-1}.

4.3.7. Minimum inhibitory concentration (MIC)

The minimum inhibitory concentration of selected microbicides were determined *in vitro* by a broth micro-dilution assay.[4] MIC is defined as the lowest concentration of antimicrobial agent that inhibits the development of visible micro-organism growth after incubation at 30 °C (24 h for the antibacterial test and 48-72 h for the antifungal test). Cell cultures were adjusted to an initial concentrationan 10^5 cfu mL^{-1}; bacterial and yeast cutures[4] were adjusted to an optical density on the McFarland scale of 0.5 and moulds cultures[5] were adjusted by direct microscopic counting procedure using the Petroff-Hausser counting chamber. The MIC assay was performed in a 96-well microtitre, where each raw was inoculated with the tested micro-organism (*ca.* 10^4 cfu mL^{-1}). Each column contained inoculated medium with different concentration of the agent (from 0.25 to 256 mg L^{-1}) and the control corresponded to the inoculated medium in absence of the biocide. The micro-organisms used were the following:

Gram-positive bacteria: *Arthrobacter oxydans* ATCC 14358, *Bacillus cereus var. mycoides* ATCC 11778, *Bacillus subtilis* ATCC 6633, *Enterococcus hirae* ATCC 10541, *Micrococcus epidermidis* ATCC 155-U, *Micrococcus luteus* ATCC 10054 and 9341, *Mycobacterium phlei* ATCC 10142, 41423, *Mycobacterium smegmatis* ATCC 3017, *Staphylococcus aureus* ATCC 25178, 9144 and 6538, *Staphylococcus epidermidis* ATCC 12228.

Gram-negative bacteria: *Bordetella bronchiseptica* ATCC 4617, *Citrobacter freundii* ATCC 13883, *Enterobacter aerogenes* ATCC 13048 and CECT 684, *Escherichia coli* ATCC 27325, 10536 and 8739, *Klebsiella pneumoniae* ATCC 13882 and 4352, *Pseudomonas aeruginosa* ATCC 9721 and 9027,

Salmonella typhimurium ATCC 14028, *Serratia marcescens* ATCC 274, *Streptococcus faecalis* ATCC 10541.
Yeasts: *Candida albicans* ATCC 10231, *Saccharomyces cerevisiae* ATCC 9763.
Moulds: *Aspergillus niger* ATCC 16404, *Aspergillus repens* ATCC 28604, *Cladosporium cladosporoides* ATCC 16022, *Penicillum funiculosum* CECT 2914, *Penicillum chrysogenum* ATCC 9480, *Trichophyton mentagrophytes* ATCC 18748.

4.3.8. Exposure of micro-organisms to biocides

Suspensions of the micro-organisms were obtained from an overnight culture of each strain on tryptone soy broth (TSB) at 30 °C. Cultures were then centrifuged at 8000 **g** for 15 min, washed twice in sterile Ringer's solution (Scharlau, Barcelona, Spain) and resuspended in Ringer's solution to obtain a cell suspension about 10^7-10^8 cfu mL^{-1}. Cell suspensions (3 mL) were used to inoculate flasks containing 27 mL of solution to obtain a cell density of about 10^6-10^7 cfu mL^{-1}. Different aliquots (7.5-360 µL, depending on the final 1/2 or 3/2 of the MIC) of the stock solution of $C_3(CA)_2$ and CHX, were added to the bacterial suspensions. After a contact time of 30 min, the biocide effect was immediately neutralized by dilution with sterile Ringer's solution.

For flow cytometry (FC) experiments, 15 mL of the samples were centrifuged at 8000 **g** for 30 min and the bacterial pellets were resuspended in 1 mL of Ringer's solution. Experiments were conducted in triplicate.

For transmission electronic microscopy (TEM) observations, the contact time was 30 min at biocide concentration 3/2 of the MIC. Then, samples (5 mL) were taken and centrifuged at 4500 **g** for 30 min. The bacterial pellets were rinsed with 0.1 M phosphate buffer pH 7.4.

For assessment of potassium leakage, 1 mM glycylglycine buffer solution pH 6.8 was employed instead of Ringer's solution. The micro-organisms were treated with the antimicrobials at 3/2 of the MIC for 30 min. Then, 5 mL of cell suspension were removed and centrifuged at 4500 **g** for 15 min. Positive controls were lysed cell suspension obtained by thermal shock (70 °C for 30 min). Experiments were conducted in triplicate.

In all cases, control experiments lacking microbicide were carried out in parallel.

4.3.9. Flow cytometry: staining procedure

Staining protocols for flow cytometry experiments were as follows: 1 μL of a 500 μM stock solution of Syto-13 in dimethyl sulphoxide and 10 μL of a 1 mg mL^{-1} stock solution of propidium iodide (PI) in distilled water were added to 500 μL of the bacterial suspension in filtered Ringer's solution. The *S. aureus* and *E. coli* suspensions were incubated with the dyes for 3 and 20 min, respectively. Stains were performed at room temperature before the FC analysis. Experiments were conducted in triplicate.

In the case of membrane potential dye, 2 μL of a 250 μM stock solution of bis-oxonol in ethanol was added to 500 μL of the bacterial suspension to a final concentration of 1 μM and incubated for 2 min. Cells killed by heat exposure (3 min at 70 °C) were used as controls for bis-oxonol staining. Experiments were conducted in duplicate.

4.3.10. Bacterial count

Viable cell counts (cfu mL^{-1}) were obtained on trypticase soy agar (TSA). After an appropriate dilution in Ringer's solution, the sample was inoculated on plates and incubated at 30 °C for 24-48 h. Rapid separation of bacteria from the antimicrobial was achieved by centrifugation at 4500 **g** in

a bench top centrifuge for 15 min and subsequent dilution on Ringer's solution prior to plating. Cell counting was performed in triplicate.

4.3.11. Transmission electron microscopy (TEM)

After treatment of cell suspensions with the biocides at 3/2 MIC for 30 min for each micro-organism (3 μg mL^{-1} and 12 μg mL^{-1} of $C_3(CA)_2$ with *S. aureus* and *E. coli*, respectively, and 0.75 μg mL^{-1} and 3 μg mL^{-1} of CHX with *S. aureus* and *E. coli*, respectively). The bacterial pellets were rinsed with 0.1 M phosphate buffer (pH 7.4), washed three times and fixed with 2.5 % buffered glutaraldehyde for 1 h at 4 °C. The cells were then postfixed in 1 % buffered osmium tretroxide for 1 h, stained with 1 % uranyl acetate, dehydrated in a graded series of ethanol and embedded in L.R. (London Resin Co. Ltd.) white resin. Ultra-thin sections were prepared and stained with 1 % uranyl acetate and sodium citrate.

4.3.12. Potassium leakage

Absorbance values were converted into potassium ion concentration (ppm) by reference to a calibration curve using potassium ion solution of 0, 0.1, 0.2, 0.5 and 1 ppm. The cell density studied were $2x10^8$ cfu mL^{-1} and $3x10^8$ cfu mL^{-1} for *S. aureus* and *E. coli*, respectively.

4.3.13. Papain immobilization

Papain (EC 3.4.22.2) from *Carica papaya* crude powder (1.7 U mg^{-1} of protein; one unit (U) will hydrolyze 1.0 mmol of benzyl-L-arginine ethyl ester per minute (BAEE) at pH 6.2, 25 °C was obtained from Sigma. Papain was immobilized by deposition onto Celite 545. The procedure was the following: papain (500 mg) and DTT (250 mg) were dissolved in boric acid-borate buffer 0.1 M pH 8.2 (5 mL, 0.5 % v/v). This solution was thoroughly mixed with Celite-545 (5 g) and dried under vacuum (80 μbar).

4.3.14. Production and purification of FSA

The cloning and overexpression in *E. coli* of the gene encoding FSA and the biochemical characterization was carried out for the first time by Schürmann *et al.*[6] This section describes the methodology to overexpress y FSA, to purify and to assess its activity.

Overexpression of FSA in Escherichia coli:

The *Escherichia coli* strain used was DH5α. This strain contains the plasmid pJF119fsa, which confer resistance to the antibiotic ampicillin. The experimental procedure to produce the FSA enzyme from *E. coli* consists of the followings steps:

1) An aliquot of *E. coli* glycerinate (1 mL) was preinoculated overnight at 37 °C with shaking (250 rpm) into 5 mL of culture medium in presence of ampicillin (0.1 mg L^{-1}). The composition of the sterilized culture medium was: yeast extract (YT, 4 g), triptone (8 g), NaCl (8 g) and, distilled water (800 mL).

2) The former preinoculated aliquot was diluted in 45 mL of culture medium and was shaked (250 rpm) at 37 °C overnight.

3) Inoculated aliquots (15 mL) were diluted in three flasks with 800 mL (total volume 2.4 L) of medium in presence of ampicillin (0.1 mg L^{-1}). The cultures were shacked (37 °C, 2 h, 250 rpm).

4) Then, isopropyl-ß-D-thiogalacto-pyranoside (IPTG, 1 mM) was added to the flasks and the cultures were shacked (37 °C, ~16 h). The addition of the inducer IPTG to recombinant cells in the exponential phase increases the production of FSA.

5) The cell suspensions were centrifuged (10000 rpm, 30 min, 10 °C). The supernatant was discarded. Pellets were washed with glycylglycine buffer (glycylglycine 50 mM, 1,4-dithio-D,L-threitol (DTT) 1 mM, pH 8.0). After that, pellets were resuspended in buffer and centrifuged (10000 rpm, 30 min, 10 °C). Again, the supernatant was discarded.

6) The pellets can be frozen and stored at -80 °C before performing the extraction and the purification of the FSA enzyme.

Extraction and purification of FSA enzyme:

The experimental procedure to purify the FSA enzyme from *E. coli* consists of the followings steps:

1) The frozen pellets of *E. coli* were resuspended with glycylglycine buffer.

2) The cell suspensions were passed through a cellular disruptor. The applied pressure was 1.37 kbar to extract cytoplasmic membrane proteins.

3) The cell-free extract was centrifuged (10000 rpm, 30 min, 10 °C). Pellets were discarded.

4) After centrifugation, the supernatant was heated (75 °C, 40 min) in order to denature other enzymes present in the cell-extract.

5) The solution was centrifuged (20000 rpm, 40 min, 10 °C) and pellets were discarded.

6) The supernatants were lyophilized yielding a light brown powder (2.8 g). The enzymatic activity of this lyophilized powder was 1.7 U mg^{-1}. This powder was stored at 4 °C, keeping the enzymatic activity constant at least after seven months.

NOTE: One unit (U) will synthesize 1 μmol of fructose-6-phosphate from D-glyceraldehyde-3-phosphate and DHA per minute at pH 8.5 (glycylglycine 50 mM buffer) and 30 °C.

Purification of FSA by chromatography

1) After performing the heat treatment and centrifugation of the solution, the cell-free extract was dissolved in glycylglycine buffer and directly applied onto a Q-Sepharose HP anion exchange column. FSA was eluted in a linear NaCl gradient (flow 1 mL min^{-1}). This purification was carried out at 4 °C.

2) The Bradford's test and the enzymatic assay were performed to determine the FSA concentration and the specific activity, respectively. The active fractions were pooled and the initial glycylglycine buffer was changed by KH_2PO_4 buffer (10 mM, pH 7.0).

3) The former solution was further purified using a hydroxyapatite ($Ca_3(PO_4)_2$) column. FSA enzyme was eluted in the first millilitres using

KH_2PO_4 buffer (10 mM, pH 7.0) as eluent (flow 1 mL min^{-1}). This purification was also carried out at 4 °C.

4) The buffer of pure fractions was changed to glycylglycine buffer since the presence of KH_2PO_4 inhibits the enzymatic activity.

5) Pure fractions of FSA were pooled, frozen and lyophilized in order to store the enzyme at 4 °C.

Determination of FSA concentration: Bradford's test

The Bradford's test was performed to determine the concentration (mg mL^{-1}) of the FSA samples. A volume of sample (1-50 µL) was mixed with glycylglycine buffer to a final volume of 50 µL. Then, 950 µL of Bradford's solution was added. After 5 min, the absorbance was measured at 595 nm. The concentration of FSA is calculated from the interpolation of the calibration curve of bovine serum albumin (BSA) (Figure 1).

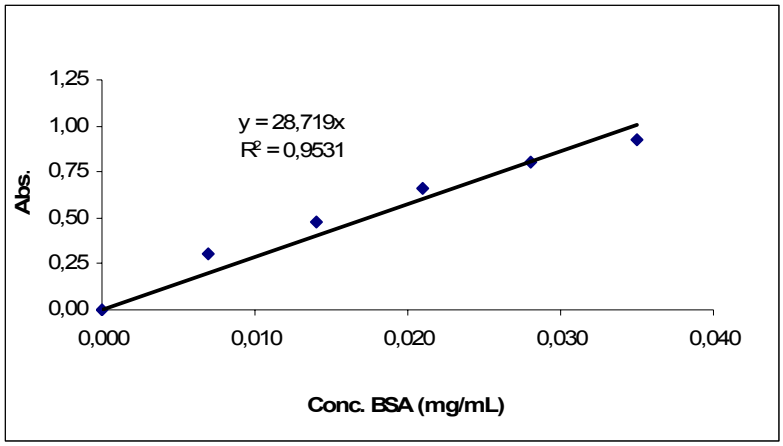

Fig. 1 Calibration curve of of bovine serum albumin (BSA).

Determination of FSA activity: aldolase assay

The activity of the FSA samples was measured by an enzymatic assay based on the formation of fructose-6-phosphate (Figure 2). The advance of this reaction is followed indirectly by the reduction of NADP to NADPH (absorbance measured at 340 nm, 30 °C, pH 8.5 (glycylglycine 50 mM buffer).

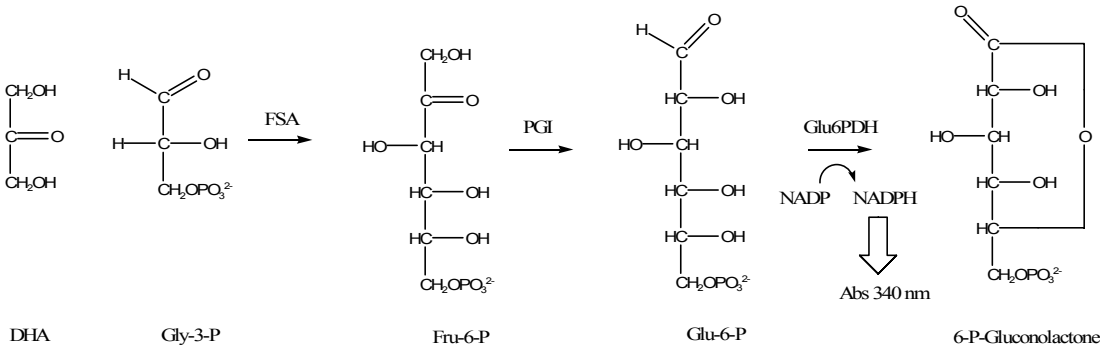

Fig. 2 Enzymatic assay performed using a spectrophotometer with a thermostated cuvette holder.

First, the following reagents are mixed in a cuvette at 30 °C:

DHA (10 µL of dihydroxyacetone dimer 2,5 M), FSA (5-10 µg determined previously by the Bradford's Test), PGI (6 µL of phosphoglucose isomerase solution 10 mg mL^{-1}, 18 U), Glu6PDH (5 µL of glucose-6-phosphate dehydrogenase solution 1010 U mL^{-1}, 5 U), NADP (10 µL of β-nicotinamide adenine dinucleotide phosphate disodium salt solution 50 mM).

After 5 min, Gly-3-P (10 µL of DL-glyceraldehyde-3-phosphate solution 0.29 M) is added into the cuvette.

Final volume: 1 mL (with buffer glycylglycine 50 mM, DTT 1 mM, pH 8.5).

NOTE: One unit (U) will synthesize 1 µmol of fructose-6-phosphate from D-glyceraldehyde-3-phosphate and dihydroxyacetone per minute at pH 8.5 (glycylglycine 50 mM buffer) and 30 °C.

SDS-polyacrilamide gel electrophoresis (PAGE)

The bands observed at the SDS-Page analysis indicate that FSA constitutes up to 10 % of the total soluble protein content of the crude extract (Figure 3, lane A). After chromatographic purification of the cell-free extract, FSA was obtained with ~95 % of purity (Figure 3, lane D).

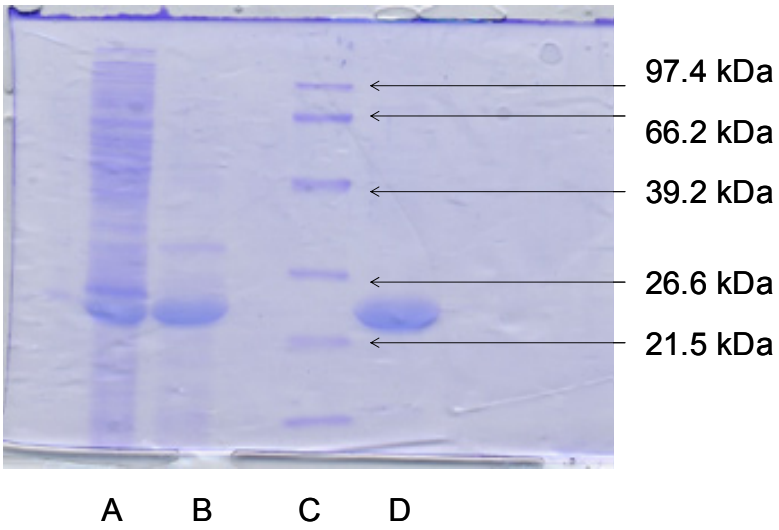

Fig. 3 SDS-PAGE analysis of the *E. coli* aldolase purification

where: lane A is crude extract of FSA before the heat treatment, lane B is pool of FSA after the heat treatment, lane C: Protein reference (bovine serum albumin), lane D is final pool of FSA (after chromatography using Q-sepharose and hydroxyapatite as stationary phases).

4.3.15. Haemolysis assays

The erythrocytes were washed three times in isotonic phosphate saline pH = 7.4 buffer (PBS): Na_2HPO_4 (22.2 mM), KH_2PO_4 (5.6 mM), NaCl (123.3 mM) and glucose (10.0 mM). The cells ($8x10^9$ cell mL^{-1}) were then suspended in isotonic saline solution (NaCl 0.9 %). Different volumes (10 to 80 μl) of stock solutions of compounds (20 mg mL^{-1}) were mixed with PBS in polystyrene tubes to final volume of 1 mL; the final concentrations of products were from 200 to 1600 μg mL^{-1}. To these solutions, aliquots of erythrocyte suspension (25 μL) were added, and the mixture incubated for 10 minutes, with constant shaking, at room temperature. After incubation, the tubes were centrifuged at 1500 **g** for 5 min. Then, the percentage of haemolysis was determined by comparing the absorbance (λ 540 nm) of the supernatant with that of control samples totally haemolysed with distilled water.[7] The dose-response curve was determined from the haemolysis results and the concentration that induces the haemolysis of 50 % of the

cells (HC_{50}) was calculated.

The potential ocular irritation of the compounds was studied with a method based on the haemolysis test (*i.e.* cellular lysis) and the damage caused on the cellular proteins by the compound (*i.e.* denaturation). The irritation index was determined according to the lysis/denaturation ratio (L/D) obtained dividing the HC_{50} (μg mL^{-1}) by the denaturation index (DI). DI of each compound was measured by comparing the haemoglobin denaturation (D) induced by the compound and sodium dodecyl sulphate (SDS) as positive control. Haemoglobin denaturation was determined after inducing haemolysis by adding SDS (10 mg mL^{-1}) to the erythrocytes and measuring the absorption ratio of the supernatant at 575 nm and 540 nm. The resulting L/D ratio was used instead of the ocular irritancy score in the acute phase of *in vivo* evaluation. The compounds can be classified according to this L/D ratio as: non irritant >100, slightly irritant >10, moderate irritant >1, irritant >0.1 and, very irritant < 0.1.[7]

4.3.16. Enzymatic inhibition assays

Commercial glycosidase solutions were prepared with the appropriate buffer and incubated in 96-well plates at 37 ºC without (control) or with inhibitor (1 mM) during 3 min for α-glycosidase, α-mannosidase, and for α-rhamnosidase, and 5 min for β-galactosidase. After addition of the corresponding substrate solution, incubations were prolonged during different time periods: 10 min for α-glucosidase, 6 min for α-mannosidase, 5 min for α-rhamnosidase and 16 min for ß-galactosidase and stopped by addition of 50 μL of 1 M Tris solution or 180 μL of 100 mM glycine buffer pH 10, depending on the enzymatic inhibition assay. The amount of *p*-nitrophenol formed was determined at 405 nm with UV/VIS Lector Spectramax Plus (Molecular Devices Corporation) spectrophotometer. α-D-Glucosidase from baker's yeast activity was determined with *p*-nitrophenyl-α-D-glucopyranoside (1 mM) in 100 mM sodium phosphate buffer (pH 7.2). α-Glucosidase activity was determined with *p*-nitrophenyl-

α-D-glucopyranoside (1 mM) in 100 mM sodium acetate buffer (pH 5.0). α-Glucosidase from rice activity was determined with *p*-nitrophenyl-α-D-glucopyranoside (1 mM) in 50 mM sodium acetate buffer (pH 5.0). α-Mannosidase activity was determined with *p*-nitrophenyl-α-D-mannopyranoside (1 mM) in 50 mM sodium acetate buffer (pH 5.0). α-Rhamnosidase activity was determined with *p*-nitrophenyl-α-D-rhamnopyranoside (1 mM) in 50 mM sodium acetate buffer (pH 5.0). ß-Galactosidase activity was determined with *p*-nitrophenyl-α-D-galactopyranoside (1 mM) in 100 mM sodium phosphate buffer 0.1 mM $MgCl_2$ (pH 7.2). The commercial glycosidase solutions were prepared as follows: α-glycosidase from rice: 100 μL commercial suspension/5 mL buffer, α-mannosidase from jack bean: 25 μL commercial suspension/10 mL buffer, naringinase from *Penicilium decumbens*: 0.3 mg/1 mL buffer; β-galactosidase from bovine liver: 0.1 mg /1 mL buffer.

Kinetics of Inhibition. The nature of the inhibition against enzymes and the K_i values were determined from the Lineweaver-Burk or Dixon plots.

4.3.17. Assay of antileishmanial activity

The antileishmanial activity of pentamidine isethionate salt and bis(PhAcArg) derivatives with spacer chain of 6, 12 and 14 methylenes (*i.e.* compounds **3a** and **3d-e**) against *Leishmania infantum* was measured. The technique is based on the assessment of the activity of acid phosphatases as measure of cell growth.

Parasite preparation. The experiments were carried out using the strain BCN 503 of *Leishmania infantum*.

Drug preparation. The selected compounds **3a** and **3d-e** and pentamidine (positive control) were diluted in DMSO (~0.01 g mL^{-1}) in order to sterilize the initial solutions. After that, 800 μM solutions were prepared.

Assay in promastigotes by the method of phosphatase. Promastigote is defined as the flagellate stage of a trypanosomatid protozoan, as that of any

of the *Leishmania* parasites. The concentration of the initial solution of parasites was *ca.* 10^6 cell mL^{-1}. Inoculated medium (100 μL) were added into the wells of a 96-well microtitre plate. Different aliquots of the drug solutions were added to each raw with the exception of the last raw (negative control). The micro-plate was kept at 26 °C for 48 h. An aliquot (40 μL) of the medium from each well was added to a new 96-well microtitre plate. Cells were lysed adding citrate buffer 90 mM (100 μL/well) and Triton-100 1 % pH 4.8 at 37 °C. Cell growth was assessed measuring the activity of the acid phosphatase with the addition of *p*-nitrophenyl phosphate 10 mM (Sigma N-6260). The enzymatic reaction was quenched after 2 h, with NaOH 0.1 M (60 μL/well). The absorbance was measured at 405 nm using a Titterteck Multiscan. The drug concentration which leads to the 50 % reduction of cell growth, *i.e.* IC_{50}, was assessed through the lineal regression adjustment by minimum squares of the cell growth *versus* the logarithm of the drug concentration.

4.4. Preparation of bis(phenylacetylarginine) derivatives

4.4.1. Synthesis of 1,14-diaminotetradecane

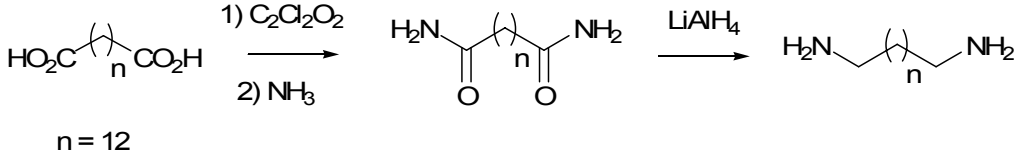

1,12-Dodecanedicarboxylic acid (5.6 g, 21.8 mmol) and DMF (1.68 mL, 21.8 mmol) were dissolved in hexane (350 mL) and the mixture was cooled at 4 °C. To this solution, oxalyl chloride (0.2 mol) was added dropwise over a period of 30 min, and then the mixture was allowed to react at room temperature overnight. The reaction mixture started as a white suspension and it was a transparent solution at the end with brown oily precipitated drops on the reactor wall. The solvent was evaporated under vacuum and the residue dissolved in freshly distilled CH_2Cl_2. This solution was

saturated with NH_3 at 4 °C and a white precipitate was formed immediately. The reaction mixture was left to proceed at room temperature overnight. Then, the solvent and the excess of NH_3 were removed under vacuum. The solid obtained was washed with cold water and cold EtOAc and finally, dried under vacuum to afford **1,12-dodecanediamide** as a brown solid (6.4 g, isolated yield 98 %). ^{1}H NMR (500 MHz, [D_6]DMSO, 40 °C): δ (ppm) = 7.16 (s, 2H), 6.57 (s, 2H), 2.09-1.92 (m, 4H), 1.58-1.38 (m, 4H), 1.24 (s, 16H). ^{13}C NMR (100 MHz, [D_6]DMSO, 40 °C): δ (ppm) = 174.1, 35.0, 28.8, 28.7, 28.6, 28.5, 24.9. IR (KBr) ν = 3387, 3189, 2923, 2848, 1650, 1416, 1337, 1281, 1230, 1179, 1122, 799, 646 cm^{-1}.

The 1,12-dodecanediamide thus obtained (2.5 g, 9.73 mmol) was added to a suspension of $LiAlH_4$ (1.5 g, 40 mmol) in freshly distilled THF (0.5 L) at 4 °C. The reaction proceeded overnight at reflux to favour the solubility of the diamide. The reaction was stopped by slow and careful addition of cold water. The solid obtained was filtered off and the filtrate was dried under vacuum affording **1,14-diaminotetradecane** as a white solid (1.6 g, isolated yield 70 %). ^{1}H NMR (500 MHz, [D_6]DMSO, 40 °C): δ (ppm) = 1.35-1.28 (m, 4H), 1.24 (s, 24H). ^{13}C NMR (100 MHz, [D_6]DMSO, 40 °C): δ (ppm) = 41.5, 33.3, 28.9, 28.8, 28.8, 26.2. IR (KBr) ν =3335, 3251, 2923, 2846, 1603, 1461, 1319, 1062, 1004, 920, 714 cm^{-1}.

4.4.2. Synthesis of N^{α}-phenylacetyl-L-arginine methyl ester hydrochloride (PhAc-Arg-OMe·HCl) (1)

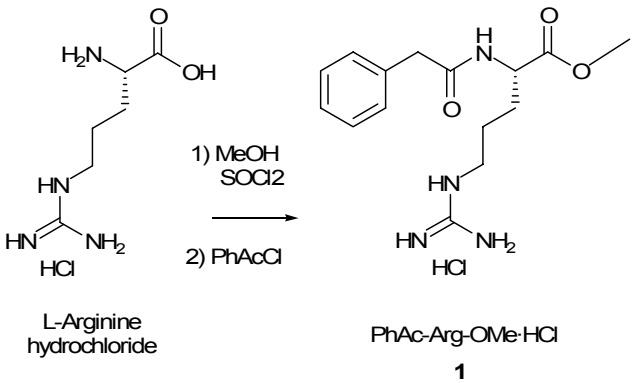

L-Arginine hydrochloride

PhAc-Arg-OMe·HCl

1

L-Arginine hydrochloride (20.0 g, 94.9 mmol) was suspended in MeOH (0.5 L) and cooled till *ca.* - 40 ºC. $SOCl_2$ (50 mL, 0.69 mol) was added dropwise to this suspension over a period of one hour. Afterwards the mixture was stirred at room temperature for 48 h to obtain a clear solution. The solvent, excess $SOCl_2$ and HCl were then removed under vacuum by repeated addition of EtOH until a solid residue was formed. The residue was filtered, washed with Et_2O and dried to afford **L-arginine methyl ester dihydrochloride** as a white solid (24.2 g, isolated yield 98 %).

The L-arginine methyl ester hydrochloride thus obtained (10.0 g, 38.29 mmol) was dissolved with ACN/H_2O 15/1. $NaHCO_3$ (6.4 g, 76.2 mmol) and Na_2CO_3 (10.1 g, 95.3 mmol) were added to this solution. The mixture was cooled with ice water and then, phenylacetyl chloride (5.6 mL, 42.12 mmol) was added dropwise. The reaction mixture was stirred overnight at room temperature. The resulting mixture was filtered, acidified at pH ~2 and the solvent removed under vacuum. The residue was dissolved in water (80 mL) and washed with EtOAc (3x100 mL) and the aqueous phase was lyophilized. The solid thus obtained was suspended in cool EtOH to precipitate the salts, which were filtered out. This desalting process was repeated three times. Finally, the ethanol was evaporated under vacuum, the residue dissolved in water and lyophilized affording the title compound as a white solid (9.83 g, isolated yield 75 %).

4.4.3. Synthesis of bis(N^{α}-phenylacetyl-L-arginine)-α,ω-dialkylamide dihydrocloride (bis(PhAcArg)) (3a-e)

(*a*)Two step procedure:

1st step: Preparation of N^{α}-phenylacetyl-L-arginine(ω-aminoalkyl)amide monohydrochloride derivatives (PhAc-Arg-NH-$(CH_2)_m$-NH_2·HCl) **2**.

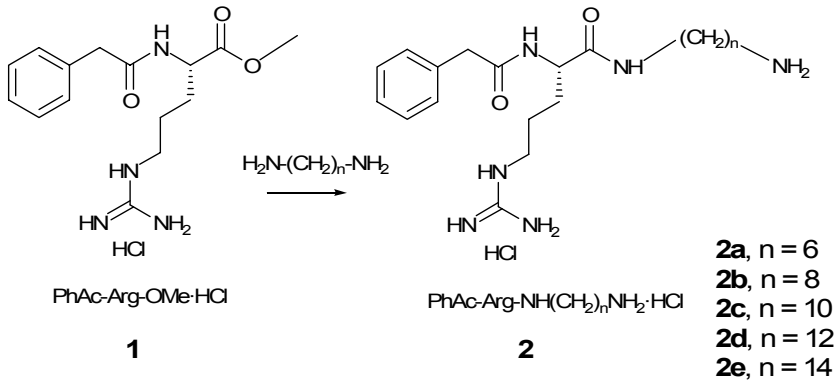

PhAc-Arg-OMe·HCl **1** (4.0 g, 11.67 mmol) was mixed with the corresponding α,ω-diaminoalkane (81.70 mmol). The mixture was heated at different temperatures depending on the diamine: 50 ºC for 1,6-diaminohexane, 55 ºC for 1,8-diaminooctane, 66 ºC for 1,10-diaminodecane, 72 ºC for 1,12-diaminododecane and 100 ºC for 1,14-diaminotetradecane, obtaining a homogeneous mixture after few minutes. After 1.5 h, the reactions were quenched by adding EtO_2 (25 mL for **2a**), ACN/EtO_2 (1:1) (25 mL for **2b**) or ACN/EtO_2 (2:1) (25 mL for **2c** and **2d**). The resulting mixture was stirred, sonicated at room temperature and finally was cooled at -40 ºC. The precipitated thus obtained was collected and washed with EtO_2 (2x25 mL). Finally, the solid was dried under vacuum to yield the title compound. These intermediate products were identified by mass spectrometry: **2a,** MS *m/z* [M^+ +1], 391; **2b**, MS *m/z* [M^+ +1] 419; **2c**, MS *m/z* [M^+ +1] 447; and **2d**, MS *m/z* [M^+ +1] 475. The treatment for the crude of **2e** failed and the 1,14-α,ω-diaminotetradecane could not be removed.

2nd step: Preparation of bis(N^{α}-phenylacetyl-L-arginine)-α,ω-diamide dihydrochloride derivatives, bis(PhAcArg) (3)

The corresponding compounds **2** (13.30 mmol) and **1** (3.04 g, 8.87 mmol) were dissolved in EtOH (150 mL), previously saturated with nitrogen and dried over molecular sieves (3Å). To this solution aqueous boric-borate buffer 0.1 M pH 8.2 (0.75 mL, 0.5 % v/v) was added. The mixture was stirred and sonicated thoroughly to obtain a homogeneous solution.

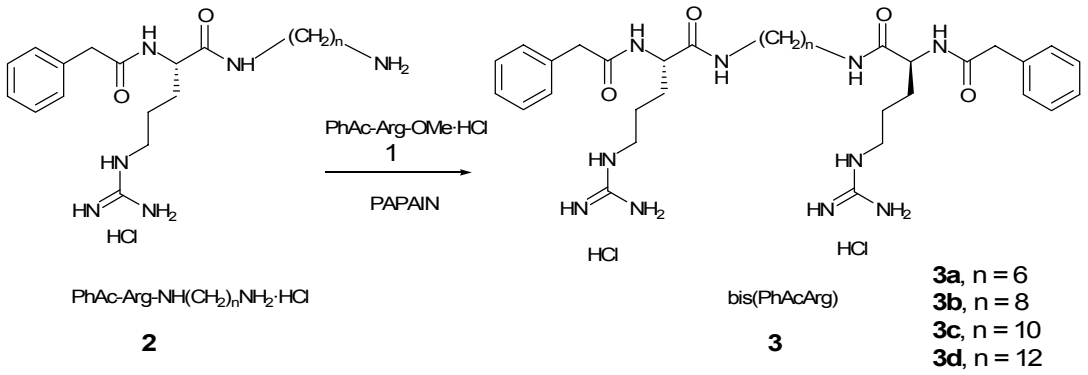

Then, the immobilized papain preparation (17 g) was added. The reaction mixture was placed in a reciprocal shaker (125 rpm) at 25 ºC under argon atmosphere. After 72 h, MeOH (100 mL) was added and the immobilized preparation was filtered off and washed with MeOH (3x100 mL). The organic phases were pooled and the solvent evaporated under vacuum. The residue was purified first by ion exchange chromatography and then by preparative HPLC as described below.

One pot procedure:

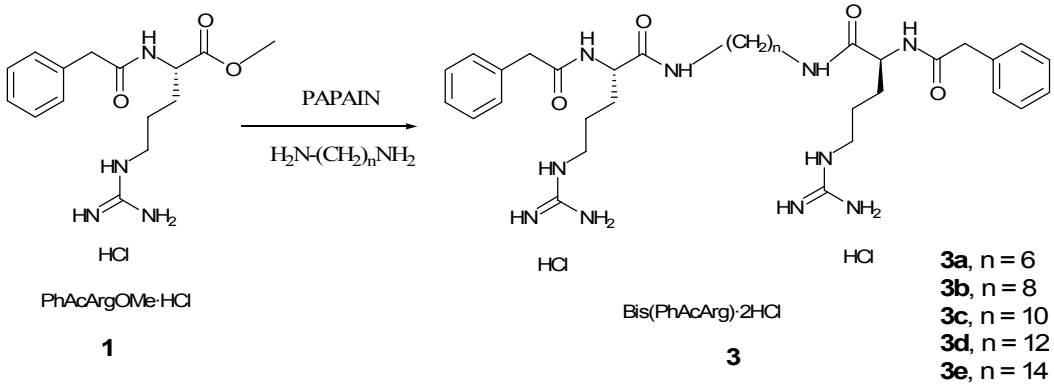

PhAc-Arg-OMe·HCl (**1**) (24 mg, 0.07 mmol) and the corresponding α,ω-alkanodiamine (0.04 mmol) were dissolved in EtOH (1 mL), free of O_2 and dried over molecular sieves (3Å). To this solution boric-borate 0.1 M pH 8.2 buffer (5 µL, 0.5 % v/v) was added. Then, the immobilized papain preparation (100 mg) was added and the reaction mixture was placed in a reciprocal shaker (125 rpm) at 25 ˚C under argon atmosphere. After 72 h, the reaction was quenched, worked up as described above and the residue

was purified first by ion exchange chromatography and then, by preparative HPLC as described below.

*Bis(N^{α}-phenylacetyl-L-arginine)-1,6-hexanediamide dihydrochloride (**3a**)*

The title compound was prepared following the general methodology described above (*a*) (1.05 g, isolated yield 25 %), 98 % purity by HPLC. HPLC conditions: gradient elution 10-70 % B in 30 min; retention factor (*k*') = 6.94. $[\alpha]_D^{20}$ = -25.3 (*c* = 1.0 in methanol). IR (KBr): ν (cm^{-1}) = 3258, 3165, 2930, 2853, 1650, 1537, 1445, 1347, 1250, 1168, 702. ^{1}H NMR (500 MHz, CD_3OD, 22 °C) δ (ppm) = 7.36-7.17 (m, 10H), 4.31 (dd, *J* = 8.5, 5.6 Hz, 2H), 3.60 (m, 4H), 3.16 (m, 8H), 1.93-1.51 (m, 8H), 1.45 (s, 4H), 1.28 (s, 4H). ^{13}C NMR (101 MHz, CD_3OD, 22 °C) δ (ppm): 174.2, 173.9, 158.5, 136.8, 130.2, 129.6 , 128.0, 54.7, 43.6, 41.9, 40.2, 30.3, 30.1, 27.3, 26.5. Elemental analysis calcd. (%) for $C_{34}H_{54}Cl_2N_{10}O_4 \cdot 3H_2O$ (Mw 791.8); C 51.57, H 7.64, N 17.69 found C 51.56, H 7.56, N 17.56.

*Bis(N^{α}-phenylacetyl-L-arginine)-1,8-octanediamide dihydrochloride (**3b**)*

The title compound was prepared following the general methodology described above (*a*) (1.37 g, isolated yield 21 %), 99 % purity by HPLC. HPLC conditions: gradient elution 10-70 % B in 30 min; retention factor (*k*') = 8.5. $[\alpha]_D^{20}$ = -23.0 (*c* = 1.0 in methanol). IR (KBr): ν (cm^{-1}) = 3268, 3155, 2930, 2853, 1650, 1537, 1455, 1358, 1250, 1163, 697. ^{1}H NMR (500 MHz, CD_3OD) δ (ppm) = 7.34-7.20 (m, 10H), 4.31 (m, 2H), 3.59 (m, 4H), 3.16 (s, 8H), 1.83 (s, 2H), 1.74-1.50 (m, 6H), 1.46 (s, 4H), 1.32-1.25 (m, 8H). ^{13}C NMR (101 MHz, CD_3OD) δ (ppm) = 174.2, 173.7, 136.9, 130.2, 129.7, 128.0, 54.5, 43.6, 42.0, 40.4, 30.4, 30.3, 30.2, 27.8, 26.4. Elemental analysis calcd. (%) for $C_{36}H_{58}Cl_2N_{10}O_4 \cdot 2H_2O$ (Mw 801.9); C 53.92, H 7.79, N 17.47 found C 54.14, H 7.83, N, 17.63.

*Bis(N^{α}-phenylacetyl-L-arginine)-1,10-decanediamide dihydrochloride (**3c**)*

The title compound was prepared following the general methodology described above (*a*) (1.61 g, isolated yield 27 %), 98 % purity by HPLC. HPLC conditions: gradient elution 10-70 % B in 30 min; retention factor (*k*') = 10.0. $[\alpha]_D^{20}$ = -22.4 (*c* = 1.0 in methanol). IR (KBr): ν (cm^{-1}) = 3268, 3176, 2925, 2848, 1650, 1537, 1455, 1358, 1245, 1163, 692. ^{1}H NMR (300 MHz, CD_3OD) δ (ppm) 7.34-7.19 (m, 10H), 4.31 (dd, *J* = 8.6, 5.6 Hz, 2H), 3.59 (m, 4H), 3.16 (m, 8H), 1.95-1.36 (m, 12H), 1.36-1.16 (m, 12H). ^{13}C NMR (75 MHz, CD_3OD) δ (ppm) = 174.2, 173.7, 158.5, 136.9, 130.2, 129.6, 128.0, 54.5, 43.6, 41.9, 40.5, 30.6, 30.4, 27.9, 26.4. Elemental analysis calcd. (%) for $C_{38}H_{62}Cl_2N_{10}O_4 \cdot 3/2H_2O$ (Mw 820.9); C 55.60, H 7.98, N 17.06 found C 55.41, H 8.12, N 16.80.

*Bis(N^{α}-phenylacetyl-L-arginine)-1,12-dodecanediamide dihydrochloride (**3d**)*

The title compound was prepared following the general methodology described above (a) (1.45 g, isolated yield 26 %), 97 % purity by HPLC. HPLC conditions: gradient elution 10-70 % B in 30 min; retention factor (*k*') = 11.2. $[\alpha]_D^{20}$ = -21.2 (*c* = 1.0 in methanol). IR (KBr): ν (cm^{-1}) = 3278, 3170, 2920, 2848, 1639, 1537, 1455, 1358, 1250, 1163, 692. ^{1}H NMR (300 MHz, CD_3OD) δ (ppm) = 7.37-7.18 (m, 10H), 4.39-4.24 (m, 2H), 3.59 (m, 4H), 3.16 (m, 8H), 1.94-1.37 (m, 12H), 1.36-1.20 (m, 16H). ^{13}C NMR (75 MHz, CD_3OD) δ (ppm) = 174.2, 173.8, 158.6, 136.9, 130.2, 129.6, 128.0, 54.6, 54.5, 43.7, 43.7, 42.0, 40.6, 40.5, 30.7, 30.7, 30.4, 30.4, 28.0, 26.4. Elemental analysis calcd. (%) for $C_{40}H_{66}Cl_2N_{10}O_4 \cdot 2H_2O$ (Mw 858.0); C 56.00, H 8.22, N 16.33 found C 56.31, H 8.39, N 16.38.

*Bis(N^{α}-phenylacetyl-L-arginine)-1,14-tetradecanediamide dihydrochloride (**3e**)*

The title compound was prepared following the general methodology described above (b) (1.80 g, isolated yield 26 %), 98 % purity by HPLC. HPLC conditions: gradient elution 10-70 % B in 40 min; retention factor (*k*') = 12.4. $[\alpha]_D^{20}$ = -22.0 (*c* = 1.0 in methanol). IR (KBr): ν (cm^{-1}) = 3283, 3165,

2920, 2848, 1644, 1537, 1455, 1358, 1250, 1158, 718. ^{1}H NMR (500 MHz, CD_3OD) δ (ppm) = 7.35-7.20 (m, 10H), 4.31 (dd, J = 8.5, 5.7 Hz, 2H), 3.59 (m, 4H), 3.16 (m, 8H), 1.83 (m, 2H), 1.74-1.50 (m, 6H), 1.50-1.41 (m, 4H), 1.29 (s, 20H). ^{13}C NMR (101 MHz, CD_3OD) δ (ppm) = 174.2, 173.7, 158.5, 136.8, 130.2, 129.7, 128.0, 54.4, 43.7, 41.9, 40.5, 30.8, 30.8, 30.7, 30.4, 28.0, 26.4. Elemental analysis calcd. (%) for $C_{42}H_{70}Cl_2N_{10}O_4 \cdot 5/2H_2O$ (Mw 895.0); C 56.36, H 8.45, N 15.65 found C 56.52, H 8.43, N 15.63.

4.4.4. Purification by chromatography

HPLC analysis

The amounts of acyl-donor, product and hydrolyzed acyl-donor produced in the reactions were measured by HPLC analysis using a Lichrosphere 100 CN (propylcyano), 5 μm, 250 x 4 mm column. The solvent system used was: solvent A; H_2O 0.1 % (v/v) trifluoroacetic acid (TFA) and solvent B; H_2O/ACN 1/4 0.095 % (v/v) TFA, flow rate 1 mL min^{-1}, detection 215 nm. Samples (50 μL) were withdrawn from the reaction medium at different times (0-96 h) depending on the synthesis and diluted with EtOH (800 μL).

Preparative Ion Exchange Chromatography

Purification by preparative ion exchange chromatography was performed as follows. The crude product was loaded onto a preparative column (285 cm^3) filled with MacroPrep High S, 50 μm stationary phase. The flow rate was 50-80 mL min^{-1}. Impurities were firstly eluted using NaCl (40 mM) in boric acid-borate 10 mM pH 9.5 aqueous buffer/ethanol 40:60. The products, bis(PhAcArg) derivatives, were finally eluted with NaCl (0.5 M) in H_2O/EtOH 40:60 solution. Analysis of the fractions was carried out by HPLC using the same conditions used as for the reaction monitoring (see above). The fractions with the product reaction were further purified by preparative HPLC.

Preparative HPLC

Purification by preparative HPLC was performed as follows. The crude products were loaded onto a preparative PrepPak (Waters) column (47x300 mm) filled with DeltaPak C4, 300 Å, 15 μm stationary phase. Products were eluted using ACN gradients in 0.1 % aqueous TFA: 20-36 % in 30 min for **3a**, 15-30 % in 30 min for **3b**, 19-34 % in 30 min for **3c**, 23-38 % in 30 min for **3d** and 16-32 % in 30 min for **3e**. The flow rate was 80 mL min^{-1} and the products were detected at 254 nm. Analysis of the fractions was carried out by analytical HPLC under isocratic conditions: 41 % of solvent B for **3a**, 45 % B for **3b**, 49 % B for **3c**, 53 % B for **3d** and 59 % B for **3e**. The pure fractions were pooled and lyophilized in the presence of aqueous HCl 37 % (2 eq.) to obtain the products in hydrochloride form.

4.5. Preparation of D-fagomine and *N*-alkyl-D-fagomine derivatives

4.5.1. Synthesis of 2-iodoxybenzoic acid (IBX)

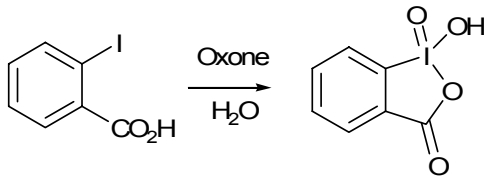

IBX

2-Iodobenzoic acid (37.2 g, 148.8 mmol) was added to a solution of OXONE (2 $KHSO_5$, $KHSO_4$, K_2SO_4, 280.4 g) in H_2O (1.5 L). This mixture was stirred at 70 °C for 3 h. Then, the reaction mixture was cooled at 4 °C overnight affording a solid. This solid was washed firstly with H_2O and finally with acetone. The residue was dried under vacuum, yielding 2-iodoxybenzoic acid (IBX) as white solid (37.2 g, isolated yield 85 %).
^{1}H NMR (300 MHz, [D_6]DMSO, 22 °C) δ (ppm) = 8.15 (d, J = 7.6 Hz, 1H), 8.06-7.96 (m, 2H), 7.84 (dt, J = 7.3, 7.3, 1.0 Hz, 1H).

4.5.2. Synthesis of *N*-benzyloxycarbonyl-3-amino-1-propanal (4)

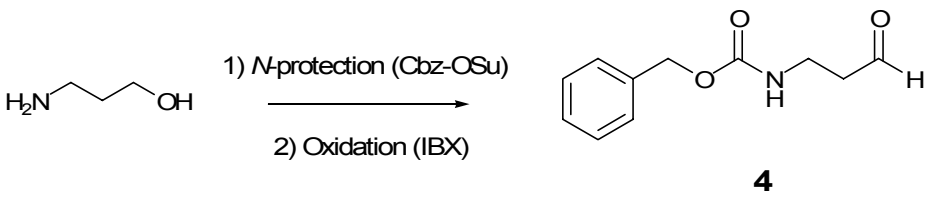

4

N-(benzyloxycarbonyloxy)succinimide (12.3 g, 49.4 mmol) dissolved in dioxane/H_2O 4:1 (150 mL) was added dropwise over a solution of 3-amino-1-propanol in dioxane/H_2O 4:1 (150 mL). The reaction mixture was stirred overnight at room temperature. The mixture was evaporated under reduced pressure affording a viscous brown solution. This solution was dissolved in EtOAc and washed with $NaHCO_3$ 5 % (2x50 mL), citric acid 5 % (2x50 mL) and brine (2x50 mL). The organic phase was dried with anhydrous Na_2SO_4, filtered and evaporated under vacuum to afford ***N*-benzyloxycarbonyl-3-amino-1-propanol** (9.28 g, isolated yield 90 %) as white solid. ^{1}H NMR (500 MHz, $CDCl_3$, 22 °C) δ (ppm) = 7.35 (m, Ar, 5H), 5.10 (s, $PhCH_2$-, 2H), 5.07 (s, -NH-, 1H), 3.67 (t, J = 5.5, -CH_2OH, 2H), 3.36 (dd, J = 12.3, 6.1, -NH-CH_2-, 2H), 1.70 (td, *J* = 11.9, 5.8 and 5.8, -$CH_2CH_2CH_2$-, 2H).

2-Iodoxybenzoic acid (IBX, 9.38 g, 34.49 mmol) was added over a stirred solution of *N*-benzyloxycarbonyl-3-amino-1-propanol (4.67 g, 22.3 mmol) in EtOAc (150 mL). Instantaneously, a white and opaque solution was formed. The reaction was stirred for 6 h at reflux. The advance of the reaction was followed by silica thin layer chromatography using EtOAc as eluent. The reaction crude was filtered and then, the filtered solution was washed with $NaHCO_3$ 5 % (2x90 mL) and brine (2x90 mL). The organic phase was dried with anhydrous Na_2SO_4, filtered and evaporated under vacuum to afford ***N*-benzyloxycarbonyl-3-amino-1-propanal** (3.77 g, isolated yield 82 %) as white solid. ^{1}H NMR (500 MHz, *CDCl3*, 22 °C) δ (ppm) = 9.80 (s, -C*H*O, 1H), 7.34 (m, Ar, 5H,), 5.17

(s, PhC*H*$_2$-, 2H), 5.08 (s, -N*H*-, 1H), 3.49 (dd, *J* = 11.9, 6.0, -NH-C*H*$_2$-, 2H), 2.75 (t, *J* = 5.6, -C*H*$_2$CHO, 2H).

4.5.3. Synthesis of (3*S*,4*R*)-6-[benzyloxycarbonyl)amino]-5,6-dideoxy-hex-2-ulose (5)

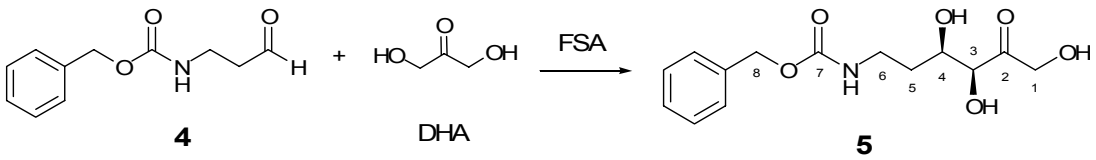

Dihydroxyacetone (2.1 g, 22.9 mmol) and FSA aldolase powder (2.09 g, 3445 U) were dissolved in boric/borate buffer 50 mM pH 7.0 (155 mL) and cooled down to 4 °C. To the mixture, *N*-Cbz-aminoaldehyde **4** (4.71 g, 22.9 mmol) dissolved in DMF (40 mL) was added. The reaction mixture was placed in a reciprocal shaker (120 rpm) at 4 °C. After 24 h, MeOH (200 mL) was added to the mixture to stop the reaction and centrifuged (1000 rpm) at 10 °C for 40 min. The supernatant was filtered on 0.45 µm filter and purified by preparative HPLC to give **5** (4.7 g, isolated yield 69 %) as a white solid. HPLC retention factor (*k*') = 3.7; $[\alpha]_D^{20}$ +9.0 (*c* 1.0 in MeOH). ^{1}H NMR (500 MHz, D_2O, 22 °C) δ (ppm) = 7.47-7.35 (5H, Ar), 5.09 (s, 2H, 8-H), 4.54 (d, *J* = 19.4 Hz, 1H, 1-H), 4.43 (d, *J* = 19.4 Hz, 1H, 1-H), 4.28 (s, 1H, 3-H), 4.02 (dt, *J* = 6.8, 6.8, 2.2 Hz, 1H, 4-H), 3.2 (m, 2H, 6-H) and 1.75 (q, *J* = 6.8 Hz, 2H, 5-H); ^{13}C NMR (101 MHz, D_2O, 22 °C) δ (ppm) = 212.9 (C-2), 158.6 (C-7), 136.7 (Ar), 128.9 (Ar), 128.5 (Ar), 127.8 (Ar), 77.7 (C-3), 69.5 (C-1), 67.0 (C-8), 66.1(C-4), 37.2 (C-6), 32.5 (C-5).

Preparative HPLC

The crude from the enzymatic reaction to obtain the aldol adduct **5** was purified by preparative HPLC as follows: the crude products were loaded onto a preparative column (47 x 300 mm) filled with Bondapack C18 (Waters), 300 Å, 15-20 µm stationary phase. Products were eluted using ACN gradient: 0 % to 28 % ACN in 35 min. The flow rate was 100 mL min^{-1} and the products were detected at 254 nm. Analysis of the fractions was

accomplished under isocratic conditions (33 % of solvent B) on the analytical HPLC. Pure fractions were pooled and lyophilized.

HPLC analyses

HPLC analyses were performed on a RP-HPLC cartridge, 250x4 mm filled with Lichrosphere® 100, RP-18, 5 μm from Merck (Darmstadt, Germany). Samples (50 μL) from the aldol reaction were withdrawn from the reaction medium, dissolved in MeOH to stop the reaction and analyzed by HPLC. The solvent system used was: solvent (A); H_2O 0.1 % (v/v) trifluoroacetic acid (TFA) and solvent (B); ACN/H_2O 4/1 0.095 % (v/v) TFA, gradient elution from 10 % to 70 % B in 30 min flow rate 1 mL min^{-1}, detection 215 nm. Retention factor (*k*') for the aldol adduct **5** is given above.

4.5.4. Synthesis of D-fagomine [(2*R*,3*R*,4*R*)-2-hydroxymethyl-piperidine-3,4-diol] (6)

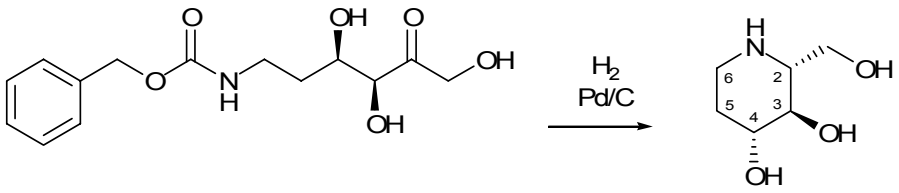

5 **6**

Pd/C (100 mg) was added to a solution of the aldol adduct **5** (373 mg, 1.26 mmol) in H_2O/EtOH 9:1 (50 mL). The reaction mixture was shaken under hydrogen gas (50 psi) and room temperature. After removal of the catalyst by filtration through neutralized and deactivated aluminium oxide, the solvent was evaporated under reduced pressure and then, lyophilized. D-Fagomine **6** (164 mg, yield 89 %, de 86 % by NMR) was afforded as a brown solid.

Purification by cationic exchange chromatography

The crude D-fagomine (24 mg) was purified by ion exchange chromatography on a FPLC system following a method described by Asano

et al.[8] Bulk stationary phase CM Sepharose CL-6B (Amersham Pharmacia) in NH_4^+ form was packed into a glass column (120x10 mm) to a final bed volume of 8 mL. The flow rate was 0.7 mL min^{-1}. The CM-Sepharose was equilibrated initially with H_2O. Then, an aqueous solution of the crude material at pH 7 was loaded onto the column. Minor coloured impurities were washed away with H_2O (2-3 column volumes). Then, D-fagomine and D-2,4-di-*epi*-fagomine were eluted in this order with NH_4OH 0.01 M. The fractions were analysed by NMR. Pure fractions were pooled and lyophilized affording D-2,4-di-*epi*-fagomine (< 1 mg) and D-fagomine (20 mg, 83 %) and as pale brown solids. $[\alpha]_D^{20}$ + 20.4 (*c* 1.0 in H_2O); ^1H NMR (500 MHz, D_2O, 22 °C) δ (ppm) = 3.86 (dd, *J* = 11.8, 3.0 Hz, 1H, 7-H), 3.66 (dd, *J* = 11.8, 6.5 Hz, 1H, 7-H), 3.56 (ddd, *J* = 11.5, 9.0, 5.0 Hz, 1H, 4-H), 3.21 (t, *J* = 9.5 Hz, 1H, 3-H), 3.06 (ddd, *J* = 12.9, 4.4, 2.3 Hz, 1H, 6-H), 2.68 (dt, *J* = 12.9, 12.9, 2.6 Hz, 1H, 6-H), 2.61 (ddd, *J* = 9.7, 6.4, 3.0 Hz, 1H, 2-H), 2.01 (tdd, *J* = 13.0, 4.9, 2.5, 2.5 Hz, 1H, 5-H), 1.53-1.43 (m, 1H, 5-H); ^{13}C NMR (101 MHz, D_2O, 22 °C) δ (ppm) = 72.9 (C-4), 72.7 (C-3), 61.1 (C-2), 60.9 (C-7), 42.6 (C-6), 32.1 (C-5).

D-2,4-di-epi-fagomine [(2S,3R,4S)-2-hydroxymethylpiperidine-3,4-diol] ***(10)****:*

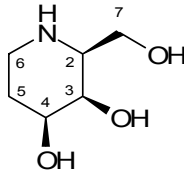

^1H NMR (500 MHz, D_2O, 22 °C) δ (ppm) = 3.91 (s, 1H, 3-H), 3.77-3.71 (m, 1H, 4-H), 3.68-3.60 (m, 2H, 7-H), 3.10-3.04 (m, 1H, 6-H), 2.74 (t, *J* = 6.8 Hz, 1H, 2-H), 2.64-2.57 (dt, *J* = 12.3, 12.3, 4.5 Hz, 1H, 6-H), 1.75-1.62 (m, 2H, 5-H); ^{13}C NMR (101 MHz, D_2O, 22 °C δ (ppm) = 69.6 (C-4), 67.6 (C-3), 61.4 (C-7), 59.2 (C-2), 42.8 (C-6), 27.0 (C-5).

4.5.5. Synthesis of *N*-alkyl-D-fagomine derivatives (7a-f)

N-butyl-D-fagomine[(2R,3R,4R)-N-butyl-2-hydroxymethylpiperidine-3,4-diol] ***(7a)***

Strategy (a): from D-fagomine

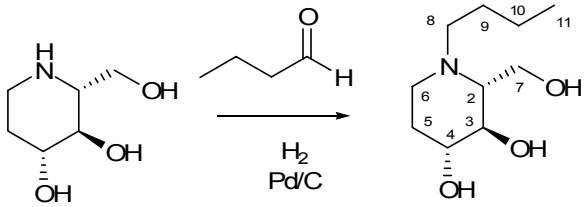

6 **7a**

Butanal (610 mg, 8.46 mmol) and D-fagomine **6** (249 mg, 1.69 mmol) were dissolved in EtOH/H_2O 20:7 (27 mL) and then, Pd/C (128 mg) was added. The mixture was shaken under H_2 (50 psi) overnight at room temperature. After removal the catalyst by filtration through neutral and deactivated alumina, the solvent was evaporated under reduced pressure. The brown oily residue obtained was purified by flash column chromatography on silica using MeOH/$CHCl_3$ from 0:1 to 4:1 as eluent. Pure fractions were pooled, the solvent was evaporated to dryness and the residue was dissolved in H_2O and lyophilized, yielding **4a** as a white-brown solid (160 mg, isolated yield 47 %). $[\alpha]_D^{20}$ -24.5 (c 1.3 in MeOH). ^{1}H NMR (500 MHz, D_2O, 22 °C) δ (ppm) = 3.90 (dd, J = 12.7, 2.4, 1H, 7-H), 3.82 (dd, *J* = 12.7, 2.9 Hz, 1H, 7-H), 3.45 (ddd, *J* = 11.5, 9.1, 5.1, 1H, 4-H,), 3.30 (t, *J* = 9.4, 1H, 3-H)**,** 2.90 (td, *J* = 12.2, 3.5, 3.5, 1H, 6-H), 2.73 (ddd, *J* = 13.3, 11.2, 5.4, 1H, 8-H), 2.50 (ddd, *J* = 13.3, 11.1, 5.2, 1H, 8-H), 2.36 (dt, *J* = 12.6, 12.6, 2.4, 1H, 6-H), 2.16 (td, *J* = 9.8, 2.6, 2.6 Hz, 1H, 2-H), 1.92 (tdd, *J* = 12.7, 5.0, 2.5, 2.5, 1H, 5-H), 1.55-1.35 (m, 3H, 5-H, 9-H), 1.30-1.21 (m, 2H, 10-H), 0.88 (t, *J* = 7.4, 3H, 11-H); ^{13}C NMR (101 MHz, D_2O, 22 °C) δ (ppm) = 73.2 (C-4), 72.0 (C-3), 65.8 (C-2), 58.1 (C-7), 52.2 (C-8), 49.1 (C-6), 30.5 (C-5), 25.6 (C-9), 20.4 (C-10) and 13.3 (C-11).

*Strategy (b): one pot reaction from the aldol adduct **5***

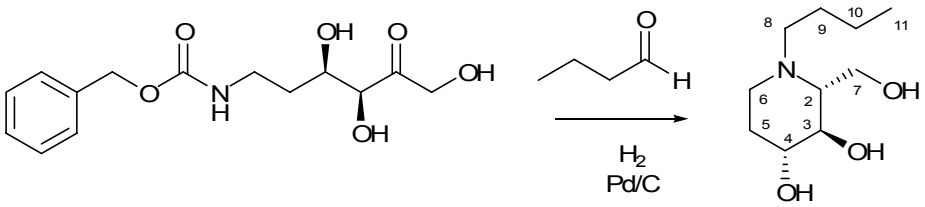

5 **7a**

Butanal (54 mg, 0.74 mmol) and the aldol adduct **5** (150 mg, 0.51 mmol) were dissolved in EtOH/H_2O 7:3 (10 mL) and Pd/C (55 mg) was added. After treatment with H_2 (50 psi) overnight at room temperature, the same procedure was followed as in *strategy a* to furnish **7a** (52 mg, isolated yield 51 %) as a solid.

*N-hexyl-D-fagomine [(2R,3R,4R)-N-hexyl-2-hydroxymethylpiperidine-3,4-diol] (**7b**)*

The title compound was obtained by the previous described *strategy a* (140 mg, isolated yield 40 %) as a solid. $[\alpha]_D^{20}$ -27.1 (*c* 1.3 in MeOH). ^{1}H NMR (500 MHz, D_2O, 22 °C) δ (ppm) = 3.94-3.84 (m, 2H, 7-H), 3.50-3.42 (m, 1H, 4-H), 3.38 (t, *J* = 9.2 Hz, 1H, 3-H), 2.97 (d, *J* = 11.7 Hz, 1H, 6-H), 2.87-2.77 (m, 1H, 8-H), 2.69-2.59 (m, 1H, 8-H), 2.46 (t, *J* = 12.0 Hz, 1H, 6-H), 2.24 (d, *J* = 9.4 Hz, 1H, 2-H), 1.97 (dd, *J* = 12.8, 2.4 Hz, 1H, 5-H), 1.58 (dq, *J* = 13.7, 13.7, 13.5, 3.2 Hz, 1H, 5-H), 1.54-1.45 (m, 2H, 9-H), 1.34-1.25 (br s, 6H, 10, 11 and 12-H), 0.88 (t, *J* = 5.8 Hz, 3H, 13-H); ^{13}C NMR (101 MHz, D_2O, 22 °C) δ (ppm) = 72.9 (C-4), 71.5 (C-3), 65.8 (C-2), 57.4 (C-7), 52.7 (C-8), 49.5 (C-6), 31.6 (C-5), 30.4 (C-9), 27.1 (C-10), 23.3 (C-11), 22.5 (C-12), 13.8 (C-13).

*N-octyl-D-fagomine [(2R,3R,4R)-N-octyl-2-hydroxymethylpiperidine-3,4-diol] (**7c**)*

The title compound was obtained by the previous described *strategy a* (79 mg, isolated yield 19 %) and *b* (153 mg, 54 %) as a solid. $[\alpha]_D^{20}$ -29.5 (*c* = 1.0 in MeOH). ^{1}H NMR (500 MHz, CD_3OD, 22 °C) δ (ppm) = 3.91-3.84 (m, 2H, 7-H), 3.38-3.31 (m, 2H, 3-H, 4-H), 2.94 (td, *J* = 11.8, 3.4, 3.4 Hz, 1H,

6-H), 2.87-2.78 (m, 1H, 8-H), 2.56 (ddd, *J* = 13.3, 10.2, 5.9 Hz, 1H, 8-H), 2.36 (dt, *J* = 12.2, 12.0, 1.5 Hz, 1H, 6-H), 2.13 (d, *J* = 8.5 Hz, 1H, 2-H), 1.92-1.85 (m, 1H, 5-H), 1.62-1.44 (m, 3H, 5-H, 9-H), 1.31 (br s, 10H, 10, 11, 12, 13 and 14-H), 0.90 (t, *J* = 6.7 Hz, 3H, 15-H); ^{13}C NMR (101 MHz, CD_3OD, 22 °C) δ (ppm) = 74.3 (C-4), 73.3 (C-3), 67.6 (C-2), 58.9 (C-7), 54.1 (C-8), 50.8 (C-6), 33.0 (C-5), 32.0 (C-9), 30.6 (C-10), 30.4 (C-11), 28.6 (C-12), 25.7 (C-13), 23.8 (C-14), 14.5 (C-15).

*N-nonyl-D-fagomine [(2R,3R,4R)-N-nonyl-2-hydroxymethylpiperidine-3,4-diol] (**7d**)*

The title compound was obtained by the previous described *strategy a* (96 mg, isolated yield 22 %) and *b* (110 mg, 40 %) as a solid. $[\alpha]_D^{22}$ -25.1 (*c* = 1.2 in MeOH). ^{1}H NMR (500 MHz, CD_3OD, 22 °C) δ (ppm) = 3.91-3.84 (m, 1H, 7-H), 3.39-3.32 (m, 2H, 3-H, 4-H), 2.96 (d, *J* = 11.9 Hz, 1H, 6-H), 2.88-2.80 (m, 1H, 8-H), 2.63-2.54 (m, 1H, 8-H), 2.43-2.34 (m, 1H, 6-H), 2.16 (d, *J* = 7.6 Hz, 1H, 2-H), 1.93-1.86 (m, 1H, 5-H), 1.62-1.46 (m, 3H, 5-H, 9-H), 1.38-1.24 (br s, 12H, 10, 11, 12, 13, 14 and 15-H), 0.90 (t, *J* = 7.0, 3H, 16-H); ^{13}C NMR (101 MHz, CD_3OD, 22 °C δ (ppm) = 74.5 (C-4), 73.5 (C-3), 67.6 (C-2), 59.2 (C-7), 54.1 (C-8), 50.9 (C-6), 33.1 (C-5), 32.2 (C-9), 30.8 (C-10), 30.7 (C-11), 30.5 (C-12), 28.7 (C-13), 25.3 (C-14), 23.8 (C-15), 14.5 (C-16).

*N-dodecyl-D-fagomine [(2R,3R,4R)-N-dodecyl-2-hydroxymethylpiperidine-3,4-diol] (**7e**)*

The title compound was obtained by the previous described *strategy a* (289 mg, isolated yield 57 %) as a solid. $[\alpha]_D^{20}$ -11.1 (*c* = 1.0 in MeOH). ^{1}H NMR (500 MHz, CD_3OD, 22 °C) δ (ppm) = 4.10 (d, *J* = 12.4, 1H, 7-H), 3.90 (dd, *J* = 12.4, 2.7, 1H, 7-H) 3.62-3.50 (m, 2H, 3-H, 4-H), 3.42 (d, *J* = 12.1 Hz, 1H, 6-H), 3.30-3.20 (br s, 1H, 8-H), 3.16-2.99 (br s, 2H, 6-H, 8-H), 2.92 (br s, 1H, 2-H), 2.11 (dd, *J* = 14.1, 3.1, 1H, 5-H), 1.82-1.63 (br s, 3H, 5-H, 9-H), 1.41-1.30 (br s, 2H, 10-H), 1.30-1.20 (16-H, 11, 12, 13, 14, 15, 16, 17 and 18-H), 0.90 (t, *J* = 6.94 Hz, 3H, 19-H); ^{13}C NMR (101 MHz, CD_3OD, 22 °C) δ (ppm) = 71.8 (C-4), 71.1 (C-3), 67.5 (C-2), 56.1 (C-7), 54.0 (C-8), 50.3

(C-6), 33.1 (C-5), 30.8 (C-9), 30.7 (C-10, C-11), 30.6 (C-12), 30.5 (C-13), 30.3 (C-14), 29.8 (C-15), 27.9 (C-16), 24.6 (C-17), 23.8 (C-18), 14.5 (C-19).

*N-phenylethyl-D-fagomine [(2R,3R,4R)-N-phenylethyl-2-hydroxymethyl-piperidine-3,4-diol] (**7f**)*

The title compound was obtained by the previous described *strategy a* (96 mg, isolated yield 23 %) as a solid $[\alpha]_D^{20}$ -21.8 (*c* 1.1 in MeOH). ^{1}H NMR (500 MHz, CD_3OD, 22 °C) δ (ppm) = 7.29-7.13 (5H, Ar), 3.96-3.88 (m, 2H, 7-H), 3.41-3.31 (m, 2H, 4-H, 3-H), 3.05-2.96 (m, 2H, 6H, 8-H), 2.93-2.72 (m, 3H, 8-H, 9-H), 2.52 (dt, *J* = 12.3, 12.3, 2.4 Hz, 1H, 6-H), 2.26 (td, *J* = 9.0, 2.7, 2.7 Hz, 1H, 2-H), 1.95-1.88 (m, 1H, 5-H), 1.65-1.54 (m, 1H, 5-H); ^{13}C NMR (101 MHz, CD_3OD, 22 °C) δ (ppm) = 141.5 (Ar), 129.71-129.1 (Ar), 74.6 (C-4), 73.5 (C-3), 67.0 (C-2), 59.4 (C-7), 56.1 (C-8), 50.9 (C-6), 32.4 (C-5), 31.5 (C-9).

References:

1. Infante, M. R.; García, J.; Erra, P.; Julia, R.; Prats, M., Surface activity molecules: preparation and properties of long chain N^{α}-acyl-L-α-amino-ω-guanidine alkyl acid derivatives. *Int. J. Cosmetic Sci.* **1984**, *6*, 275-282.
2. Piera, E.; Infante, M. R.; Clapés, P., Chemo-enzymatic synthesis of arginine-based gemini surfactants. *Biotechnol. Bioeng.* **2000**, *70*, 323-331.
3. Böttcher, C. J. F.; Van gent, C. M.; Pries, C., A rapid and sensitive sub-micro phosphorus determination. *Anal. Chim. Acta* **1961**, *24*, 203-204.
4. Woods, G. L.; Washington, J. A., Antibacterial susceptibility test: dilution in disk diffusion method. In *Manual of Clinical Microbiology*, Murray, P. R.; Baron, E. J.; Pfaller, M. S.; Ternover, F. C.; Yolken, R. H., Eds. ASM Press: Washington, 1995.
5. Madigan, M. T.; Martinko, J. M., *Brock Biology of Microorganisms*. 11 ed.; Pearson Prentice Hall: Upper Saddle River, 2006.
6. Schürmann, M.; Sprenger, G. A., Fructose-6-phosphate Aldolase Is a Novel Class I Aldolase from *Escherichia coli* and Is Related to a Novel Group of Bacterial Transaldolases. *J. Biolog. Chem.* **2001**, *276*, 11055-11061.
7. Pape, W. J.; Pfannenbecker, U.; Hoppe, U., Validation of the red blood cell test system as in vitro assay for the rapid screening of irritation potential of surfactants. *Mol. Toxicol.* **1987**, *1*, 525-536.
8. Asano, N.; Kuroi, H.; Ikeda, K.; Kizu, H.; Kameda, Y.; Kato, A. I.; Adachi, I.; Watson, A. A.; Nash, R. J.; Fleet, G. W. J., New polyhydroxylated pyrrolizidine alkaloids from *Muscari armeniacum*: structural determination and biological activity. *Tetrahedron: Asymmetry* **2000**, *11*, 1-8.

5. CONCLUDING REMARKS

The following general conclusions correspond to the four objectives previously described in section 2:

1) The interaction of arginine-based surfactant with DPPC multilamellar vesicles correlated well with their antimicrobial activity. The gemini arginine-based surfactant $C_3(CA)_2$ induced higher fluidity on DPPC unilamellar vesicles than chlorhexidine. However, from the results obtained with lipid monolayers a relation between the physico-chemical properties and the antimicrobial activity was unclear. The results point out that arginine-based surfactant are membrane-active agents.

2) $C_3(CA)_2$ and CHX induced similar types of damage to *S. aureus* and *E. coli,* though they differ in the extent of membrane depolarization and reduction of cell viability. These differences suggest that both compounds damage bacteria in a different way, and that the surfactant properties of $C_3(CA)_2$ and its ability to partition into the biological membrane from aqueous solution might be important characteristics in its microbicidal action.

3) Novel bis(PhAcArg) derivatives were prepared by a facile chemoenzymatic methodology. A clear effect of the spacer chain length on the antimicrobial activity was observed. Therefore, the hydrophilic-lipophilic balance plays a key role in the antimicrobial action of these compounds, suggesting that these compounds could target the cytoplasmic membrane.

4) D-Fagomine and some of its *N*-alkylated derivatives were prepared by a straightforward synthesis using the novel aldolase FSA. Only *N*-dodecyl-D-fagomine showed moderate antimicrobial activity. This result discards specific mechanism of antimicrobial action and suggests that these iminocyclitols target the cytoplasmic membrane.

6. ANNEXES

6.1. NMR spectra

^{1}H-NMR spectrum (CD_3OD) of compound **3a**:

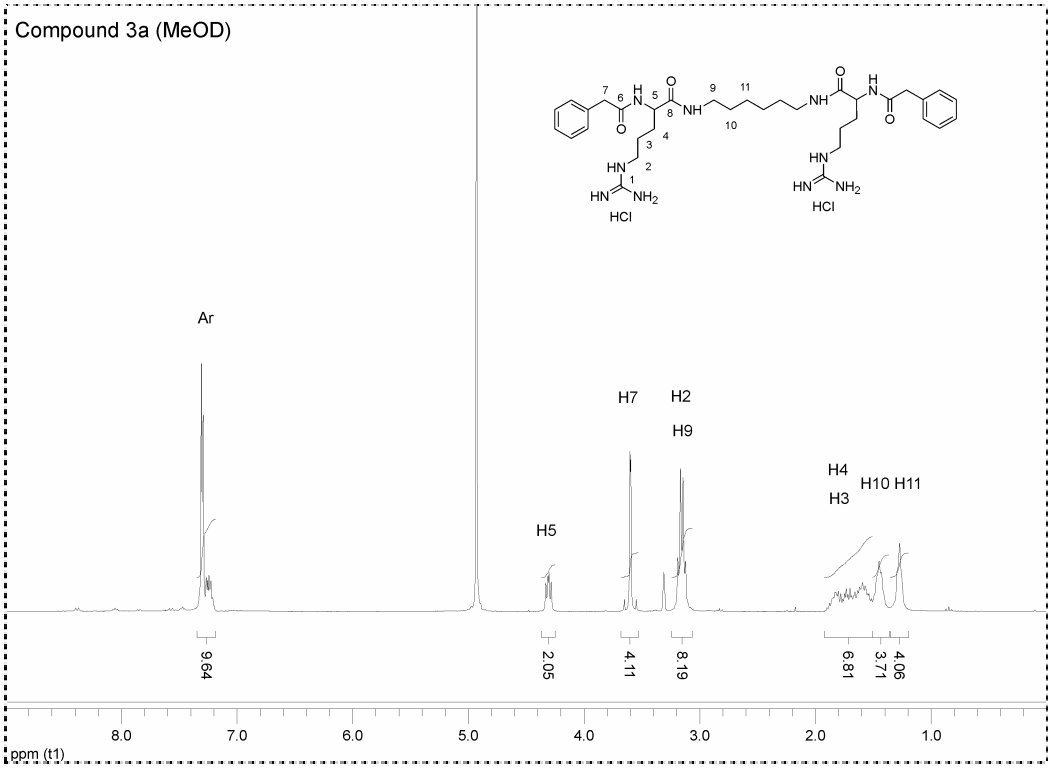

^{13}C-NMR (CD_3OD) spectrum of compound **3a**:

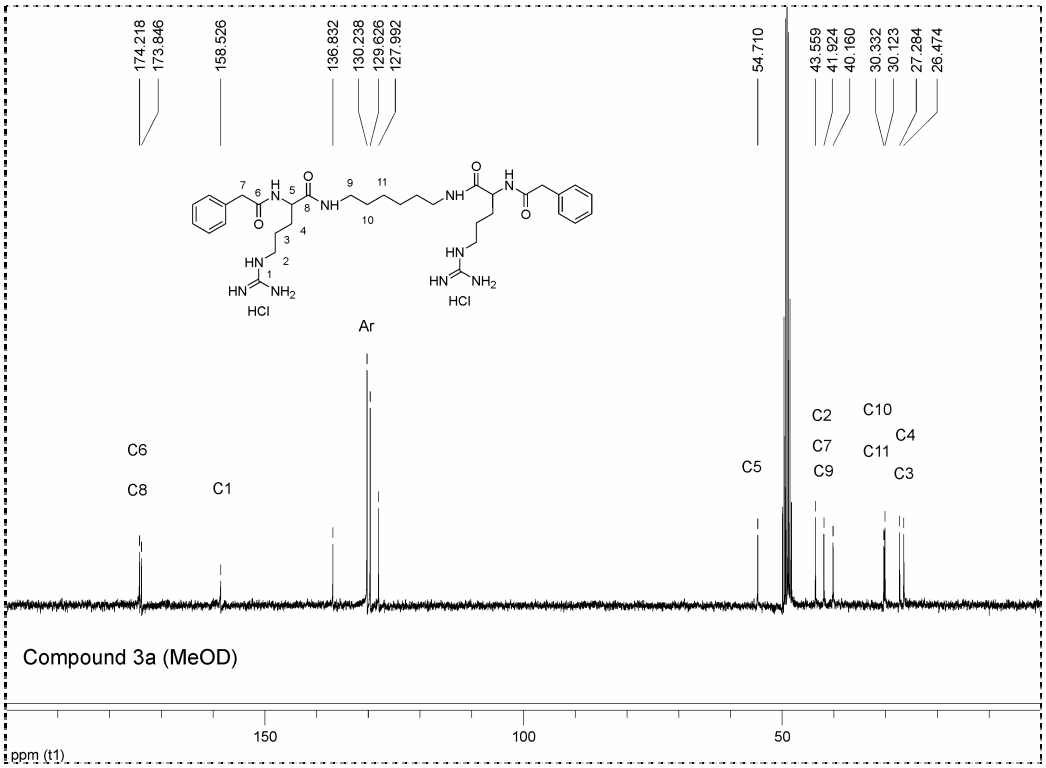

^{1}H-NMR (CD_3OD) spectrum of compound **3b**:

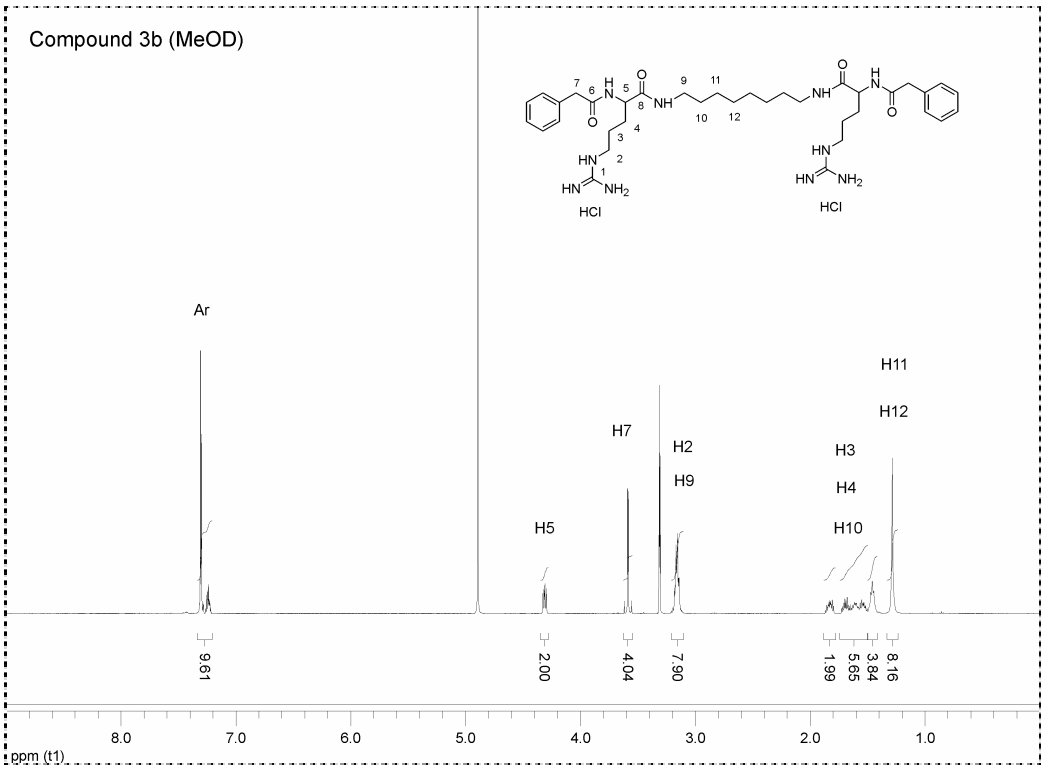

^{13}C-NMR spectrum (CD_3OD) of compound **3b**:

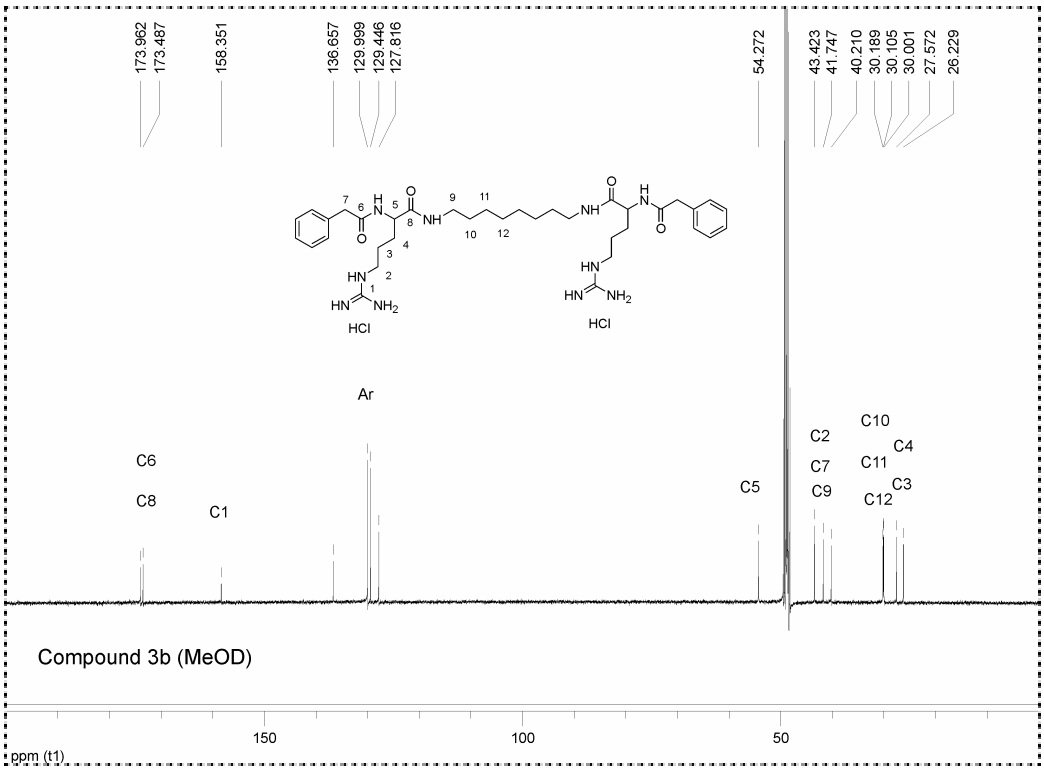

^{1}H-NMR spectrum (CD_3OD) of compound **3c**:

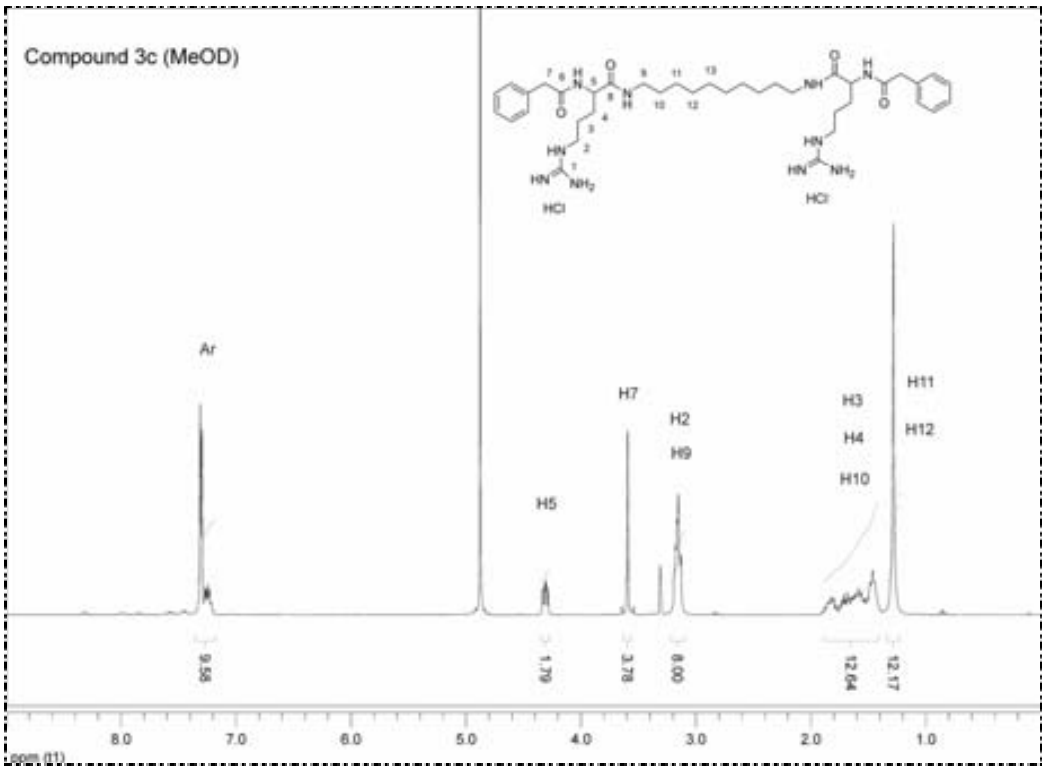

^{13}C-NMR spectrum (CD_3OD) of compound **3c**:

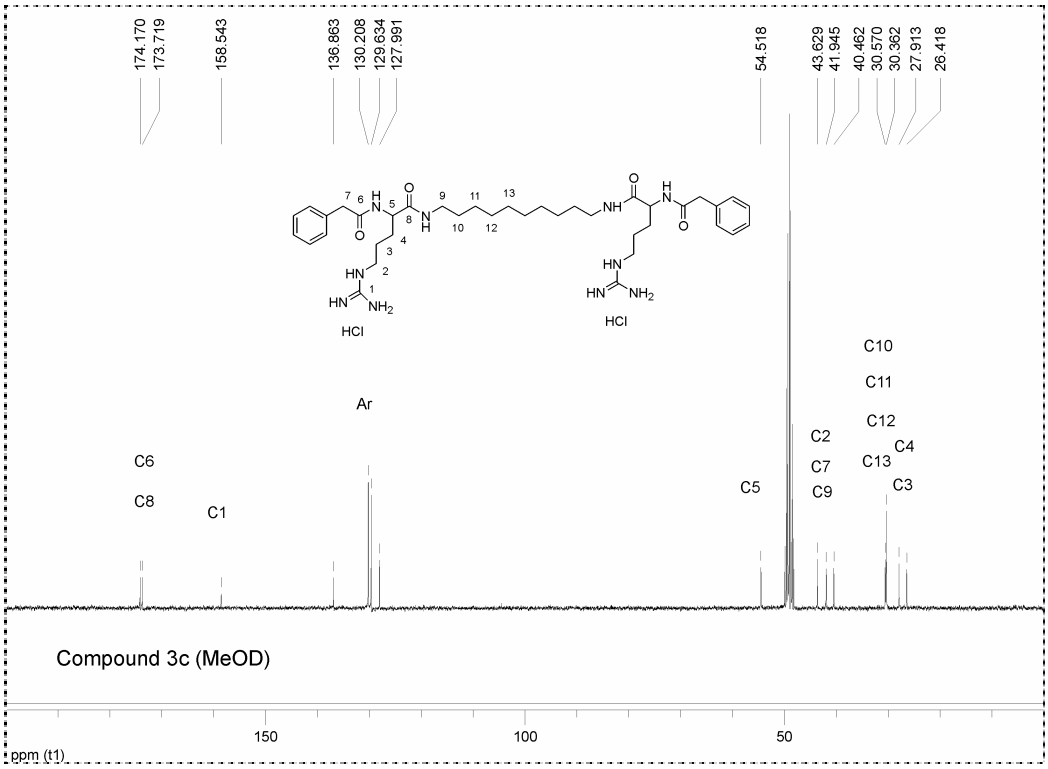

^{1}H-NMR spectrum (CD_3OD) of compound **3d**:

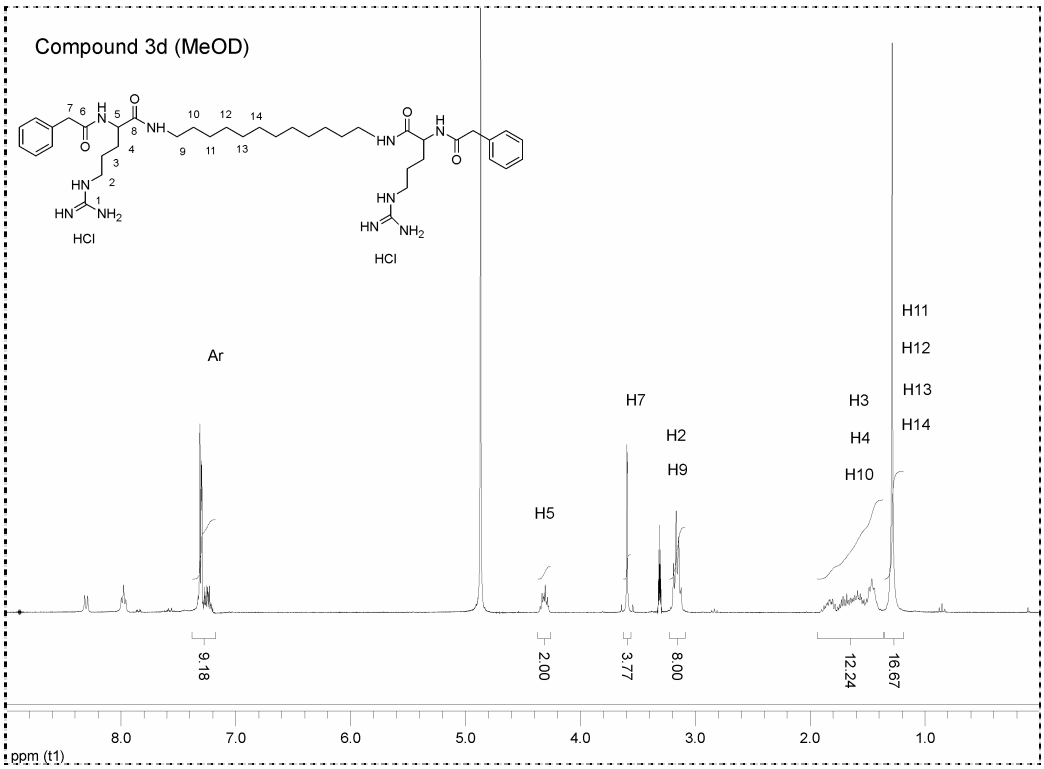

^{13}C-NMR spectrum (CD_3OD) of compound **3d**:

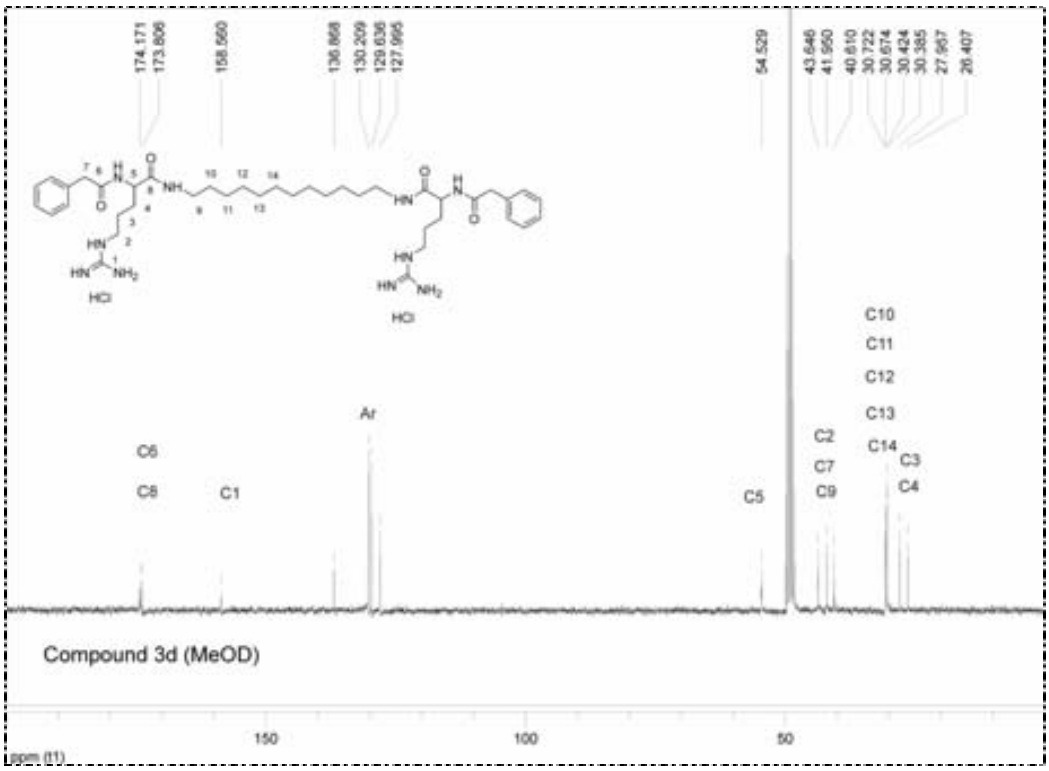

^{1}H-NMR spectrum (CD_3OD) of compound **3e**:

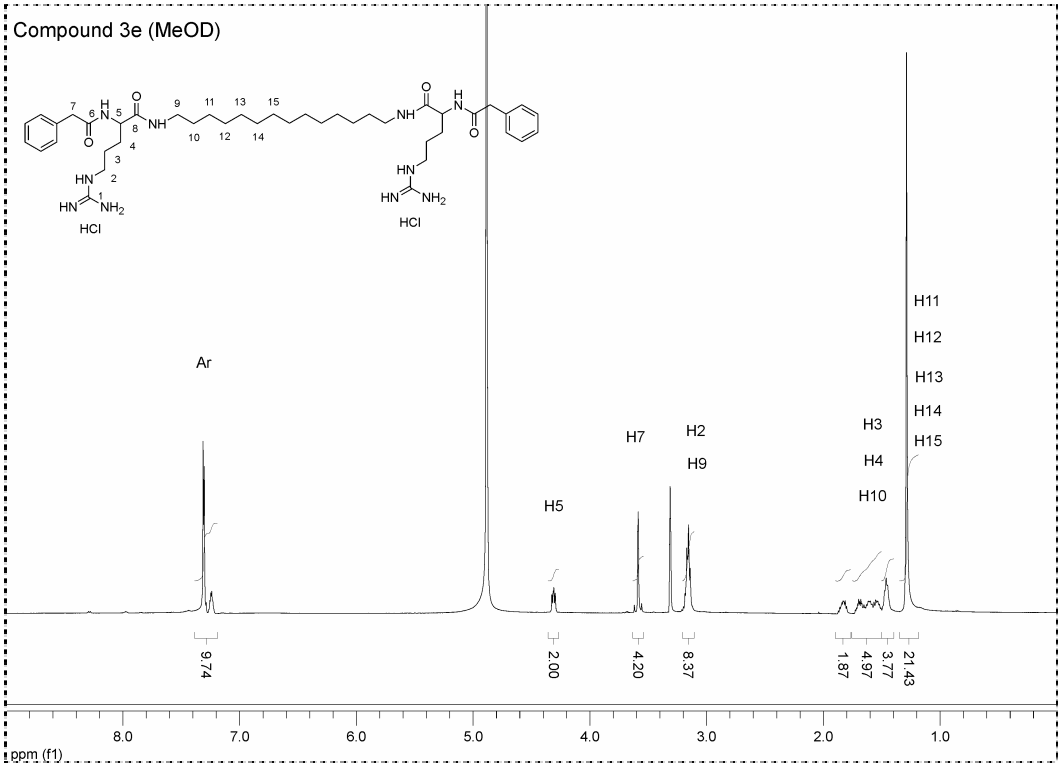

^{13}C-NMR spectrum (CD_3OD) of compound **3e**:

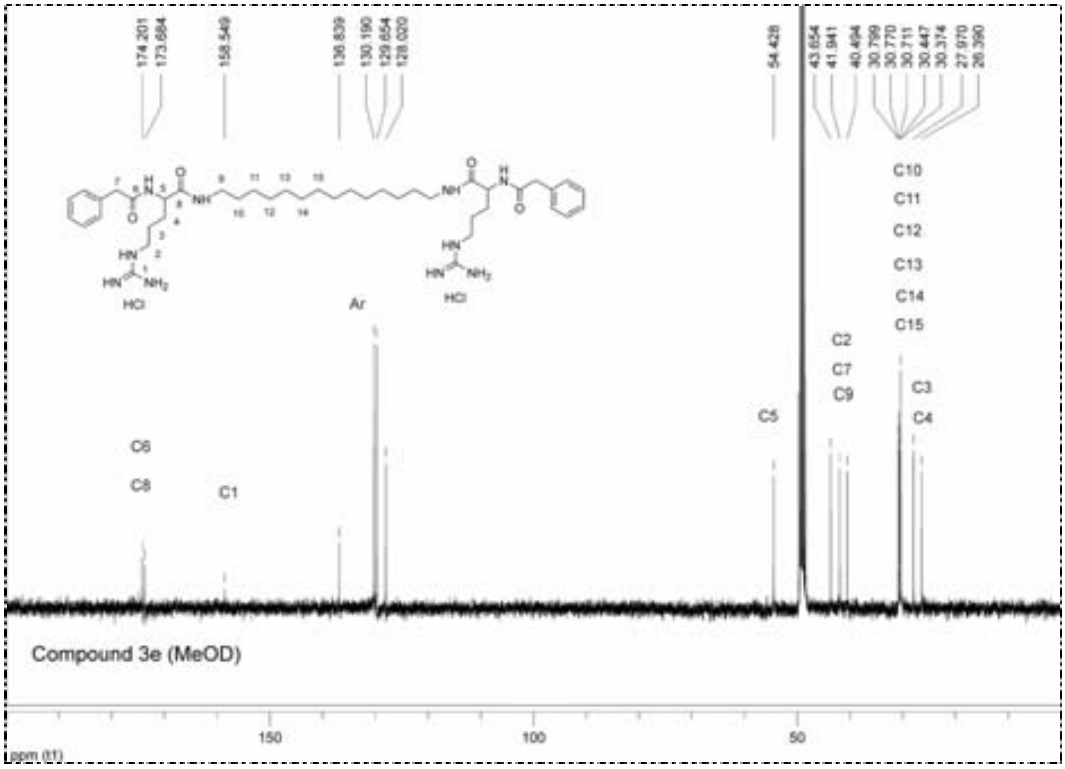

^{1}H-NMR spectrum (D_2O) of aldol adduct **5**:

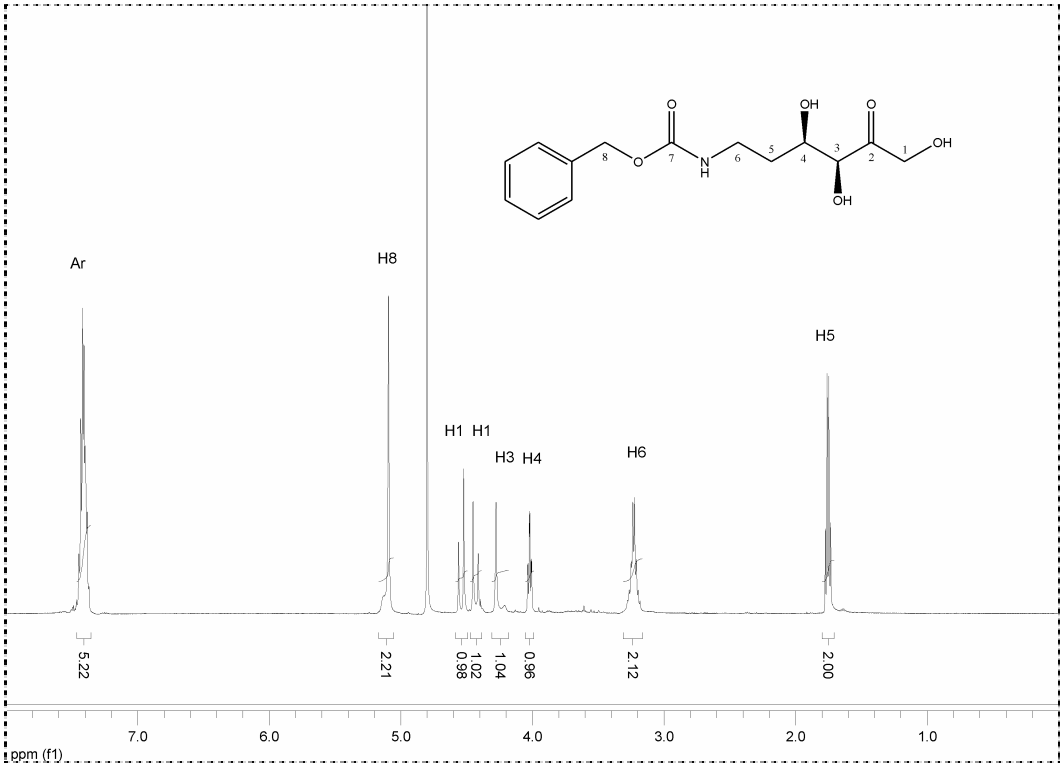

^{13}C-NMR spectrum (D_2O) of aldol adduct **5**:

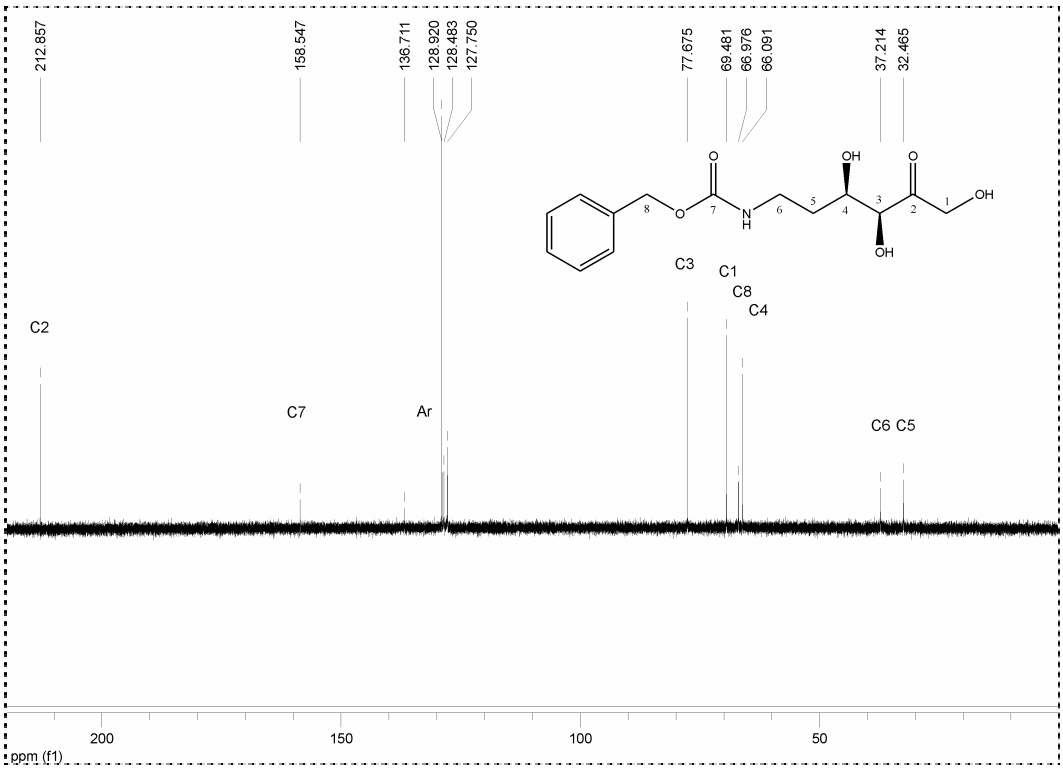

^{1}H-NMR spectrum (D_2O) of D-fagomine **6**, before purification by cation exchange chromatography:

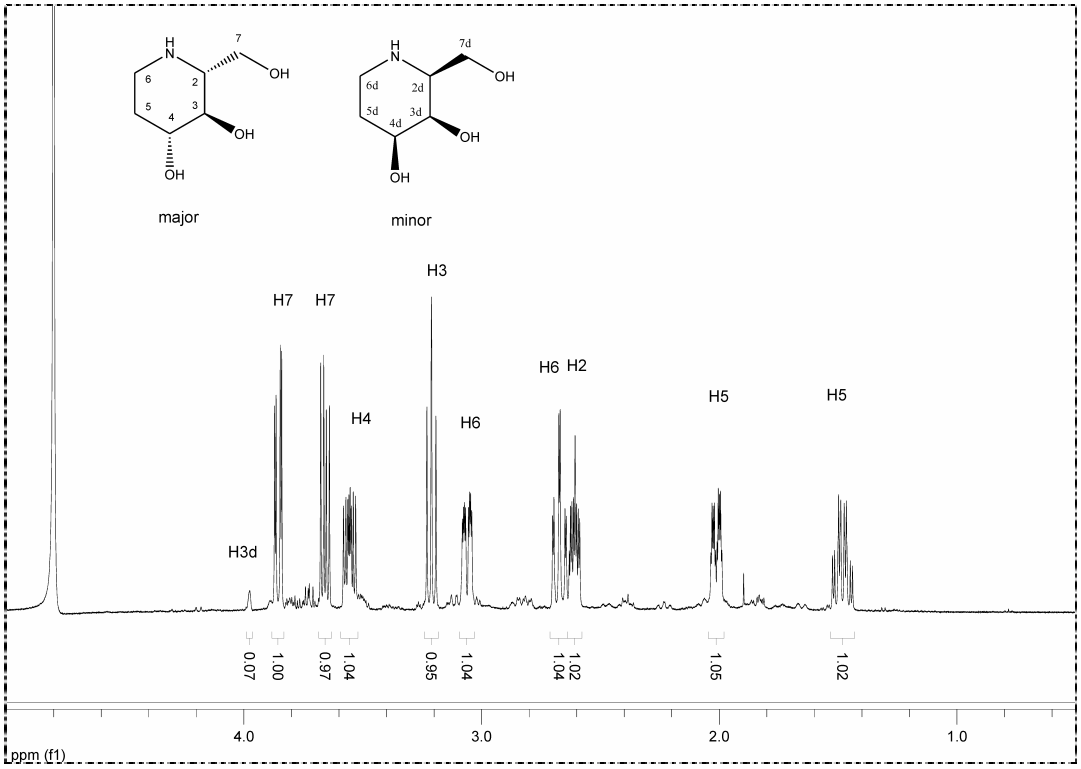

^{1}H-NMR spectrum (D_2O) of D-fagomine **6**, purified by cation exchange chromatography:

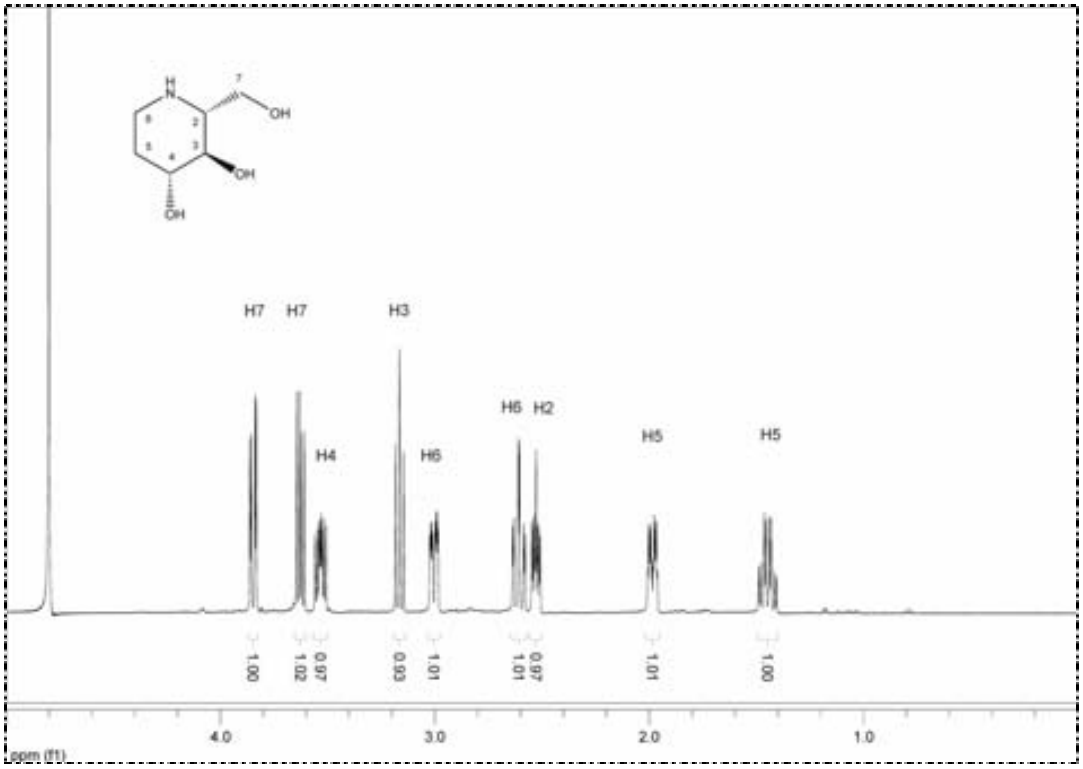

^{13}C-NMR spectrum (D_2O) of D-fagomine **6**, purified by cation exchange chromatography:

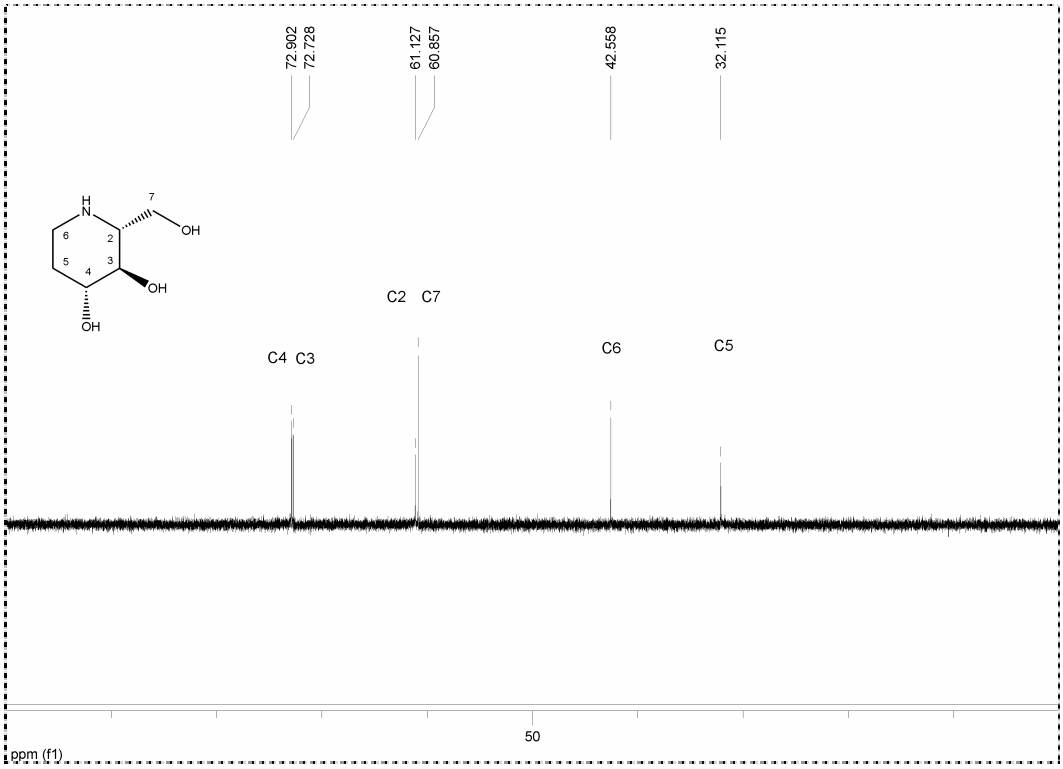

^{1}H-NMR spectrum (D_2O) of D-2,4-di-*epi*-fagomine **10**, purified by cation exchange chromatography:

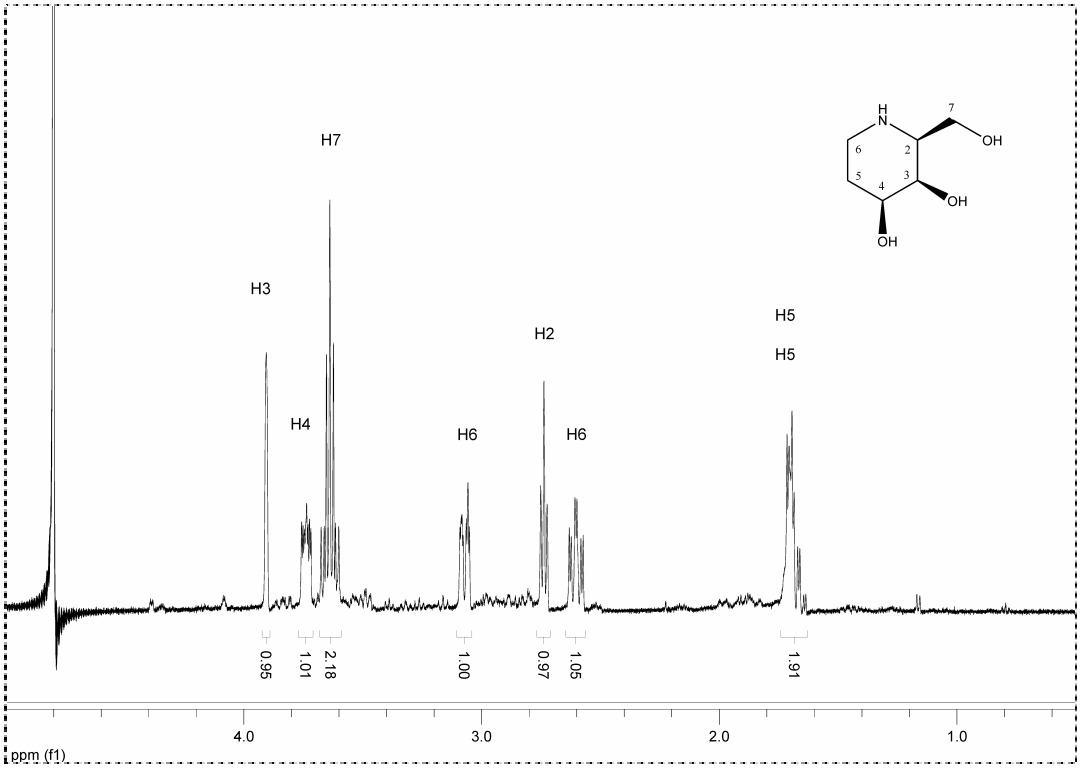

^{13}C-NMR spectrum (D_2O) of D-2,4-di-*epi*-fagomine **10**, purified by cation exchange chromatography:

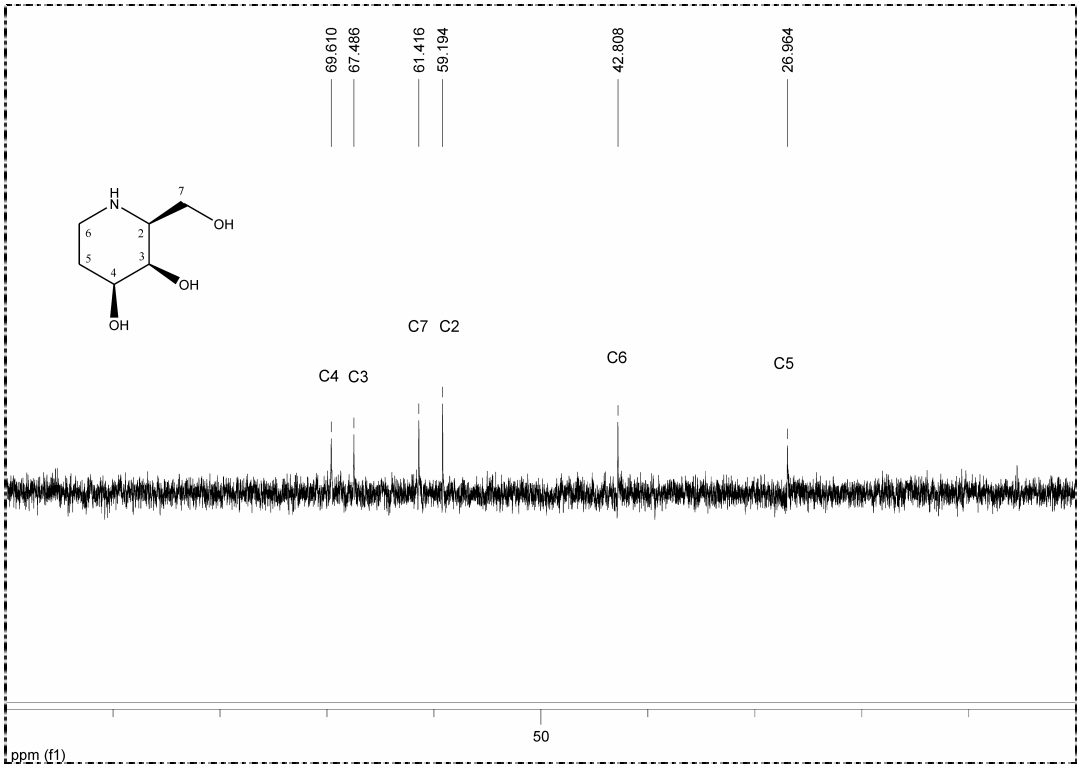

^{1}H-NMR spectrum (D_2O) of *N*-butylfagomine **7a**:

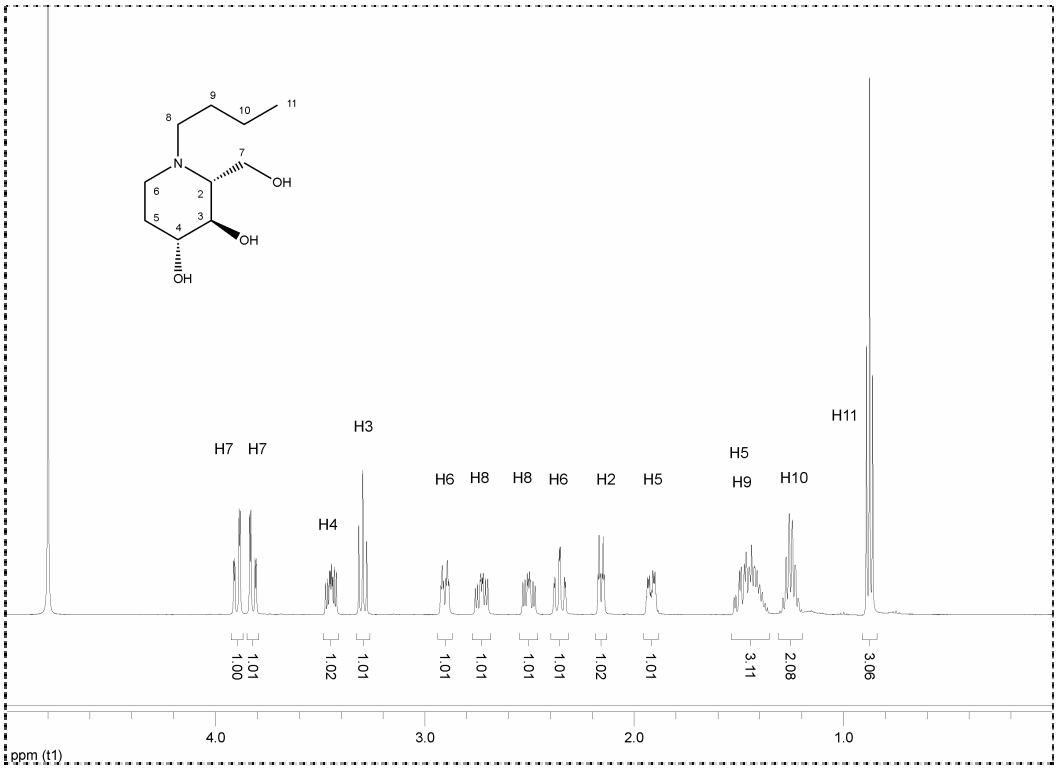

^{13}C-NMR spectrum (D_2O) of *N*-butylfagomine **7a**:

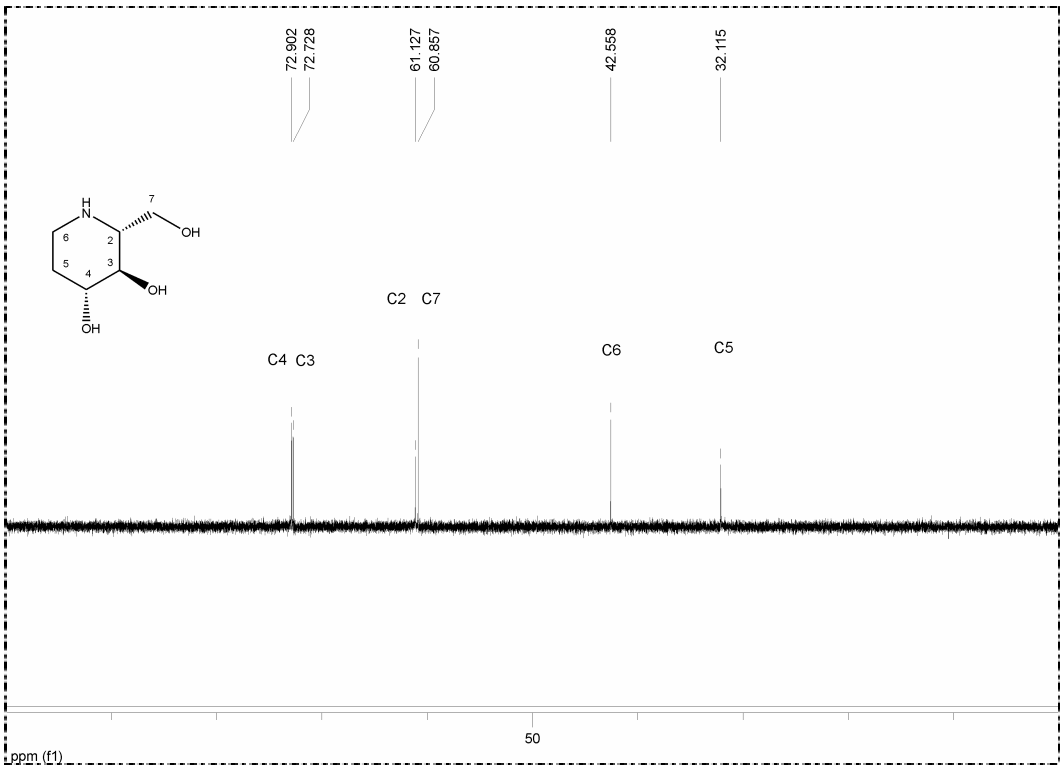

COSY-NMR spectrum (D_2O) of *N*-butylfagomine **7a**:

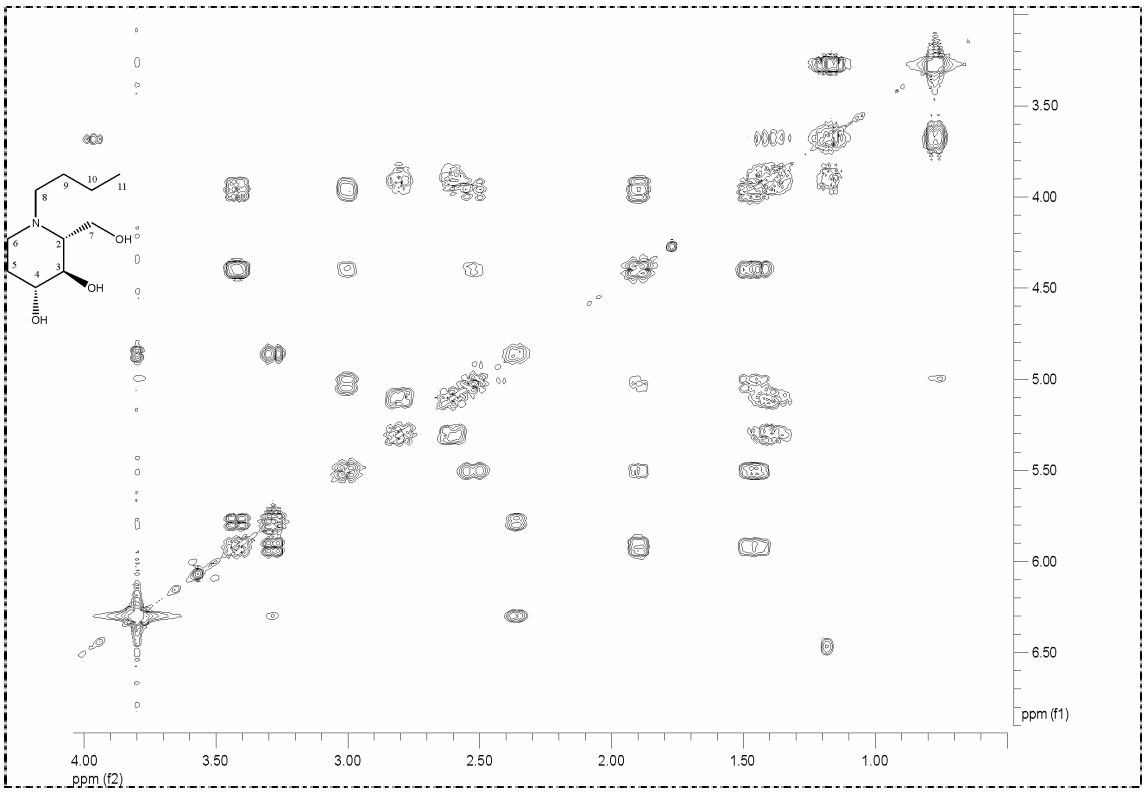

HSQC-NMR spectrum (D_2O) of *N*-butylfagomine **7a**:

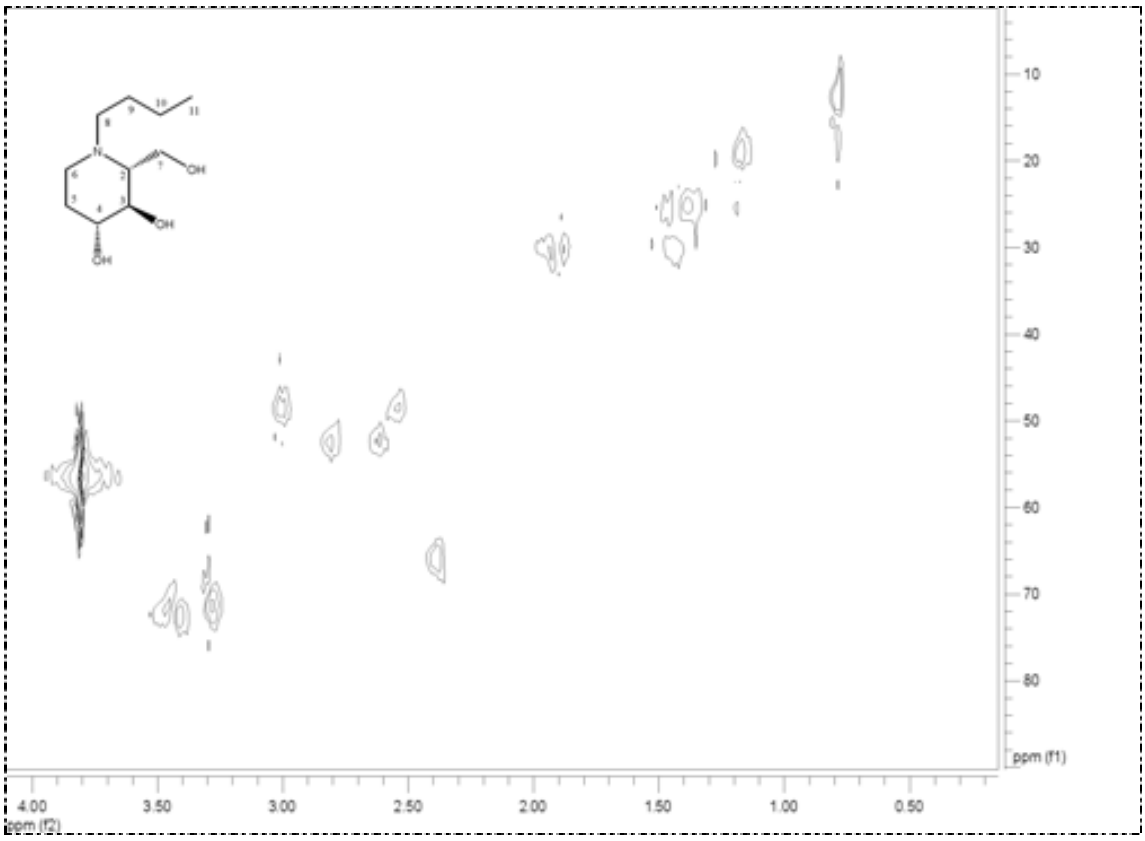

NOE-NMR spectrum (D_2O) of *N*-butylfagomine **7a**:

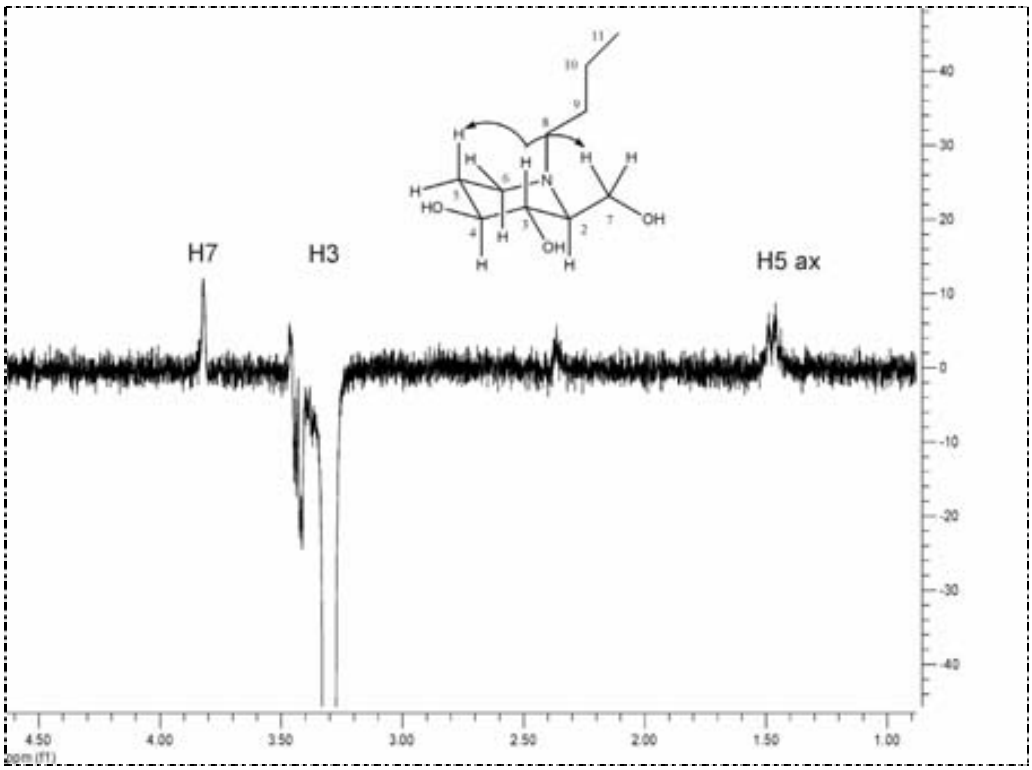

NOE-NMR spectrum (D_2O) of *N*-butylfagomine **7a**:

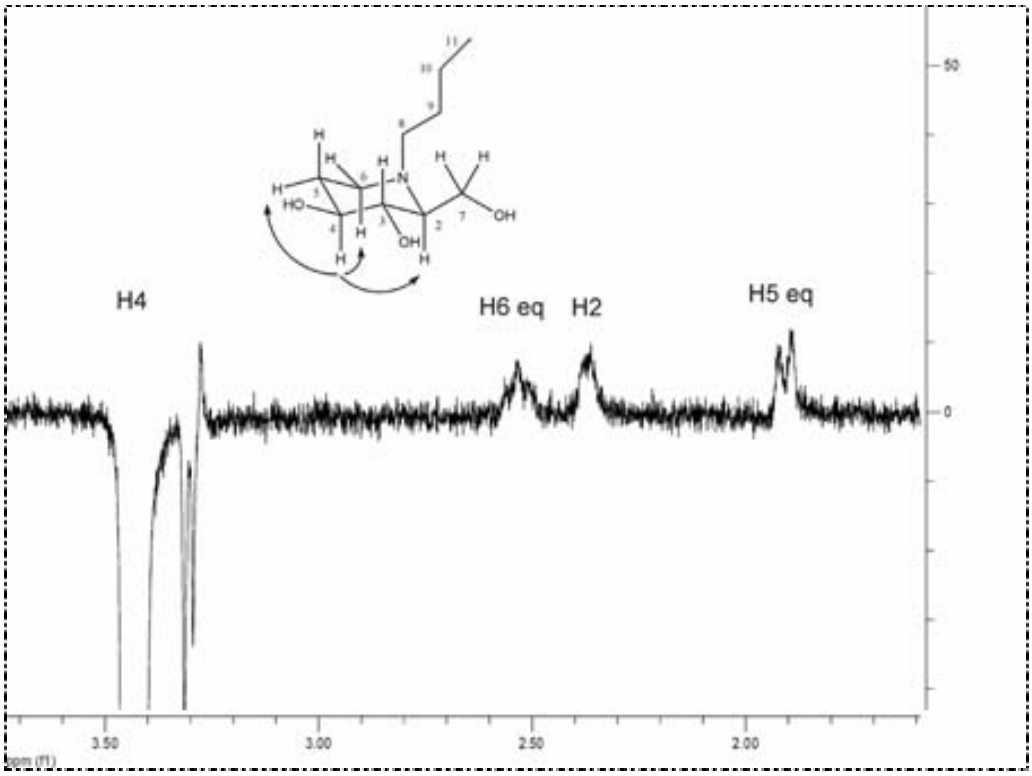

^{1}H-NMR spectrum (D_2O) of *N*-hexylfagomine **7b**:

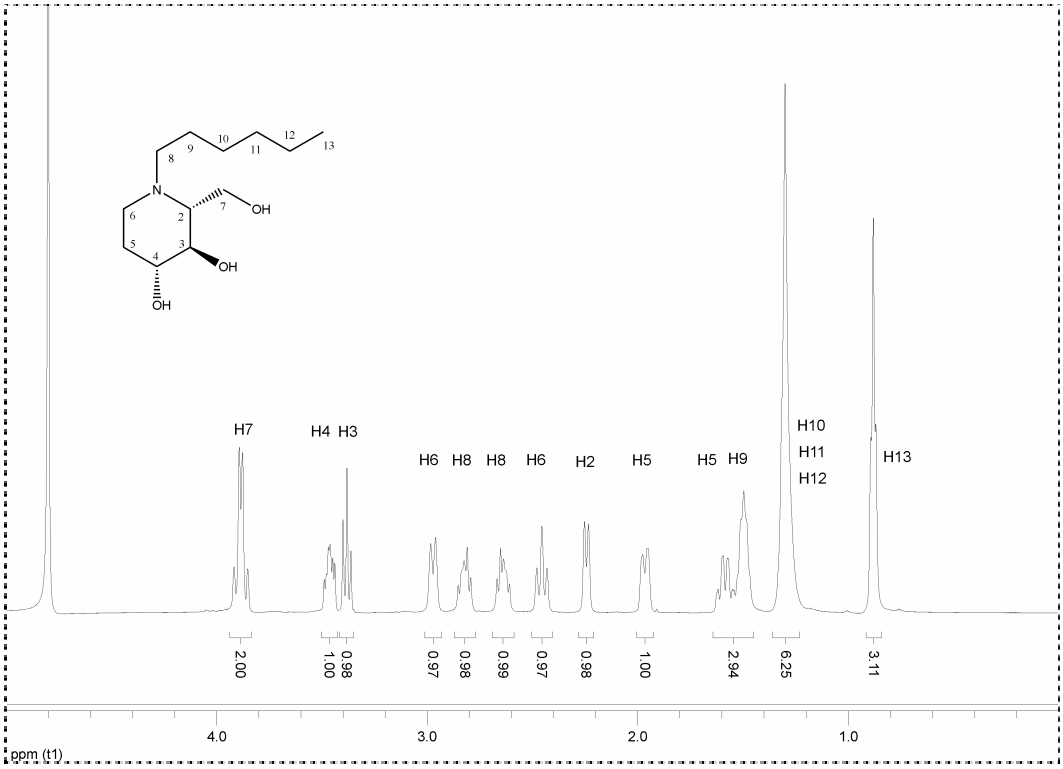

^{13}C-NMR spectrum (D_2O) of hexylfagomine **7b**:

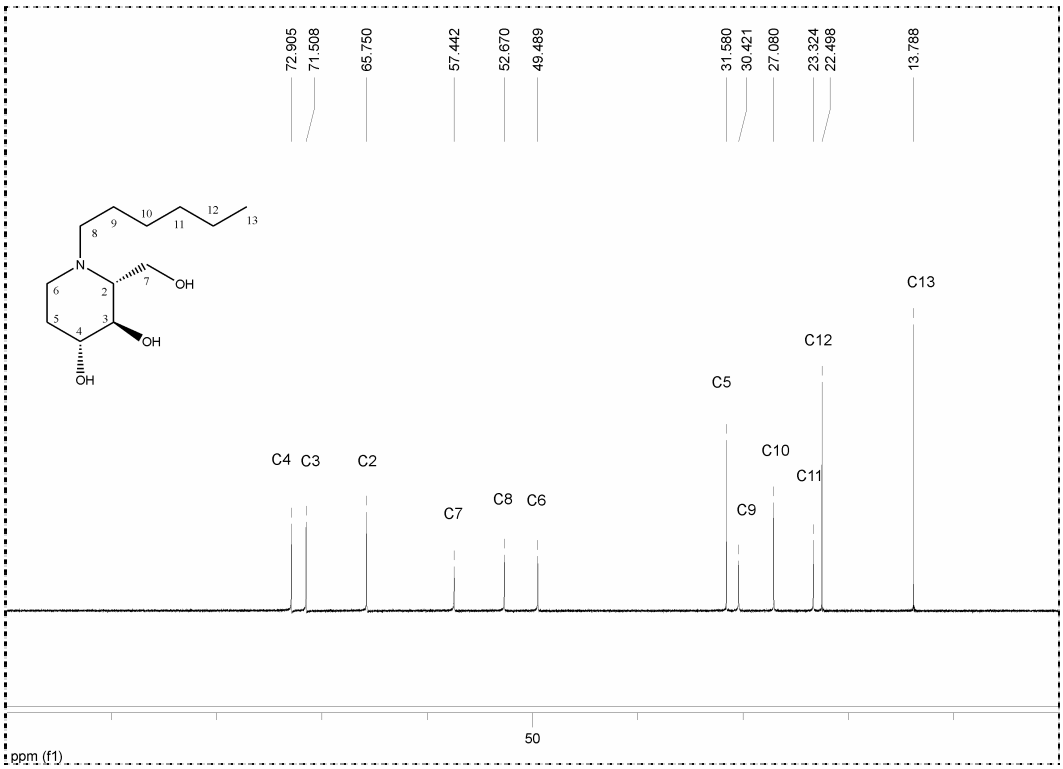

^{1}H-NMR spectrum (CD_3OD) of *N*-octylfagomine **7c**:

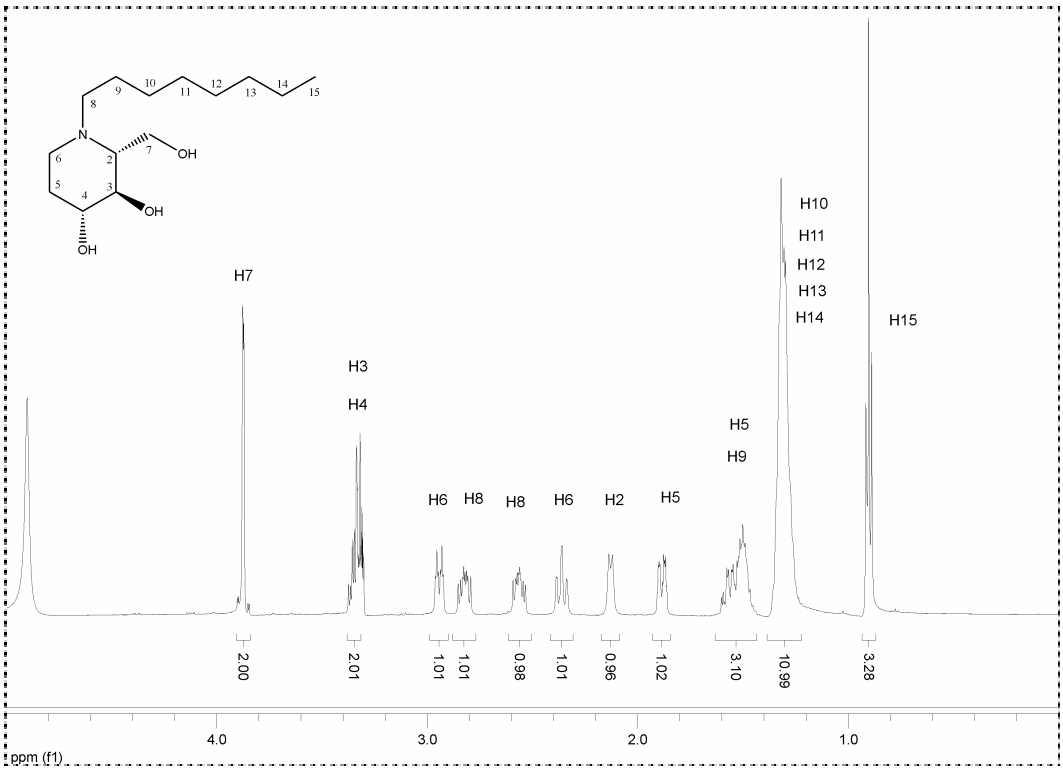

^{13}C-NMR spectrum (CD_3OD) of *N*-octylfagomine of **7c**:

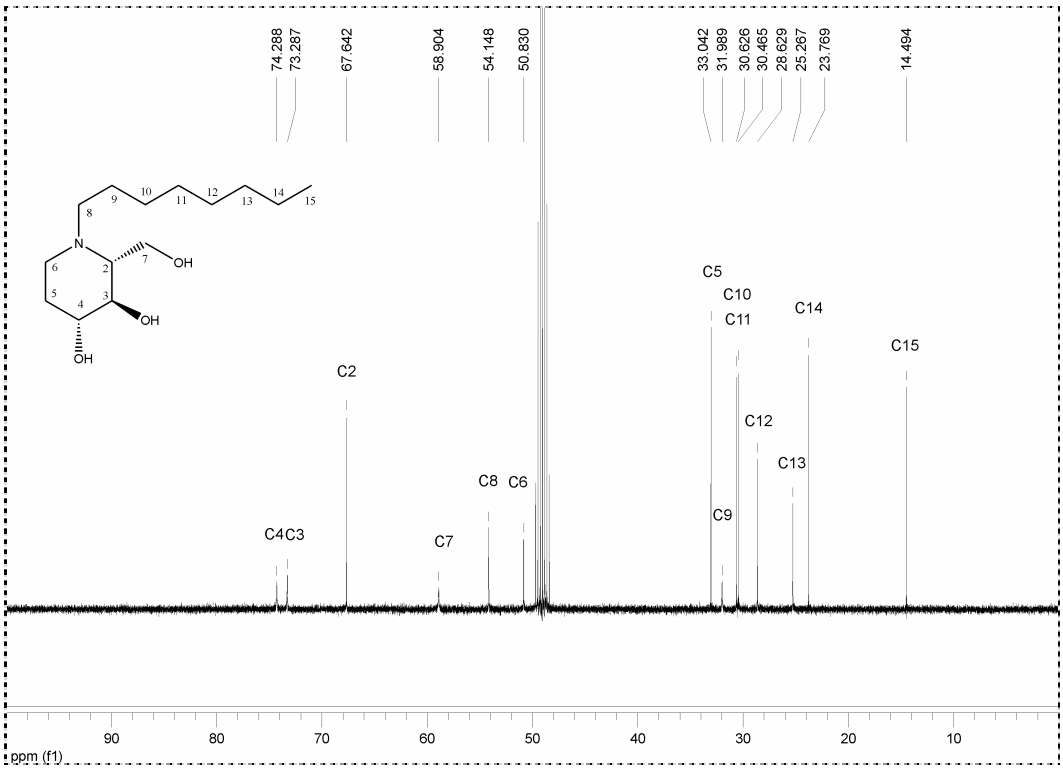

^{1}H-NMR spectrum (CD_3OD) of *N*-nonylhexylfagomine **7d**:

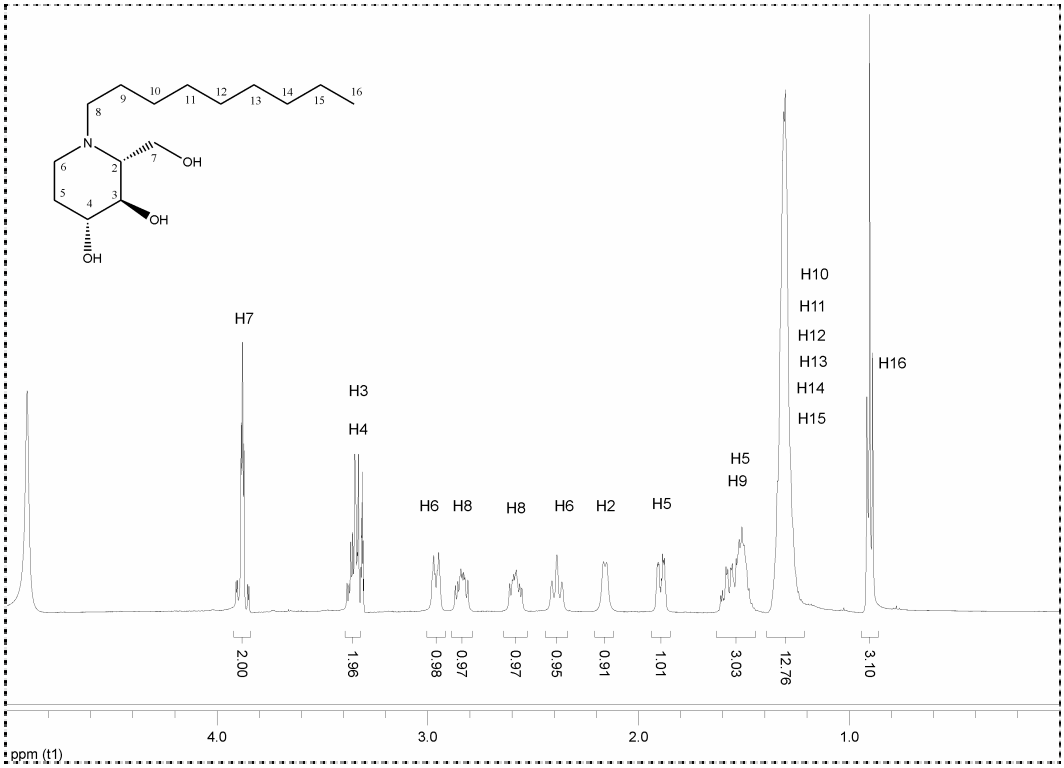

^{13}C-NMR spectrum (CD_3OD) of *N*-nonylfagomine **7d**:

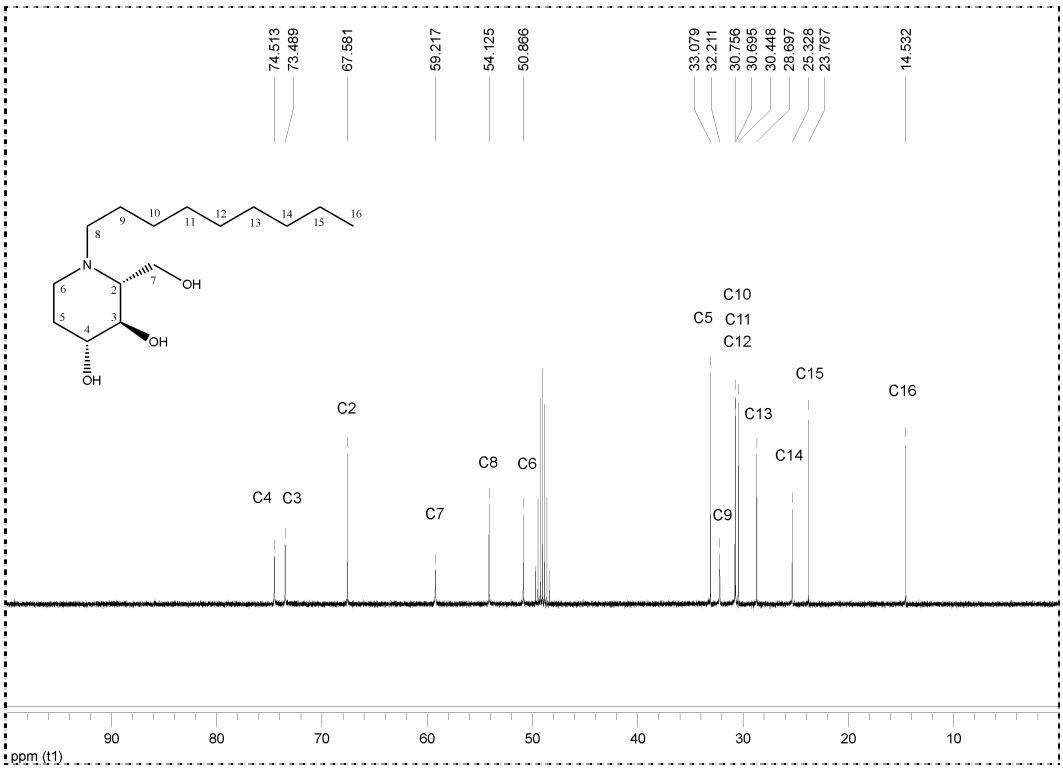

^{1}H-NMR spectrum (CD_3OD) of *N*-dodecylfagomine **7e**:

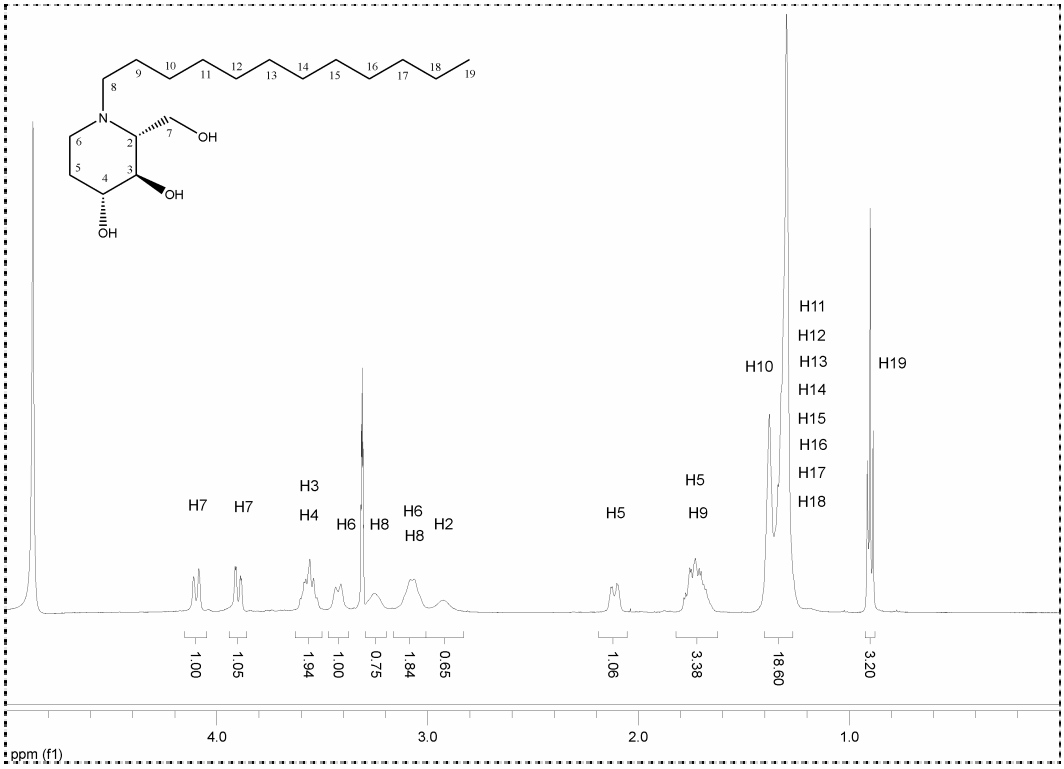

^{13}C-NMR spectrum (CD_3OD) of *N*-dodecylfagomine **7e**:

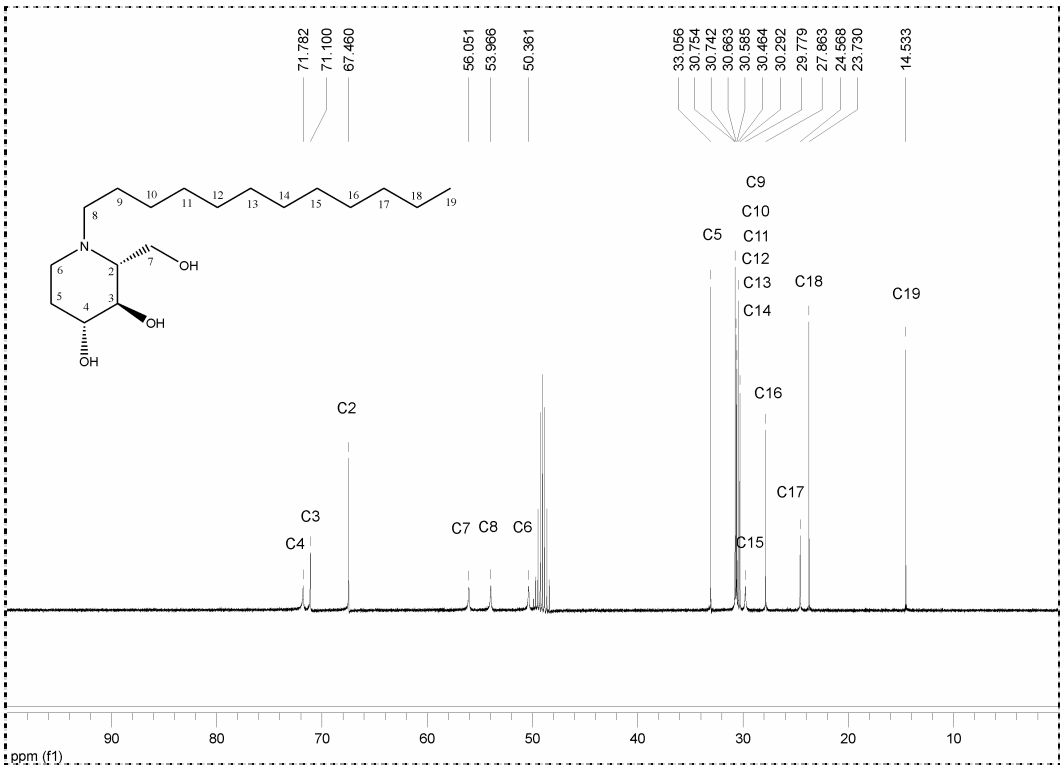

^{1}H-NMR spectrum (CD_3OD) of *N*-phenylethylfagomine **7f**:

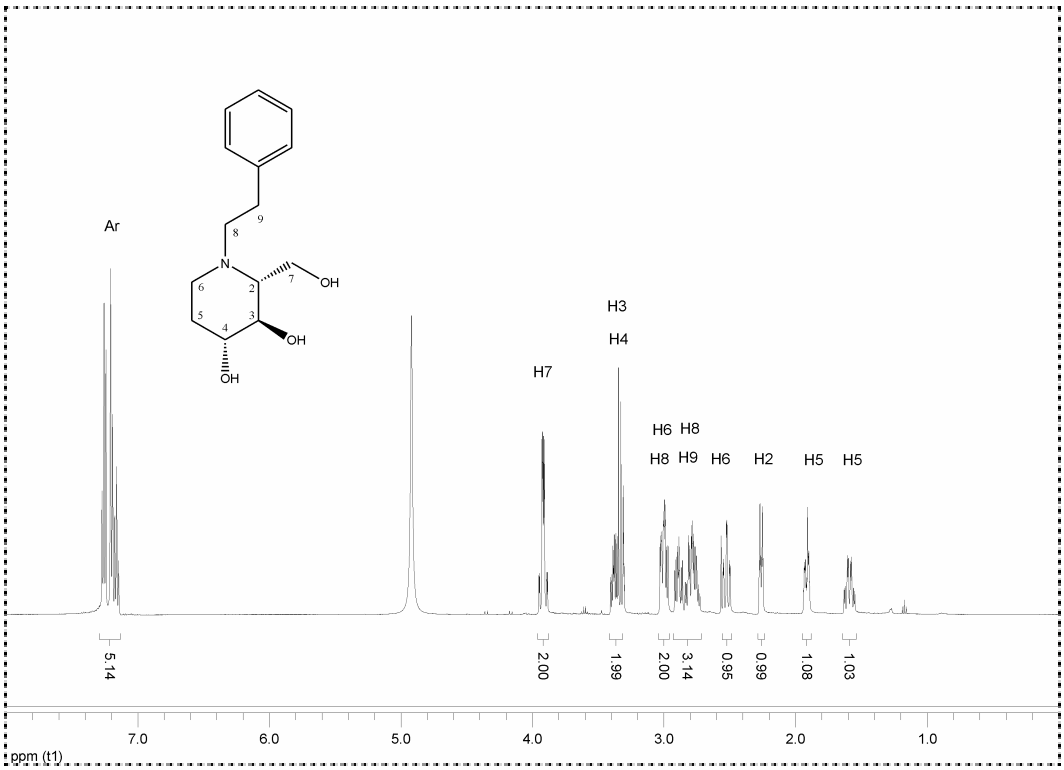

^{13}C-NMR spectrum (CD_3OD) of *N*-phenylethylfagomine **7f** :

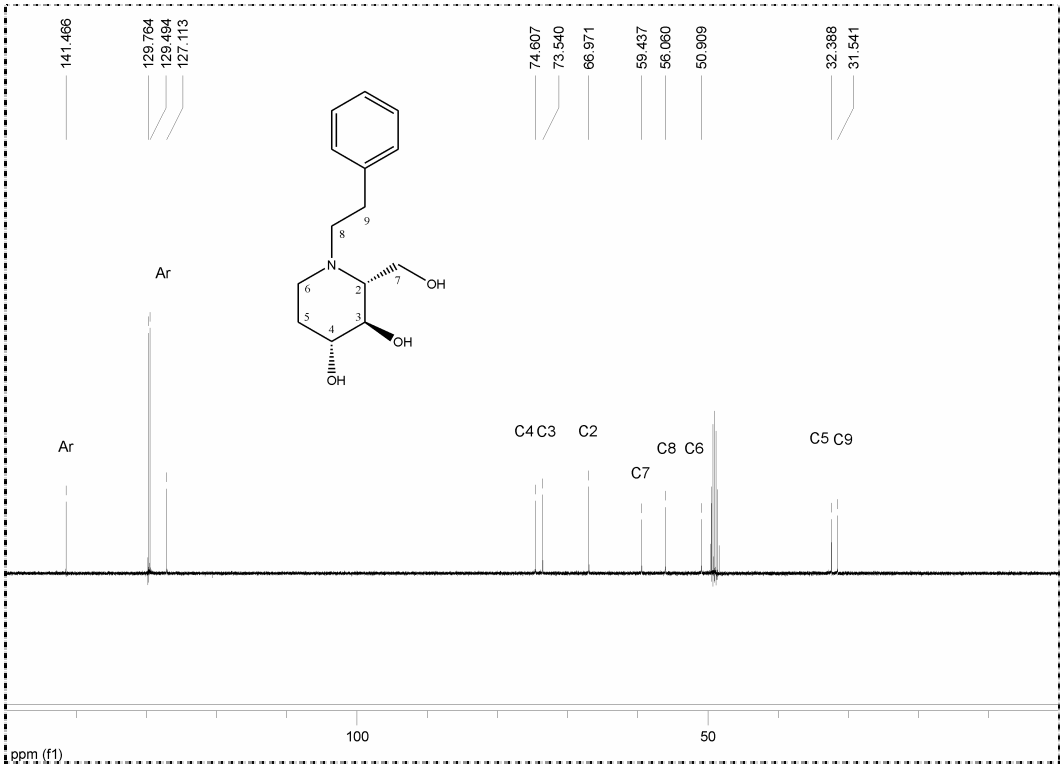

6.2. Publications:

6.2.1. Publication I:

Interaction of antimicrobial arginine-based cationic surfactants with liposomes and lipid monolayers.

José A. Castillo, Aurora Pinazo, Josep Carilla, M. Rosa Infante, M. Asunción Alsina, Isabel Haro, Pere Clapés.

Langmuir **2004**, *20,* 3379-3387.

Interaction of Antimicrobial Arginine-Based Cationic Surfactants with Liposomes and Lipid Monolayers

José A. Castillo,† Aurora Pinazo,† Josep Carilla,† M. Rosa Infante,† M. Asunción Alsina,‡ Isabel Haro,*,† and Pere Clapés*,†

Institute for Chemical and Environmental Research CSIC, Jordi Girona 18-26, 08034 Barcelona, Spain, and Unidad Asociada CSIC "Péptidos y Proteínas: Estudios Fisicoquímicos", Department of Physical Chemistry, Faculty of Pharmacy, University of Barcelona, Avgda. Joan XXIII s/n, 08028 Barcelona, Spain

Received December 24, 2003. In Final Form: February 2, 2004

The present work examines the relationship between the antimicrobial activity of novel arginine-based cationic surfactants and the physicochemical process involved in the perturbation of the cell membrane. To this end, the interaction of these surfactants with two biomembrane models, namely, 1,2-dipalmitoyl-*sn*-glycero-3-phosphocholine (DPPC) multilamellar lipid vesicles (MLVs) and monolayers of DPPC, 1,2-dipalmitoyl-*sn*-glycero-3-[phospho-*rac*-(1-glycerol)] sodium salt (DPPG), and *Escherichia coli* total lipid extract, was investigated. For the sake of comparison, this study included two commercial antimicrobial agents, hexadecyltrimethylammonium bromide and chlorhexidine dihydrochloride. Changes in the thermotropic phase transition parameters of DPPC MLVs in the presence of the compounds were studied by differential scanning calorimetry analysis. The results show that variations in both the transition temperature (T_m) and the transition width at half-height of the heat absorption peak ($\Delta T_{1/2}$) were consistent with the antimicrobial activity of the compounds. Penetration kinetics and compression isotherm studies performed with DPPC, DPPG, and *E. coli* total lipid extract monolayers indicated that both steric hindrance effects and electrostatic forces explained the antimicrobial agent−lipid interaction. Overall, in DPPC monolayers single-chain surfactants had the highest penetration capacity, whereas gemini surfactants were the most active in DPPG systems. The compression isotherms showed an expansion of the monolayers compared with that of pure lipids, indicating an insertion of the compounds into the lipid molecules. Owing to their cationic character, they are incorporated better into the negatively charged DPPG than into zwitterionic DPPC lipid monolayers.

Introduction

Bio-based surfactants are synthetic amphipathic structures based on natural structures of glycolipids, lipopeptides, phospholipids, and fatty acids. Among them, lipoamino acids and glycolipids have become increasingly important because of their chemical simplicity, surface activity, aggregation properties, broad biological activity, and low toxicity profile.[1,2] They meet four crucial requirements for the industrial development of new surfactants: low toxicity, high biodegradability, multifunctionality, and use of renewal sources of raw materials for their synthesis.

Lipoamino acids derived from arginine are a recently described family of nontoxic and biodegradable cationic surfactants with antimicrobial properties.[3−6] They are particularly interesting as preservatives for food and pharmaceutical formulations as well as active ingredients in dermatology and personal care products. Arginine-based surfactants constitute a promising alternative to other antimicrobial surfactants with high intrinsic toxicity and questioned biodegradability such as quaternary ammonium halides.[2,6,7]

The antimicrobial action of cationic surfactants is based on their ability to disrupt the integral bacterial membrane by a combined hydrophobic and electrostatic adsorption phenomenon at the membrane/water interface followed by membrane disorganization.[8] The pathogenic bacterial cell membrane is predominantly negatively charged as compared with eukaryotic cells.[9] Hence, the positive charge of the cationic amphiphiles facilitates their interaction with the bacterial membrane. In particular, the antimicrobial activity of the arginine-based cationic surfactants is directly associated with the presence of the cationic charge of the protonated guanidine group of this amino acid.[10]

Since the perturbation of the cell membrane by these compounds is directed primarily by physicochemical processes, model membrane systems can provide valuable information for understanding the mechanism of action of these molecules.[11−16] The ultimate goal is to provide the

† Institute for Chemical and Environmental Research CSIC.
‡ University of Barcelona.

(1) Infante, M. R.; Pinazo, A.; Seguer, J. *Colloids Surf., A* **1997**, *123−124*, 49−70.
(2) Clapés, P.; Infante, M. R. *Biocatal. Biotransform.* **2002**, *20*, 215−233.
(3) Infante, M. R.; Pinazo, A.; Molinero, J.; Seguer, J.; Vinardell, P. Arginine lipopeptide surfactants with antimicrobial activity. In *Protein-Based Surfactants*; Marcel Dekker: New York, 2001; Vol. 101, pp 147−167.
(4) Pérez, L.; García, M. T.; Ribosa, I.; Vinardell, M. P.; Manresa, A.; Infante, M. R. *Environ. Toxicol. Chem.* **2002**, *21*, 1279−1285.
(5) Pérez, L.; Torres, J. L.; Manresa, A.; Solans, C.; Infante, M. R. *Langmuir* **1996**, *12*, 5296−5301.
(6) Piera, E.; Infante, M. R.; Clapés, P. *Biotechnol. Bioeng.* **2000**, *70*, 323−331.
(7) Pinazo, A.; Wen, X.; Pérez, L.; Infante, M. R.; Franses, E. I. *Langmuir* **1999**, *15*, 3134−3142.
(8) McDonnell, G.; Russell, A. D. *Clin. Microbiol. Rev.* **1999**, *12*, 147−179.
(9) Oren, Z.; Hong, J.; Shai, Y. *J. Biol. Chem.* **1997**, *272*, 14643−14649.
(10) Infante, M. R.; García-Domínguez, J. J.; Erra, P.; Julia, M. R.; Prats, M. *Int. J. Cosmet. Sci.* **1984**, *6*, 275−282.
(11) Sospedra, P.; Espina, M.; Alsina, M. A.; Haro, I.; Mestres, C. *J. Colloid Interface Sci.* **2001**, *244*, 79−86.
(12) Maget-Dana, R. *Biochim. Biophys. Acta*: *Biomembranes* **1999**, *1462*, 109−140.
(13) Prenner, E. J.; Lewis, R. N. A. H.; McElhaney, R. N. *Biochim. Biophys. Acta*: *Biomembranes* **1999**, *1462*, 201−221.

10.1021/la036452h CCC: $27.50
Published on Web 03/13/2004

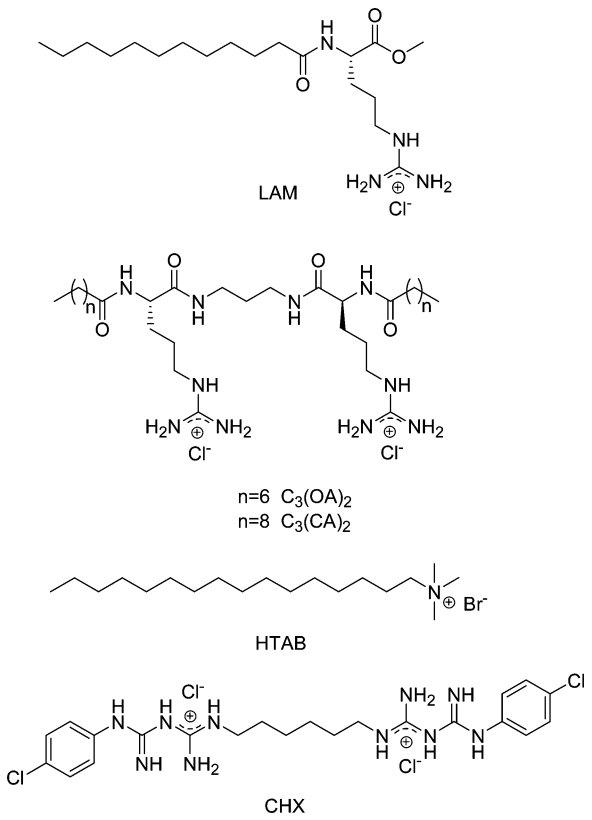

Figure 1. Structures of the selected antimicrobial compounds.

basis for a rational design of new and improved antimicrobials based on the physicochemical properties of the molecule.

In this work, we endeavored to gain insight into putative correlations between the antimicrobial activity of the arginine-based cationic surfactants (Figure 1) and their physicochemical interaction with model membranes. To this end, the antimicrobial activity of these compounds against Gram-positive and Gram-negative bacteria was determined first. Second, the physicochemical interaction of these arginine amphiphiles with multilamellar vesicles (MLVs) and monolayers of different lipid composition as biomembrane models was studied. The results were compared with those obtained with commercial antimicrobial agents such as hexadecyltrimethylamonium bromide (HTAB) and chlorhexidine dihydrochloride (CHX)[17] (Figure 1).

Experimental Procedures

Chemicals. 1,2-Dipalmitoyl-*sn*-glycero-3-phosphocholine (DPPC) and *Escherichia coli* total lipid extract (i.e., 58% of 1,2-diacyl-*sn*-glycero-3-phosphoethanolamine (DPPE), 15% of 1,2-dipalmitoyl-*sn*-glycero-3-[phospho-*rac*-(1-glycerol)] sodium salt (DPPG), 10% of cardiolipin, and 17% of other compounds) were purchased from Avanti Polar Lipids Inc. DPPG, HTAB, and CHX were purchased from Sigma. N^{α}-Lauroyl-L-arginine methyl ester monohydrochloride (LAM), bis(N^{α}-octanoyl-L-arginine)-1,3-propanediamide dihydrochloride ($C_3(OA)_2$), and bis(N^{α}-caproyl-L-arginine)-1,3-propanediamide dihydrochloride ($C_3(CA)_2$) were synthesized in our laboratory by a previously published methodology.[2,6,18,19] Solvents and reagents used were of analytical grade. Ultrapure water, produced by a Nanopure purification system coupled to a Milli-Q water purification system, resistivity = 18.2 MΩ cm, was used for the aqueous solutions.

Antimicrobial Activity. The antimicrobial activities of LAM, $C_3(OA)_2$, $C_3(CA)_2$, HTAB, and CHX (Figure 1) were determined in vitro as the minimum inhibitory concentration (MIC) values. MIC is defined as the lowest concentration of antimicrobial agent that inhibits the development of visible microorganism growth after 24 h of incubation at 37 °C.[20] The microorganisms used (15 bacteria and 1 yeast) were the following. Gram-negative bacteria: *Bordetella bronchiseptica* ATCC 4617, *Citrobacter freundii* ATCC13883, *Enterobacter aerogenes* ATCC 13048, *Salmonella typhimurium* ATCC 14028, *Streptococcus faecalis* ATCC 10541, *Escherichia coli* ATCC 27325, *Klebsiella pneumoniae* ATCC 13882, *Pseudomonas aeruginosa* ATCC 9721, *Arthrobacter oxydans* ATCC 14358. Gram-positive bacteria: *Bacillus cereus var. mycoides* ATCC 11778, *Bacillus subtilis* ATCC 6633, *Staphylococcus aureus* ATCC 25178, *Micrococcus epidermidis* ATCC 155-U, *Micrococcus luteus* ATCC 10054, *Mycobacterium phlei ATCC* 10142. Yeast: *Candida albicans* ATCC 10231.

Preparation of MLVs of DPPC. MLVs of DPPC were prepared as follows. A standard solution of DPPC (4.4 mg mL^{-1}) in $CHCl_3$/MeOH 1/1 v/v was prepared and aliquoted (100 μL) in test tubes. Then, the solvent was removed under a nitrogen stream while rotating the tube to form a thin film of lipid on the tube walls. The residual solvent was removed under a vacuum. MLVs were obtained by hydrating the lipid film with 4-(2-hydroxyethyl)piperazine-1-ethanesulfonic acid (HEPES) buffer 5 mM, pH 7.4 (100 μL), containing the corresponding amount of surfactant, followed by five alternative cycles of sonication (2 min) and heating at 60 °C (2 min).

Differential Scanning Calorimetry (DSC). Thermotropic phase transition parameters of MLVs of DPPC were measured by a DSC 821E Mettler Toledo calorimeter. Hermetically sealed aluminum pans (40 μL nominal volume) were used. DSC runs were carried out with fresh liposome preparations. Pans were loaded with DPPC MLV suspension (30 μL, corresponding to 0.13 mg of DPPC) and submitted to three heating/cooling cycles in a temperature range between 0 and 60 °C at a scanning rate of 5 °C min^{-1}. The data from the first scan were always discarded to avoid mixing artifacts. Experiments were carried out in triplicate.

Surface Activity. Surface activity measurements of LAM, $C_3(OA)_2$, $C_3(CA)_2$, HTAB, and CHX were recorded at 21 ± 1 °C by using a Langmuir film balance Nima 516 equipped with a circular Teflon trough (60.35 cm^2 and 70 mL of capacity) equipped with a Wilhelmy plate, made from chromatography paper (Whatman Chr 1) as the pressure sensor. Increasing volumes of an aqueous concentrate solution of surfactants in phosphate-buffered saline (PBS), pH 7.4, were injected beneath the air/water surface, and the pressure increases were recorded during a period of 60 min. For each compound, the saturation concentration (i.e., the minimum concentration that gives the maximum surface pressure) was determined. Dimethyl sulfoxide (DMSO) was used to prepare the concentrated solution of CHX, due to its low aqueous solubility. It has been reported that DMSO does not interfere with the surface activity measurements.[21] Surface pressure was measured with the accuracy of ±0.1 mN m^{-1}.

Penetration Kinetics at Constant Area. The interactions of LAM, $C_3(OA)_2$, $C_3(CA)_2$, HTAB, and CHX with lipid monolayers were determined with the same device described for the surface activity measurements. Lipid monolayers of DPPC, DPPG, and *E. coli* total lipid extract were spread on PBS subphases from $CHCl_3$/MeOH 2/1 v/v solutions, at the required initial pressure: 5, 10, 20, and 32 mN m^{-1}. Then, the appropriate amount of the

(14) Lohner, K.; Prenner, E. J. *Biochim. Biophys. Acta*: *Biomembranes* **1999**, *1462*, 141−156.
(15) Pignatello, R.; Toth, I.; Puglisi, G. *Thermochim. Acta* **2001**, *380*, 255−264.
(16) Pare, C.; Lafleur, M.; Liu, F.; Lewis, R. N. A. H.; McElhaney, R. N. *Biochim. Biophys. Acta*: *Biomembranes* **2001**, *1511*, 60−73.
(17) Kabara, J. J. *Cosmetic and Drug Preservation*: *Principles and Practice*; Marcel Dekker: New York, 1984.
(18) Infante, M. R.; García-Domínguez, J.; Erra, P.; Julia, R.; Prats, M. *Int. J. Cosmet. Sci.* **1984**, *6*, 275−282.
(19) Infante, M. R.; Pérez, L.; Pinazo, A.; Clapés, P.; Moran, C. Amino acid-based surfactants. In *Novel Surfactants. Preparation, Application and Biodegradability*; Holmberg, K., Ed.; Marcel Dekker, Inc.: New York, 2003; pp 193−216.
(20) Pérez, L.; Pinazo, A.; Vinardell, M. P.; Clapés, P.; Angelet, M.; Infante, M. R. *New J. Chem.* **2002**, *26*, 1221−1227.
(21) Sospedra, P.; Haro, I.; Alsina, M. A.; Reig, F.; Mestres, C. *Mater. Sci. Eng. C* **1999**, *8*−*9*, 543−549.

Table 1. Minimum Inhibitory Concentration in μg mL^{-1} of the Selected Antimicrobial Compounds

microorganism	HTAB	$C_3(OA)_2$	LAM	$C_3(CA)_2$	CHX
Gram-Negative					
1. *Citrobacter freundii*	64	64	256	32	1
2. *Bordetella bronchiseptica*	4	8	256	4	1
3. *Pseudomonas aeruginosa*	>256	256	64	32	8
4. *Salmonella typhimurium*	128	32	32	16	2
5. *Enterobacter aerogenes*	128	32	nd	16	8
6. *Arthrobacter oxydans*	2	32	64	16	1
7. *Streptococcus faecalis*	256	128	32	8	8
8. *Escherichia coli*	32	16	32	8	2
9. *Klebsiella pneumoniae*	256	8	128	8	8
Gram-Positive					
10. *Bacillus cereus*	>256	256	64	32	8
11. *Staphylococcus epidermidis*	>256	256	64	32	4
12. *Bacillus subtlis*	64	16	256	16	4
13. *Staphylococcus aureus*	2	16	64	2	0.5
14. *Micrococcus luteus*	1	8	256	4	1
15. *Microbacterium phlei*	256	256	nd	16	8
Yeast					
16. *Candida albicans*	1	8	64	2	0.5

stock solution of each product was injected in the subphase. The final concentration of each compound was fixed according to its surface pressure curve (i.e., approximately 80% of the saturation concentration). The pressure increases were recorded at 21 ± 1 °C for 30 min, to ensure that the equilibrium was reached. The subphase was stirred continuously to ensure a homogeneous distribution. The experiments were performed in triplicate and the standard error was estimated in each case.

Compression Isotherms. Compression isotherms were performed at 21 ± 1 °C using a Langmuir film balance Nima 516 equipped with a rectangular Teflon trough (19.5 × 20 cm^2 and 250 mL of capacity). Fixed amounts of DPPC, DPPG, and *E. coli* lipid extract (50 μL solution of 1 mg phospholipids/mL in $CHCl_3$/MeOH 2/1 v/v, approximately 4 × 10^{16} lipid molecules) were spread on the aqueous subphase containing the product under study at three different concentrations: 80%, 20%, and 5% of the saturation concentration. Then, the solvent was allowed to evaporate for at least 10 min. Films were compressed continuously with an area reduction rate of 12.9 Å^2 molecule^{-1} min^{-1}. The experiments were performed in triplicate, and the reproducibility was ±1 Å^2 mol^{-1}.

Results and Discussion

Antimicrobial Activity. The MIC values of LAM, $C_3(CA)_2$, $C_3(OA)_2$, HTAB, and CHX for 15 selected Gram-positive and Gram-negative bacteria and one yeast are summarized in Table 1. The lower the MIC values, the higher the antimicrobial activity. A cursory inspection of Table 1 shows that the MIC values for each compound depended exclusively on the bacterium but not on the nature of the outer membrane (i.e., Gram-positive or Gram-negative). The cell envelope of Gram-negative bacteria is more complex than that of Gram-positive bacteria, but the presence of large amounts of negatively charged phospholipids and phosphatidylethanolamine (PE) is a common feature.[14] The antimicrobial activity increased in the order of HTAB < $C_3(OA)_2$ < LAM < $C_3(CA)_2$ < CHX. Remarkably, the arginine-based surfactants possessed lower MIC values than those of the commercial HTAB, for most of the microorganisms assayed. In previous studies,[22,23] it has been shown that the optimum biological effect of single-chain arginine-based surfactants was obtained with hydrocarbon alkyl moieties of 10 methylene groups (i.e., LAM). Pérez et al.[4] have reported

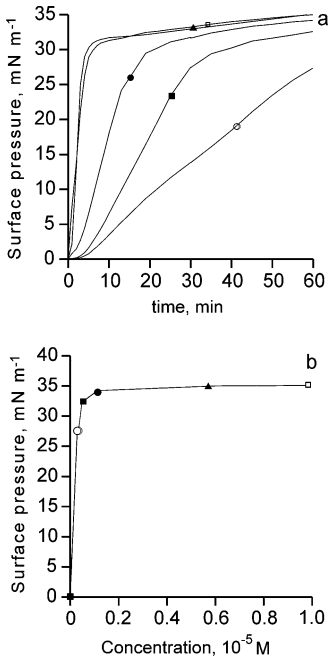

Figure 2. (a) Surface activity of $C_3(CA)_2$ as a function of time at different concentrations: 1 × 10^{-5} M (□), 5.7 × 10^{-6} M (▲), 1.1 × 10^{-6} M (●), 5.7 × 10^{-7} M (■), and 2.9 × 10^{-7} M (○). (b) Surface pressure increases as a function of $C_3(CA)_2$ concentration.

that the minimum MIC values of the arginine-based geminal surfactants were obtained with the $C_n(CA)_2$ homologues. In this work, $C_3(CA)_2$ was the most active and for some microorganisms similar to CHX. The results suggest that both the length of acyl chains and the positive charges, which determine the hydrophilic−lipophilic balance (HLB) of the molecule, are responsible for their membrane-disrupting properties.

To gain insight into the physicochemical factors that determine the antimicrobial activity of LAM, $C_3(CA)_2$, $C_3(OA)_2$, HTAB, and CHX, their interaction with model lipid-membrane systems was investigated. In the next sections, the physicochemical effects of these compounds on both MLVs and lipid monolayers are described in detail.

Surface Activity. The surface activity or accumulation at the air/water interface of the selected compounds was studied. To this end, different volumes of concentrated solutions of LAM, $C_3(CA)_2$, $C_3(OA)_2$, HTAB, and CHX were injected into the PBS subphase and the pressure increases were recorded as a function of time. When the amount of the tested compounds was increased, the surface pressure increased up to a saturation surface pressure. Figure 2a is an example of the pressure curves obtained for different concentrations of $C_3(CA)_2$. Here, at the lowest concentration assayed the maximum surface pressure was not achieved even after 60 min due to its aqueous solubility. From these plots, the curves of the surface pressure as a function of the product concentration were obtained (see Figure 2b as an example).

Surface pressure at the saturation point for the compounds under study is summarized in Table 2. The results obtained may be explained considering the number of methylene groups in the hydrophobic side chains in relation with the polar head. HTAB, with an aliphatic chain of 14 methylene groups, gave a surface pressure higher than that of LAM with 10. Similarly, the two side chains attached to the central unity of $C_3(CA)_2$ account for a total of 16 methylene units, thus explaining the remarkable surface activity of this compound. Compared

(22) Morán, C.; Clapés, P.; Comelles, F.; García, T.; Pérez, L.; Vinardell, P.; Mitjans, M.; Infante, M. R. *Langmuir* **2001**, *17*, 5071−5075.

(23) Infante, M. R.; Pinazo, A.; Seguer, J. *J. Colloids Surf. A* **1997**, 49−70.

Table 2. Surface Pressure at Saturation Concentration and at ca. 80% Saturation Concentration and the cmc for Each Antimicrobial Compound

compound	saturation concn/ 10^{-5} M	surface pressure/ mN m^{-1}	80% saturation concn/10^{-5} M	surface pressure[a]/ mN m^{-1}	cmc[b]/ 10^{-4} M
LAM	4.5	29.3	3.6	22.4	60.0[c]
$C_3(OA)_2$	11.0	19.7	3.4	15.5	7.0[d]
$C_3(CA)_2$	0.6	34.2	0.1	24.3	0.3[d]
HTAB	4.1	31.9	3.7	27.2	10.0[e]
CHX	17.0	18.0	4.0	16.8	100.0[f]

[a] Approximate values corresponding to 80% saturation concentration. [b] At 25 °C. [c] Reference 7. [d] Reference 45. [e] Reference 46. [f] Reference 47.

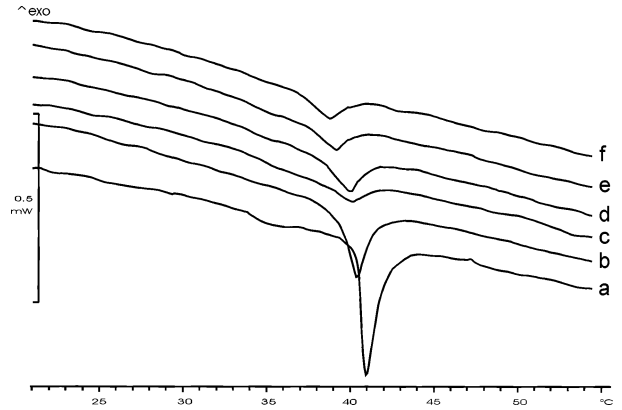

Figure 3. DSC curves obtained with DPPC−$C_3(CA)_2$ systems. The molar percentages of $C_3(CA)_2$ were (a) 0% (i.e., pure DPPC), (b) 1%, (c) 2%, (d) 3%, (e) 4%, and (f) 5%. The heating rate was 5 °C/min.

to $C_3(CA)_2$, the lower ability of $C_3(OA)_2$ to accumulate at the air−water interface may be related to its shorter side chains, as noted, for instance, in the 90 Å reduction in the van der Waals surface of the aliphatic side chain in $C_3(OA)_2$ relative to $C_3(CA)_2$.[24] Finally, CHX showed low capacity to diminish surface tension, as expected from the inclusion of a chlorobenzene unit instead of a long aliphatic side chain. The lipophilicity (octanol/water partition coefficient (log *P*)) of the side chain in $C_3(OA)_2$, which was estimated[25] to be around 3.5, is close to the lipophilicity of the side chain of CHX (i.e., chlorobenzene) (log $P = 2.8$), explaining their similar surface activity.

The surface activity data provided information on the suitable concentration of each compound that should be used in the bulk subphase for the experiments on the interaction with phospholipid monolayers (i.e., penetration kinetics and compression isotherms). This optimal concentration was the one that gave ca. 80% of the maximum surface pressure (80% saturation concentration). Under these conditions, both the saturation of the product in the trough and the formation of domains were avoided.[26] The optimal concentrations for each product, calculated from pressure/concentration curves, fell well below their respective critical micelle concentrations (cmc's) (Table 2).

Lipid Multilamellar Vesicles as a Membrane Model: DSC Studies. Analysis of MLVs of lipids with bulky polar heads (i.e., DPPC) by DSC is characterized by two-phase transitions (Figure 3, curve a): first, a pretransition around 35 °C related to the alkyl chain tilt, and second, the main transition around 41 °C between an ordered gel state ($L_{\beta'}$ phase) and a disordered liquid-crystalline state (L_α phase).[27−29]

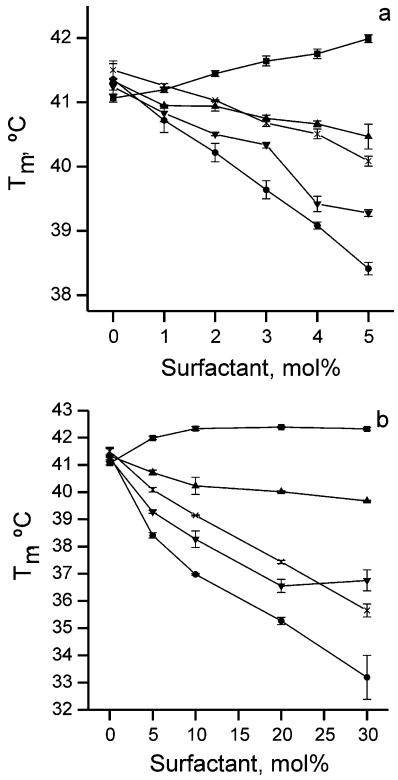

Figure 4. The phase transition temperature (T_m) of DPPC MLV liposomes as a function of the molar percentage of antimicrobial compound, in a concentration range (a) between 0 and 5 mol % and (b) between 0 and 30 mol %: LAM (×), $C_3(OA)_2$ (▲), $C_3(CA)_2$ (▼), HTAB (■), and CHX (●).

The study of the main thermotropic phase transition of MLVs by DSC represents a simple and precise method to investigate the influence of bioactive products on lipid membranes. The structural change associated with this transition is the trans−gauche isomerization of the acyl chains of the lipid molecules. The average number of gauche conformers is related to the bilayer fluidity.[27] The presence of compounds susceptible to interacting with the phospholipid molecules may cause perturbations, which can contribute to disturb the fluidity of the membrane. Two parameters related with the phase transition were studied: first, the phase transition temperature (T_m), which corresponds to the gel to liquid-crystalline transition; second, the width at half-height of the heat absorption peak ($\Delta T_{1/2}$), which is a measure of the cooperativity of this phase transition process.

The effect of the compounds on the main thermotropic phase transition parameters of zwitterionic DPPC MLVs was investigated with mixtures containing 0, 1, 2, 3, 4, 5, 10, 20, and 30 mol % of the assayed compound. As an example, in Figure 3 curves b−f depict the DSC transition profiles of DPPC MLVs in the presence of different mol % of $C_3(CA)_2$. The addition of the product always caused the complete disappearance of the pretransition.

From the DSC curves thus obtained, the T_m (Figure 4a,b) and $\Delta T_{1/2}$ (Figure 5a,b) were plotted against the mol % of each product. As seen in Figure 4a,b, the higher the concentration of the product in the MLV preparation, the lower the T_m values observed, except for HTAB. The

(24) Floris, F. M.; Tomasi, J.; Pascual-Ahuir, J. L. *J. Comput. Chem.* **1991**, *12*, 784.
(25) Leo, X. A.; Hansch, C.; Elkins, D. *Chem. Rev.* **1971**, *71*, 525.
(26) McConlogue, C. W.; Vanderlick, T. K. *Langmuir* **1998**, *14*, 4.
(27) Lo, Y.-L.; Rahman, Y.-E. *J. Pharm. Sci.* **1995**, *804*, 805−814.
(28) Pedersen, T. B.; Sabra, M. C.; Frokjaer, S.; Mouritsen, O. G.; Jorgensen, K. *Chem. Phys. Lipids* **2001**, *113*, 83−95.
(29) Ramaswami, V.; Haaseth, R. C.; Matsunaga, T. O.; Hruby, V. J.; O'Brien, D. F. *Biochim. Biophys. Acta*: *Biomembranes* **1992**, *1109*, 195−202.

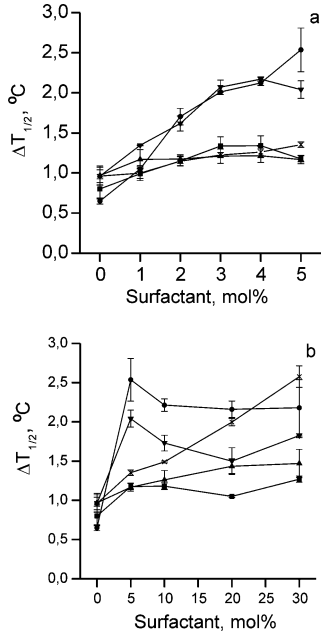

Figure 5. The transition width ($\Delta T_{1/2}$) of DPPC MLV liposomes as a function of the molar percentage of antimicrobial compound in a concentration range (a) between 0 and 5 mol % and (b) between 0 and 30 mol %: LAM (×), $C_3(OA)_2$ (▲), $C_3(CA)_2$ (▼), HTAB (■), and CHX (●).

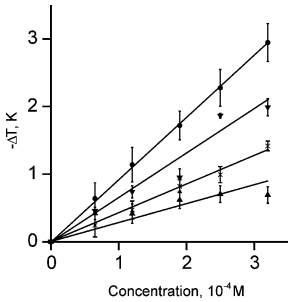

Figure 6. The depression of the transition temperature $\Delta T = T_m - T_{m,0}$ of DPPC MLV liposomes as a function of the molarity of the antimicrobial compound. Solid lines correspond to eq 1 fitted to the experimental data for the compounds LAM (×), $C_3(OA)_2$ (▲), $C_3(CA)_2$ (▼), and CHX (●).

decrease of T_m is lineal for a product concentration ranging from 0 to 5 mol %. In this concentration range, it was possible to estimate the partition coefficient (K) of the compound between the bulk solution and the lipid membrane, using eq 1:[30]

$$-\Delta T = \frac{R T_{m,0}^{\,2}}{\Delta H} \frac{K}{55.5 + C_L K} C_A^0 \qquad (1)$$

where $T_{m,0} = 314$ K (i.e., T_m of pure DPPC MLVs) and $\Delta H = 36.4$ kJ mol^{-1} corresponds to the values of the pure lipid and C_L and C_A^0 are the total concentration of the lipid and product in mol %, respectively. The partition coefficient K also reflects the interaction of the compound with the lipid molecules. The $-\Delta T = T_m - T_{m,0}$ values were plotted against the molar concentration of the compound in a range between 0 and 3×10^{-4} M (i.e., 0−5 mol %) (Figure 6). From the slope of the straight lines thus obtained, the K values were calculated and listed in Table 3. The results indicate that the partition of the compounds

Table 3. Partition Coefficient (K) of the Selected Compounds between the Bulk Solution and the DPPC MLVs Calculated from the Slopes of the Linear Regressions of Figure 5

compound	K	compound	K
LAM	10.8 ± 0.9	$C_3(CA)_2$	15.8 ± 1.2
$C_3(OA)_2$	5.1 ± 1.0	CHX	22.5 ± 1.8

into the lipid membrane increased in the order $C_3(OA)_2$ < LAM < $C_3(CA)_2$ < CHX which was consistent with the observed antimicrobial activity.

A different situation was observed for HTAB. Here, T_m increased (or $-\Delta T$ decreased) in a concentration range between 0 and 5 mol %, whereas at higher concentration T_m was constant. This result may be explained considering the effect of *n*-alkanes, alcohols, fatty acids, and tertiary alkylammonium salts on phospholipid phase transition behavior.[31−33] Compounds with hydrocarbon chain lengths of ≤10 intercalate into the hydrophobic core of the lipid bilayer, causing a void near the acyl hydrocarbon core. This void increases the ratio of trans to gauche conformers, diminishing the stability of the lamellar gel phase and, therefore, decreasing T_m. On the other hand, the longer the alkyl chain (>12 carbons) of the compound, the smaller the void formed, causing less disruption of the packing of the phospholipid acyl chains. This increases the van der Waals interactions and therefore produces a small increase of T_m.[29,34] The behavior of HTAB followed this latter trend, whereas the rest of the compounds under study performed as the shorter hydrocarbon alkyl chains.

The transition width at half-height of the heat absorption peak ($\Delta T_{1/2}$) is a measure of the cooperativity of the lipid molecules during the gel to liquid-crystalline transition. The broadening of the endothermic peak indicates that the compounds incorporated into the DPPC MLVs, disrupting the correlation between lipidic molecules in the phase transition (i.e., cooperativity).[35] Both $C_3(CA)_2$ and CHX increased $\Delta T_{1/2}$ in the concentration range studied, whereas LAM had a small effect up to 5 mol % but increased linearly between 5 and 30 mol % (Figure 5a,b).

To better correlate both T_m and the cooperativity, $\Delta T_{1/2}$ was plotted against the $-\Delta T$ values (Figure 7). HTAB was not considered here since this compound increased the T_m of the DPPC MLVs. The results may be fitted to a linear equation in accordance with a previous work.[30] Since $-\Delta T$ is directly proportional to the mole fraction of the compound in the lipid membrane, this plot reflects the extension of the perturbation of the lipid membrane by the product: the higher the slope of the straight line, the larger the perturbation of the MLVs. An inspection of the slopes for each compound, depicted in Figure 7, revealed that both CHX and $C_3(CA)_2$ caused the largest effect on the DPPC MLVs.

Considering that for most antimicrobial cationic-like compounds the mechanism of action is similar,[8] their activity on the lipid bilayer depended on the charge of the polar head and on both the structure and hydrophobicity of the lipophilic moiety: LAM has only one charged polar

(30) Inoue, T.; Miyakawa, K.; Shimozawa, R. *Chem. Phys. Lipids* **1986**, *42*, 261−270.

(31) Lohner, K. *Chem. Phys. Lipids* **1991**, *57*, 341−362.

(32) McIntosh, T. J.; Simon, S. A.; MacDonald, R. C. *Biochim. Biophys. Acta*: *Biomembranes* **1980**, *597*, 445−463.

(33) White, S. H.; King, G. I.; Cain, J. E. *Nature* **1981**, *290*, 161−163.

(34) To confirm these observations, dodecyltrimethylammonium bromide, bearing a shorter alkyl chain than that of HTAB, was also studied at concentrations ranging from 0 to 5 mol %. In this case, the DSC analyses showed a decrease of 0.3 °C mol %$^{-1}$ of the phase transition temperature suggesting the formation of voids in the hydrophobic core.

(35) Inoue, T.; Iwanaga, T.; Fukushima, K.; Shimozawa, R. *Chem. Phys. Lipids* **1988**, *46*, 25−30.

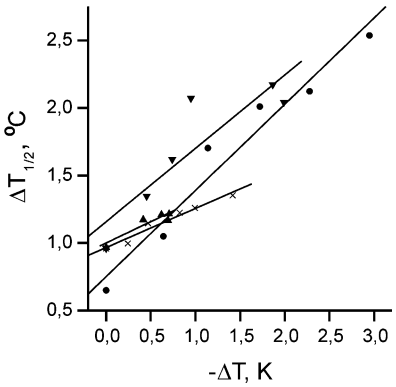

Figure 7. Correlation between the transition width ($\Delta T_{1/2}$) and the depression of the transition temperature $-\Delta T = T_m - T_{m,0}$ of DPPC MLVs in the presence of LAM (×), $C_3(OA)_2$ (▲), $C_3(CA)_2$ (▼), and CHX (●).

group, whereas $C_3(CA)_2$ has two polar groups per molecule and was more hydrophobic than $C_3(OA)_2$. As indicated above, the hydrophobicity of the side chain in $C_3(OA)_2$ was analogous to that of the CHX (log P = 2.8).[25] The differences observed between these two products stressed the importance of the structure of the lipophilic moiety in the antimicrobial activity.

The results obtained so far showed that neither the perturbation of the DPPC MLVs nor the antimicrobial activity correlate with either the cmc or the surface activity. Hence, the latter variables are not the only factors which determine the interaction of a compound with lipid membranes, in agreement with literature data.[36]

Lipid Monolayers as a Membrane Model: Kinetics of Penetration and Compression Isotherm Studies. As demonstrated thus far, lipid multilamellar vesicles are suitable membrane models for studying interactions of biologically active molecules with lipid membranes. However, they suffer from several limitations. For instance, the range over which the lipidic composition can be varied without modifying the surface curvature and phase state is limited. Besides, the degree of lipid packing is not uniform along the bilayer[12,37] and the physical state of compositionally identical bilayer dispersions depends on the method of preparation.[37] Moreover, some lipids may not form stable multilamellar vesicles suitable for DSC studies. Lipid monolayers can overcome these limitations, being considered as an excellent model system to study the interactions of active compounds with different lipid compositions at the air/water interface.

Penetration Kinetics at Constant Area. The interaction of LAM, $C_3(CA)_2$, $C_3(OA)_2$, HTAB, and CHX with monolayers of DPPC, DPPG, and *E. coli* total lipid extract was studied first by analyzing the penetration kinetics at constant area. We chose both zwitterionic DPPC and anionic DPPG phospholipids to compare the effect of the electrostatic interaction with the cationic compounds. Moreover, negatively charged phospholipids are the major components of bacterial membranes, whereas zwitterionic lipids are the major components of mammalian membranes.[9] *E. coli* total lipid extract was also investigated because it resembles a real biomembrane more closely than pure lipids. The concentration of each compound in the subphase was the corresponding value at ca. 80% saturation concentration (Table 2).

Figure 8a−c depicts the surface pressure increases ($\Delta\pi$) 30 min after injection of the compounds in the subphase

Table 4. Exclusion Density (σ_{ex}) of the Tested Compounds in DPPC, DPPG, and *E. coli* Total Lipid Extract Monolayers

compound	σ_{ex} DPPC/ molecules nm^{-2}	σ_{ex} DPPG/ molecules nm^{-2}	σ_{ex} *E. coli* extract/ molecules nm^{-2}
LAM	2.4 ± 0.2	3.0 ± 0.6	1.8 ± 0.1
$C_3(OA)_2$	2.3 ± 0.1	9.2 ± 0.5	1.8 ± 0.1
$C_3(CA)_2$	2.2 ± 0.1	4.5 ± 0.6	1.9 ± 0.1
HTAB	2.4 ± 0.1	2.9 ± 0.1	1.8 ± 0.2
CHX	2.6 ± 0.1	3.4 ± 0.2	2.1 ± 0.2

versus the initial lipid pressure (π_0) of 5, 10, 20, and 32 mN m^{-1} of DPPC, DPPG, and *E. coli* lipid extract monolayers. From these results, the exclusion density (σ_{ex}) was determined as previously described by Maget-Dana et al.[12] The plots of the pressure increases as a function of the initial densities of the lipids gave straight lines of negative slope. The intercept of these lines with the *X*-axis defines the monolayer σ_{ex}. This parameter indicates the lipid film density at which the compound no longer penetrates, and it is useful for comparing the relative penetration of a compound in various lipid monolayers. The calculated values of σ_{ex} for each antimicrobial compound are summarized in Table 4.

As a general trend (Figure 8a−c), the higher the initial monolayer pressure, the lower the pressure increase, because of the increasing packing density of the lipid molecules. Moreover, the σ_{ex} values (Table 4) show that the compounds incorporate better into the anionic DPPG monolayer than into zwitterionic DPPC.

For DPPC monolayers (Figure 8a), the pressure increases raised in the order $C_3(OA)_2 \approx$ CHX < $C_3(CA)_2$ < LAM < HTAB, indicating a low penetration capacity of gemini compounds. Here, it appears that the differences between gemini and single-chain structures arise mostly from steric hindrance.

In DPPG monolayers (Figure 8b), at π_0 of 5 and 10 mN m^{-1}, the highest pressure increases were observed for HTAB and $C_3(CA)_2$, whereas at π_0 = 32 mN m^{-1} $C_3(CA)_2$ and $C_3(OA)_2$ were the most active compounds. According to σ_{ex} (Table 4), the incorporation of the compounds into the DPPG monolayer was higher for the gemini compounds than for the single-chain surfactants. This reflects that electrostatic interactions are predominant over the steric effects between the DPPG and the surfactant. Both $C_3(CA)_2$ and $C_3(OA)_2$ have two positive charges per molecule against one of LAM and HTAB. CHX had lower interaction than arginine-based gemini surfactants, despite having also two positive charges. This may be due to the lack of the long lineal hydrophobic chains and therefore a different conformation may presumably be adopted at the air/water interface.

The penetration of the compounds in *E. coli* lipid extract monolayers at π_0 = 32 mN m^{-1} (Figure 8c) was between that found in DPPC and DPPG. The surface pressure increase at π_0 = 32 mN m^{-1} raised in the order $C_3(OA)_2$ < LAM < CHX < $C_3(CA)_2 \approx$ HTAB, but the differences between the most active antimicrobials CHX and $C_3(CA)_2$ were small. The σ_{ex} values (Table 4) indicated, however, that the incorporation of the products into this monolayer was lower than that with either DPPC or DPPG. Interestingly, the exclusion pressure[38] in the *E. coli* monolayer was ≥35 mN m^{-1} for all the tested compounds. Considering that the packing density of biological membranes[39,40] is

(36) Moncelli, M. R.; Becucci, L. *Bioelectrochem. Bioenerg.* **1996**, *39*, 227−234.

(37) Brockman, H. *Curr. Opin. Struct. Biol.* **1999**, *9*, 438−443.

(38) The exclusion pressure was calculated by plotting the pressure increases as a function of the initial pressure of the lipids and following the procedure used for the estimation of the exclusion density.

(39) Demel, R. A.; Peelen, T.; Sizen, R. J.; De Kruijff; Kuipers, O. P. *Eur. J. Biochem.* **1996**, *235*, 267−274.

(40) Marsh, D. *Biochim. Biophys. Acta* **1996**, *1286*, 183−223.

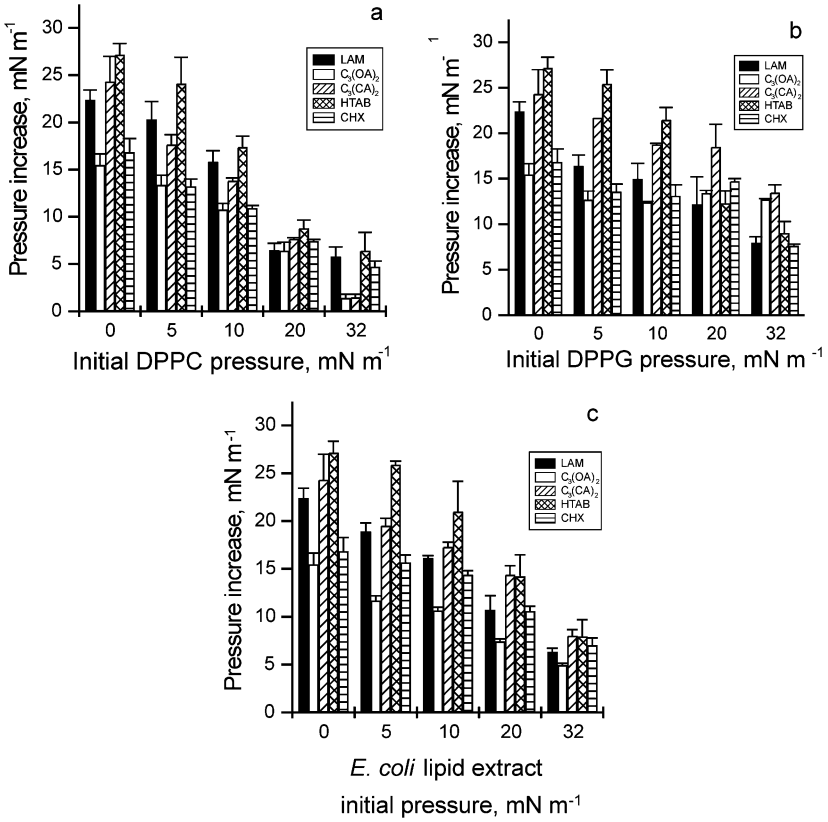

Figure 8. Pressure increases after LAM, $C_3(CA)_2$, HTAB, $C_3(OA)_2$, and CHX insertion into (a) DPPC, (b) DPPG, and (c) *E. coli* lipid extract monolayers as a function of the initial pressure.

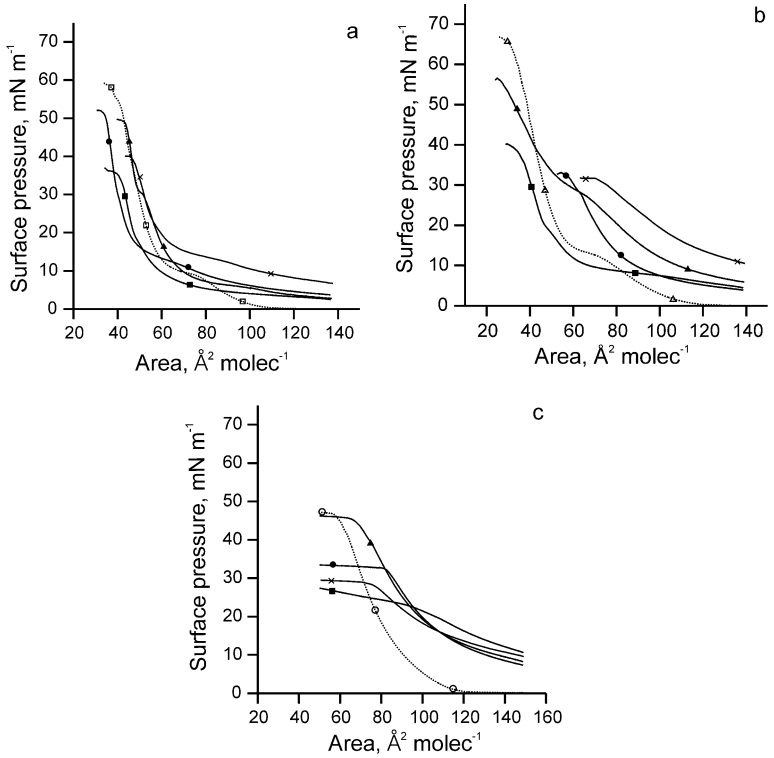

Figure 9. Compression isotherms of (a) DPPC (□), (b) DPPG (△), and (c) *E. coli* total lipid extract (○) monolayers (dotted lines) spread on subphases containing LAM (×), $C_3(OA)_2$ (▲), HTAB (■), and CHX (●) at ca. 80% saturation concentration (i.e., 4×10^{-5} M).

around 32 mN m^{-1}, the studied compounds may insert into biomembranes.

Compression Isotherms of Lipid Monolayers on Antimicrobial-Containing Subphases. The interaction of LAM, $C_3(CA)_2$, $C_3(OA)_2$, HTAB, and CHX with lipid monolayers was also investigated as the influence in the compression isotherms of DPPC, DPPG, and *E. coli* lipid extract. The isotherms taken from pure DPPC and DPPG (Figure 9a,b) showed the well-known phase transition from liquid-expanded (LE) to liquid-condensed (LC) phases

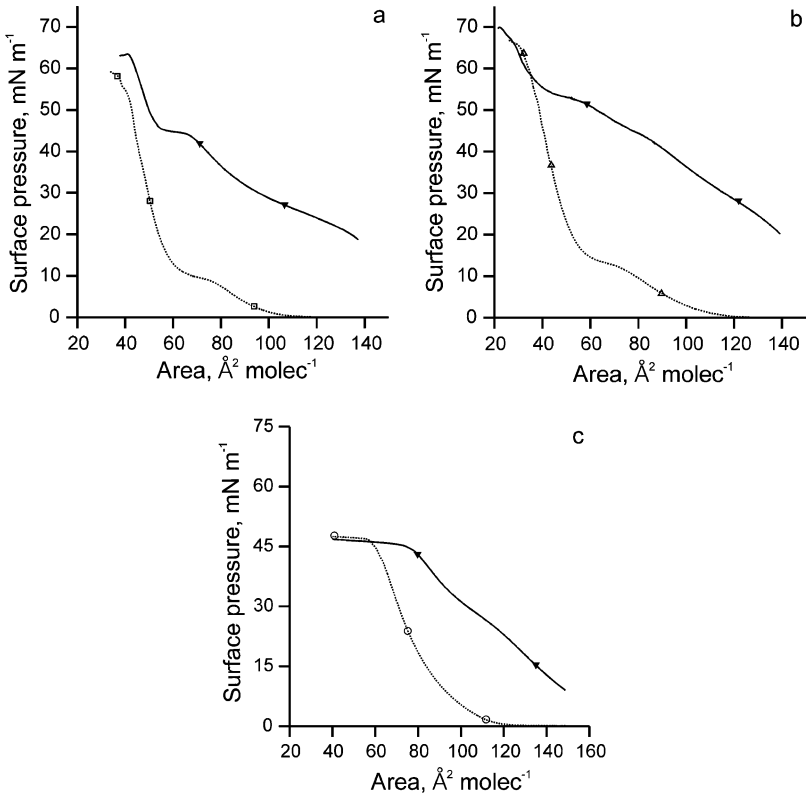

Figure 10. Compression isotherms of (a) DPPC (□), (b) DPPG (△), and (c) *E. coli* total lipid extract (○) monolayers (dotted lines) spread on subphases containing $C_3(CA)_2$ (▼) at ca. 80% saturation concentration (i.e., 10^{-6} M).

around 7 mN m^{-1} and 90 $Å^2$ mol^{-1} of molecular area.[41] The *E. coli* total lipid extract isotherm (Figure 9c) did not show the LE−LC transition, presumably because it was a mixture of three different phospholipids and contained 17% w/w of other unidentified compounds.

The shape of the compression isotherm shows the extent to which the compound is forced into the bulk subphase. If the products desorbed completely as the film was compressed, the resulting isotherm would match that of pure phospholipid. Thus, any deviation from that can be attributed to incomplete desorption of the antimicrobial.[42] Therefore, an interaction is thus expected to occur between the product and the phospholipid.

The compression isotherms obtained after spreading DPPC, DPPG, and *E. coli* lipid extract on the subphases containing the compounds under study are depicted in panels a−c of Figure 9, respectively. The compound concentration was 4×10^{-5} M (i.e., approximately 80% saturation concentration), except for $C_3(CA)_2$ (Figure 10a−c). Here, the 80% saturation concentration corresponded to ca. 1×10^{-6} M, owing to its higher surface pressure (Table 2). Therefore, for the sake of clarity, the results obtained with $C_3(CA)_2$ were plotted separately.

Analysis of the isotherms revealed that all the surfactants showed an immediate surface pressure increase at the onset of compression, due to their intrinsic adsorption at the air−water interface. We tried to reduce this effect by decreasing the product concentration in the subphase. However, a similar effect was noticed in experiments conducted at 1×10^{-5} and 3×10^{-6} M, corresponding to 20% and 5% saturation concentration, respectively, and 3×10^{-7} and 5×10^{-8} M for $C_3(CA)_2$. Analogous findings were obtained with neutral surfactants such as non-oxynol-9 and C31G (equimolar mixture of C14 amine oxide and C16 alkyl betaine).[26]

Table 5. Compressibility Moduli (C_s^{-1}) of DPPC, DPPG, and *E. coli* Lipid Extract Monolayers Spread in the Presence, at ca. 80% Saturation Concentration, or in the Absence of Cationic Compounds

	subphase					
Π (mN/m)	PBS	LAM	$C_3(OA)_2$	$C_3(CA)_2$	HTAB	CHX
			DPPC			
10	6	14	24		42	21
20	89	47	91	51	89	65
30	138	113	40	25	128	115
40	154	35	197	48	2	138
50	115			72		66
60	16			66		
			DPPG			
10	39	21	25			
20	58	38	56	82	14	33
30	91	30	36	75	41	75
40	116		41	32	44	45
50	110			22	8	
60	38			37		
			E. coli Extract			
10	45	16	16	69	48	36
20	90	36	40	53	34	51
30	83	1	73	38		75
40	96		40	64		

The presence of the compounds in the subphase shifted the lipid monolayers to higher area/molecule values (i.e., expansion effect) compared to isotherms obtained in the absence of product. This effect was reflected as a decrease in the compressibility moduli (C_s^{-1}) of the monolayer, calculated as described by Sospedra et al.[11] and summarized in Table 5.

For HTAB, CHX, and $C_3(OA)_2$, a shift toward lower values of area/molecule appeared in the DPPC or DPPG compression isotherm (Figure 9a,b). This indicates an

(41) Sospedra, P.; Espina, M.; Gomara, M. J.; Alsina, M. A.; Haro, I.; Mestres, C. *J. Colloid Interface Sci.* **2001**, *244*, 87−96.
(42) McConlogue, C. W.; Malamud, D.; Vanderlick, T. K. *Biochim. Biophys. Acta*: *Biomembranes* **1998**, *1372*, 124−134.

Table 6. Collapse Pressures (mN m^{-1}) of DPPC, DPPG, and *E. coli* Total Lipid Extract Monolayers at ca. 5%, 20%, and 80% Saturation Concentration of the Antimicrobial Compounds at the Subphase

	DPPC (60 mN m^{-1})[a]			DPPG (67 mN m^{-1})[a]			*E. coli* extract (48 mN m^{-1})[a]		
compound	80%	20%	5%	80%	20%	5%	80%	20%	5%
LAM	40	59	61	32	57	57	30	44	46
$C_3(OA)_2$	49	55	65	56	61	67	46	47	49
$C_3(CA)_2$	63	63	60	70	71	70	47	47	48
HTAB	36	53	63	40	43	58	28	40	46
CHX	52	60	63	32	39	43	34	43	46

[a] Collapse pressure of the pure lipid monolayer.

ejection of the product and lipid molecules from the monolayer to the subphase, probably by the formation of mixed micelles. $C_3(CA)_2$ always produced an expansion of the lipid monolayers regardless of the pressure and type of phospholipid (Figure 10a−c).

The collapse pressure and the variation of the LE−LC phase transition were a function of both the compound and the lipid. Overall, the higher the concentration of the compound in the subphase, the lower the collapse pressure observed (Table 6). Moreover, the LE−LC phase transition pressure tended to increase or disappear on increasing the product concentration. CHX abolished the LE−LC transition and reduced the collapse pressure regardless of the concentration, especially in DPPG monolayers. On the other hand, $C_3(CA)_2$ did not reduce the collapse pressure and the LE−LC transition shifted to higher pressures. Here, $C_3(CA)_2$ may hinder the reorientation of the alkyl chain of the lipids from horizontal to vertical position.[43]

The effects observed on the monolayer such as expansion, collapse pressure decrease, and LE−LC phase transition modification reflect a clear destabilization of the monolayer packing by the compounds under investigation. As Figures 9a,b and 10a,b show, all these perturbing effects were more important in DPPG than in DPPC, as a result of the electrostatic interactions, in agreement with the previous results on penetration kinetics.

The expansion of the DPPC and DPPG monolayers increased in the order $C_3(OA)_2$ < LAM ≈ HTAB ≈ CHX < $C_3(CA)_2$, and the collapse pressure decreased in the order $C_3(CA)_2$ > $C_3(OA)_2$ > LAM ≈ HTAB ≈ CHX. The expansion of the *E. coli* lipid extract monolayers increased in the order $C_3(OA)_2$ ≈ LAM ≈ CHX < HTAB < $C_3(CA)_2$, and the collapse pressure decreased in the order $C_3(CA)_2$ ≈ $C_3(OA)_2$ > LAM ≈ HTAB ≈ CHX. Briefly, the compounds with the highest antimicrobial activity caused a large expansion of the lipid monolayer or a large decrease in its collapse pressure together with a strong suppression of the LE−LC phase transition.

Conclusions

In summary, the interaction of the antimicrobials under study with DPPC MLVs and monolayers of DPPC, DPPG, and *E. coli* total lipid extract showed the following features:

The thermotropic parameters of DPPC MLVs correlated well with the antimicrobial activity of the compounds under study. The best antimicrobial compounds, $C_3(CA)_2$ and CHX, showed the highest partition into the lipid membrane (i.e., the highest K values) and the greatest widening of the transition width ($\Delta T_{1/2}$) with the decrease of the transition temperature (T_m).

In lipid monolayers, the penetration kinetics studies indicate that the antimicrobials incorporated better into anionic DPPG than into zwitterionic DPPC lipid monolayers. Here, mostly electrostatic forces governed the lipid−antimicrobial interaction. Concerning the compression isotherms, the highest expansion of the lipid monolayer was observed with the most active antimicrobial derived from arginine $C_3(CA)_2$, but this compound did not reduce the collapse pressure. On the other hand, CHX reduced the collapse pressure and strongly suppressed the LC−LE phase transition. From the results obtained with lipid monolayers, a relation between the physicochemical properties and the antimicrobial activity was still unclear.

With the perspective of gaining further insight into both knowledge about the mechanism of action and development of new antimicrobial surfactants, biophysical studies on leakage of vesicle-entrapped molecules are to be performed in a membrane mimetic environment.

Acknowledgment. This work was supported by the MCYT Project PPQ2000-1687-CO2-01. J.A.C. acknowledges the CSIC I3P postgraduate scholarship program for the financial support. We thank Dr. Àngels Manresa from the Faculty of Pharmacy of the University of Barcelona for her scientific assistance with the MIC measurements.

Supporting Information Available: Surface activity of the compounds as a function of time at different concentrations. Surface pressure increases as a function of the compound concentration. Pressure increases as a function of the initial density of the DPPC, DPPG, and *E. coli* total lipid extract monolayers for each compound at 80% saturation concentration. Compression isotherms of DPPC, DPPG, and *E. coli* total lipid extract monolayers spread on subphases containing the compounds under study at 80%, 20%, and 5% saturation concentration. This material is available free of charge via the Internet at http://pubs.acs.org.

LA036452H

(43) Minones, J. J.; Dynarowicz-Latka, P.; Conde, O.; Minones, J.; Iribarnegaray, E.; Casas, M. *Colloids Surf., B* **2003**, *29*, 205−215.

(44) Rosen, M. J. *Surfactants and Interfacial Phenomena*, 2nd ed.; John Wiley & Sons: New York, 1989.

(45) The cmc of $C_3(OA)_2$ and $C_3(CA)_2$ was measured in water using a tensiometer (Krúss K-12) with a Wilhelmy plate. Water/surfactant solutions of different concentrations were prepared and allowed to equilibrate for 15−30 min at 25 °C in the appropriate cells (ref 44).

(46) Fang, L.; Li, G.-Z.; Wang, H.-Q.; Xue, Q.-J. *Colloids Surf., A* **1997**, *127*, 89−96.

(47) Heard, D. D.; Ashworth, R. W. *J. Pharm. Pharmacol.* **1969**, *20*, 505−518.

6.2.2. Publication II:

Comparative study of the antimicrobial activity of bis(N^{α}-caproyl-L-arginine)-1,3-propanediamine dihydrochloride and chlorhexidine dihydrochloride against *Staphylococcus aureus* and *Escherichia coli*.

José A. Castillo, Pere Clapés, M. Rosa Infante, Jaume Comas, Ángeles Manresa.

Journal of Antimicrobial Chemotherapy **2006**, *57*, 691–698.

Journal of Antimicrobial Chemotherapy (2006) **57**, 691–698
doi:10.1093/jac/dkl012
Advance Access publication 8 February 2006

JAC

Comparative study of the antimicrobial activity of bis(N^{α}-caproyl-L-arginine)-1,3-propanediamine dihydrochloride and chlorhexidine dihydrochloride against *Staphylococcus aureus* and *Escherichia coli*

José A. Castillo[1], Pere Clapés[1], M. Rosa Infante[1], Jaume Comas[2] and Ángeles Manresa[3]*

[1]Institute for Chemistry and Environmental Research, CSIC, c/ Jordi Girona 18-26, 08034 Barcelona, Spain; [2]Serveis Científico-Tècnics, Universitat de Barcelona, c/ Josep Samitier 1-5, 08028 Barcelona, Spain; [3]Laboratori de Microbiologia, Facultat de Farmàcia, Universitat de Barcelona, Av. Joan XXIII s/n, 08028 Barcelona, Spain

Received 6 June 2005; returned 20 September 2005; revised 20 October 2005; accepted 5 January 2006

***Objectives*: The aim of this study is to gain insight into the mechanism of the antimicrobial action of a novel arginine-based surfactant, bis(N^{α}-caproyl-L-arginine)-1,3-propanediamine dihydrochloride [$C_3(CA)_2$].**

***Methods*: To this end, we compared its effects against *Staphylococcus aureus* and *Escherichia coli* with those caused by the commercial and widely known antiseptic, chlorhexidine dihydrochloride (CHX).**

***Results*: Both disrupted the cell membrane of the target bacteria to cause potassium leakage and morphological damage. The effect of $C_3(CA)_2$ on *E. coli* was concentration dependent, causing loss of membrane potential and membrane integrity leading to cell death, whereas CHX did not have these effects on *E. coli*. The effect of $C_3(CA)_2$ on *S. aureus* was the formation of mesomes and cytoplasmic clear zones, but the loss of membrane potential and membrane integrity was slightly lower than that with CHX.**

***Conclusions*: We propose that $C_3(CA)_2$ acts preferentially against Gram-negative bacteria through strong initial binding to the surface lipopolysaccharides and subsequently partitioning into the cell membrane to cause membrane damage, followed by cell death.**

Keywords: antimicrobial activity, flow cytometry, viability reduction, transmission electron microscopy, potassium leakage, cationic surfactants

Introduction

Arginine-based cationic surfactants are amphiphilic compounds that possess excellent self-assembling properties, a low toxicity profile, high biodegradability and a broad antimicrobial activity, which make them candidates of choice as preservatives and antiseptics in pharmaceutical, food and dermatological formulations.[1–5] Among the arginine-based surfactants synthesized in our laboratory, bis(N^{α}-caproyl-L-arginine)-1,3-propanediamine dihydrochloride [$C_3(CA)_2$] is a novel gemini (double-chain/double-polar head) compound which shows antimicrobial activity against a wide range of Gram-positive and Gram-negative bacteria.[1,6]

Bacterial cells offer three regions for biocide interaction: the cell wall, the cytoplasmic membrane and the cytoplasm. In general, microbicides lack target specificity, though in the case of biguanide compounds such as chlorhexidine dihydrochloride (CHX), and cationic surfactants, their main target is the bacterial membrane.[7–10] Both biguanides and cationic surfactants have a similar mechanism of action.[11] As shown in Figure 1, both compounds are dicationic but with different structures: $C_3(CA)_2$ has two arginine residues connected by three methylene groups, and two alkyl chains of ten carbon atoms that form the hydrophobic moieties. CHX, on the other hand, possess two biguanides as the polar heads connected by a spacer chain of six methylenes, and two chloro-phenyl groups as the hydrophobic core.

These cationic compounds initiate their interaction with the cytoplasmic membrane by binding to the phospholipid surface through electrostatic forces. They are then absorbed in the hydrophobic core of the membrane perturbing the packing of the lipids, leading to dissolution of the proton motive force and leakage of essential molecules.[8,10] The specificity of these

*Corresponding author. Tel: +34-934024496; Fax: +34-934024498; E-mail: amanresa@ub.edu

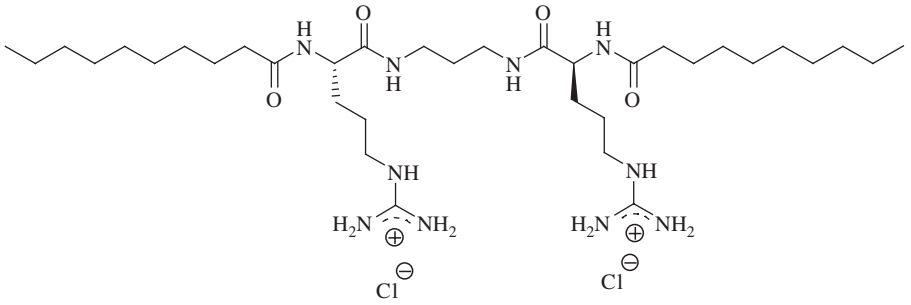

$C_3(CA)_2$

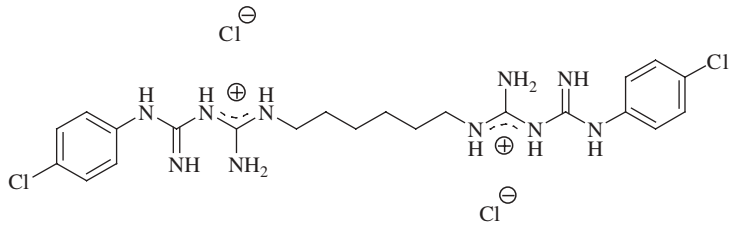

CHX

Figure 1. Structures of the selected antimicrobial compounds.

compounds towards prokaryotes, rather than eukaryotes, is thought to be due to the higher amount of anionic phospholipids in prokaryotic membranes.[12–14]

The synthesis of new biocompatible (i.e. low toxicity profile and high biodegradability) powerful antimicrobial agents is of paramount importance to prevent infectious diseases.[10,15] The design of new molecules can be aided by an understanding of their mechanism of action, and we have recently reported the interaction of arginine-based surfactants with biomembrane models (i.e. liposomes and phospholipid monolayers).[6] The purpose of this work is to elucidate the effects of the gemini surfactant $C_3(CA)_2$ on cell viability and on cell envelope integrity in *Staphylococcus aureus* and *Escherichia coli*. The well known biguanide CHX was included in these studies for comparison.

Materials and methods

Antibacterial products and chemicals

$C_3(CA)_2$ was synthesized in our laboratory as previously described.[3,16] CHX was purchased from Sigma (St Louis, MO, USA). Molecular dyes Syto-13, propidium iodide (PI) and bis-1,3-dibutylbarbutiric acid (bis-oxonol) were supplied by Molecular Probes Europe BV (Leiden, The Netherlands). The solvents and reagents used were of analytical grade. Ultra pure water, produced by a Nanopure purification system coupled to a Milli-Q water purification system, resistivity = 18.2 M·Ω·cm, was used for the aqueous solutions.

Microorganisms

Strains were obtained from the American Type Culture Collection (ATCC; Manassas, VA, USA): *S. aureus* ATCC 9144 and *E. coli* ATCC 10536. They were sub-cultured weekly on trypticase soy agar (TSA; Pronadisa, Barcelona, Spain). Strains were maintained frozen in cryovials (AES Laboratoire, Combourg, France) at –80°C.

Table 1. Minimum inhibitory concentration in mg/L and the antimicrobial concentrations tested

	S. aureus			*E. coli*		
Compound	MIC	1/2 MIC	3/2 MIC	MIC	1/2 MIC	3/2 MIC
$C_3(CA)_2$	2	1	3	8	4	12
CHX	0.5	0.25	0.75	2	1	3

MICs

The MICs of $C_3(CA)_2$ and CHX were determined by using a broth micro-dilution assay.[17] Briefly, serial dilutions of the antimicrobials were made in Mueller–Hinton broth (Oxoid, USA). A 96-well polypropylene microtitre plate (Costar, Corning Incorporated, Corning, NY, USA) was used. Each well was inoculated with 100 µL of the test organism in Mueller–Hinton broth to a final concentration of $\sim 10^5$ cfu/mL. The MIC was taken as the lowest antimicrobial concentration at which growth was inhibited after 24 h of incubation at 37°C.

Exposure of microorganisms to biocides

Suspensions of the microorganisms were obtained from an overnight culture of each strain on tryptone soy broth (TSB) (Oxoid, USA) at 30°C. Cultures were then centrifuged at 8000 **g** for 15 min, washed twice in sterile Ringer's solution (Scharlau, Barcelona, Spain) and resuspended in Ringer's solution to obtain a cell suspension of about 10^7–10^8 cfu/mL. Three millilitres of the respective cell suspensions was used to inoculate flasks containing 27 mL of Ringer's solution to obtain a cell density of about 10^6–10^7 cfu/mL.

Different aliquots (7.5–360 µL, depending on the final 1/2 or 3/2 MIC) of the stock solution of $C_3(CA)_2$ and CHX (see Table 1) were added to flasks with the respective bacterial suspensions.

After a contact time of 30 min, the biocide effect was immediately neutralized by dilution with sterile Ringer's solution, then the

bacterial suspension was centrifuged for 20 min at 8000 **g** and the pellet was resuspended with Ringer's solution to obtain the convenient cell suspension concentration (10^7–10^8 cfu/mL). The inoculated flasks were kept at room temperature.

For flow cytometry (FC) experiments, 15 mL samples were diluted, centrifuged at 8000 **g** for 30 min and the bacterial pellets were resuspended in 1 mL of Ringer's solution.

For transmission electronic microscopy (TEM) observations, the contact time was 30 min at biocide concentration 3/2 MIC. Then, samples of 5 mL were taken, diluted with Ringer's solution and centrifuged at 4500 **g** for 30 min. The bacterial pellets were then rinsed with 0.1 M phosphate buffer (pH 7.4).

In all cases, control experiments lacking microbicide were conducted in parallel.

Staining procedure

Staining protocols for FC experiments were as follows: 1 µL of a 500 µM stock solution of Syto-13 in dimethyl sulphoxide and 10 µL of a 1 mg/mL stock solution of PI in distilled water were added to 500 µL of the bacterial suspension in filtered Ringer's solution. The *S. aureus* and *E. coli* suspensions were incubated with the dyes for 3 and 20 min, respectively. Stains were performed at room temperature before the FC analysis. Experiments were conducted in triplicate.

In the case of the membrane potential dye, 2 µL of a 250 µM stock solution of bis-oxonol in ethanol was added to 500 µL of the bacterial suspension to a final concentration of 1 µM and incubated for 2 min. Cells killed by heat exposure (30 min at 70°C) were used as controls for bis-oxonol staining. Experiments were conducted in duplicate.

Flow cytometry (FC)

A Coulter Epics Elite flow cytometer (Coulter Corporation, Florida, USA) equipped with a 15 mW air-cooled 488 nm argon-ion laser (for Syto-13, PI and bis-oxonol excitation) was used. The green emission from Syto-13 and bis-oxonol was collected through a 525 nm band-pass filter. The red emission from PI was collected with a 675 nm band-pass filter. Although the maximum emission is at 620 nm, a 675 nm band-pass filter was used to minimize interference with the strong fluorescence of Syto-13.

Bacteria were counted using a Cytek Flow Module (Cytek Development, CA, USA) adapted to the flow cytometer. Forward, side-scatter and fluorescence signals were collected in logarithmic scale. A significant percentage of the bacterial population that can be detected by its Syto-13 fluorescence appears in the first channel of the scatter. Consequently, fluorescence is used to discriminate bacteria rather than scatter, thus obtaining a better resolution and decreasing the background. Data were analysed with Elitesoft version 4.1 (Coulter Corporation) and WinMDI version 2.8 software.

Particle size analysis

Cell suspensions were analysed with a Multisizer II (Coulter) using a 30 µm aperture. Cell suspensions were diluted (1/1000) in 0.9% NaCl previously passed through a 0.2 µm filter. Data were analysed by AccuComp software version 1.15 (Coulter).

Bacterial count

Viable counts (cfu/mL) were obtained on trypticase soy agar (TSA). After an appropriate dilution in Ringer's solution, the sample was inoculated on plates and incubated at 30°C for 24–48 h. Rapid separation of bacteria from the antimicrobial was achieved by centrifugation at 4500 **g** in a bench top centrifuge for 15 min and subsequent dilution in Ringer's solution prior to plating. Cell counting was performed in triplicate.

Transmission electron microscopy (TEM)

After treatment of cell suspensions with the biocides at 3/2 MIC for 30 min for each microorganism [3 and 12 mg/L of $C_3(CA)_2$ with *S. aureus* and *E. coli*, respectively, and 0.75 and 3 mg/L of CHX with *S. aureus* and *E. coli*, respectively] the bacterial pellets were rinsed with 0.1 M phosphate buffer (pH 7.4), washed three times and fixed with 2.5% buffered glutaraldehyde for 1 h at 4°C. The cells were then post-fixed in 1% buffered osmium tetroxide for 1 h, stained with 1% uranyl acetate, dehydrated in a graded series of ethanol, and embedded in LR (London Resin Co. Ltd, London, UK) white resin. Ultra-thin sections were prepared and stained with 1% uranyl acetate and sodium citrate. Microscopy was performed with a Philips EM 30 (Eindhoven, Holland) microscope with an acceleration of 60 kV.

Potassium leakage

Potassium leakage was measured as described previously.[4] Cells were grown on TSA at 37°C for 12 h, then harvested in 10 mL of Ringer's solution, washed three times with Ringer's solution and finally centrifuged at 5000 **g** for 30 min at 15°C and resuspended in 25 mL of 1 mM glycil-glycine buffer solution pH 6.8 to obtain a cell density of 2×10^8 cfu/mL and 3×10^8 cfu/mL for *S. aureus* and *E. coli*, respectively. The microorganisms were treated with the antimicrobials at 3/2 MIC for 30 min. Then, 5 mL of cell suspension was removed, diluted and centrifuged at 4500 **g** for 15 min. Positive controls were lysed cell suspension obtained by thermal shock (70°C for 30 min). Experiments were conducted in triplicate.

The potassium concentration in the supernatant was measured using an atomic absorption Philips PU9200X spectrophotometer (Philips Cambridge, UK). Absorbance values were converted into potassium ion concentration (ppm) by reference to a curve using potassium ion solution of 0, 0.1, 0.2, 0.5 and 1 ppm.

Results

As shown in Table 1, the MICs of $C_3(CA)_2$ and CHX for *S. aureus* were 2 and 0.5 mg/L, respectively, and those for *E. coli* were 8 and 2 mg/L, respectively. To study the effect of the antimicrobial agents on the bacterial population, two concentrations were selected on an MIC basis: the first was 50% greater than the corresponding MIC (3/2 MIC) and the second was 50% lower than the MIC (1/2 MIC). The concentrations of the surfactant, $C_3(CA)_2$, were always lower than the corresponding critical micellar concentration (i.e. 4×10^{-5} M).[18]

Flow cytometry (FC) and viability reduction

To assess the effect of $C_3(CA)_2$ and CHX on bacterial populations, dual staining of cells was performed with Syto-13 (a nucleic acid stain that penetrates all types of cellular membranes) and PI, a nucleic acid stain not taken up by intact cells.[19] Hence, three types of stained cells could be observed after the treatment: cells stained with Syto-13 (intact cells), double stained cells (partially damaged cells) and cells stained with PI (severely damaged cells).

To validate the FC results, and to examine the putative relation between cell damage and cell viability, viable cell counts were determined after exposure to the microbicides. The results with *S. aureus* are shown in Figure 2(a–c) and Table 2. As seen in Figure 2(a), the control population was mainly stained with Syto-13 (99 ± 1%). After 30 min of contact with 3 mg/L (3/2 MIC) $C_3(CA)_2$, 95 ± 1% of the cells were stained with Syto-13,

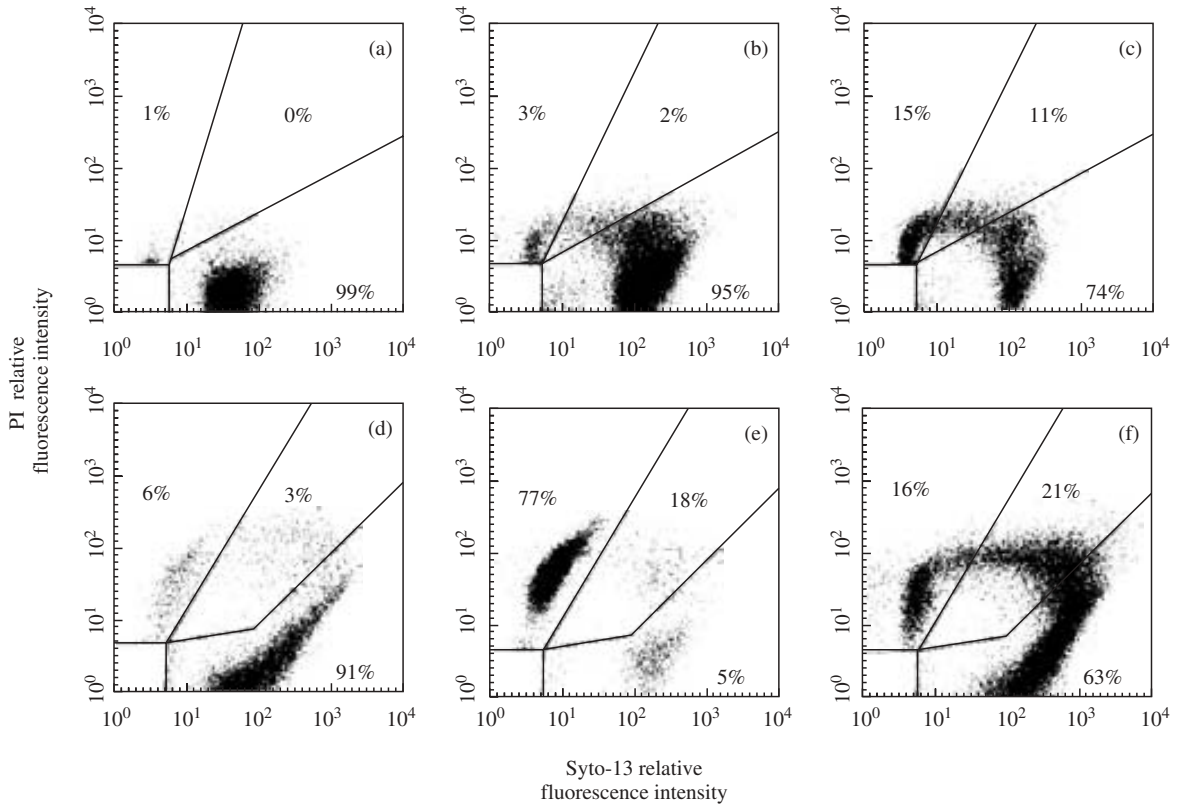

Figure 2. Effect on the membrane integrity of *S. aureus* and *E. coli* caused by exposure to $C_3(CA)_2$ and CHX, shown by dual staining with PI and Syto-13. (a) Untreated *S. aureus* control, (b) *S. aureus* treated with $C_3(CA)_2$, (c) *S. aureus* treated with CHX, (d) untreated *E. coli* control, (e) *E. coli* treated with $C_3(CA)_2$, and (f) *E. coli* treated with CHX. In all cases, time of contact was 30 min and antimicrobial concentration was 3/2 MIC.

Table 2. Effect of the antimicrobials on *S. aureus* after a dual stain with PI and Syto-13, and viability by plate counts

Entry	Sample	Conc. (mg/L)	Syto-13 (%)	PI + Syto-13 (%)	PI (%)	cfu/mL (10^6)	Viability reduction (%)
1	control	–	99 ± 1	0	1 ± 1	4.8 ± 1.3	–
2	$C_3(CA)_2$	1	93 ± 3	4 ± 1	3 ± 2	3.8 ± 1.3	21 ± 10
3	$C_3(CA)_2$	3	95 ± 1	2 ± 1	3 ± 1	3.3 ± 0.6	31 ± 6
4	CHX	0.25	80 ± 7	5 ± 1	14 ± 4	3.8 ± 3.3	21 ± 13
5	CHX	0.75	74 ± 8	11 ± 4	15 ± 1	3.4 ± 2.1	29 ± 9

Antimicrobial concentrations tested were 1/2 MIC and 3/2 MIC, and time of contact was 30 min. Data are given as the mean ± SEM of three separate experiments.

2 ± 1% were double stained and 3 ± 1% were stained with PI, indicating slight damage caused by $C_3(CA)_2$. Varying the $C_3(CA)_2$ concentration did not alter the proportion of damaged cells (Table 2, entries 2 and 3). Likewise, cell counts on plates did not change substantially with biocide concentration; viable cells dropped from 79 ± 10% at 1 mg/L (1/2 MIC) to 69 ± 6% at 3 mg/L (3/2 MIC). When *S. aureus* was treated with 0.75 mg/L CHX (3/2 MIC) (Figure 2c), 11 ± 4% partially damaged (double stained), and 15 ± 1% severely damaged cells (PI stained cells) were seen. Decreasing the biocide concentration from 3/2 to 1/2 MIC did not affect the proportion of partially damaged cells, since double stained cells only decreased from 11 ± 4 to 5 ± 1% (Table 2, entries 4 and 5). These results agree with the cell counts, where varying biocide concentration caused only a slight effect on cell viability (Table 2, entries 4 and 5).

A different pattern was observed in *E. coli* populations when they were treated with $C_3(CA)_2$ and CHX (Figure 2d–f and Table 3). The control population showed 91 ± 4% of intact cells (stained by Syto-13). After treatment with 12 mg/L $C_3(CA)_2$ (3/2 MIC), a dramatic decrease in intact cells was detected, only 5 ± 1% of the population retained Syto-13 whereas 77 ± 10% were severely damaged (stained by PI), and the remaining 18 ± 3% were partially damaged (double stained, Figure 2e). At 4 mg/L $C_3(CA)_2$ (1/2 MIC), 42% (PI and PI + Syto-13) of the population showed signs of damage and the reduction in viability was 77 ± 1% (Table 3, entry 2). Three sub-populations could clearly be observed (Figure 2f) when *E. coli* cultures were treated with CHX at 3/2 MIC: 63 ± 5% remained intact (Syto-13); 21 ± 2% showed partial damage (double stained); and 16 ± 3% of cells were severely damaged (stained by PI). As presented in Table 3 (entries

Table 3. Effect of the antimicrobials on *E. coli* after a dual stain with PI and Syto-13, and viability by plate counts

Entry	Sample	Conc. (mg/L)	Syto-13 (%)	PI + Syto-13 (%)	PI (%)	cfu/mL (10^6)	Viability reduction (%)
1	control	–	91 ± 4	3 ± 1	6 ± 3	2.5 ± 1.5	–
2	$C_3(CA)_2$	4	58 ± 11	15 ± 2	27 ± 3	0.6 ± 0.3	77 ± 1
3	$C_3(CA)_2$	12	5 ± 1	18 ± 3	77 ± 10	0.1 ± 0.1	95 ± 1
4	CHX	1	67 ± 5	13 ± 2	20 ± 3	1.4 ± 0.8	44 ± 1
5	CHX	3	63 ± 5	21 ± 2	16 ± 3	1.0 ± 0.4	61 ± 1

Antimicrobial concentrations tested were 1/2 MIC and 3/2 MIC, and time of contact was 30 min. Data are given as the mean ± SEM of three separate experiments.

4 and 5), variation of CHX concentration did not appear to have any effect as observed by FC; the population stained by Syto-13 decreased from 67 ± 5 to 63 ± 5%. However, the viability reduction changed significantly with CHX concentration, from 44 ± 1 to 61 ± 1 (i.e. 17 ± 2% of viability reduction).

Membrane potential

Membrane depolarization was measured by determining the relative fluorescence intensity of bis-oxonol labelling using FC. As shown in Figure 3, the negative controls (i.e. cell suspensions in the absence of microbicides) showed the minimum relative fluorescence intensity (Figure 3a and e). We considered the range M1 [0-350 fluorescence units (FU)] as undamaged cells showing no significant depolarization of the cytoplasmic membrane. As expected, the positive control (i.e. bacteria that underwent a thermal shock at 70°C for 30 min) showed the maximum relative fluorescence intensity (Figure 3d and h). We considered the range M2 (between 350 and 1024 FU) as damaged and dead cells. The effect of $C_3(CA)_2$ on *S. aureus* showed a bimodal profile (Figure 3b) with two distinct populations of cells: almost 50% of the population emitted fluorescence in the region of non-damaged cells; while the rest emitted in the region of the dead cells. A different pattern was observed on exposure of *E. coli* to $C_3(CA)_2$; 84% of cells were damaged or dead (increased fluorescence); and 16% remained intact. When cells were exposed to CHX, a bimodal pattern was observed (i.e. 49% intact and 51% damaged cells) with *E. coli* (Figure 3g), whereas, for the most part, *S. aureus* was undamaged (Figure 3c).

Potassium ion leakage

Potassium ion (K^+) leakage reflects an increase in the cytoplasmic membrane. Here, intracellular potassium leakage resulting from exposure to $C_3(CA)_2$ and CHX of *S. aureus* and *E. coli* at the corresponding 3/2 MIC was measured. The cell density was 2×10^8 and 3×10^8 cfu/mL for *S. aureus* and *E. coli*, respectively. The negative blank was the K^+ leakage measured from the bacterial suspensions in the absence of the antimicrobials ($363 \pm 75 \times 10^{-3}$ ppm K^+ from *S. aureus* and $769 \pm 42 \times 10^{-3}$ ppm K^+ from *E. coli*). The positive blank was the K^+ released from the bacterial suspensions heated at 70°C for 30 min ($509 \pm 29 \times 10^{-3}$ ppm K^+ from *S. aureus* and $918 \pm 33 \times 10^{-3}$ ppm K^+ from *E. coli*). Thus, the percentage of K^+ leakage was the ratio of net to total amount of K^+ released.

Experiments with the Gram-positive organism showed that $C_3(CA)_2$ caused a potassium loss of $401 \pm 32 \times 10^{-3}$ ppm K^+ (26%) and CHX $375 \pm 63 \times 10^{-3}$ ppm K^+ (8%). The results with the Gram-negative organism showed that both antimicrobials released higher amounts of potassium ion than the Gram-positive organism: the surfactant, $C_3(CA)_2$, released $951 \pm 52 \times 10^{-3}$ ppm K^+ (>100%) and CHX released, $889 \pm 42 \times 10^{-3}$ ppm K^+ (81%).

TEM

Mesosome-like structures (i.e. spiral-bodies of the cytoplasmic membrane forming within the cytoplasm) and some cytoplasmic clear zones could be seen in *S. aureus* treated with $C_3(CA)_2$ (Figure 4a). In the case of *E. coli* more severe perturbations could be seen; numerous vesicles protruded from around the cell, severe damage to the membranes, appearance of cytoplasmic white spots, and abnormal septation (Figure 4b). The morphological disturbance caused by CHX on *S. aureus* was mesosome formation, clear zones and membrane-like convoluted structures in the cytoplasm (Figure 4c). In *E. coli*, cytoplasmic damage was clearly seen with the appearance of cytoplasmic white spots, as well as clear zones, and perturbations of the cytoplasmic membrane (Figure 4d).

Discussion

$C_3(CA)_2$, and the comparator molecule CHX, change the polarity of the cell membrane bilayer of the bacteria and cause leakage of K^+ ions from the cytoplasm. Both phenomena are involved in the cell death mechanism. But, these two compounds have different bacterial selectivity suggesting a different mode of action; $C_3(CA)_2$ has a concentration dependent microbicidal effect on *E. coli*, but has little effect on *S. aureus*; whereas CHX has little effect on *E. coli*, and does cause some damage (though not loss of viability) to *S. aureus*.

Potassium leakage is a first indication of membrane damage in microorganisms.[20–22] Ultrastructural changes are also observed early on in the progress of membrane damage, with mesosome-like structures often appearing before any other effects on cell viability are noted.[23] Both $C_3(CA)_2$ and CHX induced the first stages of cytoplasmic membrane damage in *E. coli* and in *S. aureus*, as shown by loss of intracellular potassium ions from washed cell suspensions, and the presence of intracellular mesosomes. This may be due to both the physicochemical properties of the microbicides and the composition of the cell membrane of Gram-positive and Gram-negative bacteria.[7] Both, $C_3(CA)_2$ and CHX have two negative charges but the former is an amphiphilic molecule with surfactant properties whereas the later has a weak surface activity.[6,24,25]

The fluorochromes PI and Syto-13 were chosen because of their potential ability to distinguish between intermediate states of dead and live cells; PI confers fluorescence on cells which

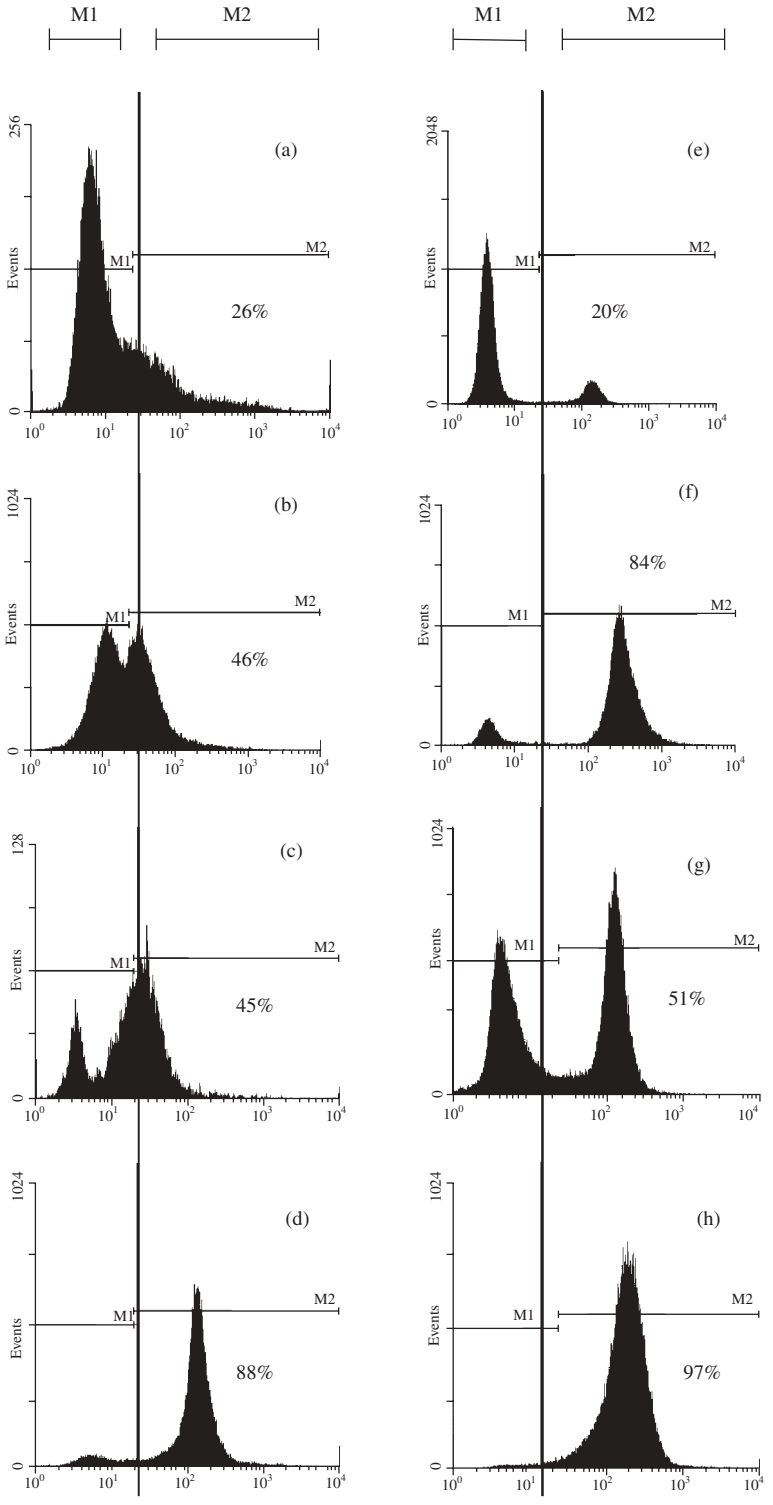

Figure 3. Effect on the transmembrane potential of *S. aureus* and *E. coli* caused by exposure to $C_3(CA)_2$ and CHX, shown by bis-oxonol staining. The relative fluorescence intensities within the M1 regions were taken as live cells, and those within the M2 regions were take as dead cells (logarithmic scale). (a) Untreated *S. aureus* control, (b) *S. aureus* treated with $C_3(CA)_2$, (c) *S. aureus* treated with CHX, (d) *S. aureus* heated at 70°C, (e) untreated *E. coli* control, (f) *E. coli* treated with $C_3(CA)_2$ (g) *E. coli* treated with CHX, and (h) *E. coli* heated at 70°C. In all cases, time of contact was 30 min and antimicrobial concentration was 3/2 MIC.

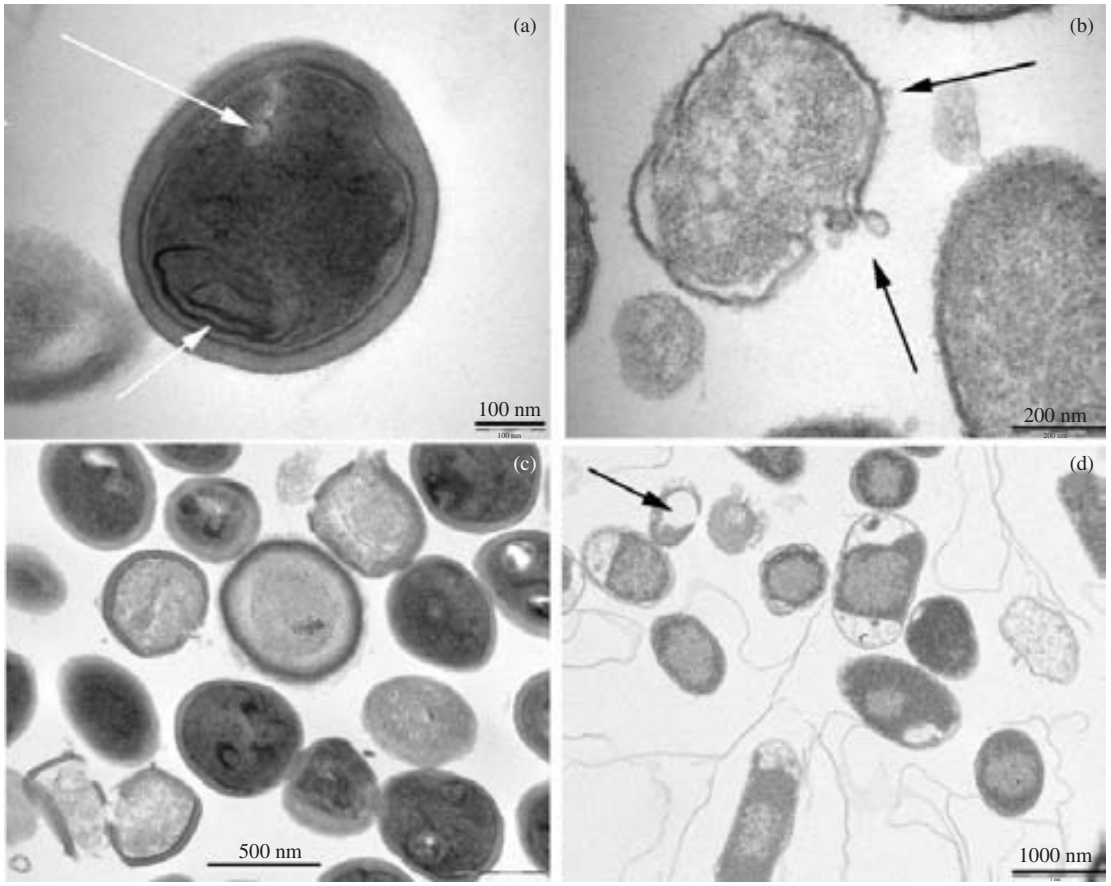

Figure 4. Effect on membrane ultrastructure of *S. aureus* and *E. coli* caused by exposure to $C_3(CA)_2$ and CHX, shown by transmission electron microscopy. (a) *S. aureus* treated with $C_3(CA)_2$, (b) *E. coli* treated with $C_3(CA)_2$, (c) *S. aureus* treated with CHX, and (d) *E. coli* treated with CHX. In all cases, time of contact was 30 min and antimicrobial concentration was 3/2 MIC.

have lost their membrane integrity, whereas Syto-13 confers fluorescence on intact cells. The fluorochrome bis-oxonol is an anionic lipophilic dye that does not accumulate to any great extent in cells with a negative transmembrane potential, and fluorescence increases as membrane potential decreases.[26] These labels, in combination with ultrastructural studies, and cell viability assays demonstrated marked differences between the microbicides in their action on the bacterial cells: when *E. coli* was exposed to $C_3(CA)_2$, 84% showed loss of membrane potential, 27–77% of cells showed membrane damage and 77–95% loss of cell viability, depending on the concentration of $C_3(CA)_2$ used. It is remarkable that the bis-oxonol fluorescence measured from the $C_3(CA)_2$-treated *E. coli* was close to that of the positive control. This indicates a complete membrane depolarization that caused irreversible damage leading to loss of viability. Electron micrographs agree with these results. Intracytoplasmic black spots were observed, similar to those reported in *E. coli* heat-treated cells.[27] The most striking ultrastructural effect observed in *E. coli* was the formation of vesicles blebbing out from the outer membrane in the presence of $C_3(CA)_2$, similar to those reported for benzalkonium chloride-treated *Pseudomonas aeruginosa*.[28] CHX had little effect on *E. coli* membrane integrity, shown by PI and Syto-13 labelling, though some intracytoplasmic changes were observed by electron microscopy. A moderate effect on *E. coli* membrane potential (51%) and cell viability (61% reduction) were also observed.

S. aureus membranes seem to be little affected by exposure of the bacteria to $C_3(CA)_2$, with just 5–7% loss of integrity shown by PI staining; a low emission of bis-oxonol fluorescence, indicating a moderate effect on the membrane potential and a low impact on the viability of the cells. Exposure to CHX caused some loss of membrane integrity (the proportion of PI stained cells increased), and a moderate reduction in membrane potential, but no reduction in viability. These data were supported by ultrastructural studies. These data are consistent with the idea that $C_3(CA)_2$ and CHX are probably working through similar overall mechanisms, but with different bacterial specificities due to their charge properties and the nature of the bacterial targets: Gram-negative cells offer a lipopolysaccharide (LPS) barrier that Gram-positive cells do not posses.[7] The anionic character of the LPS layer[14] could enhance the binding of the cationic surfactant $C_3(CA)_2$, which would not be so strong with CHX due to its weak surface activity and surfactant properties. This, together with the ability of $C_3(CA)_2$ to partition between the aqueous solution and the biological membrane, would make it an excellent molecule for targeting Gram-negative bacteria.

A lack of correlation between the membrane damaging action and cell viability seen for *S. aureus* suggests that membrane perturbation may be an important step in cell death, but is not necessarily a lethal event. Previous studies with *S. aureus* and *E. coli* have also indicated that membrane perturbation caused by antimicrobials and recovery of cells on agar are not always

directly related.[4,29] This may be due to technical factors such as the conditions for recovery of cells;[8,30,31] or that membrane perturbation does not necessarily lead to dissolution of the proton motive force and cell death.[8,30,31]

It is notable that two different populations (~50%) were registered using the bis-oxonol dye. This points to the presence of sub-populations with different degrees of damage, suggesting reversible damage or it could even represent viable and non-viable organisms.[32]

Conclusions

$C_3(CA)_2$ and CHX induce similar types of damage to *S. aureus* and *E. coli*, though they differ in the extent of membrane depolarization and reduction in cell viability. These differences suggest that both compounds damage bacteria in a different way, and that the surfactant properties of $C_3(CA)_2$ and its ability to partition into the biological membrane from aqueous solution might be important characteristics in its microbicidal action.

Acknowledgements

This work was supported by the MCYT project PPQ2000-1687-CO2-01 and CTQ-2004-7771-CO2-01/PPQ. J. A. C. acknowledges the CSIC I3P postgraduate scholarship programme for financial support.

Transparency declarations

No declarations were made by the authors of this paper.

References

1. Pérez L, Torres JL, Manresa A *et al*. Synthesis, aggregation, and biological properties of a new class of gemini cationic amphiphilic compounds from arginine, bis(args). *Langmuir* 1996; **12**: 5296–301.

2. Clapés P, Morán C, Infante MR. Enzymatic synthesis of arginine-based cationic surfactants. *Biotechnol Bioeng* 1999; **63**: 332–43.

3. Piera E, Infante MR, Clapés P. Chemo-enzymatic synthesis of arginine-based gemini surfactants. *Biotechnol Bioeng* 2000; **70**: 323–31.

4. Rodríguez E, Seguer J, Rocabayera X *et al*. Cellular effects of monohydrochloride of L-arginine, *N*-lauroyl ethylester (LAE) on exposure to *Salmonella typhimurium* and *Staphylococcus aureus*. *J Appl Microbiol* 2004; **96**: 903–12.

5. Morán C, Clapes P, Comelles F *et al*. Chemical structure/property relationship in single-chain arginine surfactants. *Langmuir* 2001; **17**: 5071–5.

6. Castillo JA, Pinazo A, Carilla J *et al*. Interaction of antimicrobial arginine-based cationic surfactants with liposomes and lipid monolayers. *Langmuir* 2004; **20**: 3379–87.

7. Denyer SP. Mechanisms of action of antibacterial biocides. *Int Biodeterior Biodegradation* 1995; **36**: 227–45.

8. Sheppard FC, Mason DJ, Bloomfield SF *et al*. Flow cytometric analysis of chlorhexidine action. *FEMS Microbiol Lett* 1997; **154**: 283–8.

9. Chawner J, Gilbert P. Interaction of the bisbiguanidines chlorhexidine and alexidine with phospholipid vesicles: evidence for separate modes of action. *J Appl Bacteriol* 1989; **66**: 253–8.

10. McDonnell G, Russell AD. Antiseptics and disinfectants: activity, action and resistance. *Clin Microbiol Rev* 1999; **12**: 147–79.

11. Denyer SP, Stewart GSAB. Mechanisms of action of disinfectants. *Int Biodeterior Biodegradation* 1998; **41**: 261–8.

12. Oren Z, Hong J, Shai Y. A repertoire of novel antibacterial diastereomeric peptides with selective cytolytic activity. *J Biol Chem* 1997; **272**: 14643–9.

13. Lohner K, Prenner EJ. Differential scanning calorimetry and X-ray diffraction studies of the specificity of the interaction of antimicrobial peptides with membrane-mimetic systems. *Biochim Biophys Acta* 1999; **1462**: 141–56.

14. Papo N, Shai Y. Can we predict biological activity of antimicrobial peptides from their interactions with model phospholipid membranes? *Peptides* 2003; **24**: 1693–703.

15. Lambert RJW. Comparative analysis of antibiotic and antimicrobial biocide susceptibility data in clinical isolates of methicillin-sensitive *Staphylococcus aureus*, methicillin-resistant *Staphylococcus aureus* and *Pseudomonas aeruginosa* between 1989 and 2000. *J Appl Microbiol* 2004; **97**: 699–711.

16. Clapés P, Infante MR. Amino acid-based surfactants: enzymatic synthesis, properties and potencial applications. *Biocatal Biotransformation* 2002; **20**: 215–33.

17. Woods GL, Washington JA. Antibacterial susceptibility tests: dilution and disk diffusion methods. In: Murray PR, Baron EJ, Pfaller MS *et al.*, eds. *Manual of Clinical Microbiology*. Washington, USA: ASM Press, 1995.

18. Pérez L, Pinazo A, Rosen MJ *et al*. Surface activity properties at equilibrium of novel gemini cationic amphiphilic compounds from arginine, bis(args). *Langmuir* 1998; **14**: 2307–15.

19. Bunthof CJ, Van Schalkwijk S, Meijer W *et al*. Fluorescent method for monitoring cheese starter permeabilization and lysis. *Appl Environ Microbiol* 2001; **67**: 4264–71.

20. Mlynarcik D, Sirotkova L, Devinsky F *et al*. Potassium leakage from *Escherichia coli* cells treated by organic ammonium salts. *J Basic Microbiol* 1992; **32**: 43–7.

21. Lambert PA, Hammond SM. Potassium fluxes, first indications of membrane damage in micro-organisms. *Biochem Biophys Res Commun* 1973; **54**: 796–9.

22. Fitzgerald KA, Davies A, Russell AD. Mechanism of action of chlorhexidine diacetate and phenoxyethanol singly and in combination against Gram-negative bacteria. *Microbios* 1992; **70**: 215–30.

23. Shimoda M, Ohki K, Shimamoto Y *et al*. Morphology of defensin-treated *Staphylococcus aureus*. *Infect Immun* 1995; **63**: 2886–91.

24. Heard DD, Ashworth RW. The colloidal properties of chlorhexidine and its interaction with some macromolecules. *J Pharm Pharmacol* 1968; **20**: 505–12.

25. Pérez L, García MT, Ribosa I *et al*. Biological properties of arginine-based gemini cationic surfactants. *Environ Toxicol Chem* 2002; **21**: 1279–85.

26. Comas J, Vives J. Assessment of the effects of gramicidin, formaldehyde, and surfactants on *Escherichia coli* by flow cytometry using nucleic acid and membrane potential dyes. *Cytometry* 1997; **29**: 58–64.

27. Woo IS, Rhee IK, Park HD. Differential damage in bacterial cells by microwave radiation on the basis of cell wall structure. *Appl Environ Microbiol* 2000; **66**: 2243–7.

28. Joynson JA, Forbes B, Lambert RJW. Adaptive resistance to benzalkonium chloride, amikacin and tobramycin: the effect on susceptibility to other antimicrobials. *J Appl Microbiol* 2002; **93**: 96–107.

29. Friedrich CL, Moyles D, Beveridge T *et al*. Antibacterial action of structurally diverse cationic peptides on Gram-positive bacteria. *Antimicrob Agents Chemother* 2000; **44**: 2086–92.

30. Comas J, Vives J. Enumeration, viability and heterogeneity in Staphylococcus aureus cultures by flow cytometry. *J Microbiol Methods* 1998; **32**: 45–53.

31. Vives J, Lebaron P, Nebe-von Caron G. Current and future applications of flow cytometry in aquatic microbiology. *FEMS Microbiol Rev* 2000; **24**: 429–48.

32. Suller MTE, Lloyd D. Fluorescence monitoring of antibiotic-induced bacterial damage using flow cytometry. *Cytometry* 1999; **35**: 235–41.

6.2.3. Publication III:

Chemoenzymatic synthesis and antimicrobial and haemolytic activities of amphiphilic bis(phenylacetylarginine) derivatives.

José A. Castillo, M. Rosa Infante, Àngels Manresa, M. Pilar Vinardell, Montserrat Mitjans, Pere Clapés.

ChemMedChem **2006**, *1*, 1091-1098.

DOI: 10.1002/cmdc.200600148

Chemoenzymatic Synthesis and Antimicrobial and Haemolytic Activities of Amphiphilic Bis(phenylacetylarginine) Derivatives

José A. Castillo,[a] M. Rosa Infante,[a] Àngels Manresa,[b] M. Pilar Vinardell,[c] Montserrat Mitjans,[c] and Pere Clapés*[a]

Novel bis(N$^{\alpha}$-phenylacetyl-L-arginine)-α,ω-alkanediamide dihydrochloride (bis(PhAcArg)) derivatives with antimicrobial activity were designed and synthesised by a chemoenzymatic strategy. The new structures consist of two N$^{\alpha}$-phenylacetyl-L-arginine moieties connected by an alkanediamine spacer chain of 6, 8, 10, 12, and 14 methylene units through amide bonds. The key step in the chemoenzymatic strategy is the double aminolysis of the N$^{\alpha}$-phenylacetyl-L-arginine methyl ester by the corresponding α,ω-alkanediamine catalyzed by papain in ethanolic media. The compounds synthesised were tested as antimicrobials against 15 bacterial and 8 fungal species. The antimicrobial activity and selectivity depend strongly on the spacer chain length. The bis(PhAcArg) derivative with the spacer chain of 12 methylene groups gave the lowest MIC values against Gram-positive bacteria, whereas that with 14 methylene units was the best against Gram-negative bacteria. Interestingly, these novel compounds showed enhanced antibacterial activity relative to the lead compound, bis(N$^{\alpha}$-caproyl-L-arginine)-1,3-propanediamide dihydrochloride ($C_3(CA)_2$), and moderate antifungal activity. Moreover, tests of haemolytic activity toward human erythrocytes revealed that haemolysis increases with spacer chain length. Importantly, the compounds were classified as not irritating to eyes, with the exception of the compound with the spacer chain of 14 methylene groups, which was a slight eye irritant.

Introduction

The synthesis, physicochemistry, and biological activity of arginine fatty acid conjugates have been the focus of our attention during the last decade.[1–3] Arginine fatty acid conjugates are a class of amphiphilic compounds that possess excellent surface and interface activity, rich self-assembly behaviour, a low toxicity profile, high biodegradability, and broad antimicrobial activity.[4,5] These exceptional characteristics make them candidates of choice as preservatives and antiseptics in pharmaceutical, food, and dermatological formulations. Among the arginine-based surfactants synthesised by our research group, bis(*N*$^{\alpha}$-caproyl-L-arginine)-1,3-propanediamide dihydrochloride ($C_3(CA)_2$), a novel dimeric (that is, double-chain/double-polar-head compound), showed the lowest minimum inhibitory concentration (MIC) values against a broad spectrum of Gram-positive and Gram-negative bacteria.[6,7]

Biguanides are powerful antiseptics widely employed in many pharmaceutical and personal-care formulations. Chlorhexidine (CHX) is the most representative commercial biguanide compound. It possesses high efficacy against both Gram-positive and Gram-negative bacteria and low toxicity.[8,9] Interestingly, the MIC values of CHX are about 2- to 48-fold lower, depending on the microorganism, than those of $C_3(CA)_2$.[7] In general, microbicides lack target specificity, although in the case of biguanides such as CHX and cationic surfactants including $C_3(CA)_2$, the main target appears to be the cytoplasmic bacterial membrane.[7,8,10] Moreover, both biguanides and cationic surfactants share similar mechanisms of action.[11] Thus, structural factors and an appropriate hydrophobic–hydrophilic balance are mostly responsible for the various antimicrobial efficiencies observed. To improve the antimicrobial potency of arginine–lipid conjugates, we sought to design new arginine derivatives, namely bis(PhAcArg)s, analogues of $C_3(CA)_2$.

$C_3(CA)_2$ and CHX are both dicationic, and their positive charges are connected through a hydrocarbon spacer chain (Figure 1). As $C_3(CA)_2$ already has good antibacterial activity, we intended to keep structural changes in the molecule to a minimum. Hence, with the CHX structure in mind, we thought of substituting the two *N*$^{\alpha}$-caproyl groups of $C_3(CA)_2$ with two *N*$^{\alpha}$-phenylacetyl residues and to vary the length of the spacer alkyl chain (see Figure 1). The spacer chain length modulates the hydrophobic–hydrophilic balance, which influences the interfacial properties and therefore, the antimicrobial activity of

[a] *J. A. Castillo, Dr. M. R. Infante, Dr. P. Clapés*
Institute for Chemical and Environmental Research, CSIC
c/Jordi Girona 18-26, 08034 Barcelona (Spain)
Fax: (+33) 34 93 204 59 04
E-mail: pcsqbp@iiqab.csic.es

[b] *Dr. À. Manresa*
Department of Microbiology, Faculty of Pharmacy
University of Barcelona, Avgda. Joan XXIII s/n, 08028 Barcelona (Spain)

[c] *Dr. M. P. Vinardell, Dr. M. Mitjans*
Department of Physiology, Faculty of Pharmacy
University of Barcelona, Avgda. Joan XXIII s/n, 08028 Barcelona (Spain)

Supporting information for this article is available on the WWW under http://www.chemmedchem.org or from the author.

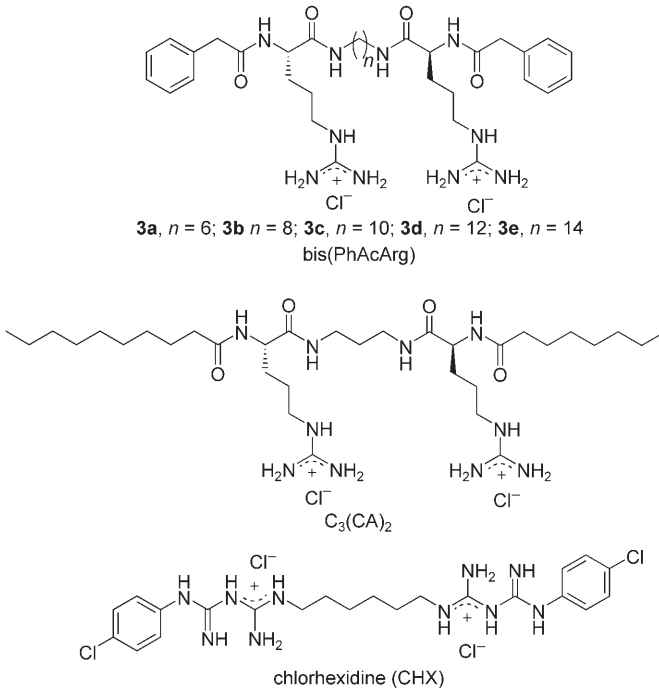

Figure 1. Structures of bis(PhAcArg), $C_3(CA)_2$, and CHX.

the molecule.[12] Based on previous work[1,13] with dimeric arginine derivatives, alkanediamine spacers of 6, 8, 10, 12, and 14 methylene groups were chosen as the most appropriate.

Herein we report the chemoenzymatic synthesis of these new bis(PhAcArg) derivatives and their antimicrobial activity against 15 bacterial and 8 fungal species. Moreover, to assess cytotoxicity and the potential for acute eye irritation, we determined their haemolytic and protein denaturation effects on erythrocytes and compared those with the effects observed in the presence of CHX by using a quick in vitro screening test.

Results and Discussion

Chemoenzymatic synthesis of bis(PhAcArg) derivatives

Based on our previous work in the chemoenzymatic preparation of arginine-based gemini surfactants,[2] the synthesis of the new bis(PhAcArg) amphiphiles was initially planned in four steps (Scheme 1).

The first two steps, esterification of the α-carboxyl group of the arginine moiety (98%) and acylation of the α-amine with phenylacetyl chloride (73%) gave access to intermediate **1**. The third step was the aminolysis of the α-methyl carboxylate group of **1** by one of the amino groups of the α,ω-alkanediamine. This reaction took place without any catalyst in good yield (Table 1) by using 5–7 equiv diamine at temperatures above the melting point of the given diamine, which acted as solvent and reagent. Derivatives **3a**–**3e** were then obtained by papain-catalysed amidation of **1** by **2** in ethanol/boric acid–borate buffer (0.1 M, pH 8.2, 99.5:0.5) in good yield (Table 2). The final purification steps required to afford highly pure products lead to moderate overall yields. The enzymatic amide bond formation failed for the reaction between **1** and α,ω-tetradecyldiamine. Excess diamine from the previous step that had not been eliminated by simple washings appears to be responsible for the low conversion. In fact, it had been observed that the diamines had a negative effect on papain activity by either acting as an inhibitor or by modifying the enzyme ionization state owing to the basicity of the product.[2]

To avoid the presence of excess diamine, the formation of bis(PhAcArg) in a one-pot enzymatic reaction was undertaken, starting from the diamine and 2 equiv compound **1**. Interestingly, the new synthetic enzymatic scheme furnished bis(PhAcArg) in three

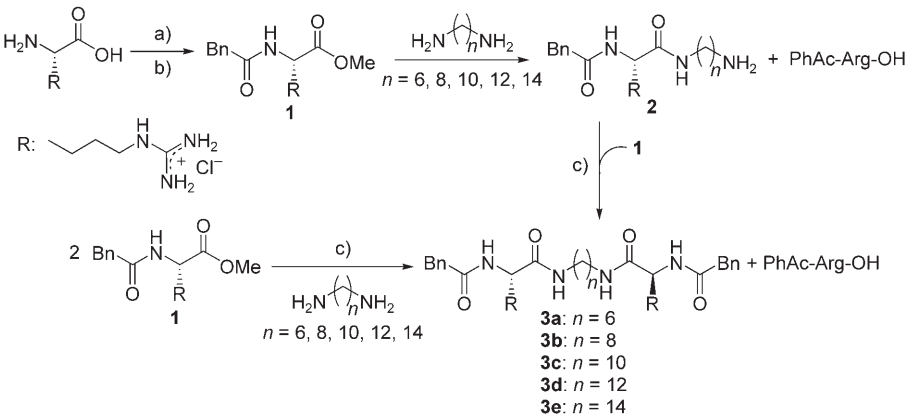

Scheme 1. Chemoenzymatic synthesis of bis(PhAcArg) derivatives: a) $SOCl_2$/MeOH; b) BnCOCl; c) Papain onto celite, EtOH/boric acid–borate buffer (99.5:0.5). Bn = benzyl.

Table 1. Aminolysis of **1** by α,ω-alkanediamines of various length.

$H_2N(CH_2)_nNH_2$	T [°C]	PhAc-Arg-OH[a] [%]	Product **2** [%][a,b]	Product **3** [%][a]
$n=6$	50	6	90	6
$n=8$	55	9	85	9
$n=10$	66	7	88	7
$n=12$	72	6	87	6
$n=14$	100	8	87	8

[a] Molar percent conversion into the corresponding product with respect to PhAc-Arg-OMe (compound **1**) measured by HPLC of the crude reaction mixture using purified standards; reaction time: 2 h. [b] Isolated yields were not calculated, as a simple workup was performed to remove excess diamine; therefore, the final product contained PhAc-Arg-OH and product **3**.

Table 2. Papain-catalyzed amide bond formation between **1** and **2**.

Product	Conversion [%][a]	PhAc-Arg-OH [%][a]	Isolated Yield [%]
3a	48	38	25
3b	48	29	21
3c	54	34	27
3d	58	25	26
3e	27	65	nr[b]

[a] Molar percent conversion into the corresponding product with respect to PhAc-Arg-OMe (compound **1**) measured by HPLC of the crude reaction mixture using purified standards; reaction time: 72 h; 1.5 equiv **2** per mol PhAc-Arg-OMe. [b] No reaction.

steps at room temperature and with reaction conversions similar to those obtained by the procedure described above (Table 3). Most importantly, this strategy allowed us to prepare the bis(PhAcArg) **3e** with α,ω-tetradecyldiamine in isolated yields similar to those obtained with shorter spacer chain lengths.

Antibacterial activity

Minimum inhibitory concentration (MIC) values for **3a**–**e** along with those for $C_3(CA)_2$ and CHX are summarised in Table 4. To compare compounds with different molecular weights precisely, MIC values are expressed in μM instead of the typical mg L^{-1}. For the novel bis(PhAcArg) series **3**, there is a clear effect of the spacer chain length on antimicrobial property. Overall, the lowest MIC values against Gram-positive bacteria were observed with **3d** (12 methylene groups in the spacer chain), whereas **3e** (14 methylene groups) showed the most potent inhibition of growth toward Gram-negative bacteria.

Table 3. Papain-catalyzed synthesis of **3** in one-pot reaction.

Product	PhAc-Arg-OH [%][a]	Product **2** [%][a]	Product **3** [%][a]
3a	13	16	55
3b	11	19	59
3c	11	17	55
3d	13	19	59
3e	10	20	37

[a] Molar percent conversion into the corresponding product with respect to PhAc-Arg-OMe (compound **1**) measured by HPLC of the crude reaction mixture using purified standards; reaction time: 176 h; 1.1 equiv α,ω-alkanediamine per mol PhAc-Arg-OMe.

Gram-negative are generally more resistant to antimicrobial agents than are Gram-positive bacteria. This can be explained by the different cell envelope structure of the two bacterial types. Gram-negative bacteria possess an outer membrane composed mainly of lipopolysaccharides and porins which restrict the entrance of biocides and amphiphilic compounds.[14,15] The perturbation of this outer membrane requires a fine tuning of the hydrophobic–hydrophilic balance of the microbicide molecule.[4] Gram-positive bacteria possess a thick, rigid, and highly porous cell wall of peptidoglycans. Thus, small hydrophilic molecules such as penicillin can move through it without difficulty, allowing easy penetration of compounds into the cell.[14] Moreover, bacteria often possess efflux proteins located in the cytoplasm membrane. These serve as a protective mechanism against antimicrobial activity by pumping antimicrobial molecules out of the cell.[16]

Table 4. MIC values (μM) for compounds **3a**–**e**, $C_3(CA)_2$, and CHX against bacteria.[a]

Species	**3a**	**3b**	**3c**	**3d**	**3e**	$C_3(CA)_2$	CHX
			Gram-positive				
Bacillus cereus var. mycoides	>323	>307	78	18	18	21	2
Staphylococcus epidermidis	>323	19	39	2	36	10	2
Bacillus subtilis	>323	154	39	2	36	21	2
Staphylococcus aureus	>323	77	19	5	36	3	1
Micrococcus luteus	>323	154	19	18	71	21	2
Enterococcus hirae	>323	>307	156	10	36	10	3
Mycobacterium phlei	>323	77	19	nd	nd	21	nd
Mycobacterium smegmatis	nd	nd	nd	nd	36	10	3
			Gram-negative				
Bordetella bronchiseptica	>323	154	39	37	36	5	2
Pseudomonas aeruginosa	>323	>307	>311	149	71	42	14
Salmonella typhimurium	>323	>307	>311	75	36	42	7
Enterobacter aerogenes	>323	>307	>311	149	18	42	14
Escherichia coli	>323	154	156	37	18	10	3
Klebsiella pneumoniae	>323	>307	>311	149	18	21	7
Serratia marcescens	>323	>307	>311	>298	>286	>333	7

[a] MIC: the lowest concentration of compound required for the inhibition of growth of test strains; nd = not determined.

Compared with $C_3(CA)_2$, compounds **3d** and **3e** have enhanced activity against Gram-positive and Gram-negative bacteria, respectively. The different antimicrobial efficiency of these compounds can be attributed to the combination of several physicochemical parameters: hydrophobicity, adsorption, aqueous solubility, and transport in the test medium. As a measure of hydrophobicity, we estimated the log octanol–water partition coefficient (log *P*) of the compounds by using KowWin, software that is based on the atom/fragment contribution method.[17] The estimated values are as follows: **3a** 0.80, **3b** 1.78, **3c** 2.76, **3d** 3.74, **3e** 4.73, $C_3(CA)_2$ 3.77, and CHX 4.85. It is important to stress that these are estimated rather than experimental values. As expected, log *P* increased with increasing spacer chain length. Interestingly, the antimicrobial activity showed good correlation with log *P* for the bis(PhAcArg)s, in good agreement with QSAR studies of biguanide biocides.[12,18] The most active compounds, including CHX, have an estimated log *P* value in the range between 3.74 and 4.85. It has been observed that the spacer chain length modulates the lipophilicity of the molecule, but is not a key structur-

al parameter for antimicrobial activity.[12] The optimal length of the spacer chain depends on the structure and nature of the polar head groups as well as on the presence of other alkyl chains in the molecule.[1,6,19] Therefore, antimicrobial activity cannot be determined by any given individual structural moiety alone. It is the right combination of positive charges and hydrophobic groups that provide the adequate hydrophilic–lipophilic balance.[20]

Apart from high activity (that is, high preservation capacity), a balance between antimicrobial activity on one hand, and low toxicity and efficient biodegradability on the other is always pursued. Hence, the relatively low activity against Gram-negative bacteria may facilitate the subsequent biodegradability of these compounds, thus decreasing their environmental impact.

Antifungal activity

The MIC values for compounds **3a**–**e**, $C_3(CA)_2$, and CHX against two yeast species and six molds are shown in Table 5. Similarly to the antibacterial activity, the results for the novel bis-(PhAcArg) series **3** against fungi indicate that there is a clear effect of the spacer chain length on antimicrobial properties. Antifungal capacity increases with increasing spacer chain length; compounds **3a** and **3b** did not show antimicrobial activity in the concentration range tested; an increase in spacer chain length did increase the antifungal effect (compounds **3c**–**e**). However, $C_3(CA)_2$ and CHX are more potent than compounds **3.** These results suggest again that the amphipathicity is the key parameter for activity.

Compounds **3c**–**e**, $C_3(CA)_2$, and CHX showed both antibacterial and antifungal activity. Fungi are eukaryotic organisms, and in many instances, antibacterial agents have no effect on them. An exception to this are the cationic biocides, the primary target of which are the bacterial cytoplasmic and fungal plasma membranes.[21]

The mechanism of action of some antifungal compounds is related to the inhibition of ergosterol biosynthesis, among other metabolic pathways.[22] However, the mode of action of amphiphilic fungicides is still poorly understood. Some amphiphilic fungicides such as amphotericin B and nystatin bind to ergosterol which disrupts membrane function and increases permeability, thus causing cell lysis.[22] Pentamidine analogues are dicationic aromatic compounds with antifungal activity equal or greater than that of fluconazole and amphotericin B.[23] The mitochondrion appears to be the primary cellular target of these compounds.[24]

Therefore, the mode of antifungal action of **3c**–**e** could be mostly through a perturbation of the plasma membrane, likely by binding to ergosterol, among other things. Furthermore, a potential effect on mitochondrial processes might be also considered; as this action requires the uptake of the compound through the membrane, an accurate lipophilic–hydrophilic balance of the molecule is also required.

Haemolytic effect and potential ocular irritation

In many cases, antimicrobial agents that kill or inhibit the growth of microbial cells can also be cytotoxic to others such as red blood cells. The determination of haemolytic action is a good way to discriminate cytotoxic from non-cytotoxic compounds and also to asses the potential for acute eye irritation.[25] Compounds **3a**, **3b**, and **3c** showed low haemolytic activity at the highest concentration tested and did not induce haemoglobin denaturation. Compounds **3d**, **3e**, and CHX showed haemolytic activity, and the results of haemolysis obtained at different concentrations are presented in a dose–response curve (Figure 2).

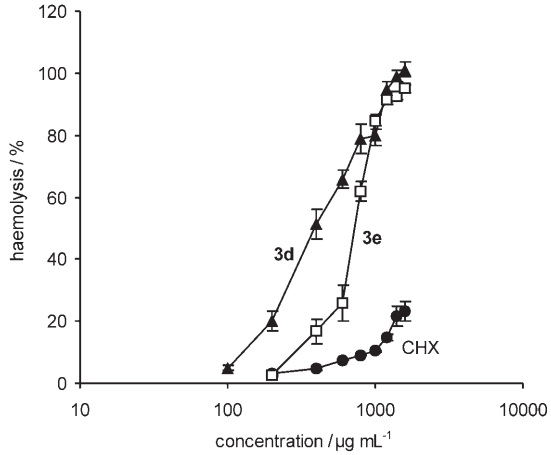

Figure 2. Haemolysis induced by **3d** (▲), **3e** (□), and CHX (●). Values are expressed as the mean ± SD of three experiments.

Table 5. MIC values (μM) for compounds **3a**–**e**, $C_3(CA)_2$, and CHX against fungi.

Fungi	3a	3b	3c	3d	3e	$C_3(CA)_2$	CHX
			Yeast				
Candida albicans	>323	>319	312	149	143	166	55
Saccharomyces cerevisiae	>323	>319	156	149	143	166	28
			Moulds				
Aspergillus repens	>323	319	78	19	36	5	7
Aspergillus niger	>323	>319	312	75	72	10	55
Penicillium chrysogenum	>323	>319	312	75	143	83	28
Cladosporium cladosporoides	>323	160	78	37	18	5	7
Trychophyton mentagrophytes	>323	>319	312	149	72	21	14
Penicillium funiculosum	>323	160	78	19	18	21	7

The values of HC_{50} for **3d**, **3e**, and CHX are presented in Table 6 along with the denaturation index (DI) and the lysis/denaturation ratio (L/D). From the L/D data, CHX and **3d** can be considered as nonirritant to the eyes, whereas **3e** was a slight irritant. Interestingly, CHX, **3d**, and **3e** were lesser irritants than $C_3(CA)_2$, which was found to be a moderate irritant and more haemolytic.[26] In the pres-

Table 6. Haemolytic data of **3d**, **3e**, and CHX determined with human erythrocytes.

Parameter	**3d**	**3e**	CHX
HC_{50} [$\mu g\,mL^{-1}$][a]	1002 ± 81	366 ± 4	2525 ± 270
DI[b]	0	8 ± 1	0
L/D[c]	∞	46	∞
Classification	Nonirritant	Slight irritant	Nonirritant

[a] Concentration giving 50% haemolysis; values expressed as the mean $\pm$SD. [b] Denaturation index. [c] Lysis/denaturation ratio.

ent study, CHX showed an HC_{50} value higher than that previously reported for which rabbit blood cells were used.[27] This could be attributed to both the different erythrocyte sources (human versus rabbit blood cells) and the different methodologies employed.[28] Human erythrocytes have been proven to be more resistant than those from other species.[29]

When the compounds were added to the erythrocyte suspension in aqueous medium, they could first distribute between the erythrocyte membrane and the solution by adsorption until equilibrium is reached. The interaction between the compound and erythrocyte membrane at sublytic concentration might be governed by the partition of the compound between the aqueous medium and the membrane. This partitioning is closely related to both the hydrophobicity of the compound and the ionic interactions present. Haemolysis probably begins when the erythrocyte membranes are saturated with the given compound. Herein, a good correlation (that is, exponential relationship) was observed between the haemolysis induced by compounds **3a**–**e** at 1000 $\mu g\,mL^{-1}$ and the number of methylene units in the spacer chain (Figure 3). Various examples of the relationship between haemolysis and alkyl chain length of surfactants have been published.[26,30] Overall, the longer the alkyl chain length, the greater the haemolytic activity within a family of structurally related compounds.

Despite the fact that the log*P* values of CHX, **3e**, and $C_3(CA)_2$ are similar, CHX showed lower haemolytic activity. It was observed that the interfacial activity of CHX was much lower than that of $C_3(CA)_2$; therefore, this may also be an important parameter to consider.[7] Again, the right combination of more than one parameter may explain the overall activity of the compounds.

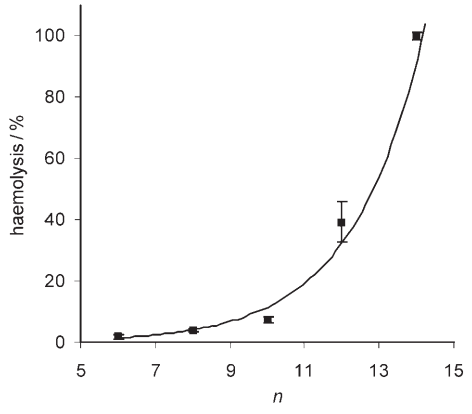

Figure 3. Haemolytic activity of **3a**–**e** at 1000 $\mu g\,mL^{-1}$ as a function of the number of methylene units (*n*) on the spacer chain. Results are expressed as mean $\pm$SD of three experiments; $R^2 = 0.986$ for the fitted curve.

Conclusions

In conclusion, the synthesis of novel bis(N^{α}-phenylacetyl-L-arginine)-α,ω-alkanediamide dihydrochloride (bis(PhAcArg)) derivatives can be carried out by an effective chemoenzymatic strategy in good reaction conversions. The key step in the synthesis is the papain-catalysed amide bond formation between the N^{α}-phenylacetyl arginine methyl ester and the corresponding α,ω-alkanediamine.

Replacement of the N^{α}-caproyl groups in $C_3(CA)_2$ by N^{α}-phenylacetyl moieties lead to novel bis(PhAcArg) compounds with enhanced antibacterial activity but lower antifungal activity than that of either $C_3(CA)_2$ or CHX. The cytoplasmic bacterial and plasma fungal membranes appear to be the target of these new arginine conjugates. The results suggest that the lipophilic–hydrophilic balance is crucial for antimicrobial activity and selectivity. Finally, the products showed low haemolytic activity against human erythrocytes and therefore low potential for ocular irritation and cytotoxicity.

Experimental Section

Chemicals and reagents: Chlorhexidine dihydrochloride, phenylacetyl chloride, oxalyl chloride and 1,12-dodecanedicarboxylic acid were obtained from Aldrich. Arginine hydrochloride, lithium sodium hydride, 1,10-diaminodecane, 1,12-diaminododecane, 1,4-dithio-D,L-threitol (DTT), and celite 545 (particle size, 26 μm; mean pore diameter, 17000 nm; specific surface area (BET method), 2.19 $m^2\,g^{-1}$) were obtained from Fluka. Papain (EC 3.4.22.2) from *Carica papaya* crude powder was obtained from Sigma (1.7 $U\,mg^{-1}$ protein; one unit (U) causes the hydrolysis of 1.0 $mmol\,min^{-1}$ benzyl-L-arginine ethyl ester (BAEE) at pH 6.2, 25 °C). 1,6-Diaminohexane and 1,8-diaminooctane were purchased from Merck. Ammonia was obtained from Praxair. bis(N^{α}-Caproyl-L-arginine)-1,3-propanediamide dihydrochloride ($C_3(CA)_2$) was synthesised in our laboratory by following previously described procedures.[2] Tetrahydrofuran and dichloromethane were distilled over sodium and CaH_2, respectively, just before use. All other solvents and reagents were of analytical grade and were used without further purification. Human blood from healthy volunteers was obtained from the Blood Bank of the Hospital Clinic (Barcelona, Spain).

Instruments: ^{1}H NMR (500 MHz) spectra of compounds were recorded with a Varian Unity-500 spectrometer, and ^{13}C NMR (100 MHz) spectra, with a Varian Unity-400. IR spectra of compounds in KBr tablets were recorded with a Nicolet Avatar 360 FTIR instrument. Elemental analyses were performed by Servei de Microanàlisi Elemental at Instituto de Investigaciones Químicas y Ambientales (IIQAB-CSIC). Specific rotations were measured with a Perkin–Elmer Model 341 polarimeter. Mass spectrometric data were obtained using MALDI-TOF MS with a VOYAGER-DE-RP at the University of Barcelona. The melting point of 1,14-diaminotetradecane was determined with a Kofler apparatus.

Enzyme immobilization: Papain was immobilized by deposition onto celite 545. The procedure was the following: papain (500 mg)

and DTT (250 mg) were dissolved in boric acid–borate buffer (0.1 M, pH 8.2, 5 mL, 0.5% *v/v*). This solution was thoroughly mixed with celite 545 (5 g) and dried under vacuum (80 μbar) until constant weight was reached.

HPLC analysis: The amounts of acyl donor, product, and hydrolyzed acyl donor produced in the reactions were measured by HPLC (Merck-Hitachi, Licrograph) analysis using a Licrosphere 100 CN (propylcyano) column (5 μm, 250×4 mm). The solvent system used was: solvent A, trifluoroacetic acid (TFA) 0.1% (*v/v*) in H_2O, and solvent B, H_2O/ACN 1:4, TFA 0.095% (*v/v*); flow rate 1 mL min^{-1}; detection at $\lambda = 215$ nm. Samples (50 μL) were withdrawn from the reaction medium at various times (0–96 h) depending on the synthesis and were diluted with EtOH (800 μL).

Preparation of 1,14-diaminotetradecane: 1,12-Dodecanedicarboxylic acid (5.6 g, 21.8 mmol) and DMF (1.68 mL, 21.8 mmol) were dissolved in hexanes (350 mL), and the mixture was cooled at 4 °C. To this solution, oxalyl chloride (0.2 mol) was added dropwise over a period of 30 min, and then the mixture was allowed to react at room temperature overnight. The reaction mixture started as a white suspension and ended as a transparent solution with brown oily precipitated drops on the reactor wall. The solvent was evaporated under vacuum, and the residue was dissolved in freshly distilled CH_2Cl_2. This solution was saturated by NH_3 at 4 °C, and a white precipitate formed immediately. The reaction mixture was left to proceed at room temperature overnight. The solvent and excess NH_3 were then removed under vacuum. The solid obtained was washed with cold water and cold EtOAc and finally dried under vacuum to afford 1,12-dodecanediamide as a brown solid (6.4 g, 98% yield); ^{1}H NMR (500 MHz, [D$_6$]DMSO, 40 °C): $\delta = 7.16$ (s, 2H), 6.57 (s, 2H), 2.09–1.92 (m, 4H), 1.58–1.38 (m, 4H), 1.24 ppm (s, 16H); ^{13}C NMR (100 MHz, [D$_6$]DMSO, 40 °C): $\delta = 174.14$, 34.95, 28.78, 28.73, 28.58, 28.51, 24.90 ppm; IR (KBr): $\tilde{\nu} = 3387$, 3189, 2923, 2848, 1650, 1416, 1337, 1281, 1230, 1179, 1122, 799, 646 cm^{-1}.

The 1,12-dodecanediamide thus obtained (2.5 g, 9.73 mmol) was added to a solution of $LiAlH_4$ (1.5 g, 40 mmol) in freshly distilled THF (0.5 L) at 4 °C. The reaction proceeded overnight at reflux to favour the solubility of the diamide. The reaction was stopped by slow and careful addition of cold water. The solid obtained was filtered off, and the filtrate was dried under vacuum to afford 1,14-diaminotetradecane as a white solid (1.6 g, 70% yield); ^{1}H NMR (500 MHz, [D$_6$]DMSO, 40 °C): $\delta = 1.35$–1.28 (m, 4H), 1.24 ppm (s, 24H); ^{13}C NMR (100 MHz, [D$_6$]DMSO, 40 °C): $\delta = 41.52$, 33.29, 28.86, 28.81, 28.79, 26.24 ppm; IR (KBr): $\tilde{\nu} = 3335$, 3251, 2923, 2846, 1603, 1461, 1319, 1062, 1004, 920, 714 cm^{-1}.

Preparation of N^{α}-phenylacetyl-L-arginine methyl ester hydrochloride (PhAc-Arg-OMe·HCl) (1): L-Arginine hydrochloride (20.0 g, 94.9 mmol) was suspended in MeOH (0.5 L) and cooled to ≈ −40 °C. $SOCl_2$ (50 mL, 0.69 mol) was added dropwise to this suspension over a period of one hour. Afterward the mixture was stirred at room temperature for 48 h to obtain a clear solution. The solvent, excess $SOCl_2$, and HCl generated were then removed under vacuum by repeated addition of EtOH until a solid residue was formed. The residue was filtered, washed with Et_2O, and dried to afford L-arginine methyl ester dihydrochloride as a white solid (24.2 g, 98% yield). The L-arginine methyl ester hydrochloride thus obtained (10.0 g, 38.29 mmol) was dissolved with ACN/H_2O (15:1). $NaHCO_3$ (6.4 g, 76.2 mmol) and Na_2CO_3 (10.1 g, 95.3 mmol) were added to this solution. The mixture was cooled with ice water, and phenylacetyl chloride (5.6 mL, 42.12 mmol) was added dropwise. The reaction medium was stirred overnight at room temperature. The resulting mixture was filtered, acidified to pH 1–2, and the solvent was removed under vacuum. The residue was dissolved in water (80 mL) and washed with EtOAc (3×100 mL), and the aqueous phase was lyophilized. The solid thus obtained was suspended in cool EtOH to precipitate the salts, which were filtered out. This desalting process was repeated three times. Finally, the ethanol was evaporated under vacuum, the residue was dissolved in water and lyophilized to afford the title compound as a white solid (9.83 g, 75% yield).

Preparation of bis(N^{α}-phenylacetyl-L-arginine)-α,ω-dialkylamide dihydrocloride (3): *a) Two-step procedure; step 1: Preparation of N^{α}-phenylacetyl-L-arginine(ω-aminoalkyl)amide monohydrochloride derivatives (PhAc-Arg-NH-(CH$_2$)$_n$-NH$_2$·HCl)* ***2***: PhAc-Arg-OMe·HCl **1** (4.0 g, 11.67 mmol) was mixed with the corresponding α,ω-diaminoalkane (81.70 mmol). The mixture was heated at different temperatures depending on the diamine: 50 °C for 1,6-diaminohexane, 55 °C for 1,8-diaminooctane, 66 °C for 1,10-diaminodecane, 72 °C for 1,12-diaminododecane, and 100 °C for 1,14-diaminotetradecane to obtain a homogeneous mixture after few minutes. After 1.5 h, the reactions were quenched by adding EtO_2 (25 mL for **2a**), ACN/EtO_2 (1:1, 25 mL for **2b**), or ACN/EtO_2 (2:1, 25 mL for **2c** and **2d**); for compound **2e**, see text. The resulting mixture was stirred, sonicated at room temperature, and finally cooled at −40 °C. The precipitate thus obtained was collected and washed with EtO_2 (2× 25 mL). Finally, the solid was dried under vacuum to yield the title compound. These intermediate products were identified by MS: **2a**, *m/z* [M^++1]: 391; **2b**, *m/z* [M^++1]: 419; **2c**, *m/z* [M^++1]: 447; and **2d**, *m/z* [M^++1]: 475.

a) Step 2: *Preparation of bis(PhAcArg) (**3**)*: The corresponding compounds **2** (13.30 mmol) and **1** (3.04 g, 8.87 mmol) were dissolved in EtOH (150 mL) free of O_2 and dried over molecular sieves (3 Å). Aqueous boric acid–borate buffer (0.1 M, pH 8.2, 0.75 mL, 0.5% *v/v*) was added To this solution. The mixture was stirred and sonicated thoroughly to obtain a homogeneous solution. Then, the immobilized papain preparation (17 g) was added. The reaction mixture was placed in a reciprocal shaker (125 rpm) at 25 °C under argon atmosphere. After 72 h, MeOH (100 mL) was added, and the immobilized preparation was filtered off and washed with MeOH (3× 100 mL). The organic phases were pooled, and the solvent was evaporated under vacuum. The residue was purified first by ion-exchange chromatography and then by preparative HPLC as described below.

b) One-pot procedure: PhAc-Arg-OMe·HCl (24 mg, 0.07 mmol) and the corresponding α,ω-alkanediamine (0.04 mmol) were dissolved in EtOH (1 mL) free of O_2 and dried over molecular sieves (3 Å). Boric acid–borate buffer (0.1 M, pH 8.2, 5 μL, 0.5% *v/v*) was added to this solution. The immobilized papain preparation (100 mg) was then added, and the reaction mixture was placed in a reciprocal shaker (125 rpm) at 25 °C under argon atmosphere. After 72 h, the reaction was stopped, worked up as previously described (see above), and the residue was purified first by ion-exchange chromatography and then by preparative HPLC as described below.

Preparative ion-exchange chromatography: Purification by preparative ion-exchange chromatography was performed as follows. The crude product was loaded onto a preparative column (285 cm^3) filled with MacroPrep High S, 50 μm stationary phase. The flow rate was 50–80 mL min^{-1}. Impurities were first eluted using NaCl (40 mM) in boric acid–borate (10 mM, pH 9.5) aqueous buffer/ethanol 40:60. The products, bis(PhAcArg), were finally eluted with NaCl (0.5 M) in H_2O/EtOH 40:60. Analysis of the fractions was carried out by HPLC under conditions used for monitor-

ing the reaction. The fractions with the reaction product were further purified by preparative HPLC.

Preparative HPLC: Purification by preparative HPLC was performed as follows. The crude products were loaded onto a preparative PrepPak (Waters) column (47×300 mm) filled with Delta-Pak C4, 300 Å, 15 μm stationary phase. Products were eluted using ACN gradients in 0.1% aqueous TFA: 20–36% in 30 min for **3a**, 15–30% in 30 min for **3b**, 19–34% in 30 min for **3c**, 23–38% in 30 min for **3d** and 16–32% in 30 min for **3e.** The flow rate was 80 mL min^{-1}, and the products were detected at $\lambda = 254$ nm. Analysis of the fractions was carried out by analytical HPLC under isocratic conditions: 41% solvent B for **3a**, 45% B for **3b**, 49% B for **3c**, 53% B for **3d**, and 59% B for **3e**. The pure fractions were pooled and lyophilized in the presence of aqueous HCl (37%, 2 equiv) to obtain the products in hydrochloride form.

Bis(N^{α}-phenylacetyl-L-arginine)-1,6-hexanediamide dihydrochloride (3a): The title compound was prepared by following the general methodology described above (a) (1.05 g, 13% isolated yield), 98% purity by HPLC: gradient elution 10–70% B in 30 min, retention factor (k') = 6.94; $[\alpha]_D^{20} = -25.3$ ($c = 1.0$ in methanol); IR (KBr): $\tilde{\nu}$ = 3258, 3165, 2930, 2853, 1650, 1537, 1445, 1347, 1250, 1168, 702 cm^{-1}; ^{1}H NMR (500 MHz, [D$_4$]CH$_3$OH, 22 °C): $\delta = 7.36$–7.17 (m, 10H), 4.31 (dd, J = 8.46, 5.58 Hz, 2H), 3.60 (m, 4H), 3.16 (m, 8H), 1.93–1.51 (m, 8H), 1.45 (s, 4H), 1.28 ppm (s, 4H); ^{13}C NMR (75 MHz, [D$_4$]CH$_3$OH, 22 °C): δ = 174.22, 173.85, 158.53, 136.83, 130.24, 129.63, 127.99, 54.71, 43.56, 41.92, 40.16, 30.33, 30.12, 27.28, 26.47 ppm; elemental analysis calcd (%) for $C_{34}H_{54}Cl_2N_{10}O_4 \cdot 3H_2O$ (791.8): C 51.57, H 7.64, N 17.69, found: C 51.56, H 7.56, N 17.56.

Bis(N^{α}-phenylacetyl-L-arginine)-1,8-octanediamide dihydrochloride (3b): The title compound was prepared following the general methodology described above (a) (1.37 g, 21% isolated yield), 99% purity by HPLC: gradient elution 10–70% B in 30 min, k' = 8.5; $[\alpha]_D^{20} = -23.0$ ($c = 1.0$ in methanol); IR (KBr): $\tilde{\nu}$ = 3268, 3155, 2930, 2853, 1650, 1537, 1455, 1358, 1250, 1163, 697 cm^{-1}; ^{1}H NMR (500 MHz, CD$_3$OD): $\delta = 7.34$–7.20 (m, 10H), 4.31 (m, 2H), 3.59 (m, 4H), 3.16 (s, 8H), 1.83 (s, 2H), 1.74–1.50 (m, 6H), 1.46 (s, 4H), 1.32–1.25 ppm (m, 8H); ^{13}C NMR (101 MHz, CD$_3$OD): δ = 174.17, 173.70, 158.56, 136.87, 130.21, 129.66, 128.03, 54.48, 43.63, 41.96, 40.42, 30.40, 30.32, 30.21, 27.78, 26.44 ppm); elemental analysis calcd (%) for $C_{36}H_{58}Cl_2N_{10}O_4 \cdot 2H_2O$ (801.9): C 53.92, H 7.79, N 17.47, found: C 54.14, H 7.83, N, 17.63.

Bis(N^{α}-phenylacetyl-L-arginine)-1,10-decanediamide dihydrochloride (3c): The title compound was prepared following the general methodology described above (a) (1.61 g, 27% isolated yield), 98% purity by HPLC: gradient elution 10–70% B in 30 min, k' = 10.0; $[\alpha]_D^{20} = -22.4$ ($c = 1.0$ in methanol); IR (KBr): $\tilde{\nu}$ = 3268, 3176, 2925, 2848, 1650, 1537, 1455, 1358, 1245, 1163, 692 cm^{-1}; ^{1}H NMR (300 MHz, CD$_3$OD): $\delta = 7.34$–7.19 (m, 10H), 4.31 (dd, J = 8.64, 5.55 Hz, 2H), 3.59 (m, 4H), 3.16 (m, 8H), 1.95–1.36 (m, 12H), 1.36–1.16 ppm (m, 12H); ^{13}C NMR (75 MHz, CD$_3$OD): δ = 174.17, 173.72, 158.54, 136.86, 130.21, 129.63, 127.99, 54.52, 43.63, 41.94, 40.46, 30.57, 30.36, 27.91, 26.42 ppm; elemental analysis calcd (%) for $C_{38}H_{62}Cl_2N_{10}O_4 \cdot 3/2H_2O$ (820.9): C 55.60, H 7.98, N 17.06, found: C 55.41, H 8.12, N 16.80.

Bis(N^{α}-phenylacetyl-L-arginine)-1,12-dodecanediamide dihydrochloride (3d): The title compound was prepared following the general methodology described above (a) (1.45 g, 26% isolated yield), 97% purity by HPLC: gradient elution 10–70% B in 30 min, k' = 11.2; $[\alpha]_D^{20} = -21.2$ ($c = 1.0$ in methanol); IR (KBr): $\tilde{\nu}$ = 3278, 3170, 2920, 2848, 1639, 1537, 1455, 1358, 1250, 1163, 692 cm^{-1}; ^{1}H NMR (300 MHz, CD$_3$OD): $\delta = 7.37$–7.18 (m, 10H), 4.39–4.24 (m, 2H), 3.59 (m, 4H), 3.16 (m, 8H), 1.94–1.37 (m, 12H), 1.36–1.20 ppm (m, 16H); ^{13}C NMR (75 MHz, CD$_3$OD): δ = 174.17, 173.81, 158.56, 136.87, 130.21, 129.64, 128.00, 54.53, 43.69, 43.65, 41.95, 40.61, 40.48, 30.72, 30.67, 30.42, 30.38, 27.96, 26.41 ppm; elemental analysis calcd (%) for $C_{40}H_{66}Cl_2N_{10}O_4 \cdot 2H_2O$ (858.0): C 56.00, H 8.22, N 16.33, found: C 56,31, H 8,39, N 16,38.

Bis(N^{α}-phenylacetyl-L-arginine)-1,14-tetradecanediamide dihydrochloride (3e): The title compound was prepared following the general methodology described above (b) (1.80 g, 26% isolated yield), 98% purity by HPLC: gradient elution 10–70% B in 40 min, k' = 12.4; $[\alpha]_D^{20} = -22.0$ ($c = 1.0$ in methanol); IR (KBr): $\tilde{\nu}$ = 3283, 3165, 2920, 2848, 1644, 1537, 1455, 1358, 1250, 1158, 718 cm^{-1}; ^{1}H NMR (500 MHz, CD$_3$OD): $\delta = 7.35$–7.20 (m, 10H), 4.31 (dd, J = 8.46, 5.70 Hz, 2H), 3.59 (m, 4H), 3.16 (m, 8H), 1.83 (m, 2H), 1.74–1.50 (m, 6H), 1.50–1.41 (m, 4H), 1.29 ppm (s, 20H); ^{13}C NMR (101 MHz, CD$_3$OD): δ = 174.20, 173.68, 158.55, 136.84, 130.19, 129.65, 128.02, 54.43, 43.65, 41.94, 40.49, 30.80, 30.77, 30.71, 30.45, 30.37, 27.97, 26.39 ppm; elemental analysis calcd (%) for $C_{42}H_{70}Cl_2N_{10}O_4 \cdot 5/2H_2O$ (895.0): C 56.36, H 8.45, N 15.65, found: C 56.52, H 8.43, N 15.63.

Minimum inhibitory concentration (MIC): The MIC values of **3a**–**e**, $C_3(CA)_2$, and CHX, were determined in vitro by using a broth microdilution assay.[31] Muller Hinton broth (Scharlau Chemie, Barcelona, Spain) was used for the antibacterial test, and Sabouraud liquid medium (ADSA Micro, Barcelona, Spain) was used for the antifungal test. Serial dilutions of compounds between 256 and 0.25 mg L^{-1} final concentration in the corresponding liquid medium were dispensed into 96-well polystyrene microtitre plates (Nunc, Roskilde, Denmark). The corresponding dilutions were inoculated with a suspension of the test organism on the corresponding liquid medium to a final concentration of $\approx 10^4$ CFU mL^{-1} (CFU = colony-forming unit). MIC is defined as the lowest concentration of antimicrobial agent that visibly inhibits the development of bacterial or fungal growth after 24 h at 37 °C and 48–72 h at 30 °C, respectively. Experiments were conducted in duplicate.

Microorganisms: The microorganisms used were: Gram-positive bacteria (eight): *Bacillus cereus var. mycoides* ATCC 11778, *Staphylococcus epidermidis* ATCC 12228, *Bacillus subtilis* ATCC 6633, *Staphylococcus aureus* ATCC *6538*, *Micrococcus luteus* ATCC 9341, *Enterococcus hirae* ATCC 10541, *Mycobacterium phlei* ATCC 41423, and *Mycobacterium smegmatis* ATCC 3017. Gram-negative bacteria (seven): *Bordetella bronchiseptica* ATCC 4617, *Pseudomonas aeruginosa* ATCC 9027, *Salmonella typhimurium* ATCC 14028, *Enterobacter aerogenes* ATCC 13048, *Escherichia coli* ATCC 8739, *Klebsiella pneumoniae* ATCC 4352, and *Serratia marcescens* ATCC 274. Fungi: Yeasts (two): *Candida albicans* ATCC 10231 and *Saccharomyces cerevisiae* ATCC 9763; Moulds (six): *Aspergillus repens* ATCC 28604, *Aspergillus niger* ATCC 16404, *Penicillium chrysogenum* ATCC 9480, *Cladosporium cladosporoides* ATCC 16022, *Trychophyton mentagrophytes* ATCC 18748, and *Penicillium funiculosum* CECT 2914.

Haemolysis assays: Erythrocytes were washed three times in isotonic phosphate saline buffer (PBS, pH 7.4): Na_2HPO_4 (22.2 mM), KH_2PO_4 (5.6 mM), NaCl (123.3 mM), and glucose (10.0 mM). The cells (8×10^9 cell mL^{-1}) were then suspended in isotonic saline solution (NaCl 0.9%). Different volumes (10–80 μL) of stock solutions of compounds (20 mg mL^{-1}) were mixed with PBS in polystyrene tubes to a final volume of 1 mL; the final concentrations of products ranged from 200 to 1600 μg mL^{-1}. Aliquots of erythrocyte suspension (25 μL) were added to these solutions, and the mixtures were incubated for 10 min with constant shaking at room temperature. After incubation, the tubes were centrifuged at 1500 *g* over

5 min. The percent haemolysis was then determined by comparing the absorbance ($\lambda = 540$ nm) of the supernatant with that of control samples totally haemolysed with distilled water.[25] The dose–response curve was determined from the haemolysis results, and the concentration that induces the haemolysis of 50% of the cells (HC_{50}) was calculated.

The potential ocular irritation of the compounds was studied with a method based on the haemolysis test (cell lysis) and the damage caused to the cellular proteins by the compound (denaturation). The irritation index was determined according to the lysis/denaturation ratio (L/D) obtained by dividing the HC_{50} value (in $\mu g\,mL^{-1}$) by the denaturation index (DI). The DI of each compound was measured by comparing the haemoglobin denaturation (D) induced by the compound and by sodium dodecyl sulphate (SDS) as positive control. Haemoglobin denaturation was determined after inducing haemolysis by adding SDS ($10\,mg\,mL^{-1}$) to the erythrocytes and measuring the absorption ratio of the supernatant at $\lambda =$ 575 nm and $\lambda = 540$ nm. The resulting L/D ratio was used instead of the ocular irritancy score in the acute phase of in vivo evaluation. The compounds can be classified according to this L/D ratio as: nonirritant: >100, slight irritant: >10, moderate irritant: >1, irritant: >0.1, and very irritant: <0.1.[25]

Acknowledgements

The authors thank the financial support of DURSI (Generalitat de Catalunya) 2005-SGR-00698 and CICYT project CTQ2004-0017/PPQ. J.A.C. acknowledges the CSIC I3P postgraduate scholarship program for financial support.

Keywords: amino acids · amphiphiles · antibacterial agents · antifungal agents · biotransformations

[1] L. Pérez, J. L. Torres, A. Manresa, C. Solans, M. R. Infante, *Langmuir* **1996**, *12*, 5296 – 5301.
[2] E. Piera, M. R. Infante, P. Clapés, *Biotechnol. Bioeng.* **2000**, *70*, 323 – 331.
[3] a) P. Clapés, C. Morán, M. R. Infante, *Biotechnol. Bioeng.* **1999**, *63*, 333 – 343; b) C. Morán, M. R. Infante, P. Clapés, *J. Chem. Soc. Perkin Trans. 1* **2002**, 1124 – 1134; c) L. Pérez, A. Pinazo, M. P. Vinardell, P. Clapés, M. Angelet, M. R. Infante, *New J. Chem.* **2002**, *26*, 1221 – 1227.
[4] M. R. Infante, A. Pinazo, J. Seguer, *Colloids Surf. A* **1997**, *123–124*, 49 – 70.
[5] a) P. Clapés, M. R. Infante, *Biocatal. Biotransform.* **2002**, *20*, 215 – 233; b) M. C. Morán, A. Pinazo, L. Pérez, P. Clapés, M. Angelet, M. T. García, M. P. Vinardell, M. R. Infante, *Green Chem.* **2004**, *6*, 233 – 240.
[6] L. Pérez, M. T. García, R. I. , M. P. Vinardell, A. Manresa, M. R. Infante, *Environ. Toxicol. Chem.* **2002**, *21*, 1279 – 1285.
[7] J. A. Castillo, A. Pinazo, J. Carilla, M. R. Infante, M. A. Alsina, I. Haro, P. Clapés, *Langmuir* **2004**, *20*, 3379 – 3387.
[8] G. McDonnell, A. D. Russell, *Clin. Microbiol. Rev.* **1999**, *12*, 147 – 179.
[9] E. Hidalgo, C. Domínguez, *Toxicol. in vitro* **2001**, *15*, 271 – 276.
[10] a) S. P. Denyer, *Int. Biodeterior. Biodegrad.* **1995**, *36*, 227 – 245; b) F. C. Sheppard, D. J. Mason, S. F. Bloomfield, V. A. Gant, *FEMS Microbiol. Lett.* **1997**, *154*, 283 – 288; c) J. Chawner, P. Gilbert, *J. Appl. Bacteriol.* **1989**, *66*, 253 – 258.
[11] S. P. Denyer, G. S. A. B. Stewart, *Int. Biodeterior. Biodegrad.* **1998**, *41*, 261 – 268.
[12] G. T. Wernert, D. A. Winkler, G. Holan, G. Nicoletti, *Aust. J. Chem.* **2004**, *57*, 77 – 85.
[13] L. Pérez, A. Pinazo, M. J. Rosen, M. R. Infante, *Langmuir* **1998**, *14*, 2307 – 2315.
[14] G. Oros, T. Cserhati, E. Forgacs, *Chemosphere* **2003**, *52*, 185 – 193.
[15] M. J. Rosen, L. Fei, Y.-P. Zhu, S. W. Morrall, *J. Surfactants Deterg.* **1999**, *2*, 343 – 347.
[16] A. D. Russell, *Am. J. Infect. Control* **2001**, *29*, 259 – 261; T. Köhler, J. C. Pechère, P. Plésiat, *Cell. Mol. Life Sci.* **1999**, *56*, 771 – 778.
[17] The Log K_{ow} (KowWin) program estimates the log octanol–water partition coefficient (log *P*) of organic compounds using an atom/fragment contribution method developed at SRC. The KowWin Program methodology is described in: "Atom/fragment contribution method for estimating octanol–water partition coefficients": W. M. Meylan, P. H. Howard, *J. Pharm. Sci.* **1995**, *84*, 83 – 92.
[18] V. D. Warner, D. M. Lynch, K. H. Kim, G. L. Grunewald, *J. Med. Chem.* **1979**, *22*, 359 – 366.
[19] a) F. M. Menger, J. S. Keiper, *Angew. Chem.* **2000**, *112*, 1980 – 1996; *Angew. Chem. Int. Ed.* **2000**, *39*, 1906 – 1920; b) L. Massi, F. Guittard, R. Levy, Y. Duccini, S. Geribaldi, *Eur. J. Med. Chem.* **2003**, *38*, 519 – 523.
[20] a) J. M. Tanzer, A. M. Slee, B. A. Kamay, *Antimicrob. Agents Chemother.* **1977**, *12*, 721 – 729; b) C. Appelt, A. Wessolowski, J. A. Soderhall, M. Dathe, P. Schmieder, *ChemBioChem* **2005**, *6*, 1654 – 1662.
[21] a) L. Massi, F. Guittard, S. Geribaldi, R. Levy, Y. Duccini, *Int. J. Antimicrob. Agents* **2003**, *21*, 20 – 26; b) C. E. Codling, J. Y. Maillard, D. Russell, *J. Antimicrob. Chemother.* **2003**, *51*, 1153 – 1158; c) I. Togashi, S. Gisusi, A. Harada, *J. Wood Sci.* **1998**, *44*, 414 – 416; d) A. M. Tortorano, M. A. Viviani, E. Biraghi, A. L. Rigoni, A. Prigitano, R. Grillot, EBGA Network, *J. Med. Microbiol.* **2005**, *54*, 955–957; e) C. E. Codling, A. C. Hann, J. Y. Maillard, A. D. Russell, *Cont. Lens Ant. Eye* **2005**, *28*, 163 – 168.
[22] F. C. Odds, A. J. P. Brown, N. A. R. Gow, *Trends Microbiol.* **2003**, *11*, 272 – 279.
[23] M. Del Poeta, W. A. Schell, C. C. Dykstra, S. Jones, R. R. Tidwell, A. Czarny, M. Bajic, M. Bajic, A. Kumar, D. Boykin, J. R. Perfect, *Antimicrob. Agents Chemother.* **1998**, *42*, 2495 – 2502.
[24] G. Ludewig, J. M. Williams, Y. Li, C. Staben, *Antimicrob. Agents Chemother.* **1994**, *38*, 1123 – 1128.
[25] W. J. Pape, U. Pfannenbecker, U. Hoppe, *Mol. Toxicol.* **1987**, *1*, 525 – 536.
[26] M. Mitjans, V. Martínez, P. Clapés, L. Pérez, M. R. Infante, M. P. Vinardell, *Pharm. Res.* **2003**, *20*, 1697 – 1701.
[27] H. C. Ansel, *J. Pharm. Sci.* **1967**, *56*, 616 – 619.
[28] M. A. Vives, M. R. Infante, M. P. Vinardell, *Pharm. Sci.* **1997**, *3*, 601 – 604.
[29] M. M. Udden, C. S. Patton, *J. Appl. Toxicol.* **1994**, *14*, 91 – 96.
[30] a) S. Dufour, M. Deleu, K. Nott, B. Wathelet, P. Thonart, M. Paquot, *Biochim. Biophys. Acta* **2005**, *1726*, 87 – 95; b) E. Galembeck, A. Alonso, N. C. Meirelles, *Chem.-Biol. Interact.* **1998**, *113*, 91 – 103; c) M. Dubnickova, M. Bobrowska-Hagerstrand, T. Soderstrom, A. Iglic, H. Hagerstrand, *Acta Biochim. Pol.* **2000**, *47*, 651 – 660; d) M. Macián, J. Seguer, M. R. Infante, C. Selve, M. P. Vinardell, *Toxicology* **1996**, *106*, 1 – 9.
[31] G. L. Woods, J. A. Washington, in *Manual of Clinical Microbiology* (Eds.: P. R. Murray, E. J. Baron, M. S. Pfaller, F. C. Ternover, Y. R. H. Yolken), ASM Press, Washington, **1995**.

Received: June 17, 2006
Revised: July 17, 2006
Published online on September 14, 2006

6.2.4. Publication IV:

Fructosa-6-phosphate aldolase in organic synthesis: preparation of D-fagomine, *N*-alkylated derivatives, and preliminary biological assays.

José A. Castillo, Jordi Calveras, Josefina Casas, Montserrat Mitjans, M. Pilar Vinardell, Teodor Parella, Tomoyuki Inoue, Georg A. Sprenger, Jesús Joglar, Pere Clapés.

Organic Letters **2006**, *8*, 6067-6670.

ORGANIC LETTERS

2006
Vol. 8, No. 26
6067−6070

Fructose-6-phosphate Aldolase in Organic Synthesis: Preparation of D-Fagomine, *N*-Alkylated Derivatives, and Preliminary Biological Assays

José A. Castillo,[†] Jordi Calveras,[†] Josefina Casas,[†] Montserrat Mitjans,[‡] M. Pilar Vinardell,[‡] Teodor Parella,[§] Tomoyuki Inoue,[||] Georg A. Sprenger,[||] Jesús Joglar,*[,†] and Pere Clapés*[,†]

Institute for Chemical and Environmental Research (IIQAB)-CSIC, Jordi Girona 18-26, 08034 Barcelona, Spain, Department of Physiology, Faculty of Pharmacy, University of Barcelona, Avgda. Joan XXIII s/n, 08028 Barcelona, Spain, Servei de Ressonància Magnètica Nuclear, Universitat Autònoma de Barcelona, 08193 Bellaterra, Barcelona, Spain, and Institute of Microbiology, University of Stuttgart, Allmandring 31, 70569 Stuttgart, Germany

pcsqbp@iiqab.csic.es

Received October 17, 2006

ABSTRACT

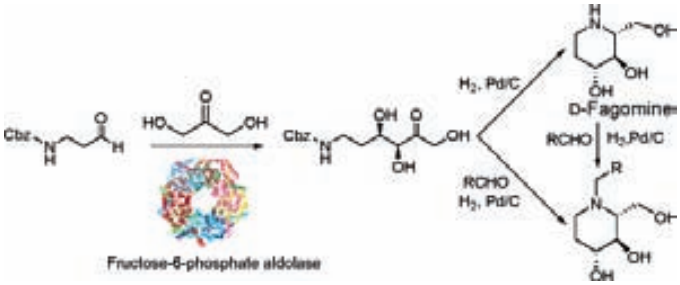

D-Fructose-6-phosphate aldolase (FSA) mediates a novel straightforward two-step chemo-enzymatic synthesis of D-fagomine and some of its *N*-alkylated derivatives in 51% isolated yield and 99% de. The key step is the FSA-catalyzed aldol addition of simple dihydroxyacetone (DHA) to *N*-Cbz-3-aminopropanal. The use of FSA greatly simplifies the enzymatic procedures that used dihydroxyacetonephosphate or DHA/esters. Some *N*-alkyl derivatives synthesized elicited antifungal and antibacterial activity as well as enhanced inhibitory activity, and selectivity against *β*-galactosidase and α-glucosidase.

D-Fagomine, (2*R*,3*R*,4*R*)-2-hydroxymethylpiperidine-3,4-diol is a naturally occurring iminosugar that was first isolated from buckwheat seeds of *Fagopyrum esculentum* Moench[1] with remarkable biological properties. This iminosugar has inhibitory activity against mammalian intestinal α-, *β*-glucosidase and α-, *β*-galactosidase.[2,3] Moreover, it appears to have a potent antihyperglycemic effect on streptozotocin-induced diabetic mice and potentiates glucose-induced insulin secretion.[4] Segraves et al.[5] have found that *C*-alkylated 3,4-di-*epi*-fagomines from *Batzella* sp. sponge have a good antimicrobial activity against *Staphylococcus epidermidis*.

[†] Institute for Chemical and Environmental Research.
[‡] University of Barcelona.
[§] Universitat Autònoma de Barcelona.
[||] University of Stuttgart.

(1) Koyama, M.; Sakamura, S. *Agr. Biol. Chem.* **1974**, *38*, 1111−1112.
(2) Scofield, A. M.; Fellows, L. E.; Nash, R. J.; Fleet, G. W. J. *Life Sci.* **1986**, *39*, 645−650.
(3) Kato, A.; Asano, N.; Kizu, H.; Matsui, K.; Watson, A. A.; Nash, R. J. *J. Nat. Prod.* **1997**, *60*, 312−314.
(4) Nojima, H.; Kimura, I.; Chen, F.-J.; Sugihara, Y.; Haruno, M.; Kato, A.; Asano, N. *J. Nat. Prod.* **1998**, *61*, 397−400. Taniguchi, S.; Asano, N.; Tomino, F.; Miwa, I. *Horm. Metab. Res.* **1998**, *30*, 679−683.
(5) Segraves, N. L.; Crews, P. *J. Nat. Prod.* **2005**, *68*, 118−121.

10.1021/ol0625482 CCC: $33.50
Published on Web 11/29/2006

Chemical synthetic approaches of D-fagomine and its derivatives involve cumbersome protection−deprotection reactions and chiral starting materials, and therefore, moderate global yields are achieved.[6,7] Recent syntheses of D-fagomine and other stereoisomers have been described starting from chiral D-serine-derived Garner aldehyde in six to seven steps with global yields around 12%.[8]

Stereodivergent asymmetric chemo-enzymatic methodologies are mostly based on dihydroxyacetone phosphate (DHAP)-dependent aldolases. The key step is the stereoselective aldol addition of DHAP or DHA/arsenate (500 mM) to synthetic equivalents of aminoaldehydes.[9,10] Given the toxicity of arsenate, it would be more attractive to find a system allowing the use of "naked" DHA.[11] Chemical synthesis of DHAP involves several steps in ca. 70% overall yield.[12] Alternatively, enzymatic methods to generate DHAP, which can be coupled with the aldol reaction, have also been described.[13] However, some limitations arising from the lack of compatibility of conditions between the coupled enzymatic reactions and the generation of complex mixtures that make the product separation and purification difficult have been observed.[14]

We report herein a straightforward procedure for the stereoselective synthesis of D-fagomine and *N*-alkylated derivatives using fructose-6-phosphate aldolase (FSA) as biocatalyst and achiral easily accessible starting materials. The key step in this synthetic scheme was the stereoselective aldol addition of simple dihydroxyacetone (DHA) to **1** catalyzed by FSA (Scheme 1). FSA is a novel class I aldolase from *E. coli* related to a novel group of bacterial transaldolases, which catalyzes the aldol addition of DHA to glyceraldehyde-3-phosphate. The cloning and overexpression in *E.* coli DH5α of the gene encoding FSA and the biochemical characterization was carried out for the first time by Schürmann et al.[15] These authors[16] reported aldol additions of either DHA or hydroxyacetone to some hydroxyaldehydes for the synthesis of sugar derivatives. The most interesting feature of FSA is that utilizes DHA instead of either DHAP or DHA/esters which greatly simplifies the chemo-enzymatic strategies to α,*β*-dihydroxyketones.

Scheme 1. Chemo-enzymatic Synthesis of **3** and *N*-Alkylated Derivatives

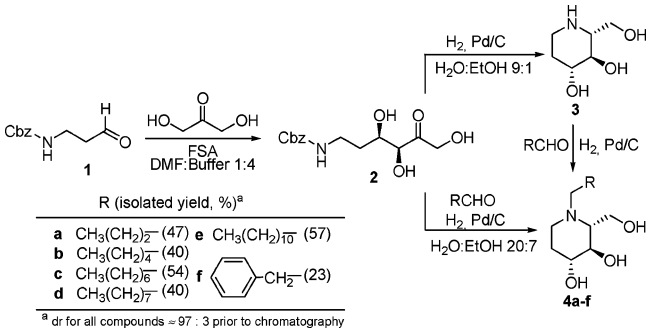

In this work, after growing and disrupting the *E. coli* cells the enzyme was purified easily by a heat treatment at 75 °C during 40 min, centrifugation, and lyophilization of the supernatant to yield a pale brown powder with 1.7 U mg^{-1}.[17] Further purification steps are not needed since they were not crucial for the activity and stereoselectivity of the enzymatic aldol addition.

Preparation of **1** was carried out by previously described procedures from 3-aminopropanol.[10,18] The FSA-catalyzed aldol addition of DHA to **1** was conducted at 4 °C in boric−borate 50 mM pH 7 buffer containing 20% v/v DMF, furnishing 79% reaction conversion by HPLC after 1 h (69% isolated yield of **2**). Glycylglycine 50 mM pH 7.0 buffer can also be used yielding 82% reaction conversion after 1 h.[11] Hence, FSA readily accepts DHA, and there is no need to in situ generate DHA esters. Furthermore, FSA tolerates organic solvents as other DHAP-dependent aldolases do. D-Fagomine (**3**) was then obtained by selective catalytic reductive amination[10] of **2** (Pd/C, H_2 50 psi) in 89% isolated yield without further purification and 93:7 diastereomeric ratio by NMR: $[\alpha]^{20}_D = +20.4$ (*c* 1.0, H_2O) (lit.[3] $[\alpha]_D^{20} = +19.5$ (*c* 1.0, H_2O)). Further purification by cation-exchange chromatography on CM-sepharose in NH_4^+ form, eluted isocratically with 0.01 M NH_4OH, gave an excellent separation of **3** (83% recovery and de ≥99%) and a minor diastereoisomer identified as D-2,4-di-*epi*-fagomine. This

(6) Fleet, G. W. J.; Fellows, L. E.; Smith, P. W. *Tetrahedron* **1987**, *43*, 979−990. Pandey, G.; Kapur, M. *Tetrahedron Lett.* **2000**, *41*, 8821−8824.

(7) Goujon, J.-Y.; Gueyrard, D.; Compain, P.; Martin, O. R.; Ikeda, K.; Kato, A.; Asano, N. *Bioorg. Med. Chem.* **2005**, *13*, 2313−2324.

(8) Banba, Y.; Abe, C.; Nemoto, H.; Kato, A.; Adachi, I.; Takahata, H. *Tetrahedron: Asymmetry* **2001**, *12*, 817−819. Takahata, H.; Banba, Y.; Ouchi, H.; Nemoto, H.; Kato, A.; Adachi, I. *J. Org. Chem.* **2003**, *68*, 3603−3607. Takahata, H.; Banba, Y.; Sasatani, M.; Nemoto, H.; Kato, A.; Adachi, I. *Tetrahedron* **2004**, *60*, 8199−8205.

(9) Ziegler, T.; Straub, A.; Effenberger, F. *Angew. Chem., Int. Ed.* **1988**, *27*, 716−717. Von der Osten, C. H.; Sinskey, A. J.; Barbas, C. F., III; Pederson, R. L.; Wang, Y. F.; Wong, C. H. *J. Am. Chem. Soc.* **1989**, *111*, 3924−3927. Pederson, R. L.; Wong, C. H. *Heterocycles* **1989**, *28*, 477−480.

(10) Espelt, L.; Parella, T.; Bujons, J.; Solans, C.; Joglar, J.; Delgado, A.; Clapes, P. *Chem.−Eur. J.* **2003**, *9*, 4887−4899.

(11) Wong et al. have recently discussed the possibility of using DHA as a substrate in the presence of borate buffer, presumably by in situ formation of borate ester to permit the direct use of DHA in DHAP-aldolase-mediated chemistry. See: Sujiyama, M.; Whalen, L. J.; Hong, Z.-Y.; Greenberg, W.A.; Wong, C.-H. *Book of Abstracts*. 232nd ACS National Meeting, San Francisco, Sep 10−14, 2006; American Chemical Society: Washington, DC, 2006; ORGN-496. In our case, FSA uses DHA, and there is no need for any ester, as demonstrated with reactions conducted in glycylglycine buffer.

(12) Jung, S.-H.; Jeong, J.-H.; Miller, P.; Wong, C.-H. *J. Org. Chem.* **1994**, *59*, 7182−7184. Gefflaut, T.; Lemaire, M.; Valentin, M.-L.; Bolte, J. *J. Org. Chem.* **1997**, *62*, 5920−5922. Ferroni, E. L.; Ditella, V.; Ghanayem, N.; Jeske, R.; Jodlowski, C.; Oconnell, M.; Styrsky, J.; Svoboda, R.; Venkataraman, A.; Winkler, B. M. *J. Org. Chem.* **1999**, *64*, 4943−4945. Charmantray, F.; El Blidi, L.; Gefflaut, T.; Hecquet, L.; Bolte, J.; Lemaire, M. *J. Org. Chem.* **2004**, *69*, 9310−9312. Meyer, O.; Ponaire, S.; Rohmer, M.; Grosdemange-Billiard, C. *Org. Lett.* **2006**, *8*, 4347−4350.

(13) Fessner, W.-D.; Sinerius, G. *Angew. Chem., Int. Ed.* **1994**, *33*, 209−212. Sanchez-Moreno, I.; Francisco Garcia-Garcia, J.; Bastida, A.; Garcia-Junceda, E. *Chem. Commun.* **2004**, 1634−1635. van Herk, T.; Hartog, A. F.; Schoemaker, H. E.; Wever, R. *J. Org. Chem.* **2006**, *71*, 6244−6247.

(14) Fessner, W.-D.; Walter, C. *Top. Curr. Chem.* **1996**, *184*, 97−194.

(15) Schürmann, M.; Sprenger, G. A. *J. Biol. Chem.* **2001**, *276*, 11055−11061.

(16) Schürmann, M.; Sprenger, G. A. *J. Mol. Catal. B: Enzym.* **2002**, *19*, 247−252.

(17) One unit of U will synthesize 1 μmol of fructose-6-phosphate from D-glyceraldehyde-3-phosphate and DHA per minute at pH 8.5 (glycylglycine 50 mM buffer) and 30 °C. The maximum specific activity observed for the purified enzyme was 7.13 U mg^{-1}.

(18) Ocejo, M.; Vicario, J. L.; Badia, D.; Carrillo, L.; Reyes, E. *Synlett* **2005**, 2110−2112.

compound arose from the *re*-face attack of the DHA−FSA complex on the aldehyde, similar to that found with D-fructose-1,6-bisphosphate aldolase.[10] *N*-Alkylated derivatives (**4a**−**f**) were easily obtained by catalytic reductive amination (Pd/C, H_2 50 psi) of a mixture of **3** and the corresponding aldehyde. Most interestingly, we carried out the preparation of **4a**−**f** by reductive amination of a mixture of **2** and the aldehyde in a one-pot reaction (Scheme 1). The isolated yields obtained by this procedure were similar to those achieved starting from **3**.

Investigations of the synthetic abilities of FSA in organic synthesis are currently in progress. We have found that this enzyme accepts, among others, *N*-Cbz-glycinal and *N*-Cbz-3-amino-2-hydroxypropanal, but α-alkyl-branched *N*-Cbz-aminoaldehydes were not tolerated as substrates.

Antimicrobial activity of **3** and **4a**−**f** was tested against 15 bacteria and 7 fungi (see the Supporting Information). Compounds **3** and **4a**−**d**,**f** did not show activity at concentrations below 256 μg mL^{-1}, thus indicating much lower potency than that found for antiseptics such as cationic surfactants and biguanides.[19] Interestingly, **4e** gave minimum inhibitory concentrations (MIC)s ranging from 32 to 64 μg mL^{-1} against most of the Gram-positive bacteria tested, whereas MICs of 128−256 μg mL^{-1} were observed for the Gram-negative bacteria. Compound **4e** was also rather potent against fungi such as *Aspergillus repens* (32 μg mL^{-1}) and *Cladosporium cladosporoides* (64 μg mL^{-1}) but less potent (128−256 μg mL^{-1}) against the rest of the fungi tested.

Since D-fagomine was reported to have inhibitory activity on α-glucosidase,[2,3] different chemical modifications have been introduced to improve its activity and selectivity. Goujon et al. synthesized α-1-*C*-substituted derivatives with or without an *N*-butyl group, which exhibited higher inhibitory activity than the parent compound against α-glucosidase from rice.[7] On the other hand, the substitution of the piperidine ring for an azepane ring decreased the inhibitory activity against both enzymes.[20]

Compounds **3** and **4a**−**f** were inhibitors of α-D-glucosidase from rice and β-D-galactosidase from bovine liver (Table 1), whereas no inhibition was observed against α-D-glucosidase from baker's yeast, β-D-glucosidase from almond, α-D-mannosidase from jack beans, and α-L-rhamnosidase from *Penicillium decumbens*. Interestingly, among the *N*-alkylated derivatives, **4d** and **4e** were the best inhibitors against α-D-glucosidase, whereas **4e** was a good inhibitor for the β-galactosidase. As shown in Table 1, the activity of **4a**−**f** against α-glucosidase increased with the aliphatic chain length up to nine carbon atoms (**4d**). Increasing the number of carbon atoms to 12 (**4e**) or including an aromatic moiety (**4f**) did not improve or caused a drastic decrease on the inhibitory activity, respectively. Kinetic studies indicated that active compounds behaved as competitive inhibitors of α-D-glucosidase from rice. These results suggested that **3** may interact with the subsite −1 of the two catalytic sites reported for α-glucosidase family II[21] and the *N*-alkyl substituent with a convenient length may fit into subsite +1, but not with the phenylethyl substitution.

Table 1. Inhibition of Glycosidases by Compounds **3** and **4a**−**f**

	α-D-glucosidase[a]		β-D-galactosidase[b]	
compd	K_i[c] (μM)	IC_{50} (μM)	K_i[d] (μM)	IC_{50} (μM)
3	9.3 ± 0.8	13.2	35.9 ± 3.9	30.4
4a	126 ± 3.6	151	NI[e]	
4b	73.3 ± 2.0	61.4	NI[e]	
4c	27.3 ± 2.8	35.3	242 ± 14	203
4d	14.9 ± 1.2	18.1	140 ± 18	108
4e	16.4 ± 2.1	20.7	9.3 ± 0.7	6.0
4f	143 ± 5.4	159	691 ± 18	416

[a] From rice. An IC_{50} value of 350 μM has been reported for compound **3**.[3] The reason may lie in the different substrate used to evaluate the glycosidase activity in the literature report (i.e., a disaccharide) and the present work (i.e., *p*-nitrophenyl glucopyranoside). [b] From bovine liver. [c] Competitive inhibition. [d] Noncompetitive. [e] No inhibition.

Inhibition of β-D-galactosidase from bovine liver by **3** and **4a**−**f** is also depicted in Table 1. For **4a**−**e**, the higher the hydrophobicity the lower the IC_{50} values, **4e** being the most active one. Inhibitory activity of **4e** was similar to that reported for the D-galacto isomer of **3**[22] and higher than that found for **3** or its α-1-*C*-ethyl derivative.[23] Active compounds inhibited this enzyme in a noncompetitive manner, with a K_i value for **4e** 4-fold lower than that for **3**.

Finally, cytotoxicity of **3** and **4a**−**f** was estimated by determination of their hemolytic and protein denaturation effects on human erythrocytes.[24] The results showed that they did not have activity, with the exception of **4e** (see the Supporting Information). The HC_{50} (i.e., concentration that induces the hemolysis of 50% of the cells) for compound **4e** was 138 ± 8 mg mL^{-1}, whereas the denaturation index (DI, i.e., hemoglobin denaturation induced by the compound) was 5 ± 1. These values compare with commercial decyl-glucoside (HC_{50} 252 ± 6 mg mL^{-1} and DI 14.2).[24]

In summary, D-fagomine can be obtained stereoselectively in two chemo-enzymatic asymmetric steps using inexpensive achiral DHA and **1** as the starting materials and FSA from *E. coli* as biocatalyst in 51% isolated yield and ≥99% de. The *N*-alkylated derivatives of **3** were obtained for the first time in one pot reaction from a mixture containing **2** and the corresponding aldehyde. Preliminary results indicated that **4e** elicited antifungal and antibacterial activity with slight selectivity against Gram-positive bacteria. Overall, alkylation of the nitrogen did not strongly improve the activity but increased the selectivity toward glucosidase and galactosidase

(19) Castillo, J. A.; Pinazo, A.; Carilla, J.; Infante, M. R.; Alsina, M. A.; Haro, I.; Clapes, P. *Langmuir* **2004**, *20*, 3379−3387.
(20) Li, H.; Bleriot, Y.; Chantereau, C.; Mallet, J.-M.; Sollogoub, M.; Zhang, Y.; Rodriguez-Garcia, E.; Vogel, P.; Jimenez-Barbero, J.; Sinay, P. *Organ. Biomol. Chem.* **2004**, *2*, 1492−1499.
(21) Kimura, A.; Lee, J.-H.; Lee, I.-S.; Lee, H.-S.; Park, K.-H.; Chiba, S.; Kim, D. *Carbohydr. Res.* **2004**, *339*, 1035−1040.
(22) Asano, N.; Oseki, K.; Kizu, H.; Matsui, K. *J. Med. Chem.* **1994**, *37*, 3701−3706.
(23) Asano, N.; Nishida, M.; Miyauchi, M.; Ikeda, K.; Yamamoto, M.; Kizu, H.; Kameda, Y.; Watson, A. A.; Nash, R. J.; Fleet, G. W. J. *Phytochemistry* **2000**, *53*, 379−382.
(24) Mitjans, M.; Martinez, V.; Clapes, P.; Perez, L.; Infante, M. R.; Vinardell, M. P. *Pharm. Res.* **2003**, *20*, 1697−1701.

inhibition. Compound **4d**, which was not cytotoxic in the red blood cell test, exhibited good inhibitory activity and higher specificity against family II α-glucosidase than that of the parent **3**.

Acknowledgment. We thank Prof. Angels Manresa at the Microbiology Department of the University of Barcelona for her assistance and fruitful discussions on antimicrobial activity. Financial support from the Spanish MEC (CTQ-2005-00063 and CTQ2005-25182-E), La Marató de TV3 foundation (20060293), and Generalitat de Catalunya DURSI 2005-SGR-00698 is acknowledged. J.A.C. and J.C. acknowledge the CSIC I3P and UAs predoctoral scholarship programs, respectively. J.A.C. also acknowledges the COST D25 STSM for financial support.

Supporting Information Available: Experimental preparations, analytical data, biological data, and ^{1}H and ^{13}C NMR spectra for all compounds; COSY, HSQC, and NOE spectra for compound **4a**. This material is available free of charge via the Internet at http://pubs.acs.org.

OL0625482